METABOLISM IN HAEMATOLOGICAL CANCER CELLS

by

ZUHAL ERASLAN

A thesis submitted to the University of Birmingham for the degree of

DOCTOR OF PHILOSOPHY

The Institute of Cancer and Genomic Sciences
College of Medical and Dental Sciences
University of Birmingham
September 2020

Dedicated to

My grandfather Mustafa Eraslan who passed away due to

Hodgkin lymphoma

Acknowledgments

Firstly, sincere thanks are due to Prof. Ulrich Günther and Dr.Farhat Khanim for their amazing supervision, support and guidance in the completion of this research. Prof. Ulrich Günther, my main supervisor, has always allowed me to chase my own ideas and provided me with a fascinating scientific journey. I always enjoyed the meetings where he was making fun of everything and encouraged me to handle difficult things just saying "well, it is simple Zuhal". Since the day I started to work with you; I know I've changed a lot that really helped me to become a better scientist. You know I appreciate you in so many ways. Dr. Farhat Khanim, my lovely co-supervisor, has been so patient to me. It is impossible to forget her willingness and ability to explain even the most complex topics at a level that I could engage with. She has such an amazing knowledge in the field of cancer biology. She always provided both practical and intellectual support for this project. Thank you for believing in me. I would like to express my special appreciation to Dr. Michelle AC Reed and Prof. Chris Bunce for insightful discussions and input to the direction of the work. Michelle, please accept my heartfelt gratitude for all the support and motivation! You are so helpful, kind, and

generous with your time and energy.

I would like to thank to all of my friends from NMR facility and the 8th floor in Biosciences for creating a friendly atmosphere to work in. Particularly, Sandro, Yao, Maiss, Bader, Anne Maria, Elis, Sanjana, Justyna and Emily, you all felt me at home, and we were like a big family! Thanks for sharing an awesome and crazy friendship that always makes me smile and never let me down. Raquel and Jennie, I was always feeling so safe when you were around me. Everything would be so tough without you… Thanks for being there always. I would like to thank Gaelle and Nuria for their helps and friendships.

I would also to thank the members of the NMR facility who were extremely warm to me. Sara and Mark, you were always patient with me even when I had no idea what was going on with the NMR spectrometer. Finally, I would like to acknowledge my parents, Zahide Eraslan and Hanifi Eraslan. There are no words to express how grateful I am to them both, for everything. And my uncles Zeynal Eraslan and Yusuf Barman, my sister Pınar Eraslan and my brother Zeynal Eraslan, thank you so much for being in my life and for your amazing supports!

Abstract

Cancer cells exhibit a rewired metabolism to meet their specific energy needs for cell proliferation. Despite remarkable efforts to unravel how cancer cells reprogram their metabolism, characterization of the metabolic differences between the different subtypes of cancer has not been well performed. Haematological cancers can be divided into subtypes with significant implications for diagnosis and treatment.

The metabolic profiles of a panel of 18 haematological cancer cell lines representing acute myeloid leukaemia (AML), chronic myeloid leukaemia (CML), multiple myeloma (MM), Burkitt's lymphoma (BL) and diffuse large B cell lymphoma (DLBCL) were characterised using an NMR approach. I found a notable widespread metabolic heterogeneity between haematological cancer subtypes, even though all haematological cancer cells showed a typical Warburg effect with lactate production. Intriguingly, MM cells were observed with a large amount of leucine uptake. The exploration of leucine metabolism using stable isotope tracer revealed that leucine is fully metabolised in MM cells and feeds the TCA cycle as well as sialic acid formation. Moreover, metabolic differences between BL and DLBCL were scrutinised, as these diseases tend to share similar morphological, immunophenotypic and genetic characteristics. Exogenous asparagine was found to regulate serine metabolism in BL cells. Furthermore, the combination of asparaginase (ASNase), a clinically used agent that depletes exogenous asparagine, with a PHGDH inhibitor (NCT503) had a synergistic effect on the viability in BL cells, exhibiting more decrease in cell viability as compared to those obtained from treatment of ASNase alone. Conversely, the combination of ASNase with NCT503 showed no synergistic effect on the viability of DLBCL cells, suggesting that the

combination of ASNase with NCT503 is solely synergistic for BL.

Hence, NMR-based metabolite profiling has revealed how metabolism alters in haematological cancers. This thesis has highlighted and investigated metabolic dependencies and vulnerabilities in different haematological cancer which can be utilised for diagnostic and therapeutic purposes in future.

Table of contents

List of figures

List of tables

List of abbreviations used in the thesis

Abbreviation	Full form
ABC	Activated B-cells
ACAT	Acetyl transacylase
ACC	Acetyl-CoA carboxylase
ACLY	ATP-citrate lyase
ACP	Acyl carrier protein
ADP	Adenosine diphosphate
AGC	Aspartate-glutamate transporter
ALD	Aldolase
ALL	Acute lymphoblastic leukaemia
AML	Acute myeloid leukaemia
AMP	Adenosine monophosphate
ANOVA	Analysis of variance
APL	Acute promyelocytic leukaemia
ASNS	Asparagine synthetase
ASS	Argininosuccinate synthetase
AST	Aspartate aminotransaminase
ATP	Adenosine triphosphate
BCAA	Branched-chain amino acid
BCAT	Branched chain aminotransferase
BCH	2-aminobicyclo-(2,2,1)-heptane-2-carboxylic acid
BCKA	Branched-chain α-keto acid
BCR	B-cell antigen receptor
BL	Burkitt lymphoma
BPTES	Bis-2-(5-phenylacetamido-1,3,4-thiadiazol-2-yl) ethyl sulphide
BSA	Bovine serum albumin
CAD	Carbamoyl phosphate synthetase
CAF	Cancer-associated fibroblasts
CBF	Core-binding factor
CI	Complex I
CII	Complex II
CIII	Complex III
CIV	Complex IV
CLP	Common lymphoid precursor
CML	Common myeloid precursor
CMP	Chronic myeloid leukaemia
COSY	Correlated spectroscopy
COX	Cytochrome c oxidase

CPT	Carnitine palmitoyl transferase
CRC	Colorectal cancer
CSF	Colony-stimulating factor
CTL	Cytotoxic T lymphocytes
DC	Dendritic cells
DLBCL	Diffuse large B-cell lymphoma
DMSO	Dimethyl sulfoxide
DNA	Deoxyribonucleic acid
DNMT	DNA (cytosine-5)-methyltransferase
EBV	Epstein-Barr virus
ECM	Extracellular matrix
EDTA	Ethylenediaminetetraacetic acid
ENO	Enolase
EZH	Enhancer of zeste homolog
FA	Fatty acid
FACS	Fluorescence-activated cell sorting
FAD	Flavin adenine dinucleotide
FADH	Reduced flavin adenine dinucleotide
FAK	Focal adhesion kinase
FAO	Fatty-acid oxidation
FASN	Fatty acid synthase
FBS	Fetal bovine serum
FDG	Fluoro-2-deoxy-D-glucose
FGFR	Fibroblast growth factor receptor
FID	Free induction decay
FLT	Fms related receptor tyrosine kinase
FT	Fourier transform
FU	Fluorouracil
GAPDH	Glyceraldehyde 3-phosphate dehydrogenase
GBM	Glioblastoma multiforme
GC	Germinal centre
GCB	Germinal centre B cell
GDH	Glutamate dehydrogenase
GDP	Guanosine diphosphate
GLS	Glutaminase
GLUD	Glutamate dehydrogenase
GLUT	Glucose transporter
GMP	Guanosine monophosphate
GS	Glutamine synthetase
GSH	Glutathione
GTP	Guanosine diphosphate

HCL	Hydrochloric acid
HG	Hydroxyglutarate
HIF	Hypoxia-inducible factor
HIV	Human immunodeficiency virus
HK	Hexokinase
HMDB	Human metabolome database
HPLC	High-performance liquid chromatography
HSC	Haematopoietic stem cells
HSQC	Heteronuclear single quantum correlation
IDH	Isocitrate dehydrogenase
IMP	Inosine 5-monophosphate
IMPDH	Inosine 5-monophosphate dehydrogenase
JAK	Janus kinase
KGCDH	Ketoglutarate dehydrogenase
LAT	L-amino acid transporter
LDH	Lactate dehydrogenase
MCT	Monocarboxylate transporter
MDH	Malate dehydrogenase
MDS	Myelodysplastic neoplasm
MEF	Mouse embryonic fibroblast
MGUS	Monoclonal gammopathy of undetermined significance
MM	Multiple myeloma
MPN	Myeloproliferative neoplasms
MRI	Magnetic resonance imaging
MRS	Magnetic resonance spectroscopy
MS	Mass spectrometry
NAD	Nicotinamide adenine dinucleotide
NADH	Reduced nicotinamide adenine dinucleotide
NADP	Nicotinamide adenine dinucleotide phosphate
NADPH	Reduced nicotinamide adenine dinucleotide phosphate
NGS	Next-generation sequencing
NHL	Non-Hodgkin lymphoma
NOE	Nuclear Overhauser effect
NOESY	Nuclear Overhauser effect spectroscopy
NUS	Non-uniform sampling
OXPHOS	Oxidative phosphorylation
PAGE	Polyacrylamide gel electrophoresis
PBS	Phosphate-buffered saline
PCA	Principle component analysis
PCR	Polymerase chain reaction

PDGFRA	Platelet-derived growth factor receptor A
PDH	Pyruvate dehydrogenase
PDHK	Pyruvate dehydrogenase kinase
PET	Positron emission tomography
PFK	Phosphofructokinase
PGI	Phosphoglucoisomerase
PGK	Phosphoglycerate kinase
PGM	phosphoglycerate mutase
PHGDH	Phosphoglycerate Dehydrogenase
PKM	Pyruvate kinase
PML	Promyelocytic leukaemia gene
PPP	Pentose phosphate pathway
PQN	Probabilistic quotient normalization
PRPP	5-Phosphoribosyl-1-pyrophosphate
PRPS	Phosphoribosylpyrophosphate synthetase
PTEN	Phosphatase and tensin homolog
PTLD	Posttransplant lymphoproliferative disorders
PVDF	Polyvinylidene fluoride
PYC	Pyruvate carboxylase
RAR	Retinoic acid receptor
RIPA	Radio-Immunoprecipitation Assay
RNA	Ribonucleic acid
ROS	Reactive oxygen species
SDH	Succinate dehydrogenase
SDS	Sodium dodecyl sulphate
STAT	Signal transducer and activator of transcription
TCA	Tricarboxylic acid
THF	Tetrahydrofolate
TKT	Transketolase
TMSP	Timethylsilyl-propanoic acid
TOCSY	Total correlation spectroscopy,
UDP	Uridine diphosphate
VEGF	Vascular endothelial growth factor
WHO	World Health Organization

CHAPTER 1

INTRODUCTION

1.1 Cell metabolism

Cellular metabolism is defined as the set of chemical reactions that take place in the cell so as to maintain life. Products of these chemical reactions provide cells with materials that are necessary for growth, reproduction, and maintenance of their structure. Metabolic processes have two distinct classes: anabolism and catabolism (Sánchez López de Nava & Raja, 2020). Both anabolic and catabolic reactions are critical to maintaining life.

Anabolism is the construction of molecules from smaller molecules utilising energy in the form of ATP molecules. Examples of anabolic reactions, also called biosynthesis reactions, are fatty acid synthesis, nucleic acid synthesis and the pentose phosphate pathway that generates NADPH and pentoses (5-carbon sugars) (Stincone et al., 2015). Catabolism is the breaking down of complex molecules into smaller units releasing the energy contained in the chemical bonds. The energy yielded from a catabolic reaction is released in the form of ATP and heat. Important sets of catabolic reactions occur in glycolysis, the tricarboxylic acid cycle (TCA) and β-oxidation (Tortora & Derrickson, 2018). During starvation, the amino acids are broken down to their carbon and nitrogen skeletons. While the nitrogen backbone is discarded through the urea cycle from the body, the carbon backbone can be funnelled into molecules involved in glycolysis and the TCA cycle (Gurina & Mohiuddin, 2020).

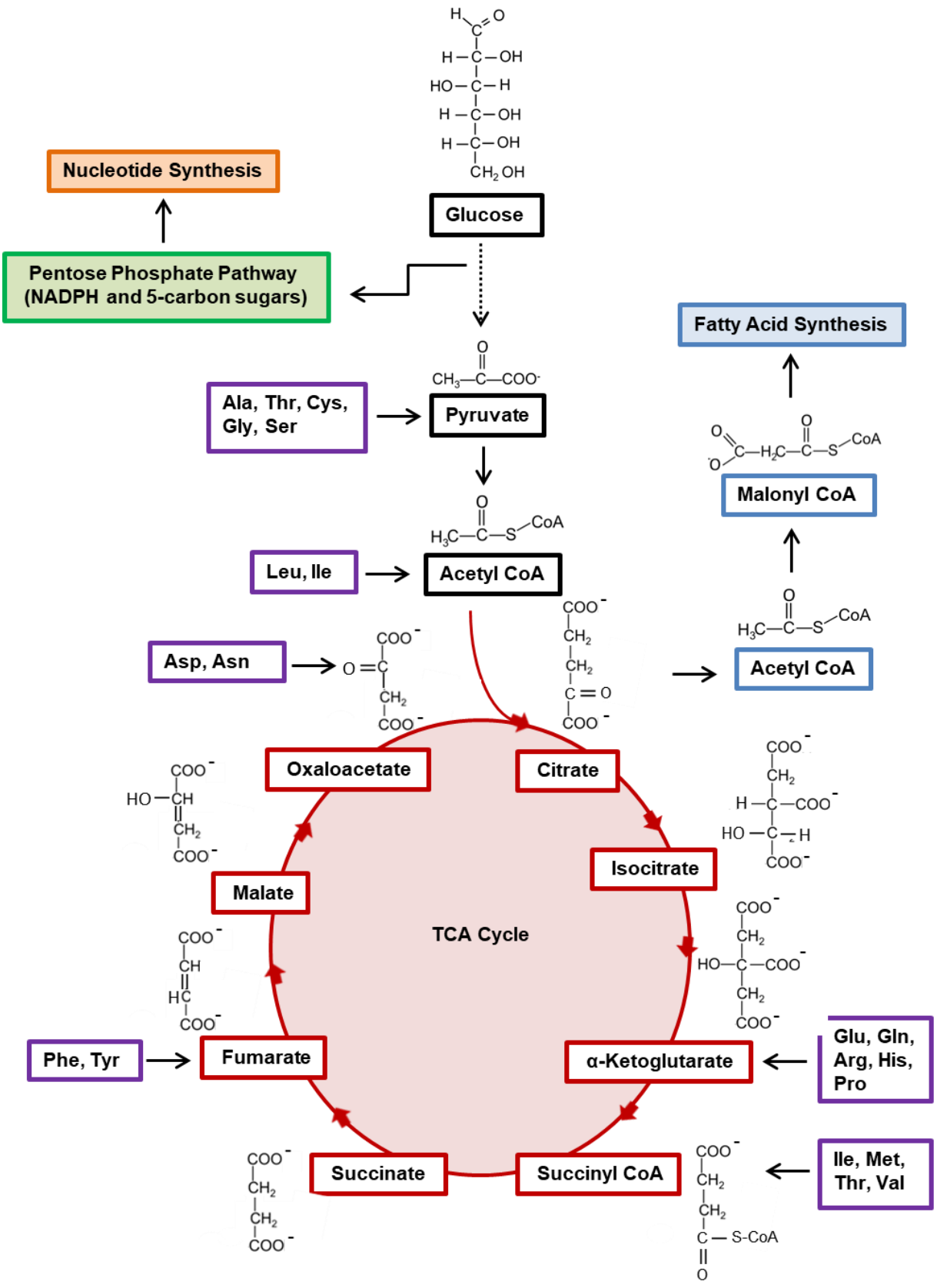
Nucleotide Synthesis
Glucose
Pentose Phosphate Pathway (NADPH and 5-carbon sugars)
Fatty Acid Synthesis
Ala, Thr, Cys, Gly, Ser
Pyruvate
Malonyl CoA
Leu, Ile
Acetyl CoA
Acetyl CoA
Asp, Asn
Oxaloacetate
Citrate
Isocitrate
Malate
TCA Cycle
Phe, Tyr
Fumarate
α-Ketoglutarate
Glu, Gln, Arg, His, Pro
Succinate
Succinyl CoA
Ile, Met, Thr, Val

Figure 1.1.1 Anabolic and catabolic pathways.

A simplified overview of the major anabolic and catabolic pathways. Glucose can either be directed to pentose phosphate pathway (PPP) or oxidised to pyruvate. Carbon atoms of alanine (Ala), serine (Ser), cysteine (Cys), glycine (Gly) and threonine (Thr) are used in the production of pyruvate. Pyruvate is converted to acetyl-CoA to enter the TCA cycle. Glutamine (Gln), glutamate (Glu), arginine (Arg), histidine (His) and proline (Pro) are converted into a-ketoglutarate; isoleucine (Ile), methionine (Met), threonine (Thr) and valine (Val) into succinyl-CoA, phenylalanine (Phe) and tyrosine(Tyr) into fumarate; aspartate (Asp) and asparagine (Asn) into oxaloacetate. The carbon skeletons of leucine (Leu) and isoleucine (Ile) are ultimately broken down to yield acetyl-CoA. Acetyl-CoA is then condensed with oxaloacetate yielding citrate. Citrate can either be cleaved to acetyl-CoA or converted to isocitrate in the TCA cycle. The carboxylation of acetyl-CoA to malonyl-CoA starts fatty acid synthesis.

1.2 Major metabolic pathways

1.2.1 Glycolysis and pentose phosphate pathway

Glycolysis is one of the main metabolic pathways of cellular respiration to synthesise the high energy molecules of ATP and NADH. Glycolysis is an anaerobic source of energy that has evolved in many living organisms but can occur in the presence of oxygen as well.

In glycolysis, glucose is split to yield two molecules of pyruvate and produce a net total of two ATP molecules and NADH through a series of reactions in the cytosol (see Figure 1.2.1). In the first reaction of glycolysis, glucose is phosphorylated with a phosphate group from ATP by hexokinase (HK), producing glucose 6-phosphate and ADP. HK catalyses the rate-limiting first step of glycolysis. Glucose 6-phosphate is then converted to fructose 6-phosphate by phosphoglucoisomerase (PGI) which catalyses the aldose-ketose isomerization. Phosphofructokinase-1 (PFK-1) catalyses production of fructose 1,6-bisphosphate from fructose 6-phosphate. Fructose 1,6-bisphosphate is split into two triose phosphates, glyceraldehyde 3-phosphate and dihydroxyacetone phosphate by aldolase (ALD). Glyceraldehyde 3-phosphate is then converted to 1,3-biphosphoglycerate in a reaction which reduces a molecule of NAD^+ to NADH by the action of glyceraldehyde 3-phosphate dehydrogenase (GAPDH). 1,3-biphosphoglycerate is now used to generate the first ATP as part of glycolysis. Phosphoglycerate kinase (PGK) transfers a phosphate group from 1,3-biphosphoglycerate to ADP, producing ATP and 3-phosphoglycerate. Then, phosphoglycerate mutase (PGM) catalyses the transfer of the phosphate group from one hydroxyl group to another hydroxyl group of 3-phosphoglycerate, generating 2-phosphoglycerate. In the next step, 2-phosphoglycerate

is dehydrated to form phosphoenolpyruvate by enolase (ENO). In the last reaction, the phosphoryl group of phosphoenolpyruvate is transferred to a molecule of ADP by pyruvate kinase (PKM), forming ATP and pyruvate. In the absence of sufficient oxygen, oxidation of NADH to NAD^+ occurs in a reaction which converts pyruvate to lactate catalysed by lactate dehydrogenase (LDH). The production of NAD^+ in this reaction allows further glycolysis. On the other hand, if oxygen is plentiful, glycolytically produced pyruvate is transported to mitochondria in order to become completely oxidised in the TCA cycle (Chaudhry & Varacallo, 2020).

Glycolytic intermediates act as a starting point for the pentose phosphate pathway (PPP). Once glucose is phosphorylated to generate glucose 6-phosphate, it can enter the PPP in the cytosol (see Figure 1.2.1). The PPP can be grouped into an oxidative stage and a non-oxidative stage. In the oxidative stage, NADPH is produced while ribulose 5-phosphate is formed from glucose 6-phosphate. The non-oxidative reactions are catalysed by transketolase (TKT) and transaldolase (TA) that exchange two and three-carbon fragments between sugar phosphates. Ribose 5-phosphate and its derivatives are required for the biosynthesis of essential cellular molecules such as RNA, DNA, and certain coenzymes. NADPH is the pyridine nucleotide coenzyme used for biosynthesis pathways that require reducing power, particularly for the synthesis of fatty acids (Cho et al., 2018).

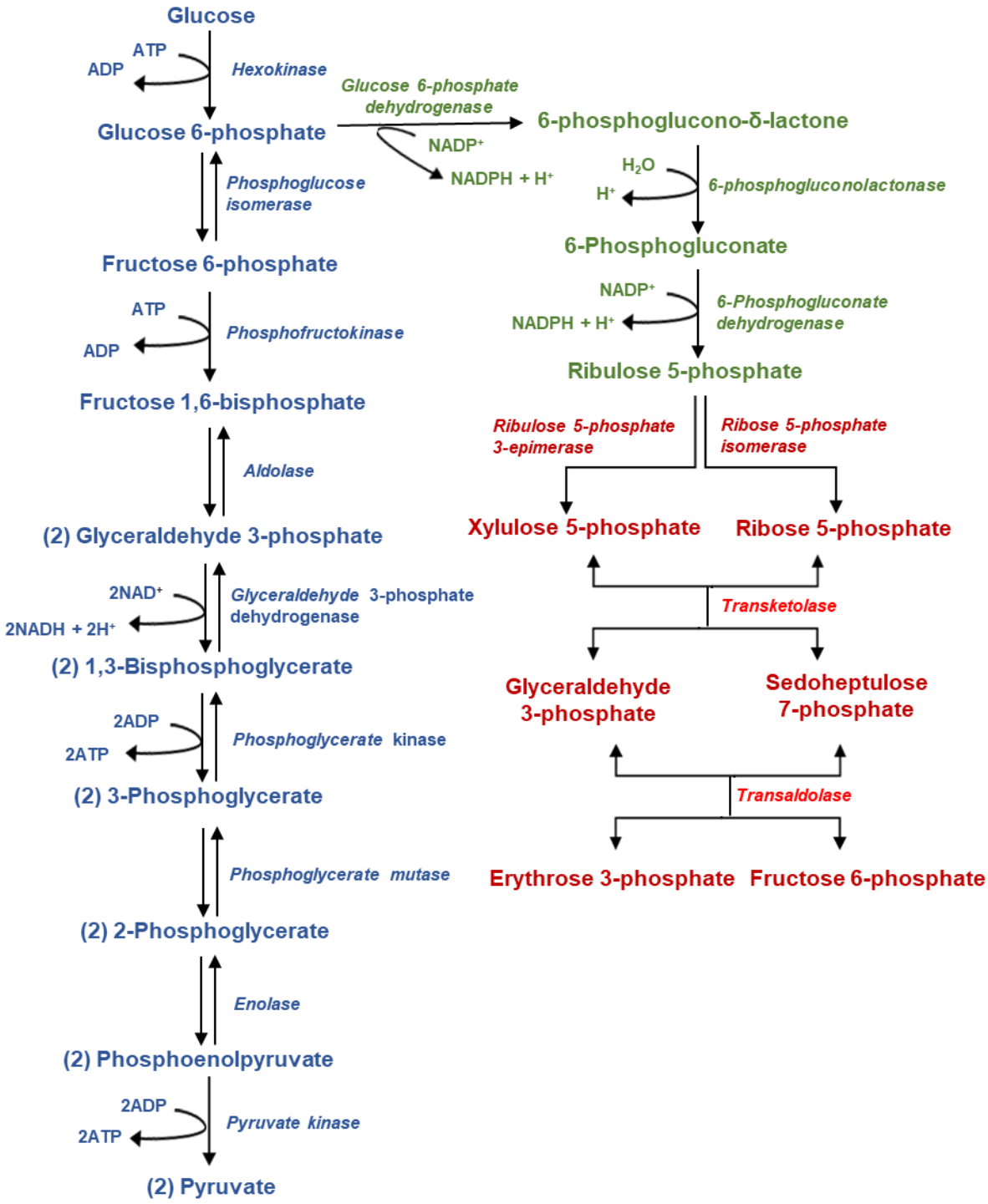
Glucose
ATP
ADP
Hexokinase
Glucose 6-phosphate
Glucose 6-phosphate dehydrogenase
NADP+
NADPH + H+
6-phosphoglucono-δ-lactone
H2O
H+
6-phosphogluconolactonase
6-Phosphogluconate
NADP+
NADPH + H+
6-Phosphogluconate dehydrogenase
Ribulose 5-phosphate
Phosphoglucose isomerase
Fructose 6-phosphate
ATP
ADP
Phosphofructokinase
Fructose 1,6-bisphosphate
Aldolase
(2) Glyceraldehyde 3-phosphate
Ribulose 5-phosphate 3-epimerase
Ribose 5-phosphate isomerase
Xylulose 5-phosphate
Ribose 5-phosphate
Transketolase
Glyceraldehyde 3-phosphate
Sedoheptulose 7-phosphate
Transaldolase
Erythrose 3-phosphate
Fructose 6-phosphate
2NAD+
2NADH + 2H+
Glyceraldehyde 3-phosphate dehydrogenase
(2) 1,3-Bisphosphoglycerate
2ADP
2ATP
Phosphoglycerate kinase
(2) 3-Phosphoglycerate
Phosphoglycerate mutase
(2) 2-Phosphoglycerate
Enolase
(2) Phosphoenolpyruvate
2ADP
2ATP
Pyruvate kinase
(2) Pyruvate

Figure 1.2.1 Glycolysis and pentose phosphate pathway.

The diagram represents glycolysis (blue), the oxidative phase of the pentose phosphate pathway (green) and the non-oxidative phase of the pentose phosphate pathway (red). The glycolysis and pentose phosphate pathway (PPP) are metabolically connected. Glucose in cells is rapidly phosphorylated to generate glucose 6-phosphate (G6P). The G6P can be either metabolised by the PPP to produce NADPH or by the glycolytic pathway to produce ATP, NADH and pyruvate. The PPP consists of two biochemical branches: an oxidative branch that produces NADPH and a non-oxidative branch that generates fructose 6-phosphate and glyceraldehyde 3-phosphate. Abbreviations: ADP: adenosine diphosphate; ATP: adenosine triphosphate; NAD: nicotinamide adenine dinucleotide; NADH: reduced nicotinamide adenine dinucleotide; NADP: nicotinamide adenine dinucleotide phosphate; NADPH: reduced nicotinamide adenine dinucleotide phosphate.

1.2.2 Fatty acid metabolism

Fatty acid (FA) metabolism, including de novo synthesis and oxidation of FAs, contributes to important needs of cells. Fatty acids serve as building blocks of complex membrane lipids as well as acting as fuel molecules.

Fatty acid synthesis is the process by which acetyl-CoA and NADPH are converted to fatty acids in the cytosol (see Figure1.2.2). Since acetyl-CoA is produced in mitochondria and the inner mitochondrial membrane is not permeable for acetyl-CoA, it is shuttled into the cytosol by the citrate transport system after condensation with oxaloacetate to form citrate by citrate synthase (CS). Then citrate is cleaved to regenerate acetyl-CoA and oxaloacetate by ATP-citrate lyase (ACLY) in the cytoplasm. The first committed step in fatty acid biosynthesis consists of carboxylation of acetyl-CoA to form malonyl-CoA using HCO_3^- by acetyl-CoA carboxylase (ACCase). As the elongation steps of fatty acid synthesis require the phosphopantetheine reactive unit in acyl carrier protein, ACP, the formation of acetyl-ACP and malonyl-ACP occurs by the action of the acetyl transacylase (ACAT) and malonyl transacylase (MCAT) activity, respectively. The synthesis of C16 palmitate from acetyl-ACP and malonyl-ACP is catalysed by the multiple enzymatic

activities of fatty acid synthase (FASN), which requires NADPH as reductant. Then, palmitate can undergo elongation and desaturation to yield a wide variety of other fatty acids (Berg et al., 2002).

Fatty acids are particularly important energy storage compounds in nature. Degradation of fatty acids plays a pivotal role in energy homeostasis in organs such as the heart, liver and skeletal muscles. Fatty acids can deliver more energy per gram than glucose; thus, they compete with carbohydrates as the primary oxidative substrate. During fasting and strenuous exercise, when glucose supply becomes limited, oxidation of fatty acids becomes vital for many organs to generate energy. Fatty acid β-oxidation is the catabolic process of breaking down a fatty acid into acetyl-CoA units in the mitochondria in eukaryotes. Free fatty acids cannot cross any cell membrane because of their negative charge. Hence, fatty acids must be actively transported into the mitochondrial matrix where β-oxidation takes place. The transport of fatty acids into mitochondria occurs by facilitated diffusion. Firstly, fatty acids are activated by conjugation with coenzyme A (CoA) in the cytosol, catalysed by acyl-CoA synthetase. Then, fatty acyl-CoA is esterified to carnitine to yield acylcarnitine for transport across the mitochondrial membrane. Once acylcarnitine is inside the mitochondrial matrix, fatty acyl-CoA is removed and beta-oxidation occurs by cleaving two carbons every cycle to form acetyl-CoA, along with high energy compounds NADH and $FADH_2$. In β-oxidation, two carbon subunits in the form of acetyl-CoA are repeatedly cleaved to form acetyl-CoA, which is further oxidised completely to CO_2 and H_2O with the generation of additional NADH and $FADH_2$ in the TCA cycle (Berg et al., 2002).

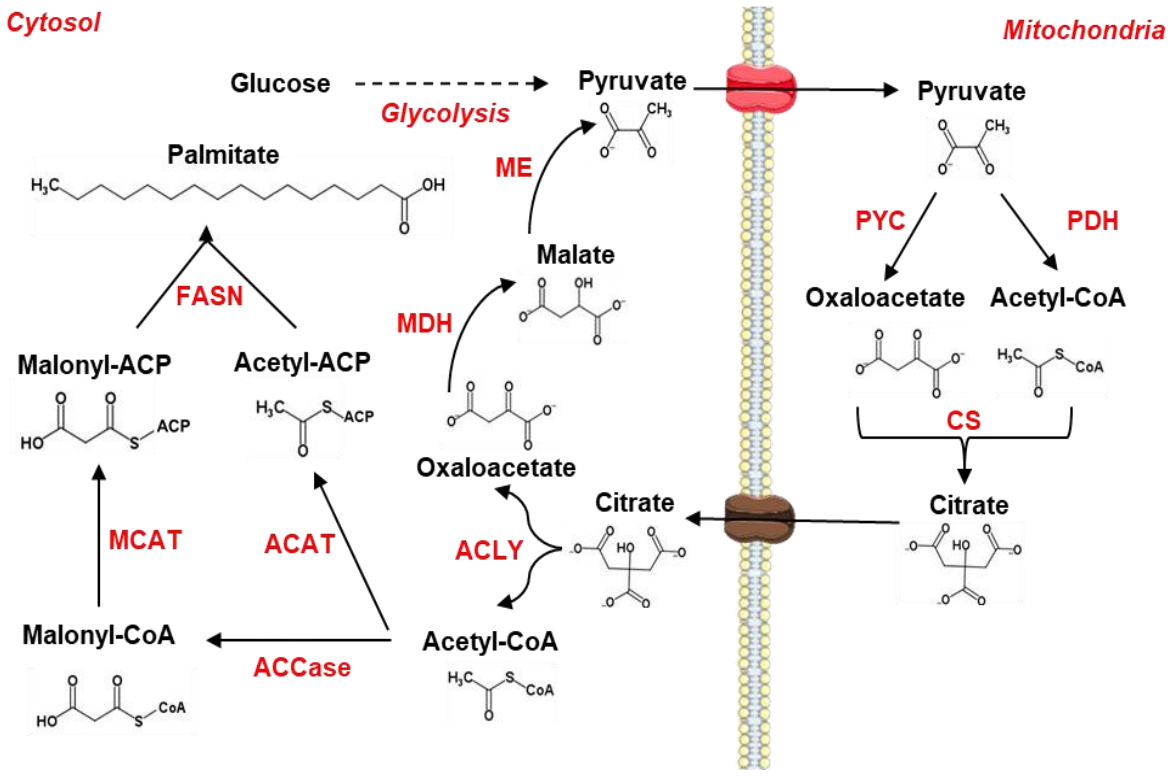

Figure 1.2.2 Fatty acid synthesis.

The figure shows the fatty acid synthesis in a cell. Fatty acid synthesis starts by transportation of citrate out of the mitochondria. Then citrate is cleaved to yield acetyl-CoA and oxaloacetate in the cytosol. Acetyl-CoA is converted to malonyl-CoA. CoA portions of acetyl-CoA and malonyl-CoA are replaced by a carrier protein, ACP. Synthesis of C16 palmitate from acetyl-ACP and malonyl-ACP is catalysed by the multiple enzymatic activities of FASN. Abbreviations: PYC: pyruvate carboxylase; PDH: pyruvate dehydrogenase; CS: citrate synthase; ACLY: ATP-citrate lyase; ACCase: acetyl-CoA carboxylase; ACAT: acetyl transacylase; MCAT: malonyl transacylase; MDH: malate dehydrogenase; ME: malic enzyme; FASN: fatty acid synthase.

1.2.3 TCA cycle and oxidative phosphorylation

The TCA cycle, also known as the citric acid cycle, is a series of chemical reactions in the cells that oxidises acetyl-CoA to CO_2 and H_2O, with the concomitant production of energy (Alabduladhem & Bordoni, 2020). Acetyl-CoA can be derived from the oxidation of glycolytically produced pyruvate by PDH or degradation of ketogenic amino acids and β-

oxidation of fatty acids. The TCA cycle provides cells with precursor metabolites for the synthesis of fatty acids, amino acids and nucleotides. Thus, the TCA cycle is considered to be the hub of aerobic metabolism as it fulfils energetic, biosynthetic and redox balance requirements of cells.

The TCA cycle consists of eight reactions in the matrix of mitochondria of eukaryotes and in the cytoplasm of prokaryotes. It begins with the generation of citrate formed from the condensation of oxaloacetate and acetyl-CoA (see Figure 1.2. 3). The citrate formation is followed by the two-step reactions in which citrate is converted to isocitrate by aconitase (AH). Then, isocitrate dehydrogenase (IDH) oxidizes isocitrate to α-ketoglutarate and CO_2 while reducing NAD^+ to NADH. The next step of the cycle is oxidative decarboxylation of α-ketoglutarate to succinyl-CoA and CO_2, with the formation of a molecule of NADH by α-ketoglutarate dehydrogenase (KGCDH). Succinate thiokinase (SST) removes the CoA group from succinyl-CoA to produce succinate; this first generates GTP by substrate-level phosphorylation. Succinate is oxidised to fumarate by succinate dehydrogenase (SDH) using FAD^+ as a proton acceptor. Then, fumarate hydratase (FH) catalyses the reversible addition of one molecule of H_2O to the double bond of fumarate to yield malate. The last step of the TCA cycle is the regeneration of oxaloacetate, the starting compound of the cycle, from malate by malate dehydrogenase (MDH). During this oxidation, NAD^+ is required as a cofactor and is reduced to NADH (Haddad & Mohiuddin, 2020).

The TCA cycle shuttles high-energy NADH and $FADH_2$ molecules to the electron transport chain. The electron transport chain is the site of oxidative phosphorylation and consists of a series of proteins and electron carriers found in the mitochondrial inner membrane. Briefly, oxidative phosphorylation is ATP production that links to the re-oxidation of NADH and $FADH_2$ by the electron transport chain. Electrons are transferred from one member

of the electron transport chain to another releasing some energy. The energy released by electron flow is used to pump protons to the intermembrane space in order to create an electrochemical proton gradient between the inner and outer mitochondrial membrane. Therefore, protons flow back down the gradient into the matrix through ATP synthase (ATPase) which uses the energy of protons in the synthesis of ATP from ADP.

Furthermore, the TCA cycle provides the substrates for amino acid synthesis by transamination, as well as for fatty acid synthesis and nucleotide synthesis (Anderson et al., 2018). For instance, malate generated in the TCA cycle can be shuttled into intermembrane space of mitochondria by a malate-alpha-ketoglutarate transporter (OGC) and converted into oxaloacetate, during which NAD^+ is reduced with two electrons to form NADH (see Figure 1.2.3). Then aspartate aminotransferase (AST) produces aspartate from oxaloacetate (Todisco et al., 2019).

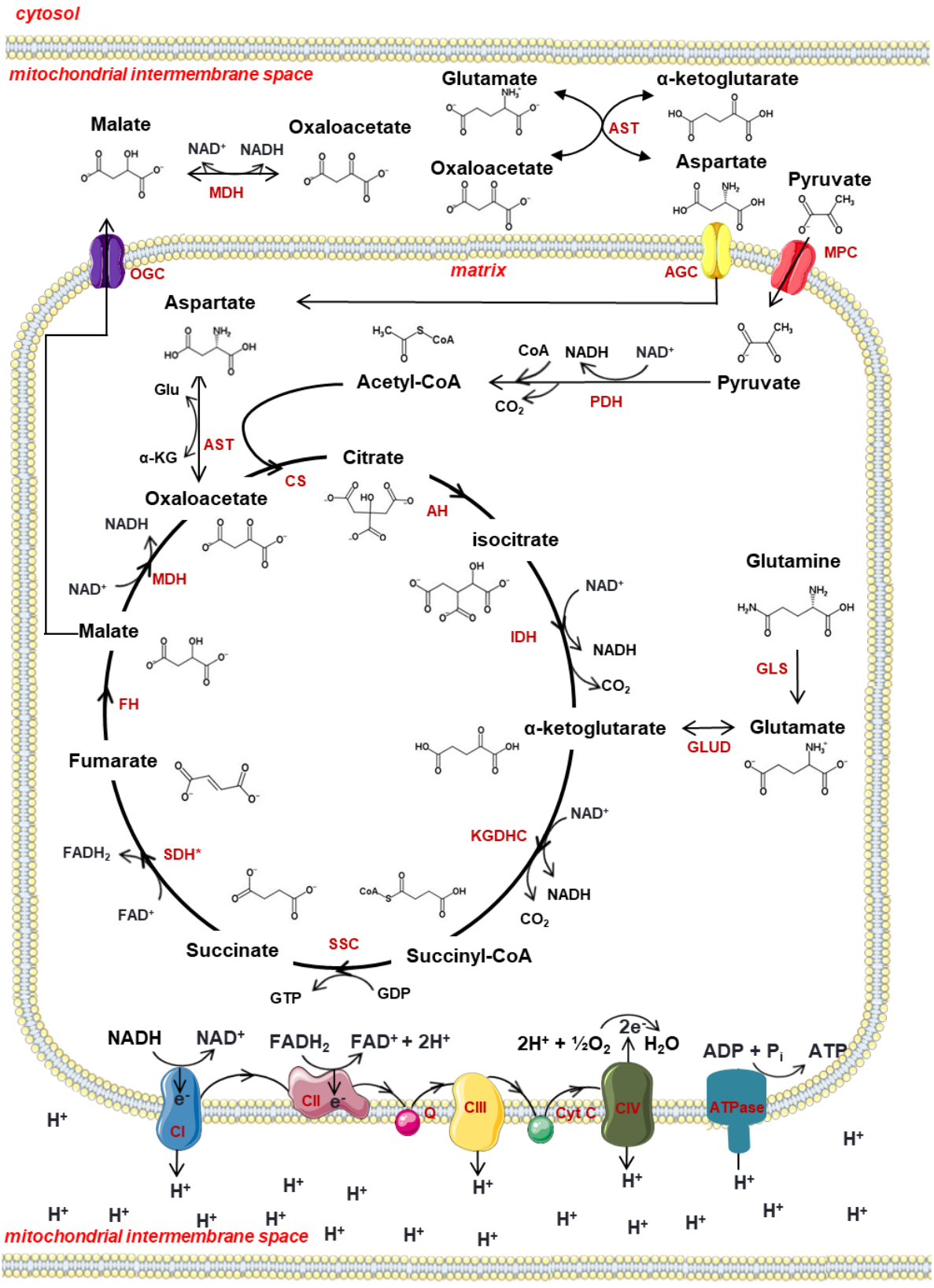
cytosol
mitochondrial intermembrane space
Glutamate
α-ketoglutarate
AST
Malate
NAD+
NADH
MDH
Oxaloacetate
Oxaloacetate
Aspartate
Pyruvate
OGC
matrix
AGC
MPC
Aspartate
Acetyl-CoA
CoA
NADH
NAD+
Pyruvate
CO2
PDH
Glu
α-KG
AST
Citrate
CS
Oxaloacetate
AH
NADH
NAD+
MDH
isocitrate
Glutamine
NAD+
IDH
NADH
CO2
GLS
Malate
FH
α-ketoglutarate
GLUD
Glutamate
Fumarate
NAD+
KGDHC
FADH2
SDH*
FAD+
NADH
CO2
Succinate
SSC
Succinyl-CoA
GTP
GDP
NADH
NAD+
FADH2
FAD+ + 2H+
2H+ + ½O2
2e-
H2O
ADP + Pi
ATP
e-
CI
CII
e-
Q
CIII
Cyt C
CIV
ATPase
H+
mitochondrial intermembrane space

Figure 1.2.3 Main pathways of mitochondrial energy production.

The diagram shows the TCA cycle and oxidative phosphorylation. The TCA cycle is a set of eight enzymatic reactions that begins with the transfer of an acetyl group from acetyl-CoA to oxaloacetate, then, in other steps, the acetyl group of acetyl-CoA are released as CO_2, restoring the oxaloacetate molecule for another round. Glutamine acts as an anaplerotic substrate to replenish the cycle intermediate, α ketoglutarate. The TCA cycle gives rise to three NADH molecules and one $FADH_2$ molecule. Electrons of NADH and $FADH_2$ are used to create a chemical gradient to produce ATP by electron transport chain found in the mitochondrial inner membrane. The malate produced in the TCA cycle moves into the intermembrane space of mitochondria. In the intermembrane space, malate is oxidised into oxaloacetate. The oxaloacetate is transaminated to produce aspartate using glutamate. The aspartate is then shuttled into the mitochondrial matrix and converted back to oxaloacetate. Abbreviations: MDH: malate dehydrogenase; AST: aspartate aminotransferase; AGC: glutamate-aspartate transporter; OGC: malate-alpha-ketoglutarate transporter; MPC: mitochondrial pyruvate carrier; PDH: pyruvate dehydrogenase; CS: citrate synthase; AH: aconitase; IDH: isocitrate dehydrogenase; KGDHC: α ketoglutarate dehydrogenase; SSC: succinate thiokinase; SDH: succinate dehydrogenase; FH: fumarate hydratase; FAD: flavin adenine dinucleotide; $FADH_2$: reduced flavin adenine dinucleotide; GDP: guanosine diphosphate; GTP: guanosine triphosphate; GLS: glutaminase; GLUD: glutamate dehydrogenase; ADP: adenosine diphosphate; ATP: adenosine triphosphate; NAD: nicotinamide adenine dinucleotide; NADH: reduced nicotinamide adenine dinucleotide; CI: NADH ubiquinone oxireductase; CII: succinate dehydrogenase; CIII: cytochrome bc1 complex; CIV: cytochrome c oxidase; ATPase: adenylpyrophosphatase.

1.3 Metabolism in cancer cells

Cancer is characterised by the uncontrolled growth of abnormal cells that destroys normal body tissue. Normal cells acquire specific mutations and subsequently traits to become tumorigenic and eventually malignant. One of the most fundamental traits of the cancer cell is dysregulation of growth-promoting signals that prevent progression through the cell cycle (Hanahan & Weinberg, 2011). Whilst normal cells carefully control cell cycles and differentiation to ensure homeostasis of cell number and tissue composition, cancer cells constitutively stimulate many signalling pathways that support growth and proliferation. Mutations in tumour suppressor genes endow cancer cells with the ability to evade growth suspension and cell death (Hanahan & Weinberg, 2011).

Cell metabolism is closely linked to cell proliferation. The uncontrolled proliferation and growth of cancer cells correlate with corresponding adjustments of energy metabolism in order to promote cell growth and division (Pavlova & Thompson, 2016). The alterations in metabolism are generally performed as a coordinated response of a cell to distinct cellular processes. For instance, cells with high proliferation reorganize the biosynthetic pathway for cell cycle progression, leading to a shift toward anabolic metabolism (Fritz & Fajas, 2010). Cancer cells uniquely alter their metabolism to meet the anabolic requirements associated with cell proliferation and also to enable invasion, metastasis and resistance to therapy (Phan et al., 2014). Thus, metabolic reprogramming in cancer cells has been recognised as one of the main hallmarks of malignancies (Pavlova & Thompson, 2016).

Cell proliferation entails the production of building block, intermediary metabolites and NADPH as reducing power. Several cancer cells were shown to be addicted to glucose so that they adapt to rapid proliferation (Fang & Fang, 2016; Gandhi & Das, 2019;

Strickland & Stoll, 2017). Catabolism of glucose provides cancer cells with intermediary metabolites which are diverted into branching pathways (Boroughs & DeBerardinis, 2015). For instance, glucose 6-phosphate produced by phosphorylation of glucose can be oxidised to generate NADPH in the PPP. Another important example is the use of glycolytic 3-phosphoglycerate generated from glycolysis as a precursor for the synthesis of serine that facilitates the folate metabolism and nucleotide synthesis (Newman & Maddocks, 2017). In normal cells, glycolysis is suppressed by energy-rich metabolites produced in mitochondria under aerobic conditions (Luengo et al., 2017). In a marked contrast to normal cells, cancer cells maintain a high rate of glycolysis in the presence of oxygen (Bhattacharya et al., 2016). Although glycolysis is bioenergetically less favourable than oxidative phosphorylation with less ATP production per molecule of glucose, cancer cells prefer glycolysis to oxidative phosphorylation(San-Millán & Brooks, 2017) .

Paradoxically, many cancer cells show an addiction to glutamine, despite the fact that glutamine is a non-essential amino acid (DeBerardinis et al., 2007). Glutamine plays a key role in the maintenance of the TCA cycle by replenishing TCA intermediates. Furthermore, the efflux of glutamine is coupled to the import of leucine that maintains the activity of the mammalian target of rapamycin (mTOR) pathway, which regulates, cell motility, cell survival, protein synthesis and autophagy (Nicklin et al., 2009). Thus, the high rate of glutamine increases proliferation as well as survival in cancer cells.

Many cancer cells also alter fatty acid metabolism to maintain cellular structure, provide energy and to regulate multiple signalling pathways (Huang & Freter, 2015). The increased de novo synthesis of fatty acids (FAs) is also believed to provide cancer cells with a constant supply of FAs for protein modification (Munir et al., 2019).

1.3.1 The Warburg effect

In normal differentiated cells, glucose metabolism begins with the oxidation of one molecule of glucose to two molecules of pyruvate, two molecules of NADH and two molecules of ATP; followed by the citric acid cycle in which three molecules of NADH, one molecule of $FADH_2$ and one molecule of GTP are produced in preparation for oxidative phosphorylation in the presence of oxygen (Chaudhry & Varacallo, 2020). Non-transformed cells ferment glucose to lactate in hypoxic conditions, which is known as anaerobic glycolysis. In the 1920s, Otto Warburg and colleagues had observed that tumour cells converted glucose into lactate for obtaining energy as evidenced by a high rate of glucose uptake and an enormous production and export of lactate even in the presence of the abundant oxygen (Warburg et al., 1927). Fermentation of glucose in the presence of oxygen is also known as aerobic glycolysis. This phenomenon was later termed the Warburg effect and accepted as an anomalous characteristic of cancer cells (Vander Heiden et al., 2009) (see Figure 1.3.1). For example, although leukaemic cells are present in blood and thus live under aerobic conditions, they display a glycolytic phenotype (Cunningham & Kohno, 2016). Nolop and colleagues showed that the rate of uptake of 18-fluoro-2-deoxy-D-glucose (^{18}FDG) by pulmonary tumour cells of 12 patients was significantly higher than normal tissue and revealed that pulmonary tumours had elevated rates of glucose uptake despite being in airways (Nolop et al., 1987).

Several hypotheses have been made so far to understand why cancer cells metabolise glucose via aerobic glycolysis. The fact is that complete catabolism of glucose using mitochondrial oxidative phosphorylation is a more efficient way to meet the energy requirements of cells and maximize ATP production. Specifically, insight from the study of aerobic glycolysis has helped to shed light on why cancer cells shut down the complete

oxidation of glucose in the TCA cycle. Rather than maximising ATP yield, cancer cells are in a much greater need for production of cellular building blocks for cell division (Vander Heiden et al., 2009). One molecule of glucose can be diverted into the pentose phosphate pathway to generate cytosolic NADPH and ribose 5-phosphate required for the biosynthesis of essential cellular molecules such as RNA and DNA. For instance, synthesis of lipids, amino acids and nucleotides require more equivalents of carbon and NADPH than of ATP (Boroughs & DeBerardinis, 2015). From this perspective, it becomes clear that aerobic glycolysis provides macromolecular precursors instead of focusing on ATP production in rapidly proliferating malignant cells.

1.3.2 The role of lactate in cancer cells

The increased glucose uptake and metabolism by neoplastic cells results in the accumulation of intracellular lactate (Romero-Garcia et al., 2016). The accumulation of lactic acids in cancer cells promotes lactic acid transport by the proton-linked monocarboxylate transporters (MCTs) across the plasma membrane, which in turn makes extracellular pH drop to 6.0–6.5 (Erra Díaz et al., 2018). The acidic microenvironment contributes to immunologic escape mechanisms in different ways (Romero-Garcia et al., 2016). The high concentration of lactate in the tumour environment was found to have a deleterious effect on the differentiation of monocytes to dendritic cells (DC) and proliferation of cytotoxic T lymphocytes (CTLs) which are important in the anti-tumoural response (Fischer et al., 2007). Since the export of lactate depends on the concentration gradient between intracellular and extracellular lactate, high extracellular lactate concentrations generated by tumour cells blocks lactate secretion from cytotoxic T cells. As a consequence of this, the accumulation of lactate in the tumour microenvironment

impairs metabolism and function of the activated T cells, thereby making T cells unable to adequately eliminate cancer cells (Fischer et al., 2007).

Beyond contribution to immune escape, lactate plays a central role in angiogenesis and metastasis. There is a renaissance of interest in the contribution of tumour acidity to local invasion and metastasis in cancer research, as the high rate of aerobic glycolysis impacts the development of the metastatic phenotype (San-Millán & Brooks, 2017). It has been shown that inhibition of lactate production reduces the development of metastasis in an established murine model of breast cancer (Rizwan et al., 2013). Furthermore, lactate assists angiogenesis through acid-induced expression of VEGF in endothelial cells (San-Millán & Brooks, 2017).

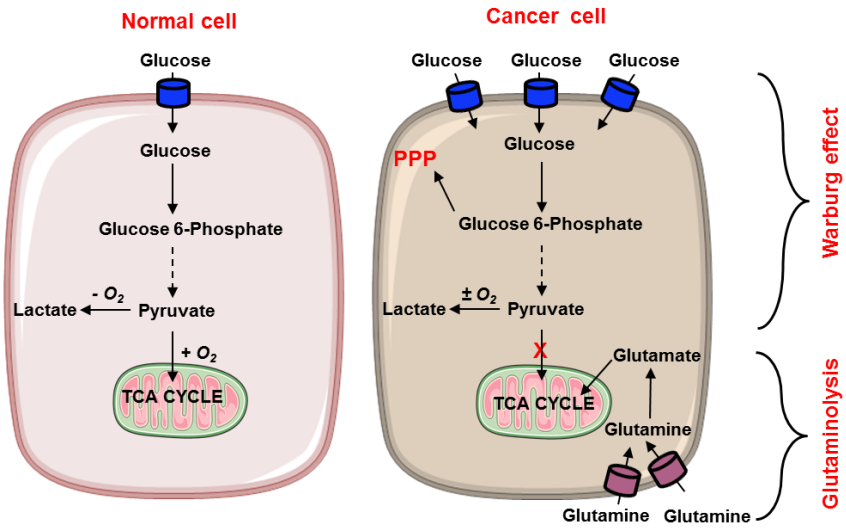

Figure 1.3.1 Glucose metabolism in a normal and a cancer cell.

In normal cells, glucose is processed through glycolysis and completely oxidised through the TCA cycle. Only if oxygen is not sufficient, pyruvate is converted to lactate. Unlike normal cells, cancer cells metabolise glucose into lactate regardless of presence oxygen (Warburg et al., 1927). The increased glucose uptake is used to fuel the pentose phosphate pathway in cancer cells (Jin & Zhou, 2019). Glutamate produced during glutaminolysis maintains the TCA cycle.

1.3.3 Genetic alterations and the Warburg effect

The weight of the evidence to date supports that the Warburg effect is facilitated by orchestrated oncogene activation and tumour suppressor mutations (Koppenol et al., 2011; Ward & Thompson, 2012). Therefore, numerous studies have investigated the regulation of the Warburg effect in cancer cells.

Hypoxia-inducible factor 1 alpha (HIF-1α), p53 and proto-oncogene c-Myc drive the Warburg effect by regulating the gene expression of many glycolytic enzymes (Marbaniang & Kma, 2018). Given the importance of glucose transporter 1 (GLUT1) as a key rate-limiting factor in the glucose transport in cells, point mutations in the DNA-binding domain of p53 were found to abolish the inhibitory effect of p53 on transcriptional activity of the GLUT1 gene, resulting in increased GLUT1 protein levels and consequently increased glucose uptake (Schwartzenberg-Bar-Yoseph et al., 2004). Elevated HIF-1α and c-Myc also continuously induce expression of hexokinase 2 (HK2), pyruvate kinase isoenzyme 2 (PKM2) and lactate dehydrogenase A (LDHA) (Burns & Manda, 2017). Studies identified that aberrant induction of HK2 expression is in part responsible for the high rate of glycolysis and accelerated glucose flux into the PPP in breast and lung cancer cells (Patra et al., 2013; T. Yang et al., 2018).

Aberrant tyrosine kinase signalling plays a significant role in regulating the activity of glycolytic enzymes in numerous different cancers, including both blood cancers and solid tumours. As a notable example, phosphorylation of PKM2 by oncogenic kinases (e.g., FGFR1, BCR-ABL, and Jak2) restricts the terminal reaction in glycolysis (Hitosugi et al., 2009).

1.3.4 Drug resistance associated with the Warburg effect

The Warburg effect enhances cancer cell growth and aggressiveness. In addition to promoting tumourigenesis, a series of recent studies has revealed that the Warburg effect is one of the essential components for the resistance of cancer cells to chemo-and radiotherapy (Cao et al., 2017; Tan et al., 2019). The enzymes directly catalysing the reactions in glycolysis have been implicated in the development of a drug-resistant phenotype in cancer cells (Bhattacharya et al., 2016).

Glycolytic enzymes have been shown to promote cell survival and drug resistance through intervention in apoptosis (X. Yu & Li, 2017). HK2 can confer cell survival by direct insertion in the mitochondrial outer membrane to inhibit binding of apoptotic Bcl-2 family proteins to mitochondria. Thus, HK2 induces drug resistance by the inhibition of intrinsic apoptotic pathways (Majewski et al., 2004). Overexpression of PKM2, the final rate-limiting enzyme of glycolysis, was shown to prevent apoptosis by regulating Bcl-xL at the transcriptional level in gastric cancer cells (Kwon et al., 2012). Clinically, increased PKM2 levels have been highly associated with resistance to 5-fluorouracil (5-FU) in patients with colorectal cancer compared with complete responders to 5-FU-based chemotherapy (Bhattacharya et al., 2016). In support of this data, gene silencing of PKM2 increases the effects of docetaxel and cisplatin in lung carcinoma cells (Bhattacharya et al., 2016). In addition to PKM2, Inhibition of GLUT1 by a specific inhibitor significantly overcomes 5-FU resistance of colon cancer cells indicating the importance of glucose uptake in colon cancer cells (W. Liu et al., 2014).

1.3.5 Glutaminolysis

Tumour cells undergo a metabolic reprogramming that is required for tumour development. Although cancer cells preferentially convert glucose into lactate instead of entering pyruvate into the TCA cycle, even under oxygen-rich conditions, they remain dependent on mitochondrial metabolism. As a result of limited pyruvate availability due to the Warburg effect, glutamine is used to replenish TCA cycle intermediates in order to maintain mitochondrial function (Reitzer et al., 1979).

Through glutaminolysis, glutamine is first deaminated to glutamate and further to α-ketoglutarate by glutaminase (GLS) and glutamate dehydrogenase (GLUD) respectively Glutaminolysis enables ATP production through oxidative phosphorylation and provides nitrogen and carbon skeletons for generation of antioxidants, nonessential amino acids, purines, pyrimidines and fatty acids (Conrad & Sato, 2012; Son et al., 2013). Thus, glutamine metabolism contributes to the increased levels of tumour growth and metastasis by the biosynthesis of proteins, lipids, and nucleotides, and overcomes oxidative stress through glutathione synthesis (L. V. Yang, 2017). Yang and co-workers reported that glucose deprivation resulted in a gradual rise in ammonia production in glioblastoma cells through increasing GLS activity. Indeed, inhibition of GLUD activity in glioblastoma cells has been shown to enhance the effect of drugs that suppress glycolysis (Xiang et al., 2015). As has been previously reported, GLUD over-expression is associated with metastatic lymph nodes and liver metastases lesions in colorectal cancer (G et al., 2015). Furthermore, specific inhibition of GLS by BPTES prolongs survival of an immune-competent Myc-mediated mouse model of liver cancer (Xiang et al., 2015).

1.3.6 Interplay between genetics and glutaminolysis in oncogenesis

Cancer cells alter their glutamine metabolism to benefit their metabolic needs, growth, proliferation, and survival. Several findings have provided evidence that mutations in oncogenes and or tumour suppressor genes reprogram glutamine metabolism in cells (L. Yang et al., 2017). The proto-oncogene c-Myc is well known to regulate cell metabolism (Shim et al., 1997). With regard to glutamine metabolism, the oncogene c-Myc has been shown to enhance glutamine uptake by directly activating the expression of glutamine transporters SLC1A4 and SLC1A5 genes, promoting the influx of glutamine (Wise et al., 2008). Indeed, c-Myc was found to induce expression of glutamine synthetase (GS) through upregulation of thymine DNA glycosylase (TDG), which promotes active demethylation of the GS promoter in a number of human and murine cells (Bott et al., 2015). A further role for c-Myc in glutaminolysis stems from the observations that the expression of GLS gene is increased via transcriptional repression of the GLS repressor micro RNAs (miR)-23a/b by c-Myc (Bott et al., 2015).

Mutations in RAS proteins are one of the most prevalent oncogenic alterations observed in human and experimentally induced animal tumours. Several reports suggest that oncogenic Ras proteins, such as KRAS, exhibit increased utilisation of glutamine for anabolic synthesis (Bryant et al., 2014; Gaglio et al., 2011). Oncogenic KRAS was found to increase the gene expression of enzymes associated with glutaminolysis in KRAS-mutant cells (Bryant et al., 2014). Specifically, KRAS-transformed cells elevate expression of AST to release aspartate into the cytoplasm for NADPH production (M. S. Miller & Miller, 2011).

The PI3K/AKT/mTOR pathway is crucial for many aspects of cell growth and survival and deregulated in several cancers (Paplomata & O'Regan, 2014; Porta et al., 2014).

Activation of mTORC1 has been shown to positively regulate the anaplerotic entry of glutamine into the TCA cycle and glutamine flux by activating GLUD and GLS. (Csibi et al., 2014). Furthermore, the P13K/AKT axis stimulates glutathione (GSH) synthesis through the transcriptional up-regulation of the GSH biosynthetic genes in breast cancer cells(Lien et al., 2016).

In addition to oncogenes, tumour suppressors also profoundly regulate glutamine metabolism. For example, the tumour suppressor retinoblastoma protein (RB) suppresses the expression of the glutamine transporter ASCT2 and the activity of GLS1 by E2F transcription factor 3 (E2F3). Loss of Rb-1 function markedly elevates glutamine uptake and conversion to glutamate in mouse embryonic fibroblast (MEF) cells (Reynolds et al., 2014).

1.3.7 Aberrant lipid metabolism in tumour cells

The enhanced proliferation of tumour cells requires specific alterations in their metabolic activity. This metabolic reprogramming supports their high growth rates and high energy demand. In addition to the changes in glucose and glutamine metabolism, another a fundamental feature of metabolic reprogramming in transformed cells is the elevated *de novo* synthesis of fatty acids (FAs). Lipids serve as a source of energy and provide cells with a constant supply of FAs required by the proliferating tumour cells for membrane biogenesis and other associated functions during growth (Mounier et al., 2014).

In normal adults, the *de novo* synthesis of FAs and cholesterol largely occurs in the liver and adipose tissues, while the circulating dietary lipids provide for the demand of other mammalian tissues (Beloribi-Djefaflia et al., 2016). However, up-regulation of lipogenic enzymes such as FASN and ACCase has been widely observed in cancer tissues (Ray

& Roy, 2018). The expression of lipogenic enzymes has been found in androgen-responsive prostate cancer cells (Swinnen et al., 2004). An elevated FASN expression has been reported to induce progression of cancer cells into S phase (Cheng et al., 2014). Furthermore, inhibition of FASN by cerulenin, a natural product of *cephalosporium caerulens,* causes suppression of DNA replication and induction of apoptosis in colon carcinoma cells (Flavin et al., 2010). In addition to FASN, increased ACCase, a rate-limiting enzyme of the pathway in fatty acid biosynthesis, was associated with a higher risk of infiltration in breast cancer (Lz et al., 1997). Furthermore, the ACCase gene in breast cancer cell was found to be deregulated by high-level amplifications in ACCase gene copy number (Chin et al., 2006).

1.3.8 *De novo* purine and pyrimidine biosynthesis and anticancer therapy

Purines (adenine and guanine) and pyrimidines (cytosine, thymine, and uracil) are basic components of nucleotides for DNA and RNA. Besides acting as building blocks for nucleic acids, ribonucleotides are fundamental for energy supply (ATP and GTP), components of co-enzymes (NAD and FAD) and signal transduction (cAMP and cGMP). Therefore, purines and pyrimidines provide essential components for cell survival and proliferation (Yin et al., 2018).

Cancer cells enhance the *de novo* synthesis of purines (see Figure 1.3.2) and pyrimidines to maintain sufficient pools to support DNA replication, and other anabolic pathways necessary for cell proliferation; hence impaired purine and pyrimidine metabolism is associated with the progression of cancer (Lane & Fan, 2015; Qiao et al., 2020; Sigoillot et al., 2004). Phosphoribosylpyrophosphate synthetase 1 (PRPS1), which catalyses the first step of the synthesis of nucleotide to synthesise ribose-5-phosphate, has been shown

to be overexpressed in colorectal cancer (CRC), with knockdown of PRPS1 significantly reducing glucose consumption and adenosine triphosphate in level CRC cells (Qiu et al., 2015) . A recent study concluded that PRPS1 has a notable effect on cell proliferation and apoptosis in glioblastoma multiforme (GBM) (Li et al., 2016). Moreover, multiple types of cancer cells were shown to highly express inosine 5-monophosphate dehydrogenase 2 (IMPDH2) (Collart et al., 1992), which catalyses the oxidation of inosine monophosphate (IMP) to xanthosine monophosphate (XMP) in *de novo* biosynthesis of guanine nucleotides. IMPDH2 considerably promotes proliferation, invasion, and metastasis and is associated with cancer progression and poor prognosis of cancer patients (Duan et al., 2018; Ying He et al., 2018). IMPDH2 was found to enhance G1/S phase cell cycle transition through activation of the PI3K/AKT/mTOR pathway (Duan et al., 2018). Furthermore, inhibition of IMPDH2 activity sensitised resistant HT29 human colon cancer cells to methotrexate (Peñuelas et al., 2005, p. 29).

Many studies to date have reported that pyrimidine biosynthetic enzymes are elevated in cancer cells in response to the increased demand for pyrimidine nucleotides (Siddiqui & Ceppi, 2020; Villa et al., 2019) Particularly, the activity of carbamoyl phosphate synthetase (CAD), which catalyses the first and rate-limiting step of pyrimidine synthesis, is elevated in cancer cells (Weber, 2001).

New insights into increased metabolic demand of cancer cells for nucleotide biosynthesis have provided novel therapeutic strategies. Since the discovery of aminopterin in 1947, antimetabolites that resemble nucleotide metabolites, have been used to treat many cancers. Antimetabolites inhibit the activity of enzymes involved in *de novo* purine and pyrimidine synthesis. Notable examples include methotrexate and pemetrexed, which inhibit one-carbon transfer reactions required for *de novo* nucleotide synthesis (Norris &

Adamson, 2010). Particularly, methotrexate is very effective for the treatment of several cancers, either alone or in combination with other chemotherapy agents. Furthermore, the purine analogue 6-mercaptopurine (6-MP), which inhibits PRPP amidotransferase in purine synthesis, has been successful to treat childhood leukaemia (Alsous et al., 2017).

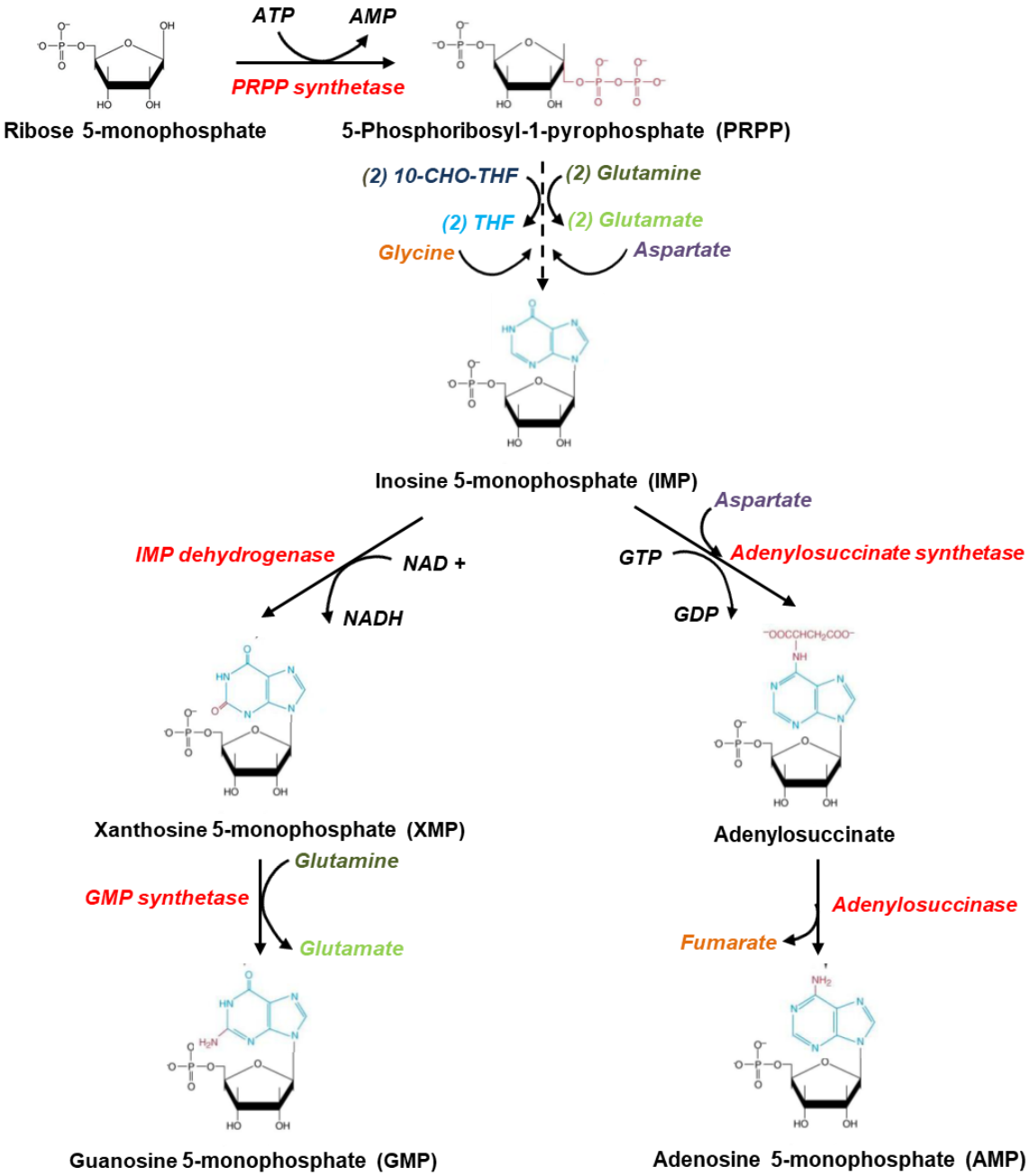

Figure 1.3.2 Purine biosynthesis.

5-Phosphoribosyl-1-pyrophosphate (PRPP) is generated from ribose 5-monophosphate by the action of PRPP synthetase. Inosine 5-monophosphate (IMP) is synthesised from PRPP through a series of reactions utilizing 10-formyltetrahydrofolate, glutamine, glycine and aspartate. IMP can be converted into either guanosine 5-monophosphate (GMP) or adenosine 5-monophosphate (AMP).

1.3.9 Tumour microenvironment and metabolism

The uncontrolled growth of tumour can lead to deficiencies in amino acids, glucose, and oxygen in their microenvironment as they exceed their blood supply. While oxygen deprivation causes an accumulation of unfolded proteins in the endoplasmic reticulum by the perturbation of the oxidative environment, amino acid deprivation leads to a build-up of uncharged tRNAs within cells. These microenvironmental stresses activate the integrated stress response (ISR) in cells (McConkey, 2017). ISR includes phosphorylation of the alpha subunit of eukaryotic translation initiation factor 2 (eIF2a) due to amino acid depletion, oxidative stress and endoplasmic reticulum (ER) stress. eIF2α phosphorylation leads to a net reduction in global protein synthesis while stimulating the translation of selected genes including activating transcription factor 4 (ATF4). ATF4 initiates an expansive pro-survival response, including further inhibition of global protein synthesis, the upregulation of autophagy and glutamine transporter SLC1A5 with concomitant build-up of essential amino acids (Rasmussen & Adams, 2020). In cancer cells, ATF4 was found to promote metabolic homeostasis and cell survival in response to a diverse array of microenvironmental stresses (Singleton & Harris, 2012).

The crosstalk between transformed and non-transformed cells, such as cancer-associated fibroblasts (CAFs), immune cells and nerve fivers, creates the tumour microenvironment (TME). Intercellular communication is driven by growth factors,

chemokines, inflammatory and matrix remodelling enzymes, thereby providing additional oncogenic signals that enhance cancer progression.

Cancer cells are engaged in a complex dialog with surrounding non-malignant cells in order to satisfy their need for energy and biomass. CAFs are one of the most important components of the tumour microenvironment. In pancreatic cancer cells, CAFs elicit deep metabolic alterations by enriching fatty acid biosynthesis, glycolysis and also gluconeogenesis that strengthen pancreatic tumour progression (Sherman et al., 2017). Moreover, CAFs are instructed to decrease their mitochondrial function with the ensuing increase on glycolysis by breast tumour cells within the microenvironment. This metabolic shift leads to release of lactate from CAFs to their microenvironment. Cancer cells take up lactate produced from CAFs to use as a fuel source for the TCA cycle to increase their tumourigenic potential (A. Miller et al., 2017). This type of catabolite transfer and subsequent increase in mitochondrial function of tumour cells have been recently described as the Reverse Warburg effect (Pavlides et al., 2009). Furthermore, some cancer cells that suffer from OXPHOS insufficiency were shown to take up whole mitochondria from stromal cells in order to further support cell growth and metastasis (Moschoi et al., 2016). This has been shown in co-culture studies, where both primary and cultured acute myeloid leukaemia (AML) raised their mitochondrial mass up to 14% by taking up of mitochondria from bone marrow stromal cells (Moschoi et al., 2016).

Within the tumour microenvironment, there is substantial evidence of the contribution of (extracellular matrix) ECM to metabolic reprogramming of tumour cells (Pickup et al., 2014). At its most basic level, the ECM is essential for the uptake of extracellular nutrients as well as serving as the scaffold. The uniqueness of ECM for tumour metabolism lies in the interaction between integrins and growth factor receptors accessing the cytoplasmic

signalling network (Ata & Antonescu, 2017). Importantly, β1-Integrin interacts with the monocarboxylate transporter 4 (MCT4) and CD98 that mediates transport of leucine, isoleucine and arginine in exchange for glutamine (Gallagher et al., 2009). Thus, integrins can be involved in glucose uptake and amino acid transport. Intriguingly, detachment of cancer cells from ECM leads to a reduction in glucose uptake and an increase in the generation of reactive oxygen species (ROS) (Schafer et al., 2009). Moreover, focal adhesion kinase (FAK), a regulator of integrin signalling, cooperates with oncogenic drivers such as c-Myc, thereby supporting glutaminolysis in cancer cells to maintain high cell proliferation (Pickup et al., 2014). Additionally, focal adhesion signalling enhances the activation of the PI3K pathway which increases glycolysis by upregulating the expression of GLUT1 and GLUT4 (Pickup et al., 2014).

1.4 Haematopoiesis

Haematopoiesis refers to the process of generation and development of a variety of distinct blood cell types from haematopoietic stem cells (HSCs) (see Figure 1.4.1). HSCs are characterised by the ability to self-renew and to produce circulating blood cells. Under steady-state, only a fraction of HSCs enters cell cycle to generate differentiated progenies. As HSCs divide, they give rise to common lymphoid and common myeloid precursor cells (CLP and CMP respectively). CMPs are an early ancestor of the mature white blood cells, red blood cells, and platelets, all of which are normally present in circulating blood. Common myeloid progenitors are capable of differentiating into proerythroblasts, megakaryoblasts, and myoblasts giving rise to erythrocytes, thrombocytes, and all granulocytes respectively. Common lymphoid progenitors are responsible for forming the lymphoid lineages. CLP further differentiate into lymphoblast and dendritic cells. Depending on the stimuli, lymphoblasts differentiate into natural killer cells or B and T lymphocytes.

The differentiation and proliferation of CLPs and CMPs are regulated via cell-cell interactions and by way of the generation of growth factors and cytokines, such as granulocyte-monocyte colony-stimulating factor (GM-CSF) and erythropoietin. These growth factors and cytokines influence the differentiation and proliferation of progenitor cells by regulating the expression of transcription factors. These secreted molecules can act over long or relatively short distances. For instance, production of erythropoietin by the kidney primarily regulate the development of the erythroid lineage while IL-7 produced from stromal cells in the bone marrow drives the differentiation of hematopoietic stem cells into CLPs (Chapman & Zhang, 2020).

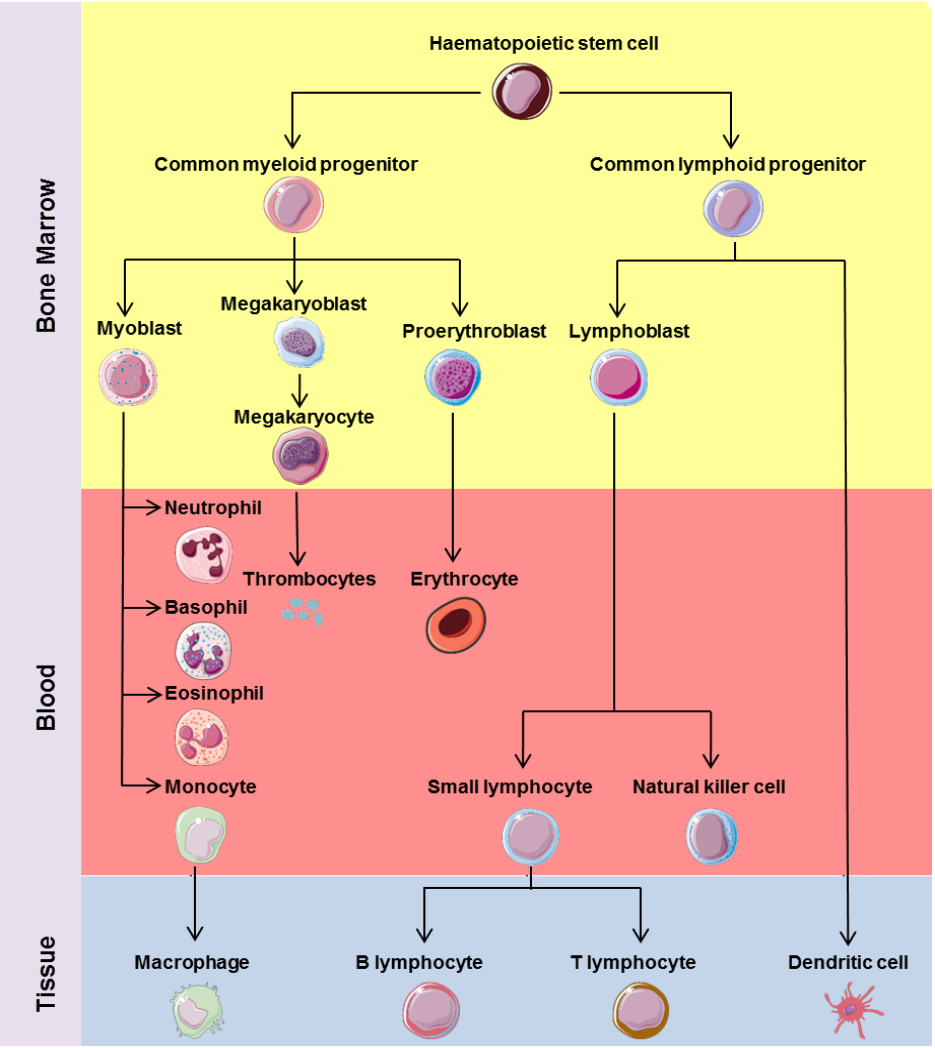

Figure 1.4.1 Haematopoiesis.

The figure shows the maturational sequence of different blood cells. In adults, haematopoiesis starts in the bone marrow from haematopoietic stem cells (HSCs). The HSCs differentiate into both myeloid or lymphoid cell lines in blood and other tissues such as thymus and spleen.

1.5 Haematological malignancies

Haematological malignancies are a diverse group of cancers that originate from cells of the bone marrow and the lymphatic system. In most blood cancer cells, the normal cellular processes are interrupted by a variety of molecular and cytogenetic abnormalities. As a consequence, malignant blood cells fail to develop into functional myeloid or lymphoid

cells (Snowden et al., 2017).

The first haematological malignancy was described in 1832 by Thomas Hodgkin (Hodgkin, 1832). The particular lymphoma that Hodgkin described bears his name in his honour. Since that time, other hematologic malignancies have been further described with the assistance of several technologies, including morphology, immunophenotyping, cytogenetics and molecular genetics (see Table I). To define distinct types of haematological cancers, the World Health Organization (WHO) published the fourth editions of the *WHO Classification of Tumours of Haematopoietic and Lymphoid Tissues 2008* with the efforts of pathologists, haematologists, oncologists, and geneticists from around the world (Campo et al., 2011; Vardiman et al., 2009). Then, the major subtypes of myeloid neoplasms, acute leukaemia, lymphoid, histiocytic, and dendritic neoplasms according to the WHO classification was updated incorporating morphology, immunophenotype, genetic features, and clinical features to define disease entities of clinical significance in 2016 (Arber et al., 2016).

In this thesis, I have mainly focused on acute myeloid leukaemia (AML), chronic myeloid leukaemia (CML), multiple myeloma (MM), Burkitt's lymphoma (BL) and diffuse large B cell lymphoma (DLBCL).

Table I. *Main types of haematological malignancies according to the 2016 WHO classification.*

Haematological malignancies
Myeloproliferative neoplasms (MPN)
Myeloid/lymphoid neoplasms with eosinophilia and rearrangement of PDGFRA or FGFR1
Myelodysplastic/myeloproliferative neoplasms (MDS/MPN)
Myelodysplastic syndromes (MDS)
Acute myeloid leukaemia (AML) and related neoplasms
Blastic plasmacytoid dendritic cell neoplasm
Acute leukaemia's of ambiguous lineage
B-lymphoblastic leukaemia/lymphoma
Blastic plasmacytoid dendritic cell neoplasm
T-lymphoblastic leukaemia/lymphoma
Mature B cell neoplasms
Mature T and NK neoplasms
Hodgkin lymphoma
Posttransplant lymphoproliferative disorders (PTLD)
Histiocytic and dendritic cell neoplasms

1.5.1 Acute myeloid leukaemia

Acute myeloid leukaemia (AML) is a rapidly progressing haematological cancer, characterised by the accumulation of clonal myeloid progenitor cells that do not differentiate normally. The differentiation arrest of clonal myeloid cells causes multilineage cytopenias in AML patient. The signs and symptoms of AML are mainly the results of the decrease in the number of normal myeloid cells, including red blood cells, platelets, and granulocytes, that eventually contributes to morbidity in this disease. General signs and symptoms of the early stages of AML may mimic other common illnesses, like the flu. However, the symptoms of AML usually become worse, as the disease progresses with

more leukaemia cells filling the bone marrow.

Genetic abnormalities play a big role in the progression of AML. These genetic abnormalities include point mutations, amplifications, specific chromosomal aberrations and translocations, which ultimately impair the normal developmental process of myeloid cells. Among them, cytogenetic abnormalities are the most powerful independent prognostic factors in AML, which serve to determine biologically discrete subsets of disease (Kihara et al., 2014). However, nearly half of AML patients lack typical prognostic karyotypic changes and structural abnormalities in their genomes (Lin & Falini, 2015). Next-generation sequencing (NGS) revealed a total of 5234 driver mutations across 76 genes in 1540 patients with AML (Papaemmanuil et al., 2016). Nevertheless, a comprehensive analysis of genetic alterations in 197 adult patients with AML reported that only FLT3, NPM1, CEBPA, DNMT3A and KIT genes were mutated in more than 10% of the patients, while a total of 505 mutations in 44 genes was identified (Kihara et al., 2014). The most common cytogenetic abnormality in AML patients is t(8;21)(q22;q22). The t(8;21)(q22;q22) involves the AML1 (RUNX1) gene on chromosome 21 and the ETO (RUNX1T1) gene on chromosome 8, producing a novel chimeric gene, AML1–ETO. The AML1 gene encodes the alpha subunit of the core-binding factor (CBF), which controls normal haematopoiesis. AML1–ETO fusion gene disrupts the CBF transcription complex, thereby initiating the leukaemogenesis (Lin et al., 2008).

Acute promyelocytic leukaemia (APL) is one of the major groups of AML with cytogenetic abnormality t(15;17) in which the promyelocytic leukaemia gene (PML) on chromosome 15 fuses with retinoic acid receptor-alpha (RARα) gene on chromosome 17, resulting in the expression of a PML-RARα chimeric protein. PML-RARα causes an arrest of differentiation at the promyelocytic stage (Adams & Nassiri, 2015). So far, typical APL with

PML-RARα has shown a good response to all-trans retinoic acid (ATRA) (X. Wang et al., 2019). ATRA stimulates the terminal differentiation of immature leukaemic clone into granulocytes. Although the majority of APL are characterised by the expression of a PML-RARα protein, a few variant chromosomal mutations have been also described, including PLZF-RARα, F1P1L1-RARα, STAT5b-RARα, et al. Unlike APL with PML-RARα protein, both PLZF-RARα and STAT5b-RARa do not respond to ATRA (X. Wang et al., 2019).

1.5.2 Metabolism in AML

Metabolic deregulation has been identified as a hallmark of cancer (Warburg et al., 1927). The identification of mutations in human cytosolic isocitrate dehydrogenase 1 (IDH1) and mitochondrial isocitrate dehydrogenase 2 (IDH2) occurring somatically in AML cells has led to renewed interest in metabolic reprogramming in myeloid leukaemia cells and their therapeutic applications (see Figure 1.4.2) (L. Dang et al., 2009).

The IDH1 and IDH2 proteins catalyse the oxidative decarboxylation of isocitrate to α-KG outside of the TCA cycle by generating NADPH from $NADP^+$. All mutations identified to date appear to effect arginine residue 132 (R132) in IDH1 or the analogous residue in IDH2 (R172). Since these residues are located in the active site of the enzymes, the missense mutations at R132 in IDH1 and R172 in IDH2 abolish their normal catalytic activity because of impaired isocitrate binding (Ward et al., 2010). However, *in vitro* studies have shown that the mutated IDH1/2 gain the ability to convert α-KG to R(-)-2-hydroxyglutarate (2-HG) which is regarded as an oncometabolite owing to its impact on alterations in the aberrant DNA methylation and also on cellular metabolism (Reiter-Brennan et al., 2018). Altered IDH1/2 results in a decrease in cellular α-KG because of the suppressed capacity to convert isocitrate to α-KG and abnormal production of 2-HG.

AML cells with IDH mutations were found to be addicted to glutamine so that the reduction in the α-KG production could be compensated, as glutamine is another cellular source of α-KG. Thus, targeting glutaminolysis in AML cells with IDH1/2 mutations has been a promising metabolic targeted therapy (Emadi et al., 2014). Somatic mutations of IDH1 or IDH2 genes have been reported in approximately 6-16% and 8-19% of AML, respectively. Indeed, these oncogenic mutations are more frequent in cytogenetically normal AML (25-30% of cases) (Ok et al., 2019).

Metabonomic analysis of serum samples of 183 AML patients and 232 age- and gender-matched healthy controls has shown that AML patients have significant differences in glycolysis, gluconeogenesis, TCA cycle and metabolism of fatty acids (Y. Wang et al., 2013). Particularly, glycolysis is frequently upregulated in most cases of AML. High glycolytic activity is implicated in AML leukaemogenesis driven by over-activated mTORC1 and FLT3-ITD mediated signalling (Chapuis et al., 2019). Accordingly, constitutive mTORC1 activation renders AML cells addicted to glucose. Furthermore, AML cells increase glucose uptake mainly for its subsequent diversion into the PPP, notably through the production of glucose-6-phosphate from glucose (see Figure 1.4.2). Targeting the PPP was also identified as a potential therapeutic strategy for AML cells (Y. Wang et al., 2013).

The fatty-acid oxidation (FAO) pathway enables cells to produce ATP through OXPHOS. In AML, carnitine palmitoyl transferase 1A (CPT1A) protein which catalyses an essential step in FAO pathway, is highly expressed (see Figure 1.4.2). Targeting CPT1A has been shown to promote apoptosis and to suppress cell proliferation without affecting normal $CD34^+$ haematopoietic cells (Shi et al., 2016).

1.5.3 Chronic myeloid leukaemia

Chronic myeloid leukaemia (CML) is a pluripotent hematopoietic stem cell disorder characterised by unrestricted proliferation of granulocytes in the blood that occurs due to the presence of the Philadelphia chromosome. Philadelphia (Ph) chromosome is present in nearly 90% of patients with CML (Y. Chen et al., 2010).

The Ph chromosome is a reciprocal translocation of the ABL1 gene on chromosome 9 to breakpoint cluster region BCR on chromosome 22 causing the formation of the BCR-ABL fusion gene that encodes BCR-ABL protein (see Figure 1.5.1). This translocation results in the generation of shorter derivative chromosome 22 and longer derivative chromosome 9. The BCR-ABL protein has an increased tyrosine kinase activity as a result of the deletion of the SH3 domain of ABL (Kang et al., 2016). The oncogenic BCR-ABL protein is involved in the activation of RAS and STAT proteins; thus enhances cell growth and proliferation (Salesse & Verfaillie, 2002).

CML's progression consists of three phases based on laboratory findings. These phases are chronic, accelerated and blast crisis (Apperley, 2015). Some patients with chronic phase CML have either mild symptoms which can be easily controlled or no symptoms at all. The chronic phase CML is characterised by the accumulation of myeloid progenitors and mature cells. In the absence of effective treatment, the disease progresses through a period of enhancing instability known as accelerated, to terminal transformation to an aggressive blast crisis. Blast crisis arises due to additional cytogenetic and molecular changes. e.g. deletion of p53 and duplication of chromosomes 8, 17 and 22 (Radich et al., 2006).

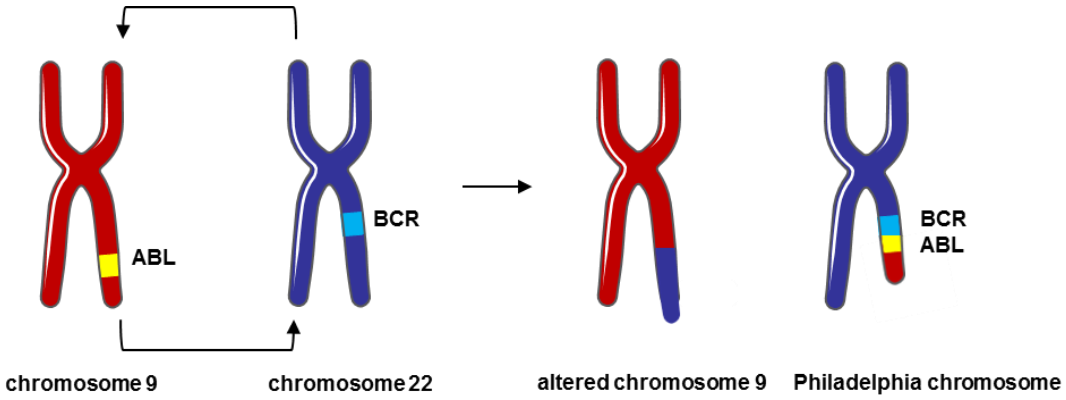

Figure 1.5.1 Philadelphia chromosome.

The figure illustrates the formation of Philadelphia (Ph) chromosome. Ph chromosome results from a reciprocal translocation between chromosome 9 and chromosome 22.

1.5.4 Metabolism in chronic myeloid leukaemia

Metabolism is frequently dysregulated in CML cells due to the expression of the constitutively active tyrosine kinase oncoprotein BCR-ABL. BCR-ABL protein can activate distinct intracellular signalling pathways that enhance cell proliferation further regulating cell metabolism (Sontakke et al., 2016).

Regarding glycolysis, BCR-ABL positive cells displayed increased glucose uptake by glucose transporter GLUT1, which is involved in the suppression of apoptosis in CML (Barnes et al., 2005). Upon entering cells, glucose and fructose were immediately phosphorylated in CML cells in comparison with controls (Karlíková et al., 2016). In contrast with the high phosphorylated hexose level, the leukocytes of CML patients showed a decrease in the majority of TCA cycle intermediates. The decrease in the majority of TCA cycle intermediates coincided with a significant increase in the activity of pyruvate dehydrogenase kinase 1 (PDHK1), which negatively regulates the conversion of pyruvate to acetyl-CoA (see Figure 1.4.2) (Karlíková et al., 2016).

Moreover, CML cells were shown to aberrantly generate branched-chain amino acids (BCAAs) by activating the expression of BCAT1, a cytosolic aminotransferase (Hattori et al., 2017).

1.5.5 Diffuse large B cell lymphoma

Diffuse large B-cell lymphoma (DLBCL) is an aggressive B-cell neoplasm, histologically characterised by dense proliferation of neoplastic B blasts. DLBCL is the most common form of non-Hodgkin lymphomas (NHLs), accounting worldwide for ~40% of adult NHL (Chapuy et al., 2016).

DLBCL is a clinically and pathologically heterogeneous disease. Over the past twenty years, there have been significant efforts to understand what transcriptional heterogeneity drives the differences in outcomes. To date, two separate classification schemes have addressed the transcriptional heterogeneity of DLBCL, consensus cluster classification (CCC) and cell-of-origin classification (COC) (Alizadeh et al., 2000; Monti et al., 2005). According to CCC, groups of DLBCLs are characterised by the OXPHOS cluster, the BCR/proliferation cluster and the host response cluster (see Table II). The OXPHOS cluster typifies some genes whose products take part in mitochondrial oxidative phosphorylation, electron transport chain and apoptosis. Some of these genes are nicotinamide adenine dinucleotide dehydrogenase (NADH) complex, cytochrome c oxidase (COX) complex and antiapoptotic BCL2 related family member, BFL-1/A1. The BCR/proliferation cluster displays abundant expression of genes involved in cell cycle and B-cell receptor (BCR) signalling such as cyclin-dependent kinase 2 (CDK2). Unlike the other clusters, the host response cluster is associated with increased expression of inflammatory mediators and markers for the classical complement pathway (Monti et al.,

2005).

COC classification is based on the type of B cells which cancer originates. According to COC classification, molecular subsets of DLBCL are characterised by the germinal centre B cell (GCB), activated B cell (ABC) and undefined type 3. GCB DLBCLs arise from centroblasts in the germinal centre. The main oncogenic pathways related to GCB DLBCLs involve BCL6, EZH2 and PTEN (Béguelin et al., 2013). BCL6 is a transcription repressor and required for germinal centre formation. Therefore, the BCL6 gene is downregulated after germinal centre forms (Schafer et al., 2009). It has a role in the suppression of genes in lymphocyte differentiation and cell cycle control. Overexpression of BCL6, which results from translocations or mutations, leads to GCB DLBCL due to differentiation blockade of centroblasts. The increased expression of EZH2 promotes lymphomagenesis through cooperating with BCL6 to block further differentiation of B cells (Béguelin et al., 2013). ABC-DLBCLs derive from plasmablasts before they differentiate into mature plasma cells. The constitutive activation of the nuclear factor-κB (NF-κB) signalling pathway is specific for ABC-DLBCLs. Apart from constitutive activation of the nuclear factor-κB (NF-κB), the constitutive expression of BCL6 is particularly present in ABC-DLBCL (Ye et al., 1993).

Table II. *Molecular classification of diffuse large B cell lymphoma*.

Consensus cluster classification (CCC)	Cell-of-origin classification (COC)
OXPHOS cluster	Germinal centre B cell (GCB) - like
BCR/proliferation cluster	Activated B-cell (ABC) - like
Host response cluster	Undefined type 3

1.5.6 Metabolism in diffuse large B cell lymphoma

DLBCL is a highly heterogeneous disease with recognised discrete clusters or subtypes defined based on distinct clinical, pathologic or biologic features. The molecular heterogeneity in DLBCL results in subsequent metabolic heterogeneity between different groups of DLBCL.

The spectrum of fuel utilisation pathways within DLBCL has been investigated in order to predict the precise metabolic landscape of distinct subtypes of DLBCL (Caro et al., 2012). Among transcriptionally-defined groups of DLBCL, the OXPHOS cluster exhibits up-regulation of genes encoding for subunits of NADH dehydrogenase (complex I), succinate dehydrogenase (complex II) and ATP synthase (complex V) involved in electron transport chain as well as enzymes involved in FAO (see Figure 1.4.2) (Caro et al., 2012). Particularly, a larger enrichment of fatty acid derived TCA intermediates was detected in OXPHOS cell lines in comparison with other subtypes of DLBCL. In contrast to the Warburg effect, the OXPHOS cluster relies on mitochondrial oxidative metabolism and secrets less lactate than BCR cluster cells. BCR cluster cells were found to have markedly higher intracellular and secreted lactate and contribute more glucose into the synthesis of pentose sugars (see Figure 1.4.2) (Caro et al., 2012). Samples from DLBCL patients with the OXPHOS phenotype revealed that stromal cells of neoplastic lymphatic tissue shifted their metabolism to glycolysis so that the end product of glycolysis, lactate, could be taken up by neighbouring neoplastic cells for the TCA cycle (see Figure 1.4.2). This finding can suggest that DLBCL cells reprogram metabolism of stromal cells, creating a metabolic ecosystem (Gooptu et al., 2017).

In addition to metabolism in distinct subtypes of the CCC scheme, metabolic rewiring in GCB-DLBCL has been studied. GCB-DLBCLs are exposed to different environmental

conditions with varying levels of oxygen and nutrients in the germinal centre (Mlynarczyk et al., 2019). Particularly, GC-derived lymphoma cells exposed to reduced oxygen availability stabilize HIF1-α that promotes aerobic glycolysis. GCB-DLBCL cells were also found to depend on the serine/threonine protein phosphatase 2A (PP2A) to divert glucose carbon usage from glycolysis to the PPP in comparison with the GC B cells (G. Xiao et al., 2018).

1.5.7 Burkitt's lymphoma

Burkitt's lymphoma (BL) is a highly aggressive germinal centre B cell-derived lymphoma first described by Denis Burkitt in malaria-endemic regions of Africa (Burkitt, 1958). Shortly after its first description in Africa, many pathologists recognised similar lymphomas in Europe and the United States.

Endemic, sporadic, and immunodeficiency-associated BL are three clinical variants of BL. The endemic form is particularly prevalent in children aged 4 to 7 years in equatorial Africa, frequently affecting facial lymph nodes and kidneys. Sporadic BL (sBL) is the most common variant and occurs most often in the western world where malaria is not endemic. It affects young adults and children and is seen as an abdominal tumour with abdominal swelling and an enlarged thyroid. sBL accounts for 35-40 percent of childhood lymphoma cases in the U.S and western Europe. The immunodeficiency-associated BL presents in association with human immunodeficiency virus (HIV) infections and affects mostly the central nervous system although it shows similarity to sporadic form (Dozzo et al., 2016). Gene expression profiling of BL revealed that BL cells are more akin to dark zone germinal centre B cell centroblasts.

In 1975, a balanced translocation between chromosome 8 and chromosome 14 was

discovered in BL patients (L et al., 1976). A few years later, the proto-oncogene c-Myc gene was showed to juxtapose the immunoglobulin heavy chain (IgH) locus at the breakpoint of the t(8;14) translocation (Dalla-Favera et al., 1982; Taub et al., 1982). Virtually all cases of BL are characterised by c-Myc translocation. The typical translocation of c-Myc into IgH locus is observed in about 75%-90% of BL. The translocation of c-Myc into immunoglobulin light chain loci on chromosome 2 (kappa) or 22 (lambda) occurs at a frequency of about 10%. Hence, c-Myc is brought under the control of immunoglobulin enhancer elements resulting in constitutive upregulation of c-Myc gene in BL cells (Schmitz et al., 2014). The c-Myc protein is a transcription factor that regulates cell growth, proliferation and survival by inducing expression of genes required for these processes. In contrast to the tightly regulated expression of c-Myc in normal B cells, BL cells overexpress c-Myc resulting in the uncontrolled proliferation of BL cells (Meyer-Bahlburg et al., 2009)

1.5.8 Metabolism in BL

BL is characterised by chromosomal rearrangements of the c-Myc pro-oncogene, resulting in overexpression of c-Myc oncoprotein (Klein, 2009). c-Myc has been shown to induce a set of genes involved in glycolysis, glutaminolysis, fatty acid synthesis and mitochondrial biogenesis (C. V. Dang, 2011). Particularly, c-Myc was reported to directly induce virtually all genes involved in glycolysis, many of them through c-Myc binding site E-box DNA sequences (CACGTG). Inhibition of the transactivating ability of c-Myc resulted in the downregulation of genes responsible for the Warburg effect in BL cells. (see Figure 1.4.2) (Mushtaq et al., 2015).

The eBL is consistently associated with EBV (Mawson & Majumdar, 2017). This oncovirus

was shown to contribute to metabolic alteration in cancer cells to meet the amplified bioenergetic and biosynthetic demands, by interfering with cell metabolism (Xiao et al., 2014). In particular, during EBV infection, cells elevate lipogenesis and aerobic glycolysis by enhancing the expression of FASN and HK2 (see Figure 1.4.2) (L. Xiao et al., 2014). Metabolomics has been used to discover novel biomarkers in BL for the diagnosis and prognosis (Nicholson & Lindon, 2008). Comparison of serum metabolomics of BL mice and normal mice demonstrated that the concentration of glucose, glutamate, and unsaturated lipids was remarkably distinctive between two groups (F. Yang et al., 2017). Furthermore, cases of BL-induced lactic acidosis and hypoglycemia in adults have been reported (see Figure 1.4.2) (Glasheen & Sorensen, 2005).

1.5.9 Multiple myeloma

Multiple myeloma (MM) is a malignant disease of monoclonal plasma cells in the bone marrow, leading to the production of non-functional immunoglobulins or immunoglobulin chains known as a monoclonal protein (M protein) associated, in more 50% of cases, with renal impairment (Rajkumar, 2018). MM has a worldwide incidence of 2 -3 cases per 100 000 persons per year and accounts for 10% of all hematologic malignancies (Cowan et al., 2018).

Nearly all cases of MM are developed from an asymptomatic precursor state, such as monoclonal gammopathy of undetermined significance (MGUS) (Gerecke et al., 2016). MGUS is referred to as a benign condition defined as the presence of an M-spike with a concentration <3g/dL, <10% plasma cells on bone marrow biopsy and absence of hypercalcemia, renal insufficiency, anaemia and bone lesions (CRAB) (Rajkumar, 2005). The diagnosis of MM requires a serum M protein ≥ 3 g/dL, bone marrow plasma cells ≥

60%, plasma free light chain ≥100 mg/L and one or more of the CRAB features. MM cells influence the balance between bone build up and bone breakdown resulting in osteolytic lesions (Gerecke et al., 2016).

Genetic studies on MM show a remarkable heterogeneity among patients although it is a monoclonal disorder (Brigle & Rogers, 2017; Weaver & Tariman, 2017). So far, studies reported that aneuploidy and translocation are the hallmark genetic lesions in MM cells (Hallek et al., 1998; Weaver & Tariman, 2017). Although nearly 40% of MM of patients carry at least a trisomy of a chromosome, some patients can carry translocations involving immunoglobulin heavy chain (IgH) locus along with trisomies (Hallek et al., 1998).

1.5.10 Metabolism in MM

Metabolic rearrangements are common features of cancers, including MM (El Arfani et al., 2018). Investigation of glucose metabolism in MM showed that HK2 and PKM2 are widely overexpressed and inhibition of these enzymes suppresses the production of ATP in MM cells (see Figure 1.4.2) (Yunhua He et al., 2015; Nakano et al., 2012). The increases in HK2 expression and lactate production is supported by osteoclasts (OCs) within the bone marrow microenvironment (Nakano et al., 2012). However, myeloma cells also incorporate lactate that originates from the surrounding elements, into the cytoplasm to use as fuel for OXPHOS (El Arfani et al., 2018).

Besides alterations in glucose metabolism, MM cells are remarkably dependent on extracellular glutamine (Dalva-Aydemir et al., 2015). Consistent with this dependence, MM cells were found to express high levels of glutaminase and glutamine transporters (SNAT1, ASCT2, and LAT1) compared to leukaemia cells (Bolzoni et al., 2016). These findings lead to the assumption that MM cells rely on extracellular glutamine uptake to

fuel the intracellular pool of the TCA cycle. Moreover, metabolic profiles of MM patients at diagnosis based on ^{1}H-NMR spectroscopy analysis of serum samples displayed decreased level of glutamine compared with the healthy controls (Puchades-Carrasco et al., 2013). However, MM patients after achieving complete remission exhibited a closer metabolic profile to those of healthy individuals (Puchades-Carrasco et al., 2013).

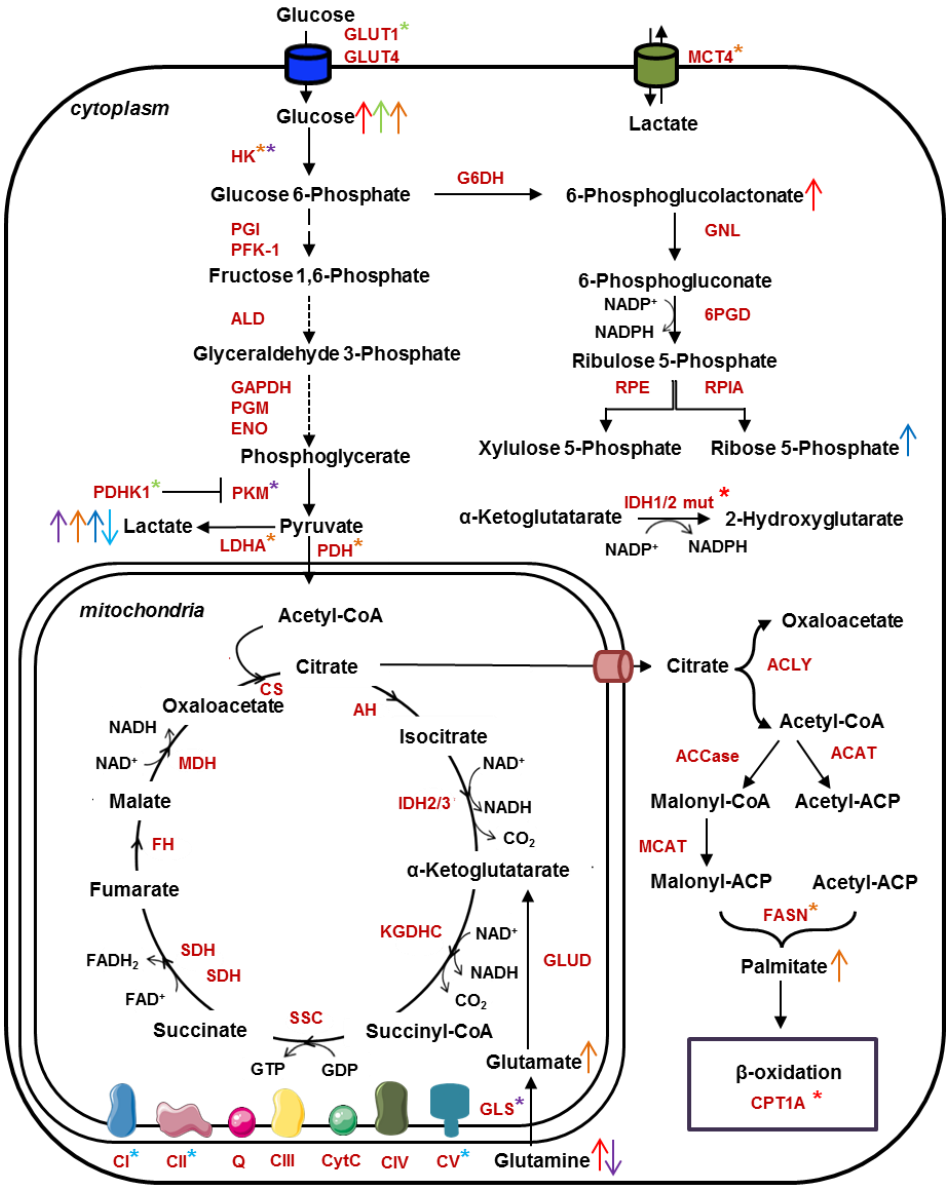

Figure 1.5.1 Metabolic changes in leukaemia, lymphoma and myeloma.

The figure shows the levels of metabolites and enzymes involved in glycolysis, PPP, TCA cycle, fatty acid synthesis, and β-oxidation in AML, CML, DLBCL, BL and MM (Star sign represents the increase in the expression level of the enzyme; arrow shows the change in the level of metabolites. AML: red star and red arrow; CML: green star and green arrow; OXPHOS cluster DLBCL: light blue star and light blue arrow; BCR cluster DLBCL: dark blue star and dark blue arrow; BL: orange star and orange arrow; MM: purple star and purple arrow.

1.6 Techniques and approaches to study metabolism

Elucidating how metabolic pathways differ from normal cells may be one of the best ways to find biomarkers for cancer detection, diagnosis, and prognosis and also to develop new treatments (Fuss & Cheng, 2016). Identification of altered metabolic pathways can provide novel insights into the phenotypic changes relative to biological function.

In general, the primary analytical techniques used for exploring tumour metabolism are mass spectrometry (MS) coupled with separation techniques and nuclear magnetic resonance (NMR) (Saborano et al., 2019). Molecular imaging of tumour metabolism holds great potential as a measurement tool for tumour staging, radiation treatment planning and monitoring of tumour response to therapy (Fuss & Cheng, 2016). At present, several modalities can be used for clinically translatable metabolic imaging, including magnetic resonance spectroscopy (MRS) and positron emission tomography (PET).

Quantitative metabolomics, in which the concentration of metabolites in biological mixtures is measured, provides reliable insights into systems biology. Numerous approaches within NMR and MS enable accurate metabolite concentration measurements and to identify unknown metabolites (A.-H. M. Emwas, 2015). The greatest advantage of NMR spectroscopy is to observe and rigorously quantify compounds present in biological fluids, cell extracts, and tissues with minimal requirements for sample preparation (Markley et al., 2017). Through the use of stable isotope labels, NMR spectroscopy can determine the positional isotopomer distributions of metabolites in a given segment of a metabolic network (Lane & Fan, 2017). NMR spectroscopy detects only medium to high abundance metabolites (concentrations >1mM) but does not require a chromatographic separation. In contrast, MS is more

sensitive and offers quantitative analyses with much higher sensitivity (Aretz & Meierhofer, 2016). Currently, chromatographic separation techniques such as liquid chromatography (LC) and gas chromatography (GC) are almost always combined with MS to reduce the complexity of the mass spectra. MS based techniques suffer from a lack of standardisation which renders it difficult to compare results from different instrumentation. MS also requires more elaborate sample preparation or fractionation because of the complexity of biological matrices compared to NMR spectroscopy. Hence, sample preparation in MS can cause metabolite losses. Unlike NMR, MS cannot readily determine each positional isotopomer (Lane & Fan, 2017), but is more powerful in determining mass increments (Dudek et al., 2020). Besides the quantitative analysis of biomacromolecules by NMR and MS, metabolic imaging techniques magnetic resonance imaging (MRI) and PET hold great potential for the evaluating diagnosis and prognosis of diseases in the clinic (Fuss & Cheng, 2016). These techniques are commonly used to diagnose and improve the treatment of these disorders. MRI is used to characterise tissue, usually using the ^{1}H-NMR signal of water molecules but can be extended to detect other nuclei and allows the detection of metabolites without the use of ionising radiation (Kurhanewicz et al., 2019). PET is based on the detection of pairs of gamma rays emitted indirectly by a radioactive tracer, most commonly fluorine-18, carbon-11, and nitrogen-13. The most widely utilised PET metabolic probe has been radiolabelled glucose analogue 18-fluorodeoxyglucose [^{18}F]-FDG (Plathow & Weber, 2008), which accumulates in highly glycolytic tissues and thereby enables to measure rates of glucose consumption. In the clinic, PET is used mostly in patients with cancer because of its potential to distinguish between benign and malignant tumours as malignant tumours usually consume glucose at faster rate.

1.7 Nuclear magnetic resonance

Nuclear Magnetic Resonance (NMR) is a technique in which nuclei are placed in an external magnetic field and absorb and emit radiofrequency radiation. In an NMR experiment, the precession of magnetisation is detected. It is used in physics, physical chemistry, chemistry and biology to study liquid crystals, membranes, the structure of molecules, metabolism etc.

1.7.1 Nuclear spin polarisation

Nuclear spin (I) is a quantum mechanical property of many nuclei which can be described in a classical model as the total angular momentum of a nucleus (Cavanagh, 1995). The concept of spin is fundamental for NMR theory. Protons, neutrons, and electrons possess net spins of ½. The spin nuclear quantum number S can adopt values between S = 0 and S = 8 in ½-unit increments between elements. There are some rules to predict the nuclear spin value of a nucleus (see Table III). Nuclei with a non-zero spin quantum numbers are NMR active.

Table III. The rules for determining the nuclear spin states.

No.of protons	No.of neutrons	Spin quantum No. (S)	Examples
Even	Even	0	^{12}C, ^{16}O
Odd	Even	1/2	^{1}H, ^{13}F
		3/2	^{11}B, ^{23}Na
Even	Odd	1/2	^{13}C
		5/2	^{17}O
Odd	Odd	1	^{2}H

Since nuclei with non-zero spin have angular momentum and charge, they possess a nuclear magnetic moment (μ). As a result of having this magnetic moment property, nuclei with non-zero spins align themselves with or against the external magnetic field. The

degeneracy of the ground state is determined by 2S+1 (Cavanagh, 1995). For instance, the nuclear spin quantum number S of ^{1}H is ½; allowing for two spin states denoted as +½ (α state) and -½ (β state) in the external magnetic field (B_o). Thus, spin ½ nuclei placed in an external magnetic field can only exit in two energy states:

- α low energy state where spins align with the external magnetic field
- β high energy state where spins oppose to the external magnetic field

At thermal equilibrium, the number of spins in the lower energy level is slightly higher than the number of spins in the upper level (see Figure 1.7.1). The Boltzmann distribution describes the distribution of the nuclei between α state and β state:

$$\frac{\mathbf{Nupper}}{\mathbf{Nlower}} = \mathbf{e}^{-\frac{\Delta \mathbf{E}}{\mathbf{kT}}} \qquad \textbf{(1.1)}$$

For instance, nuclear spin quantum number of ^{1}H is ½; so allowed the spin state of ^{1}H is 2 denoted as +½ and -½. In the external magnetic field (B_o), ^{1}H nuclei are visualised around the magnetic field direction and against the magnetic field (Cavanagh, 1995).

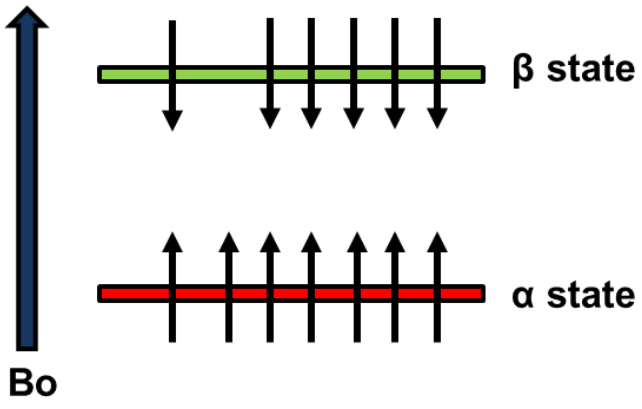

Figure 1.7.1 Demonstration of the degeneracy of ground state of ^{1}H.

Some of the ^{1}H nuclei align with the external magnetic field at lower energy stage (α) and some of them oppose to the field at higher energy stage (β).

1.7.2 Vector model

Nuclei with non-zero spin have a magnetic moment associated with angular momentum. Thus, nuclei act like a bar magnet and generate a small magnetic field. In the absence of the external magnetic field, the energy levels of quantum states corresponding to 2S+1 values of a spin-S nucleus are equal or degenerate. Application of an external magnetic field removes this degeneracy, leading to formation of discrete energy levels.

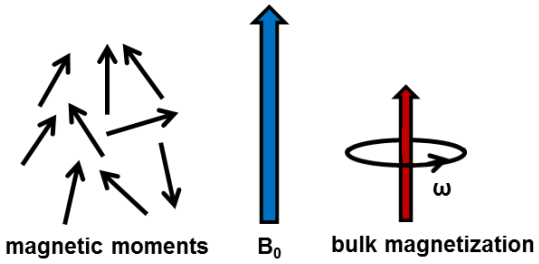

Figure 1.7.2 Generation of bulk magnetisation in an external magnetic field.
In the absence of an applied magnetic field, the direction of the spin of the nuclei is randomly oriented, producing no overall magnetic effect. By placing the spins in high magnetic fields, they orientate with this magnetic field, generarating bulk magnetization.

At thermal equilibrium, the different energy states are unequally populated by nuclei. The small population differences between energy levels produces the bulk magnetisation vector. The bulk magnetisation vector is parallel to the static magnetic field, B_0 , which, by convention, points toward the z-axis (see Figure 1.7.2). The net magnetisation along the z-axis precesses around static magnetic field with a frequency called the *Larmor frequency.* The Larmor frequency (ω_0) is related to magnetic field strength (B_0) and gyromagnetic ratio (γ) of the individual nucleus through the relation:

$$\omega_0 = -\gamma . B_0 \qquad (1.2)$$

The Larmor frequency is what we actually observe in an NMR experiment. To detect an NMR signal in an NMR experiment, the magnetisation vector is rotated away from z-axis by applying a radiofrequency field (RF field) from the x or y-axis for a short period of time at the Larmor frequency. RF field that applied around x-axis at Larmor frequency makes coordinate axes x and y rotate at Larmor frequency. Thus, in the on-resonance case, the angular frequency of the magnetisation (ω_0) relative to the angular frequency of the rotating frame (ω_{rf}) becomes zero. In this case, the influence of the external magnetic field (B_0) is removed. In the rotating frame, the apparent Larmor frequency is modified and is given by the symbol Ω:

$$\Omega = \omega_0 - \omega_{rf} \quad (1.3)$$

The precession of the magnetization vector is detected by a coil aligned in the xy plane in an NMR experiment. At equilibrium, there is no transverse magnetisation to be detected as the magnetisation precesses along the z axis. The precession of magnetisation vector at the Larmor frequency on the xy plane can be written as:

$$M_x = M_0 \sin \beta \cos(\omega_0 t) \quad (1.4)$$

$$M_y = M_0 \sin \beta \sin(\omega_0 t) \quad (1.5)$$

To detect the precession of the magnetization, the magnetisation along z axis must be tilted by some means to create a spin coherence. Thus, RF field is turned on for only a short period of time to create a spin coherence. If a RF pulse at the Larmor frequency is applied along x axis, the z and y component of the magnetisation is written as (Cavanagh, 1995):

$$M_Z = M_0 \cos \beta \quad M_Y = -M_0 \sin \beta \quad (1.6)$$

1.7.3 Fourier transformation

In an NMR experiment, the precession of magnetisation is detected. The precessing magnetisation in a transverse plane rectangular to the static B_0 field induces a current in a detection coil aligned in the xy-plane. This current is amplified and recorded as a time-domain signal. Since this current eventually decays away as a result of relaxation, the signal is called the free induction decay (FID). As the frequency-domain signal is more interpretable than the time domain signal, the time-domain function is Fourier transformed in order to convert it into frequency-domain function.

T_2 is spin-spin relaxation decay constant which causes magnetisation decay over time (t). The precession of the magnetisation in the xy-plane induces a voltage (signal S) in a coil and decays as an exponential decay:

$$S_x = S_0 \cos\Omega t \exp\left(\frac{-t}{T2}\right) \qquad S_y = S_0 . \sin\Omega t \exp\left(\frac{-t}{T2}\right) \tag{1.7}$$

$$S(t) = S_0 \exp(i\Omega t) \exp\left(\frac{-t}{T2}\right) \tag{1.8}$$

Fourier transformation of the FID gives rise to the frequency domain NMR spectrum. Fourier transformation of time domain function to frequency domain function is written as:

$$S(t) \xrightarrow{\text{FT}} S(\omega) \tag{1.9}$$

$$S_0 \exp(i\Omega t) \exp\left(\frac{-t}{T2}\right) \xrightarrow{\text{FT}} S_0 [A(\omega) + iD(\omega)] \tag{2.0}$$

The frequency-domain signal is complex, with real and imaginary parts. The real part of the spectrum gives a lineshape known as the absorption mode Lorentzian while the imaginary part shows the dispersion mode Lorentzian (see Figure 1.7.3). Phase correction is used to obtain pure absorption Lorentzian lineshapes in the spectrum.

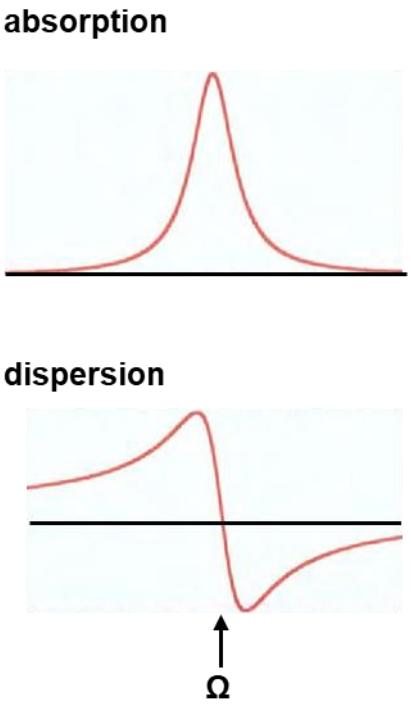

Figure 1.7.3 Illustration of absorption and dispersion Lorentzian lines.

The absorption mode Lorentzian line shape is always positive while the dispersion mode Lorentzian line shape has positive and negative parts.

1.7.4 Relaxation

NMR relaxation is the re-establishment of the equilibrium condition by the loss of energy imparted to the system. A 90^0(x) RF pulse on a sample perturbs the net bulk magnetisation along z axis and results in magnetisation in the xy-plane which corresponds to an alteration in the spin polarisation. Following this perturbation, recovery of magnetisation along z- axis occurs. This is termed longitudinal relaxation and leads to the equilibrium population to be restored. Longitudinal relaxation is known as spin lattice-relaxation and corresponds to a complete loss of energy of the spins by transfer of energy into the surroundings. As the energies transferred in the form of heat are so small, temperature changes are not detected. The Bloch theory assumes that nuclear spins

relax to the equilibrium values following exponential behaviour, defined by:

$$dM_Z / dt = (M_0 - M_Z) / T_1 \quad (1.10)$$

where M_0 is the bulk magnetisation at thermal equilibrium, M_Z is the recovery of the z-magnetisation and T_1 is the relaxation time (s^{-1}).

A bulk magnetisation vector in the transverse plane represents the sum of many individual vectors that have phase coherence. The transverse spin components precesses around the z-axis at Larmor frequency after the radiofrequency pulse. While transverse spin components move together in the transverse plane, the interaction between their intrinsic magnetic fields slightly modifies their precession rates. Moreover, inhomogeneities in the static magnetic field induce slight local changes in the precession frequency. The transverse magnetisation is gradually lost due to inhomogeneities in the static magnetic field and/or direct interactions between transverse spin components. The decay of the transverse magnetisation is referred to as spin-spin relaxation.This relaxation occurs with an exponential decay defined by the time constant T_2:

$$M_{xy}(t) = M_{xy}(0)e^{-t/T_2} \quad (1.11)$$

In most situations, spin-spin relaxation proceeds more rapidly than spin-lattice relaxation (Cavanagh, 1995).

1.7.5 Chemical shift

Information about the chemical environment of nuclei can be derived from its resonance frequency. The precise resonance frequency of a particular nucleus is dependent on the

effective magnetic field, B_0, at the nucleus. The B_0 field, experienced by a nucleus in an atom varies moderately from the external B_0 field because the magnetic field observed by the nucleus depends on the nature of the chemical bonds of the atom. Therefore different nuclei do not resonate at the same frequency. The difference between the resonance frequencies of nuclei is described by the chemical shift which depends upon the chemical nature of the molecule.

The electrons circulating around the nucleus create a secondary induced magnetic field (B_e). The magnetic field created by the electron circulation within an s orbital opposes B_0 field. Thus, the B_0 field is shielded from the nucleus by the B_e field, leading to shifts of lower frequency. In opposition, the magnetic field created by the circulation of electrons between the ground and excited states of p orbitals augments the external B_0 field. Consequently, the B_e field produced by electrons between the ground and excited states of p orbitals gives rise to deshielding. There are also effects in aromatic compounds where ring currents in aromatic rings enhance the B_0 field leading higher NMR frequencies (down-field shifts).

In practice, NMR spectroscopy measures the chemical shifts relative to a given standard, according to the following equation:

$$\text{Chemical shift, } \delta = \frac{\text{frequency of signal} - \text{frequency of reference}}{\text{spectrometer frequency}} \times 10^6$$

NMR spectrometers operate at different field strenghts. The chemical shift scale is expressed in parts per million (ppm), being independent from the spectrometer frequency

so that chemical shifts of a nucleus determined from experiments on NMR spectrometers at different field strenghts will be the same (Cavanagh, 1995).

1.7.6 1D and 2D NMR spectroscopy to study metabolism

NMR has profoundly emerged as a tool to mine an abundant amount information about metabolism of cells. The accurate identification of metabolites in cells or tissue can be carried out by one dimensional (1D) NMR and two dimensional (2D) NMR methods (Fan & Lane, 2016).

To achieve a well designed metabolomics experiment, the type of NMR measurement must be chosen carefully. A suprising amount of information can be obtained from 1D-^{1}H NMR spectra, including chemical shifts, homonuclear coupling constant (^{1}H -^{1}H) and the integral of the signal. The 1D-^{1}H NMR spectrum can only be used to measure metabolites at higher levels (Dona et al., 2016). 2D methods can be used to overcome overlap of signals and can yield additional information to identify molecues (Dona et al., 2016). For example, a 2D ^{1}H-^{13}C heteronuclear single quantum correlation (HSQC) spectra is used to correlate the chemical shifts of ^{1}H and ^{13}C directly bonded to each other (Öman et al., 2014).

An NMR experiment is simply based on a pulse sequence consisting of a series of radio frequency (RF) pulses and delays. A general 1D pulse sequence is made up of the preparation phase and detection phase (Mckay, 2011) (see Figure 1.7.4.A). During the preparation period, the sample is exited for a sufficient period of time by combination of RF pulses in order to create the desired state of magnetisation prior to detection. Due to precession of the magnetisation vector, the signal evolves in time and returns to its initial state, causing a signal as a free induction decay (FID) of the transverse magnetisation.

The FID is recorded during the detection period before repeating the acquisition of the FID for improved signal-to-noise ratio. 1D Fourier transformation (FT) of the FID yields the 1D spectrum with one frequency axis.

2D NMR spectroscopy, which yields an spectrum with two frequency axes, is sometimes needed to extract more information about connectivity or interactions within the various spin networks. 2D NMR spectroscopy introduces two additional sections into the pulse sequence of 1D NMR, namely the evolution time and the mixing time (Dona et al., 2016) see Figure 1.7.4.B). During the evolution time t_1, the desired state, which is created by RF pulses in the preparation period, evolves with chemical shift and/or scalar couplings. In the case of NOESY spectra the mixing period transfers the coherence from the first spin to a second one via relaxation mechanisms. In heteronuclear experiements such as the HSQC, the chemical shift in the 2^{nd} dimension is developed by increasing a delay between 1D slices which generates an alternating sinusoid in the incremented dimension. In order to obtain a two-dimensional data set, a 2D pulse scheme is repeated over and over again with systematically incremented t_1. After the execution of the pulse sequence many times, two-dimensional time domain data set is generated, one is from direct detection and other is from systemically incrimination of t_1. FT in both dimensions yields the 2D spectrum with two frequency axes containing the chemical shift of nuclei in the sample. Examples for 2D NMR experiments are NOESY, COSY, TOCSY and HSQC. The 2D HSQC experiment is used to correlate the chemical shift of ^{1}H in the F2 dimension with that of the directly bonded X-heteronuclei (commonly, ^{13}C or ^{15}N) in the F1 dimension (see Figure 1.7.4.C.).

Stable isotope-resolved metabolomics (SIRM) is an approach that enables us to follow the metabolic fate of labelled substrates in vivo and in vitro (Bruntz et al., 2017). Use of

isotope-labeled precursor metabolites in 1D and 2D NMR experiments offers a unique ability to analyse the fate of individual atoms from stable isotope-enriched precursors. ^{13}C NMR spectroscopy allows measuring the activity of a large variety of metabolic pathways by the detection of resonances from ^{13}C (Hollinshead et al., 2016). However, ^{13}C NMR spectroscopy is relatively insensitive compared to ^{1}H NMR due to low natural abundance of ^{13}C and weak magnetic moment of ^{13}C. Thus, ^{13}C-enriched substrates are used to observe more carbon signals. For instance, [1,2-^{13}C]-glucose, can be used to determine and quantify the activity of metabolic pathways. As a result of tracing the fate of stable isotopically-enriched nutrients, ^{13}C substitution in multiple positions in the same molecule can be distinguished (see Figure 1.7.5). However, ^{13}C-optimized NMR probes restrict us to large concentrations of metabolites. As MS can also provide information on isotopomers by yielding mass increments, the combined analysis of NMR with MS (CANMS) can be used together to obtain long range information on isotopomer contributions in ^{13}C-labeled cells for metabolic pathway analysis (Chong et al., 2017).

The HSQC experiment can be performed using metabolites generated using isotopically labeled precursors in order to decipher the carbon or nitrogen flows in cells (Fan & Lane, 2016). The 2D-HSQC offers high resolution data that allows the detection of positional isotopomer distributions of metabolites. The measurement of label incorporation can be performed by either quantification of intensities from metabolite spin systems or analysis of multiplet patterns in the incremented ^{13}C-dimension arising from the scalar coupling (J_{CC} couplings) (Saborano et al., 2019).

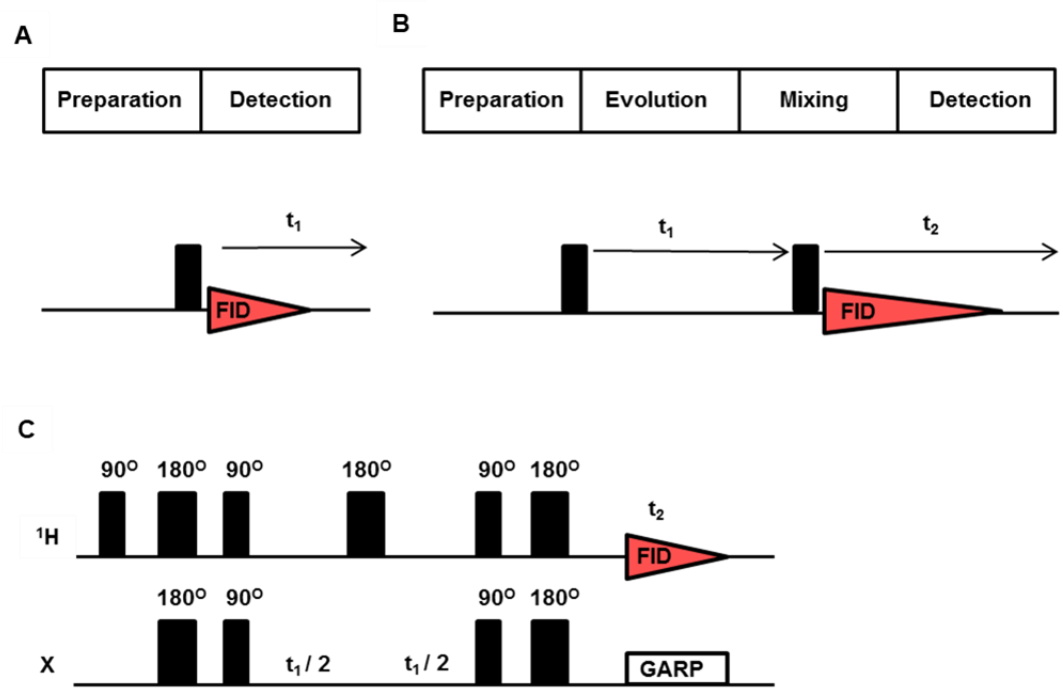

Figure 1.7.4 1D and 2D NMR spectroscopy.

(A) Schematic presentation of the pulse sequences of a simple 1D-NMR experiment. (B) The construction of a simple 2D-NMR experiment. (C) Pulse sequence of a 2D HSQC experiment.

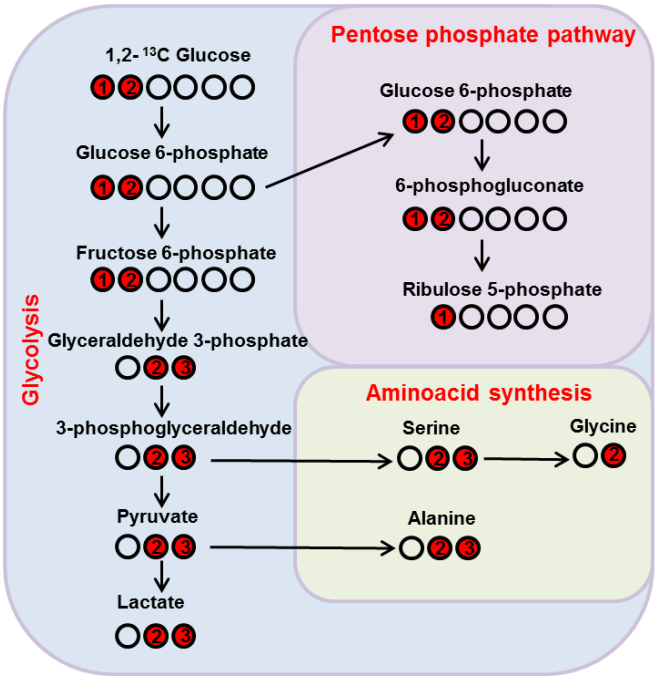

Figure 1.7.5 Isotope tracing to probe metabolic pathways.

The figure shows [1,2-^{13}C] glucose tracing pentose phosphate pathway and aminoacid synthesis. Empty circles, ^{12}C; red filled circle, ^{13}C.

1.4 The aim of this thesis

Cancer cells exhibit altered metabolism, regulating the dynamics of the central metabolic pathways in a different manner to fulfil the demands of unbridled cell growth and proliferation (DeBerardinis & Chandel, 2016). A significant effort has been made toward understanding how cancer cells converge multiple biochemical pathways to support the increased energy request, rapid proliferation, and other characteristics typical of malignant cells. Contemporary research has led to the discovery of the dependence of cancer cells on specific metabolic pathways to improve cellular fitness (Nie et al., 2018; Patil et al., 2016). Thus, a comprehensive description of the metabolic landscape in cancer cells has guided the development of drugs that target cancer-cell-selective metabolic pathways. Accordingly, there has been considerable interest in the mapping of the metabolic profiling of cancer cells to exploit metabolic vulnerabilities.

Haematological malignancies are cancers that comprise a diverse set of lymphoid and myeloid neoplasms in which normal haematopoietic differentiation is perturbed (Snowden et al., 2017). With the advent of high throughput technologies, common genetic variations with prognostic and therapeutic value have been identified across the different types of haematological cancers (Arber et al., 2016; Swerdlow et al., 2016). However, a landscape of metabolic variation across the haematological cancer types has not been well exploited so far. Therefore, the overall aim of this thesis was ‘to map metabolic profiling of a panel of haematological cancers for diagnostic or therapeutic purposes. This was achieved by employing a variety of cellular, molecular and analytical techniques, including NMR spectroscopy, flow cytometry and western blotting. To do this I focused on a series of specific experimental objectives:

First, I characterised metabolic phenotypes of the haematological cancer cell lines using

18 cell lines, covering 5 different subtypes using 1D NMR spectroscopy (chapter 3).

Then, based on the findings from this study (described in chapter 3) I aimed to further investigate the role of BCAAs in MM cells using 1D and 2D NMR spectroscopy, flow cytometry and *in vitro* cell viability assays (chapter 4).

Finally, I focused on metabolic differences between BL and DLBCL. I compared the effect of extracellular asparagine on serine metabolism for BL vs DLBCL using 1D and 2D NMR spectroscopy, flow cytometry, *in vitro* cell viability assays and western blotting (chapter 5).

CHAPTER 2

MATERIALS AND METHODS

2.1. Cell culture

2.1.1 Maintenance of cell lines

Acute myeloid leukaemia (NB4, HL60, U937, KG1a), Burkitt's lymphoma (Glor, BL31, Sav, Ezema, Dante), diffuse large B cell lymphoma (Farage, SUDHL4, SUDHL5, SUDHL6), chronic myeloid leukaemia (K562) and multiple myeloma (UM3, JJN3, U266, RPMI8226) cell lines were purchased from DSMZ (Braunschweig, Germany). Cell lines were maintained in exponential growth in RPMI-1640 media (Gibco-Invitrogen Ltd, Paisley, UK) supplemented with 10% fetal bovine serum (FBS, Gibco-Invitrogen) and penicillin (100 U/ml) and streptomycin (100 µg/ml) (Gibco-Invitrogen) at 37°C with 5% CO_2. The cultures were routinely passaged every 2 days to maintain exponential phase. Cells were authenticated regularly with NorthGene service for STR profiling. Mycoplasma test was performed with DAPI stain (Sigma Aldrich).

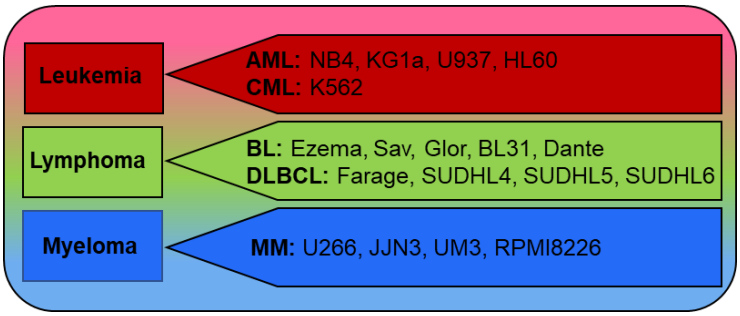

Figure 2.1.1 Haematological cancer cell lines.

Classification of 18 cell lines representing acute myeloid leukaemia (AML), chronic myeloid leukaemia (CML), Burkitt's lymphoma (BL), diffuse large B cell lymphoma (DLBCL) and multiple myeloma (MM).

2.1.2 Preparation of customised complete RPMI-1640 medium

RPMI-1640 medium powder, modified w/o glutamine, w/o amino acids, glucose was purchased from MyBioSource.com,US. Firstly, the amino acid and glucose stock solutions were prepared in ddH_2O. A nutrient mixture that consists of glucose and amino

acids based on the composition of RPMI-1640 media formulation was prepared (Moore et al., 1967) (see Table IV.).

Then, 3.70 g RPMI-1640 medium w/o L-glutamine, w/o amino acids, glucose powder was dissolved in 450 ml ddH_2O. 1 g of $NaHCO_3$ was added under stirring. Nutrient mixture was added to the medium. To bring the final volume to 500 ml, ddH_2O was added before adjusting the pH to 7.0 by addition of HCL or NaOH. The medium containing amino acid mixture and glucose was filter-sterilised using a 0.22 μm membrane.

Table IV. RPMI-1640 (21875) culture medium composition. Source: Sigma-Aldrich.

Components	Final Concentration (mg/mL)	Stock Concentration (mg/mL)
Glycine	0.01	10.0
L-Arginine hydrochloride	0.24	50.0
L-Asparagine	0.5	10.0
L-Aspartic acid	0.02	50.0
L-Cystine	0.05	25.0
L-Glutamic Acid	0.02	50.0
L-Glutamine	0.3	15.0
L-Histidine	0.015	15.0
L-Hydroxyproline	0.02	100.0
L-Isoleucine	0.05	20.0
L-Leucine	0.05	10.0
L-Lysine hydrochloride	0.04	40.0
L-Methionine	0.015	15.0
L-Phenylalanine	0.015	10.0
L-Proline	0.02	100.0
L-Serine	0.03	30.0
L-Threonine	0.02	40.0
L-Tryptophan	0.005	5.0
L-Tyrosine	0.02	25.0
L-Valine	0.02	25.0
D-Glucose (Dextrose)	2.0	100.0

2.1.3. Isotopic labelling of cells

For tracer-based metabolic analysis, cells were centrifuged (at 1500 rpm, for 5 minutes, at 21°C), then resuspended in a medium prepared with labelled precursors (see Table V). The number of cells was determined based on the metabolic pathway that would be studied in order to obtain a strong NMR signal for analysis. Cells were cultured at a density of 0.5 x 10^6 to 1.0 x 10^6 based on the incubation time and cell doubling time.

Table V. Isotopes used for metabolic tracer-based studies.

Description	Company	Catalog number
[U-^{13}C]-Glucose, 99% ^{13}C	Cortecnet	CC860P1
[U-^{13}C]-Serine, 98% ^{13}C, 98% ^{15}N	Cortecnet	CCN3000P025
[3-^{13}C]-Glutamine, 99% ^{13}C	Sigma-Aldrich	604941
[U-^{13}C]-Leucine, 98% ^{13}C	Sigma-Aldrich	605239

2.2 *In Vitro* cytotoxicity assays

2.2.1 Preparation of inhibitor solution

Asparaginase, NCT503 and 2-aminobicyclo-(2,2,1)-heptane-2-carboxylic acid (BCH) were purchased from Sigma Aldrich. JPH203 was the gift of J-Pharma (see Table VI) Asparaginase solution (100 U/ml) prepared in distilled water. NCT503 solution (50 mM) was prepared in DMSO. JPH203 solution was prepared as 100 mM in DMSO-d6 (Sigma-Aldrich). BCH solution was prepared as 200 mM in the cell culture medium**.**

Table VI. Inhibitors used in this study.

Inhibitor	Company	Catalog number
BCH	Sigma-Aldrich	A7902
Asparaginase from Escherichia coli	Sigma-Aldrich	A3809
NCT-503, ≥98% (HPLC)	Sigma-Aldrich	SML1659
JPH203 HCl salt, >99%	Gift from J-Pharma Tokyo, Japan	

2.2.2 Cell viability assay: CellTiter-Blue

Cells were plated in a 96-well plate. $20x10^4$ cells were seeded in volumes of 200 µl/well. To limit evaporation, the outer wells were loaded with PBS. Cells were treated with inhibitors or amino acid deprived media. At the end of the study, 10 µl of CellTiter-Blue®reagent (Promega) was added to each well for four hours incubation. The fluorescence intensity with the setting of Ex=560 nm and Em= 600 from the Cell Titer-Blue Reagent was read by a Victor2 plate reader (PerkinElmer).

2.3 Protein analysis: Western Blotting

2.3.1 Preparation and quantification of protein samples

Exponentially growing $5x10^6$ cells were centrifuged at 1500 rpm for 5 minutes and supernatant discarded. Cells were washed with 1 ml of ice-cold PBS, and spun again. The cell pellet was lysed with 200 µl RIPA buffer (see Appendix A) supplemented with 1 x EDTA-free protease inhibitor cocktail (Sigma) and incubated on wet ice for 1 hour. Samples were centrifuged at 14000 rpm at 4°C, for 10 minutes and the supernatant containing the soluble proteins collected and stored at -20°C.

The concentration of the protein extracts was determined using the Bio-Rad DC Protein Assay (Bio-Rad). Briefly, 25 µl of solution 'A+S' (made by adding 20 µl reagent S to each 1ml of reagent A) were pipetted in 96 well plate wells. 2 µl of BSA standards (0, 0.625, 1.25, 2.5, 5 and 10 mg/ml) or protein extract was added in triplicate wells. A colorimetric reaction was obtained by adding 200 µl of reagent B to each well. The plate was incubated for 15 min at room temperature to allow the reaction to develop. The absorbance of the samples was read using a plate reader (Perkin-Elmer Victor X3 plate reader) at 690 nm. The absorbance obtained for BSA standards with known concentration was used to construct a standard calibration curve; this was then used to calculate the concentration of cell lysates.

2.3.2 Sodium dodecyl sulphate –polyacrylamide gel electrophoresis (SDS-PAGE)

A 1.5 mm SDS-polyacrylamide resolving gel was prepared with 12% acrylamide (see Appendix A) using the Mini-Protean 3 gel system (Bio-Rad). Distilled water was poured over the resolving gel to avoid oxydation and dehydration. After resolving gel had polimerised, stacking gel was poured and a 10-well 1.5 mm comb inserted. Once gel was

set, it was loaded on mini-Protean 3 gel electrophoresis cells, and 1x SDS-PAGE running buffer (see Appendix A) was poured in the inner and outer chamber.

50 µg of cell lysate was mixed with 12.5 µl 4 x SDS gel loading buffer (see Appendix A). RIPA buffer was added to adjust the final volume to 50 µl. Samples were then denatured for 10 minutes at 70°C in a thermocycler. 20 µl of denatured protein samples or 5 µl BLUeye Prestained Protein Ladder (Geneflow Ltd) were loaded on the gel and run at 120 V (see Appendix A) until the dye front reached the edge of the gel.

2.3.3 Western blot

After SDS-PAGE, the stacking gel was removed, and the resolving gel was equilibrated in transfer buffer for 5 minutes before western blot. Briefly, 6 pieces of 3 mm filter paper soaked in 1 x transfer (see Appendix A) were placed on the anode plate of a Bio-Rad Semi-Dry Transfer cassette (Bio-Rad). Polyvinylidene fluoride (PVDF) membrane (Millipore, Watford, U.K.) was activated for 10’ in methanol (Fisher) and equilibrated in 1x transfer buffer until use. The activated PVDF membrane was placed on top of the filter papers, followed by the gel. A further 6 pieces of 3 mm filter paper soaked in 1 x transfer were put on the gel. Bubbles were gently removed from the sandwich by gentle pressure. Proteins were transferred onto membranes at 25 V for 60 minutes.

2.3.4 Immunodetection of proteins

After transfer, the PVDF membrane was blocked for 60 minutes at RT in 5% w/v non-fat milk powder in Tris-Buffered Saline (TBS) with Tween 20 (TBS-T) (5% blocking solution) (see Appendix A). The blocked membrane was incubated with the appropriate dilutions of primary antibody (according to Table VII) in 5% blocking buffer overnight in 4°C on a shaker. After incubation, the membrane was washed in three times with TBST for 5

minutes, at 70 rpm on a gyro-rocker (Scientific laboratory supplies). The membrane was then incubated with the recommended dilution of fluorescent tagged secondary antibody (according to Table VII) in 5% blocking buffer at room temperature for an hour. The membrane was then washed 3 times in TBS-T supplemented with 0.01% sodium dodecyl sulphate (SDS), followed by the last wash in TBS (see Appendix A). Protein bands on the blot were scanned and quantified using LI-COR Odyssey®. Protein levels were normalised using the housekeeping protein β-actin.

Table VII. Antibodies used for the Western blot analysis.

Antibody	Source	Company	Cat. No	Dilution
Anti-PHGDH	Rabbit	Sigma-Aldrich	HPA021241	1:750
Anti-β actin	Mouse	Sigma-Aldrich	A1978-100 µL	1:15000
Anti-rabbit	Goat	LI-COR	926-32211	1:10000
Anti-mouse	Goat	LI-COR	926-68029	1:10000

2.4 Analysis of cell surface expression of proteins: flow cytometry

100 µl of exponentially growing cells was aliquoted into flow cytometry tubes. 2 µl of fluorophore-conjugated antibody (see Table VIII) or matched isotype (see Table VIII) was added and incubated for 30 min at 4 °C in the dark. After incubation, cells were washed with 2 ml of cold PBS, cells were fixed with 300 µl fluorescence-activated cell sorting (FACS) fix buffer (see Appendix A) and stored at 4°C in the dark until run. All samples were analysed using a BD FACSCalibur and CELLQuestTM Pro (BD Bioscience) as per the manufacture instructions.

Table VIII. Antibodies used for surface staining.

Primary antibody	Matched Isotype Control	Volume Per Facs Tube
CD98 FITC-conjugated (BD Biosciences)	Ms IgG1, κ	2 µl
LAT1 (BU53) Alexa Fluor® 647-conjugated (NovusBio)	Ms IgG2α (NovusBio)	2 µl

2.5 NMR spectroscopy

2.5.1 Cell extraction

The metabolic activity of cells was halted as described before (Saborano et al., 2019). Briefly, cell suspensions were centrifuged in falcon tubes at 1500 rpm for 5 minutes at 21°C. 10 ml of the supernatant was stored for media analysis and the remaining supernatant was disposed of. Cell pellets were then washed once with 1 ml of pre-warmed PBS and transferred to Eppendorf tubes. Supernatants were discarded after centrifugation at 14000 rpm for 20 seconds. After this, 400 µl of HPLC grade methanol was rapidly added. Cell pellets were resuspended in methanol on dry ice and vortexed for 10 seconds before storing at −80 °C until extraction. For the extraction, cell pellets in methanol were transferred into the Wheaton™ lear glass sample vials (MERK). 325 µl of distilled HPLC grade H_2O and 400 µl of chloroform, pre-chilled on wet ice, were added. Samples were vortexed for 40 seconds and then incubated on the bench for 5 minutes. After centrifugation at 4000 rpm, for 10 minutes at 4°C, polar and nonpolar samples were transferred to Eppendorf tubes and the Wheaton™ clear glass sample vials, respectively. Polar samples were dried using a vacuum dryer.

2.5.2 NMR sample preparation

All polar extracts were dissolved in 50 µl of 100 mM sodium phosphate buffer (pH 7.0) prepared with 90%H_2O/10% D_2O or 100% D_2O (99.9% pure; GOSS Scientific Instruments Ltd.), 3 mM sodium azide (NaN_3) and 0.5 mM timethylsilyl-propanoic acid (TMSP, Cambridge Isotope Laboratories) as a chemical shift reference. Samples were sonicated for 15 minutes and vortexed for 10 seconds. 35 ml of sample was transferred into 1.7 mm NMR tubes. Samples that were dissolved in sodium phosphate buffer containing 90% H_2O/10% D_2O were transferred into 1.7 mm NMR tubes using the GILSON sample preparation unit, while samples that were prepared with 100% D_2O buffer were manually transferred.

For preparation of media samples for NMR, 162 µl of the previously saved media was resuspended in 18 µl of metabolomics buffer made from 1 M phosphate buffer (pH 7.0) prepared with D_2O, 0.5 mM TMSP and 3 mM NaN_3. Then the samples were transferred to 3.0 mm NMR tubes. All samples were kept at 4°C until measurement.

2.5.3 NMR data acquisition

All 1D ^{1}H-NOESY and ^{1}H-^{13}C HSQC spectra for cell extracts were acquired at 300 K using a Bruker 600 MHz spectrometer, equipped with a 1.7-mm TCI probe and a cooled Bruker SampleJet autosampler.

The ^{1}H 1D spectra were obtained using the 1D NOESY pulse sequence (noesygppr1d) with water pre-saturation. Key parameters were as follows: spectral width 7183.9 Hz; complex points, TD 32768; interscan delay, d1=4 seconds; NOE mixing time, d8=10 milliseconds; number of transient, ns = 128; steady state transient, ds = 8. Total acquisition time was 14 minutes. For the ^{1}H 1D spectra of media samples, Bruker 600

MHz spectrometer with a 5-mm TXO cryogenic probe with a cooled Bruker SampleJet autosampler was used. The standard Bruker pulse sequence noesygppr1d was used to obtain ^{1}H 1D spectra. The key parameters used were as follows: spectral width: 7183,9 Hz; TD=32768; d1=5 seconds; NOE mixing time, d8=10 milliseconds; ns=32; ds=8. Total acquisition time was 5 minutes. The ^{1}H-^{13}C HSQC spectra were obtained using a modified version of the Bruker pulse program, hsqcgphprsp.ug4 which uses States-TPPI gradient selection, with additional gradient pulses during the INEPT periods echo periods to improve signals. The spectral width for 2D ^{1}H,^{13}C spectra was set to 7812.5 Hz for the ^{1}H observe dimension while 24154.6 Hz was set to for ^{13}C observe dimension. For the ^{1}H dimension of 2D HSQC spectra, 1024 complex data points were acquired. For the ^{13}C dimension, 2048 complex data points were acquired. Spectra were acquired with 2 transients and an interscan delay of 1.5 seconds as I had sufficient samples due to using of minimum $10x10^{6}$ cells for the cell extraction. For HSQC spectra with a high resolution in the incremented dimension that allowed to see the J_{CC} couplings, Non-Uniform Sampling (NUS) incrementation was used (Hyberts et al., 2014). 25% of the 8192 complex points were sampled for the ^{13}C dimension using Wagner's schedule generator (http://gwagner.med.harvard.edu/intranet/hmsIST/gensched_new.html) with a tolerance of 0.01. Total acquisition time was 4.30 hours.

2.5 4 Analysis of 1D spectra

2.5.4.1 One dimensional NMR spectra of cell extracts

The NMRLab/MetaboLab software (Günther et al., 2000; Ludwig & Günther, 2011) in the MATLAB, version R2017a (MathWorks, Massachusetts, USA) programming environment was used to process all one-dimensional NMR data. The free induction decay (FID) signal

was zero filled to 32768 points once and Fourier transformed using an exponential line broadening of 0.3 Hz. After all spectra were phase corrected and referenced to TMSP at δ 0.00 ppm, they were aligned on the TMSP signal. Then, a spline-based baseline correction was applied to all spectra. The water region and regions devoid of signal at the edges of the spectrum were excluded. The icoshift software was used to subject the shifted regions to segmental alignment (Savorani et al., 2010). The spectra were scaled to a probabilistic quotient normalisation (PQN-scaling). For multivariate analysis, log-transformation was applied in MATLAB. Subsequently principal component analysis (PCA) was carried out using the mean centered x-block data employing PLS toolbox (Eigenvector Research). Chenomx NMR Suite (version 5.0) (Alberta, Canada, 2015) was used to assign resonances of metabolites. The intensity of metabolites was determined by semi-manual integration (ITN tool) in MetaboLab within Matlab, version R2017a (MathWorks, Massachusetts, USA). Concentration of metabolites calculated as follows:

$$\frac{Ia}{Ib} = \frac{Ha \times Ca}{Hb \times Cb}$$

Where Ia is the intensity of TMSP signal; Ib is the intensity of sample signal, Ha and Hb are the number of protons of TMSP and sample respectively and Ca and Cb are the concentrations of TMSP and sample respectively.

2.5.4.2 One dimensional NMR spectra of cell culture media

The raw NMR data (FIDs) of media samples were manually phase-adjusted and baseline-corrected using the NMRLab/MetaboLab within Matlab, version R2017a (MathWorks, Massachusetts, USA) after referencing to TMSP chemical shift at δ=0.0ppm. The spectral region 5.15 ppm – 4.65 ppm was removed to exclude the effect of imperfect water

suppression. Then, segmental alignment (using icoshift) was performed in order to align several metabolites. Resonances of metabolites were assigned using Chenomx NMR Suite (version 5.0) (Alberta, Canada, 2015). The intensity of metabolites was measured by semi-manual integration (ITN tool) in MetaboLab in the MATLAB, version R2017a. Finally, metabolite intensities are normalised according to cell number as follows:

$$\text{normalization factor} = \frac{1x10^{6}}{\text{cell density}}$$

normalized signal intensity value = signal intensity x normalization factor

2.5.4.3 Two-dimensional NMR spectra

2D HSQC spectra were processed using NMRPipe software, version 9.2 (Delaglio et al., 1995) and loaded into Metabolab within Matlab, version R2017a (MathWorks, Massachusetts, USA). Cosine-squared window functions were applied to both dimensions and spectra were phased manually. Calibration was carried out manually using the L-lactic acid methyl signal as a reference (δ 1.31/22.9 ppm). Metabolite identification was performed using the MetaboLab library that was originally derived from the Human Metabolome Database (HMDB). For 2D NUS-HSQC spectra, data processing was initially performed using NMRPipe software (version 9.2) with the Hyberts extension (Hyberts et al., 2012) for processing NUS spectra and subsequent analysis was then performed with Metabolab within Matlab, version R2017a as described above for regular HSQC spectra.

PQN scaling factors from the corresponding 1D ^{1}H spectra were used to scale the associated 2D HSQC spectra for both labelled and unlabelled samples. The percentage of label incorporation in specific metabolites was calculated as follows:

$$\text{Ratio } {}^{13}C = \frac{I_{lab} \times S_{lab}}{I_{ctl} \times S_{ctl}}$$

Where I_{lab} is the intensity of the resonance from the labelled sample, S_{lab} is the scaling factor in the corresponding 1D NOESY spectrum for labelled sample, I_{ctl} is the intensity of the resonance from the reference unlabelled sample, S_{ctl} is the scaling factors in the corresponding 1D NOESY spectrum for the control sample. Although, ^{13}C makes up about 1.1% of all natural carbon, I assumed that the natural abundance of ^{13}C is 1% of all natural carbon using the formula to determine the percentage of label incorporation.

2.6 Transcriptomic data and RNA-seq data analysis

Publicly available gene expression (RNA-seq) data of eBL (Abate et al., 2015) and GCB-DLBCL (Teater et al., 2018) primary tumors were downloaded from Sequence Read Archive (SRA) database (Cochrane et al., 2011) using the SRA Toolkit. The accession number for eBL study is SRP062178 and for GCB-DLBCL is SRP1000105. Both studies generated paired-end RNA-seq data with Illumina HiSeq2000 platform. In total, RNA-seq data from 19 eBL and 12 GCB-DLBCL cases were used for gene expression analysis. Significant altered genes were calculated with Sleuth using the “Wald Test”. Based on this parametric statistical test, a ‘beta’ value (a biased estimator of the fold change) is assigned to every transcript, describing the expression in each condition. False discovery rate (FDR) was also calculated to correct for multiple testing comparison with a threshold at 1%. Finally, advanced gene set enrichment analysis (GSEA) was applied with “SetRank” (Simillion et al., 2017). R/Bioconductor software package to identify pathways using 980 gene sets from KEGG annotated database (Kanehisa et al., 2019). Gene set

network maps were generated with “Cytoscape v3.5.1” software (Shannon et al., 2003), considering a level of significance with FDR and setRank p-values at 1%. Transcriptomic data were retrieved and analysed jointly by Mr. Grigorios Papatzikas and Prof. Jean-Baptiste Cazier using the recent computational workflow of Kallisto-Sleuth (Bray et al., 2016).

2.7 Statistical analysis

Statistical analysis of data was performed using Prism version 7.0 (GraphPad Software, Inc., La Jolla, CA, USA). To determine whether two populations are statistically different, t-test for paired data was used. One-or two-way analysis of variance (ANOVA) was used to determine whether three or more populations are statistically different from each other. Pearson correlation analysis was carried to estimate whether there was a statistically significant linear relationship between datasets. The dose-response curves were plotted to calculate IC_{50} values. To determine IC_{50} values, concentration values were converted to log(concentration) values before performing non-linear regression (log(inhibitor) vs. response - variable slope). All error bars in the experiments represent standard error of the mean (SEM) for a minimum of three independent experiments. Data were considered significant when p-values were less than 0.05 and were represented in figures following the standard convention: * $p<0.05$, ** $p<0.01$, *** $p<0.001$, **** $p<0.0001$.

CHAPTER 3

METABOLIC PROFILING OF HAEMATOLOGICAL CANCER CELLS

3.1 Introduction

Most cancer cells exhibit an altered metabolism compared to normal cells, utilising nutrients in a different manner to produce large amounts of biomass for rapid proliferation (Pavlova & Thompson, 2016). Haematological malignancies are multi-factorial diseases of unclear molecular underpinnings. There are growing consciousness and understanding that metabolic pathways are commonly dysregulated in hematologic malignancies (Wojtowicz et al., 2018).

Metabolism is frequently dysregulated in haematological cancer cells. Unlike the genetic characteristics, the metabolic alterations of haematological cancers are poorly understood. The identification of mutations in human cytosolic isocitrate dehydrogenase enzymes IDH1 and IDH2 in acute myeloid leukaemia (AML) cells has led to renewed interest in metabolic reprogramming in haematological cancers and their therapeutic applications (Mardis et al., 2009). For instance, the striking genetic heterogeneity in diffuse large B cell lymphoma (DLBCL) was found to result in subsequent metabolic heterogeneity between different groups of DLBCL (Caro et al., 2012). In addition to these findings, c-Myc protein, whose overexpression is characteristic of BL, was reported to induce virtually all genes involved in glycolysis (Goetzman & Prochownik, 2018).

Metabolome reflects not only catabolic and anabolic reactions but also cellular regulation and genetic variations. Metabolomics has a marked potential to uncover the critical metabolic pathways recruited in carcinogenesis. Despite remarkable efforts to determine genetic characteristics, the metabolic alterations of haematological cancers and characterisations of metabolic differences in cancer subtypes have not been well focused. In this chapter, metabolic phenotypes of the most frequently occurring haematological

cancers representing AML, CML, BL, DLBCL and MM, have been studied using 1D NMR spectroscopy. Both intracellular and extracellular metabolites were monitored to explore the differences or similarities between these distinct haematological cancer subtypes.

3.2 Results

3.2.1 ^{1}H-NMR profiles show discrimination between blood cancer cell lines

In order to study the metabolic phenotype of haematological cancers, 1D ^{1}H - NMR spectra of 18 exponentially growing cell lines were acquired with 6 replicates per cell line. These cell lines represent AML (NB4, HL60, U937, KG1a), BL (Glor, BL31, Sav, Ezema, Dante), CML (K562), DLBCL (Farage, SUDHL4, SUDHL5, SUDHL6) and MM (UM3, JJN3, U266, RPMI8226). To explore the metabolic discriminations, all 1D ^{1}H - NMR spectral data from AML, CML, BL, DLBCL and MM were subjected to multivariate statistical modelling using unsupervised PCA.

The score plot of the first principal component (PC1) versus PC2 from PCA of the 1D ^{1}H-NMR spectral data of 18 cell lines is shown in Figure 3.1. PC1, that captures the greatest amount of total variance in the dataset, accounted for 29.08% of the variation while PC2 that captures the second greatest contribution to variance, includes 14.93% variability. The PCA score plot revealed a clear separation between AML, CML, DLBCL and BL underscoring the metabolic variation between these haematological cancers. However, the PCA score plot did not give a clear distinction between MM and other groups.

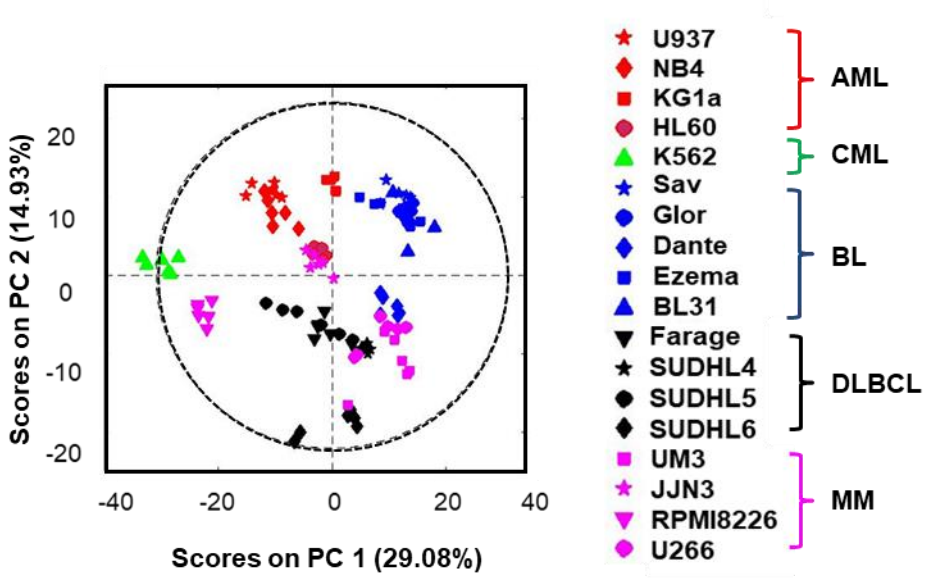

Figure 3.1 Principal component analysis (PCA) score plot of metabolic profiles of haematological cancers cells.

PCA score plot of ^{1}H NMR spectra of cell extracts. The PCA score plot displays the first and second PC components, PC 1 and PC 2 namely. Key; red: AML cell lines, green: CML cell line, blue: BL cell lines, black: DLBCL cell lines, magenta: MM cell lines.

3.2.2 ^{1}H-NMR profiles show discrimination from a same tumour type

To reveal the metabolic similarity between cell lines derived the same disease, ^{1}H - NMR spectra for the cell lines from the same group were evaluated by PCA.

Statistical evaluation by principal component analysis (PCA) showed a clear separation between the AML cells and CML cells reflecting underlying differences in metabolite composition. The first two principal components (PCs) explain 68.58% of the total variation in the spectra from AML and CML cells (see Figure 3.2.A). The observed metabolic differences between AML and CML can be reasoned by the specific genetic differences, such as the presence of the Philadelphia chromosome in K562 cells. The

PCA score plot showed almost no separation between the BL cell lines, except for Dante cells, indicating that the metabolite profiles of these BL cells are very similar (see Figure 3.2.B). This marked overlap in metabolic profiles of BL cells may reflect the strong metabolic effect of overexpression of c-Myc in BL cells. In opposition to the metabolic homogeneity of BL cells, PCA analyses computed for the spectral data from the DLBCL and MM reported a notable metabolic divergence between cell lines. The PCA that performed on the NMR data of different DLBCL cells revealed a clear separation between DLBCL cells lines, with the PC1 and PC2 accounting for 41.26% and 24.94% of the total variance respectively (see Figure 3.2.C). The PCA score plot for PC1 and PC2 for the comparison of metabolic profiles in MM cells showed that MM cell lines distinctly separated from each other due to their biochemical backgrounds (see Figure 3.2.D).

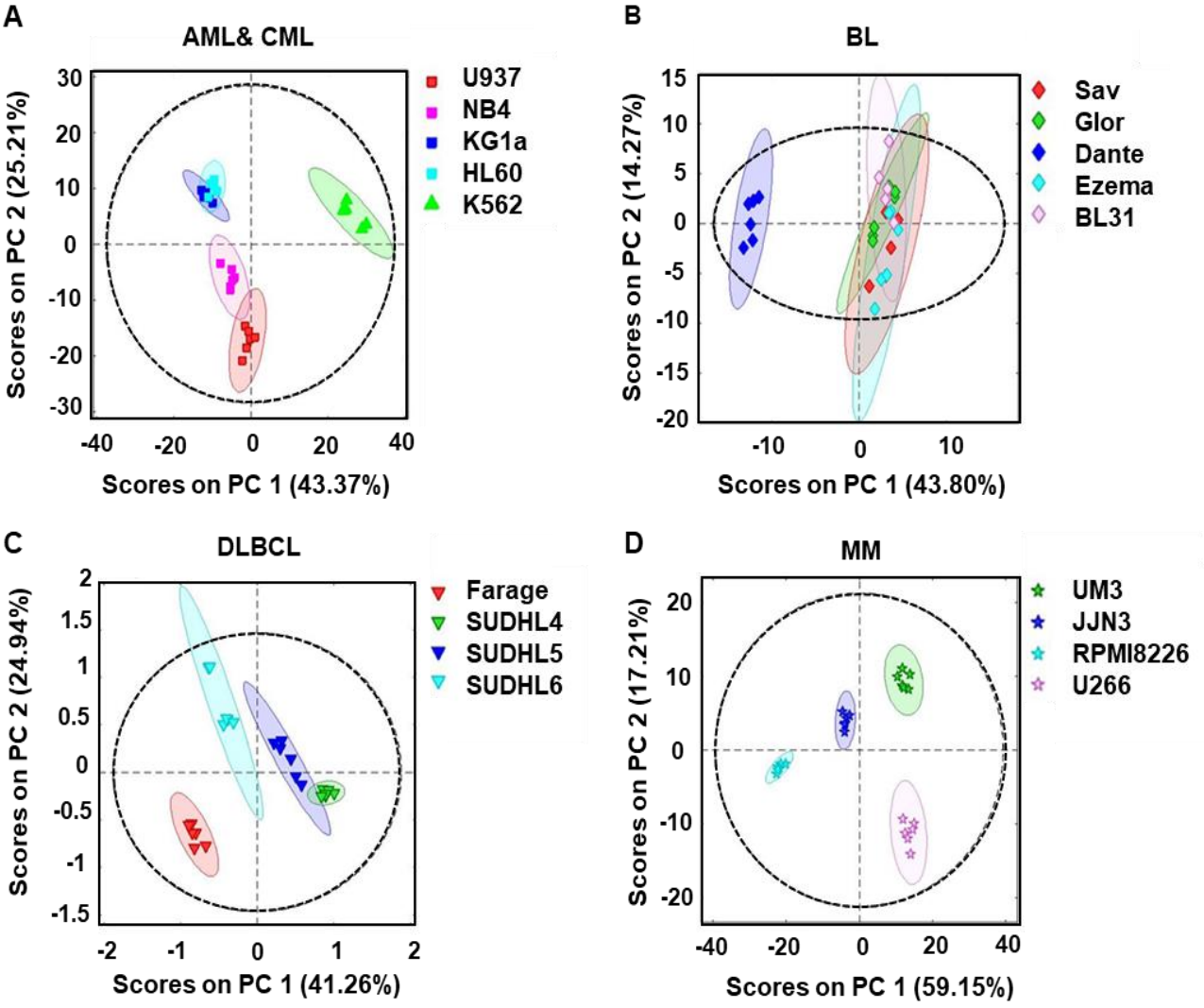

Figure 3.2 PCA score plots of metabolic profiles of different types of haematological malignancies.

PCA score plots for PC 1 versus PC 2 of 1D ^{1}H-NMR data of cell extracts from AML (NB4, HL60, U937, KG1a) & CML (K562) (A), BL (Glor, BL31, Sav, Ezema, Dante) (B), DLBCL (Farage, SUDHL4, SUDHL5, SUDHL6) (C) and MM (UM3, JJN3, U266, RPMI8226) (D) cell lines. 95% confidence intervals are indicated by ellipses.

3.2.3 ^{1}H-NMR profiles of intracellular metabolites show discrimination between blood cancer cell lines

To construct metabolic maps of AML, CML, BL, DLBCL, and MM, intracellular metabolites in NMR samples were identified. 1D NMR experiment provided well resolved spectra for intracellular polar samples (see Figure 3.3), thus enabling identification of several metabolites from several metabolic pathways (see Figure 3.4).

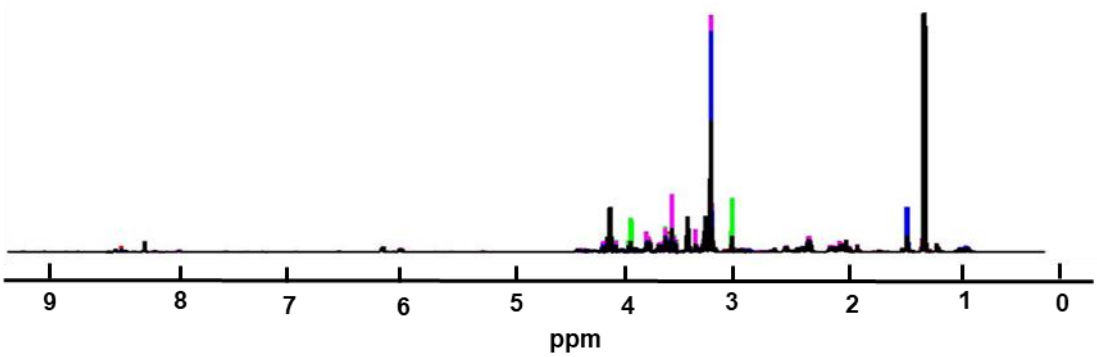

Figure 3.3 1D ^{1}H-NOESY NMR spectrum of cell extracts of 18 cell lines.

Showing an overlay of 103 ^{1}H-NOESY NMR spectra of intracellular polar samples extracted from AML, CML, MM, BL and DLBCL cells. The spectral regions including water and TMSP resonance peaks were excluded. Key; red: AML, green: CML, blue: BL, black: DLBCL, magenta: MM.

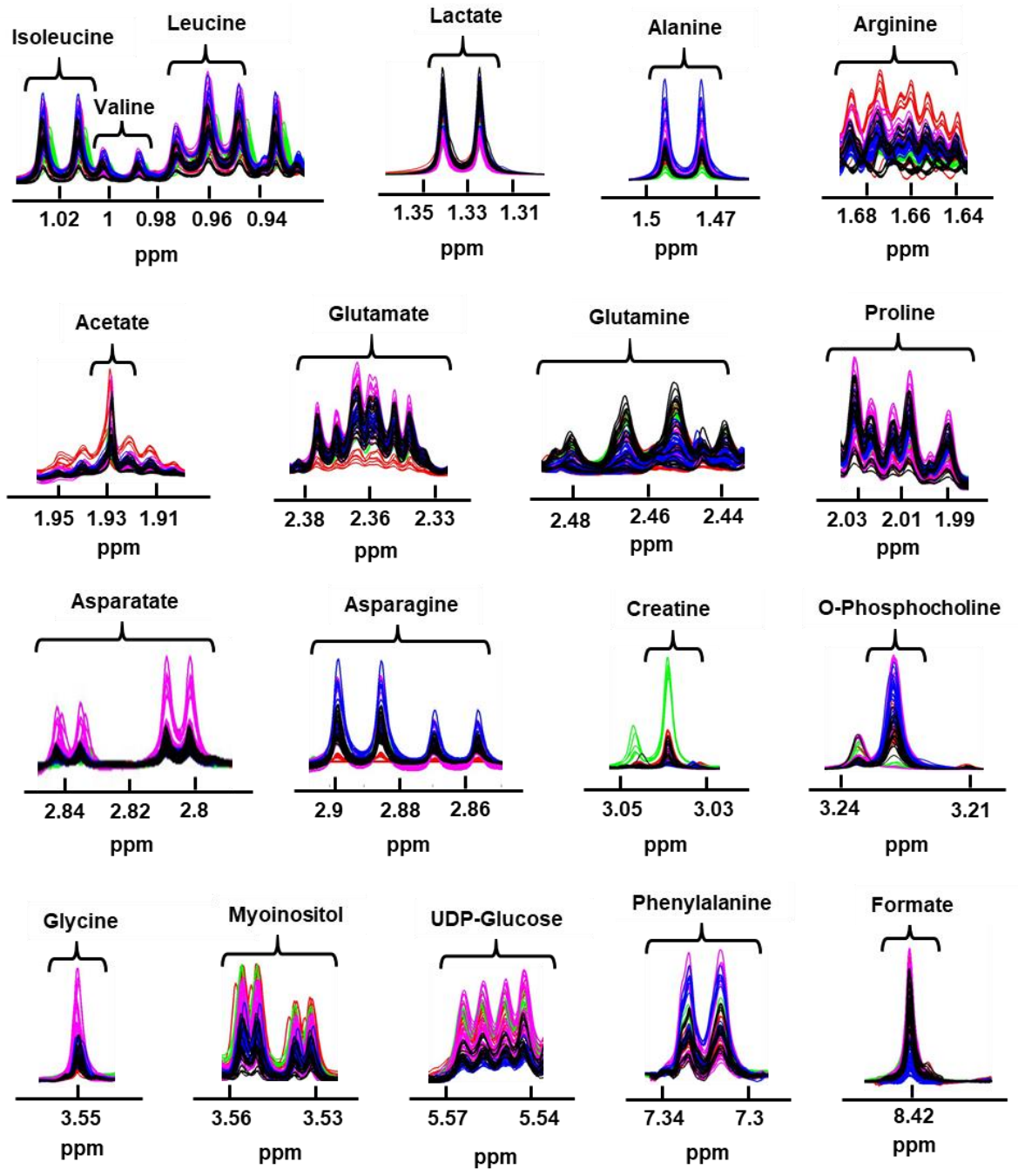

Figure 3.4 Assignment of intracellular metabolites.

Metabolite assignments in 103 1D ^{1}H-NMR spectra of intracellular polar samples from AML (red), CML (green), MM (magenta), BL (blue) and DLBCL (black) cell lines.

3.2.4 Glucose and one carbon metabolism in blood cancer cells

The high glycolytic rate and glucose catabolism forming lactate even with ample oxygen has been regarded as the most ubiquitous metabolic phenotype in cancer cells (Hsu & Sabatini, 2008). For this reason, metabolites that could be directly or indirectly *de novo* synthesised from glucose (see Figure 3.5) were studied across the 18 cell lines from different haematological cancer types.

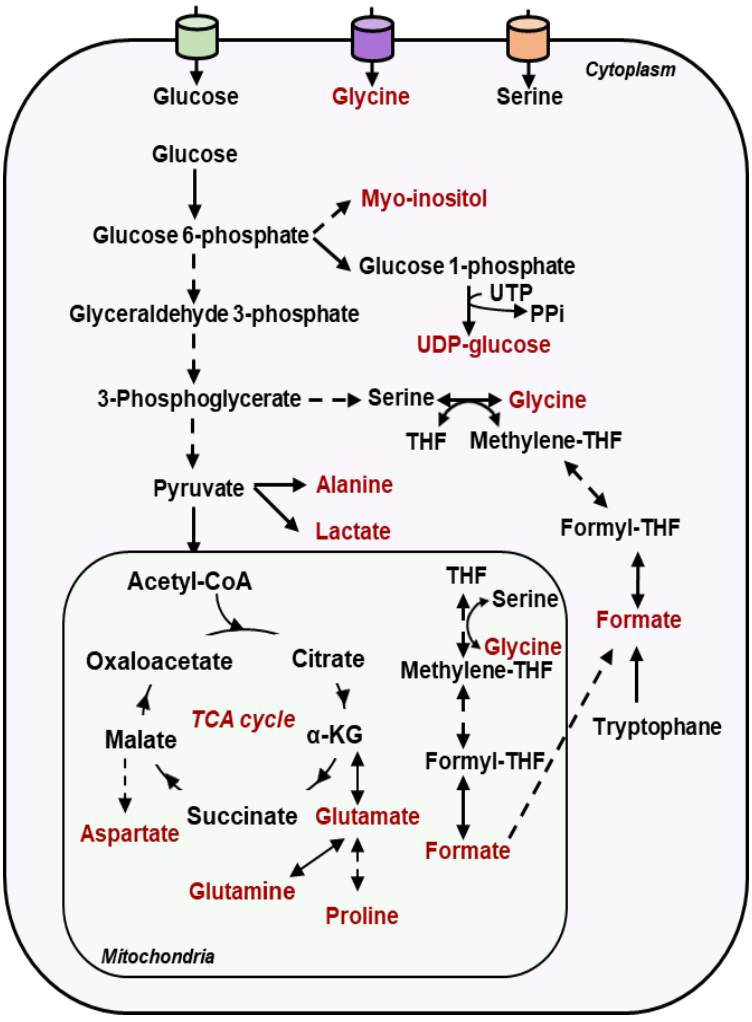

Figure 3.5 Major metabolic pathways.

Glycolysis, the TCA cycle and the folate cycle are the major pathways of central metabolism. Glycolysis gives rise to several precursor metabolites for the biosynthesis of other macromolecules. In glycolysis, glucose is converted into pyruvate. Glucose-6-phosphate is a glycolytic intermediate that lies at the crossroads of synthesis of myo-inositol and UDP-glucose. The glycolytic intermediate 3-phosphoglycerate can be converted into serine. Serine can be converted to glycine yielding methylene tetrahydrofolate (THF) which starts the folate cycle. The enzymes involved in the folate cycle are expressed in both the mitochondria and cytosol. Serine and glycine can be also imported from the extracellular environment. The glycolytic product pyruvate is converted to acetyl-CoA, which enters the TCA cycle.

Lactate was found at a higher level in CML, DLBCL and BL cells than AML and MM cells (see Figure 3.6.A). The least lactate production was observed in MM cells with the exception of JJN3 cells. On the other hand, MM and BL cells exhibited a higher alanine level than that in AML, CML and DLBCL cells (see Figure 3.6.B), suggesting that there may be a negative correlation between lactate and alanine in haematological cancer cells, as pyruvate can be converted to either lactate, alanine or acetyl-CoA. However, the Pearson correlation test did not reveal a significant negative association between alanine and lactate in haematological cancer cells (see Figure 3.6.C).

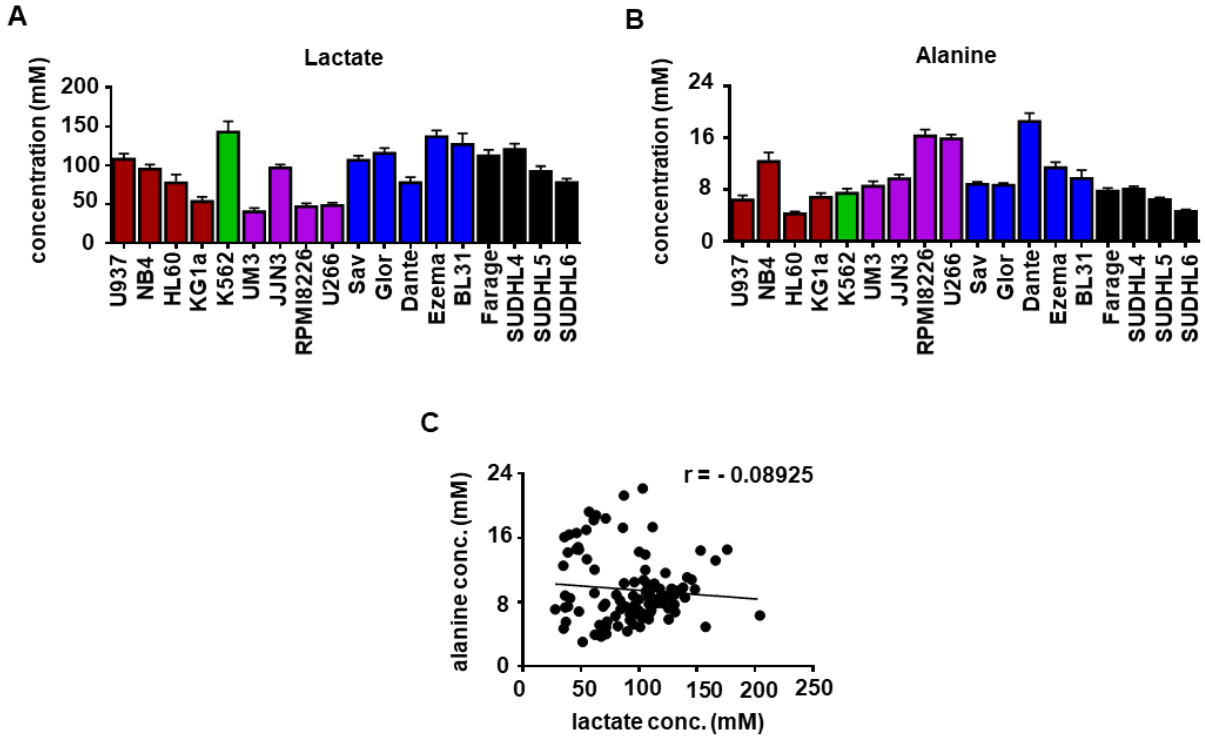

Figure 3.6 Graphical demonstration of the quantification of lactate and alanine.

Signal intensities of lactate (A) and alanine (B) across the 18 haematological cancer cell lines which represent AML (red), CML (green), MM (magenta), BL (blue) and DLBCL (black). Correlation between alanine and lactate in AML, CML, MM, BL and DLBCL cell lines (C). Bar graphs represent mean ± SEM, with n=6. Pearson rank correlation coefficient (r) was used to

detect associations between metabolites.

Cells require one-carbon units for the production of nucleotides to support the high proliferation rate of cancer cells (Newman & Maddocks, 2017). Serine, which can be synthesised from glucose or taken up from the extracellular environment, is a major source for maintenance of one carbon units which leads to formation of glycine and formate (see Figure 3.5). Figure 3.7.A and Figure 3.7.B demonstrate that U266 and K562 cells, which represent MM and CML respectively, had the largest amount of glycine and formate. The Pearson correlation was applied to show the relationship between the level of glycine and formate in haematological cancers. A significant positive correlation between glycine and formate was observed in the combined dataset that contains data from AML, CML, MM, DLBCL and BL cells (see Figure 3.7.C),

The production of lactate through aerobic glycolysis indicates the rate of glucose metabolism in cells (Vazquez et al., 2010). Even though lactate production was highest in BL and DLBCL, the level of UDP-glucose and myoinositol, which are synthesised from glucose was observed less in BL and DLBCL than other haematological cancers (see Figures 3.7.D and 3.7.E).This finding may suggest that glucose 6-phosphate derived from glucose in BL and DLBCL cells is mostly used to produce lactate rather than synthesis of UDP-glucose and myoinositol.

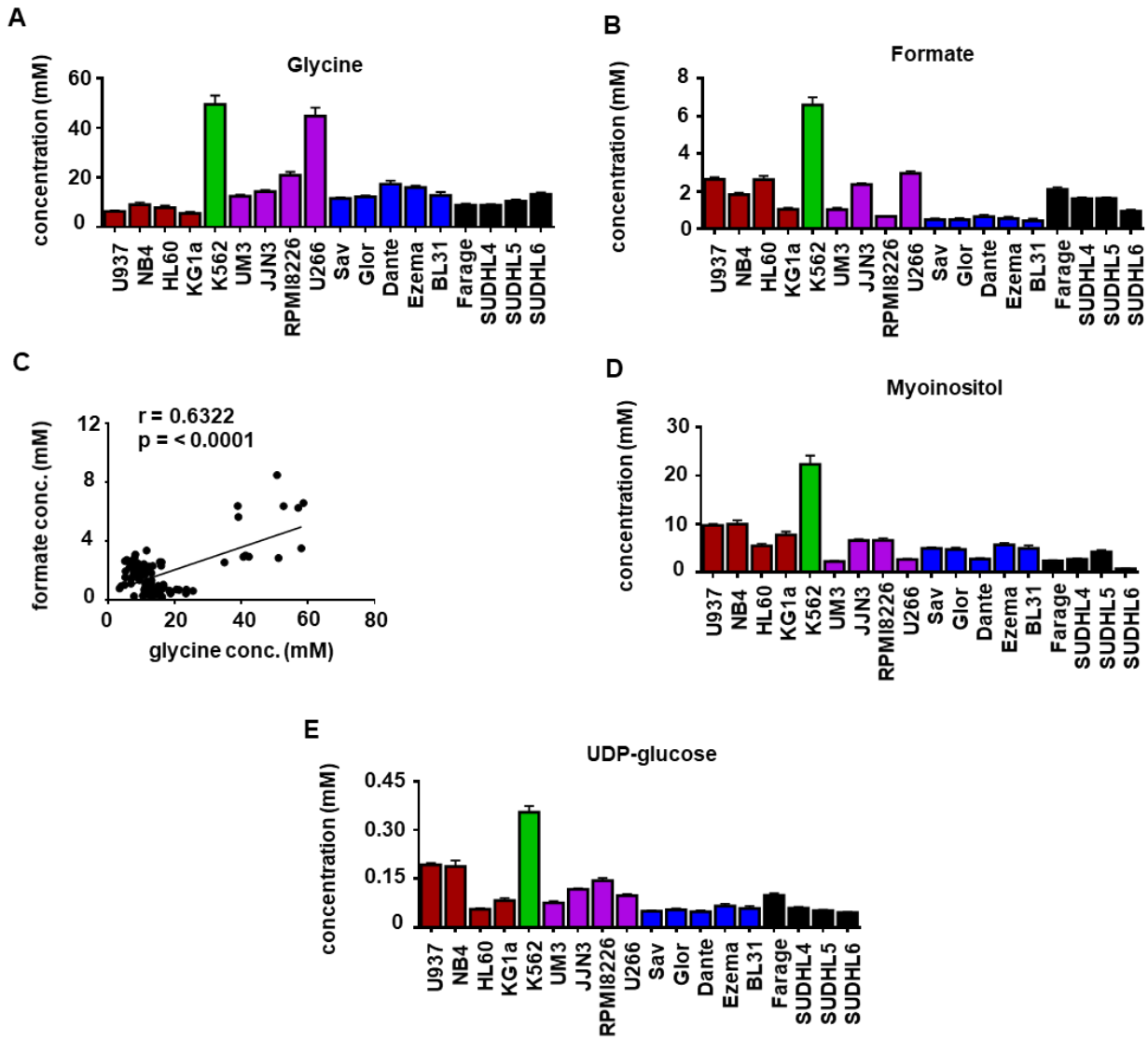

Figure 3.7 Graphical demonstration of the quantification of intracellular metabolites involved in glucose metabolism.

Signal intensities of glycine (A) and formate (B) across the 18 haematological cancer cell lines which represent AML (red), CML (green), MM (magenta), BL (blue) and DLBCL (black). Correlation between formate and glycine in AML, CML, MM, BL and DLBCL cells (C). Peak intensities of myoinositol (D) and UDP-glucose (E) across the 18 haematological cancer cell lines. Bar graphs represent mean ± SEM, with n=6. Pearson rank correlation coefficient (r) was used

to detect associations between metabolites.

3.2.5 The TCA cycle and amino acid metabolism in blood cancer cell lines

In the light of the accepted belief that cancer cells exhibit substantial alterations in the TCA cycle (Hammoudi et al., 2011), metabolites relative to the TCA cycle were studied to uncover how or to what extent different types of haematological cancers rely on the TCA cycle. 1D ^{1}H-NMR spectra showed that acetate levels in different cell line cells were in a similar range except for NB4, KG1a, JJN3, U266, and SUDHL6 cells (see Figure 3.8.A). The levels of glutamate, glutamine and succinate were almost the same in different BL cell line cells except for glutamine level in Ezema cells. By contrast, the levels of these metabolites noticeably varied across the AML, CML, DLBCL, and MM cells (see Figures 3.8.B - 3.8.D).

Glutamine is an important anaplerotic source of carbons for the TCA cycle. In cells, glutamine is converted to glutamate and next to α-KG. So, the association between glutamate and glutamine was studied to understand whether or to what extent a relationship between glutamate and glutamine is present in haematological cancers. In addition, the correlation between succinate and glutamate was questioned to see whether glutamate fuels the TCA cycle in haematological cancers. The Pearson correlation test was used to probe for relationship between the TCA cycle intermediates in AML, CML, BL, DLBCL and MM cells. This analysis demonstrated that there are pronounced positive significant associations between succinate and glutamate and also between glutamate and glutamine in haematological cancer cells (see Figures 3.8.E and 3.8.F).

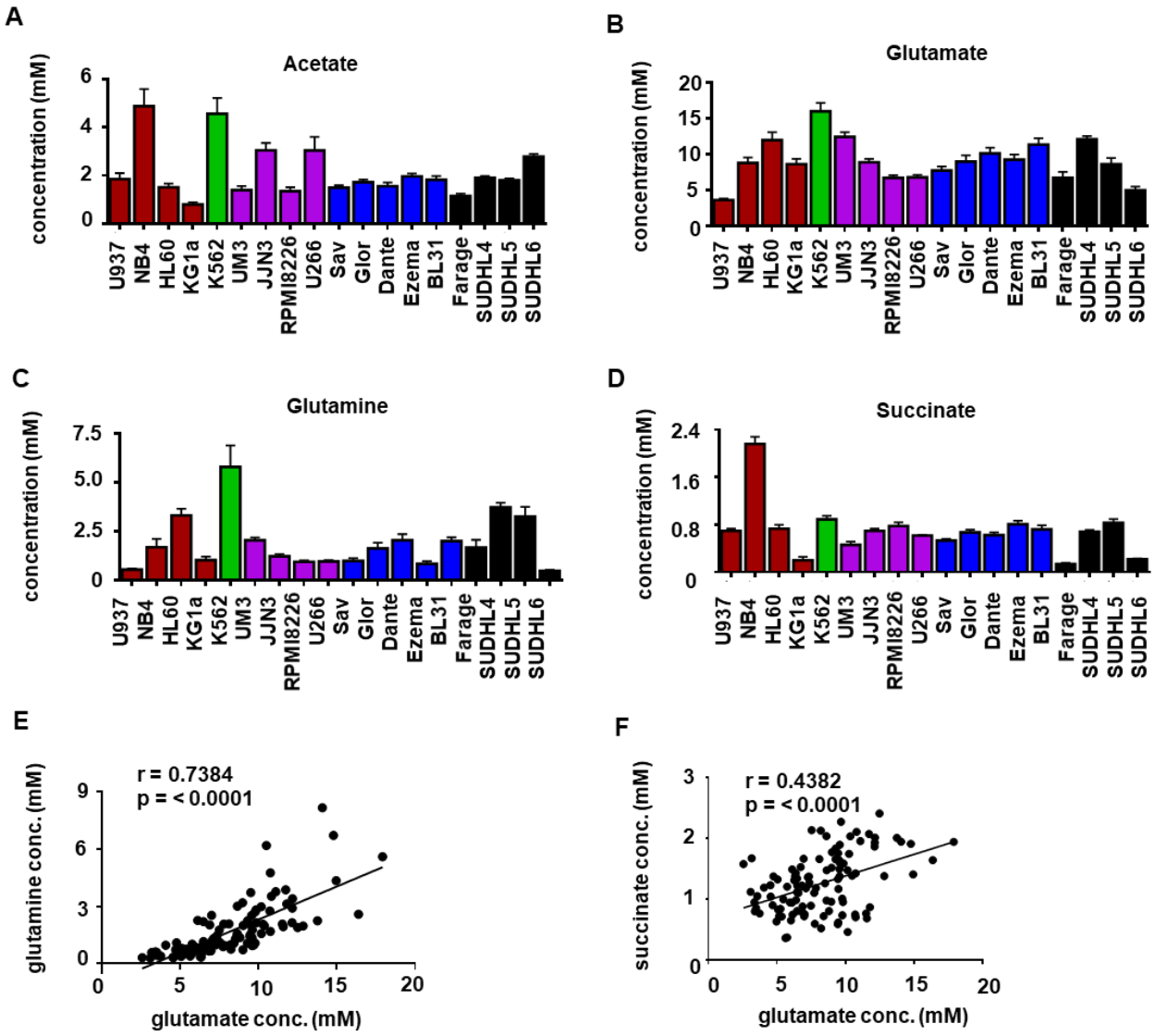

Figure 3.8 Graphical demonstration of the quantification of intracellular metabolites involved in TCA cycle and glutamine metabolism.

Peak intensities of acetate (A), glutamate (B), glutamine (C) and succinate (D) across the 18 haematological cancer cell lines which represent AML (red), CML (green), MM (magenta), BL (blue) and DLBCL (black). Correlation between glutamate and glutamine (E). Correlation between glutamate and succinate (F). Bar graphs represent mean ± SEM,

with n=6. Pearson rank correlation coefficient (r) was used to uncover associations between metabolites in AML, CML, MM, BL and DLBCL cells.

The levels of aspartate and proline noticeably varied across the AML, CML, DLBCL, BL and MM cells (see Figures 3.9.A and 3.9.B). The other noteworthy metabolite choline, which plays a key role in the formation of the cell membrane and serves as a precursor for many signalling molecules, was found at lower levels in K562 cells and higher levels in UM3, U266, Sav, Glor, Ezema and BL31 (see Figure 3.9.C). Furthermore, the comparison of the intracellular arginine level revealed that there is no remarkable difference for the level of arginine between cell lines except for NB4 and Farage cells (see Figure 3.9.D). NB4 cells had the highest level of arginine while the Farage cells possessed the smallest amount of arginine.

Arginine mainly acts as a nitrogen donor and maintains the nitrogen balance in cells. Aside from the maintenance of nitrogen balance, arginine is also used to generate creatine that supplies cellular adenosine triphosphate reservation by the generation of phosphocreatine. The most abundant amount of cellular creatine was found in K562 cells whereas the least amount of creatine was observed in BL cells (see Figure 3.9.E).

The levels of BCAAs and phenylalanine greatly varied across the haematological cancer cell lines (see Figures 3.10.A - 3.10.D). Although leucine and isoleucine levels were rather high in MM cells, the level of valine in MM cell lines except for U266 cells was found much lower compared to valine levels in other cells from different haematological cancer subtypes. Since the System L-amino acid transporters (LATs) mediate transport of BCAAs and phenylalanine (see Figure 3.11.A), the correlation between these amino acid levels was investigated. The Pearson correlation test revealed that there is a strong correlation

with a very high statistical significance between leucine and isoleucine valine and phenylalanine (see Figures 3.11.B - 3.11.D).

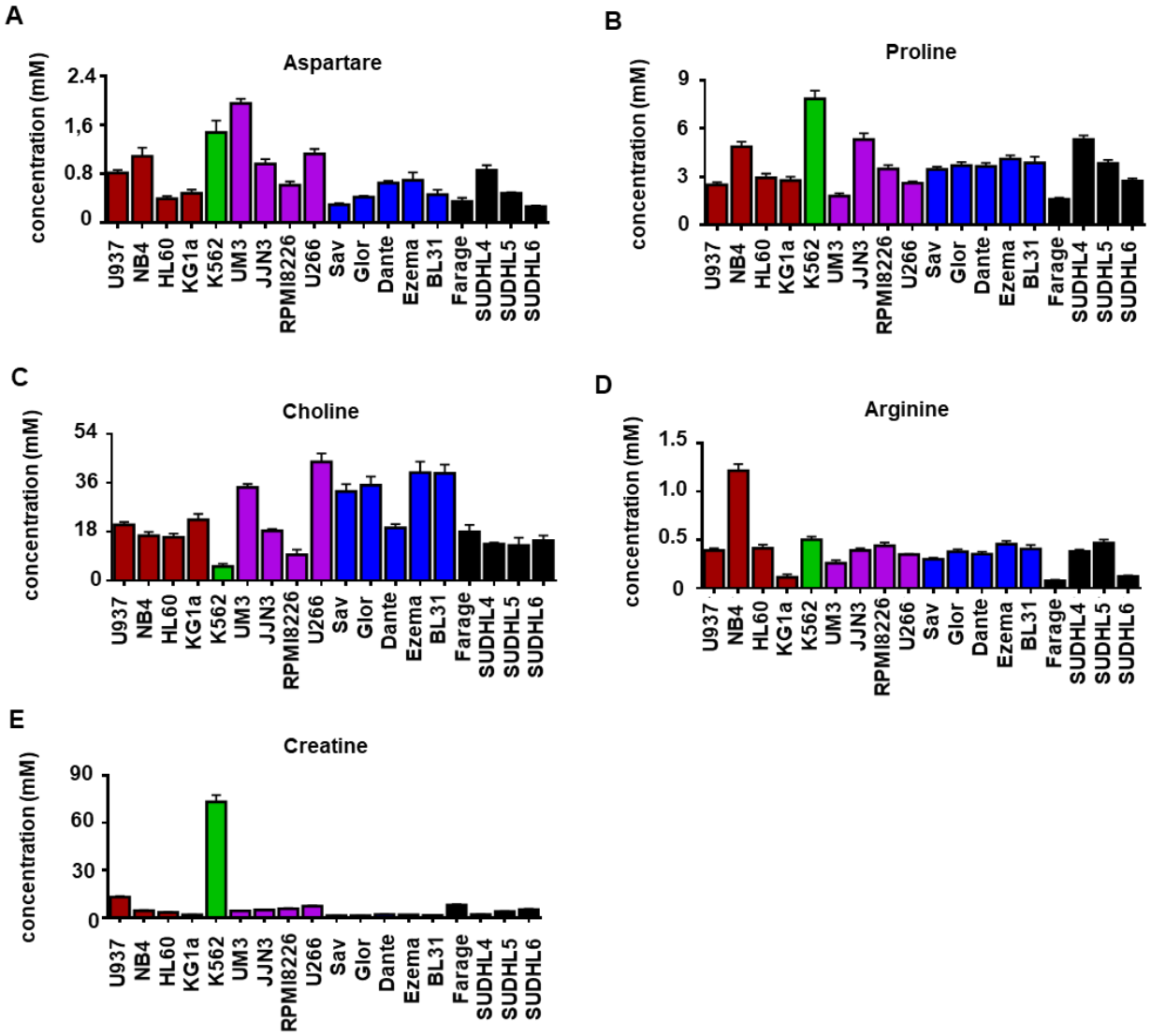

Figure 3.9 Graphical demonstration of the quantification of metabolites.

Peak intensities of aspartate (A), proline (B), choline (C), arginine (D) and creatine (E) across the 18 haematological cancer cell lines which represent AML (red), CML (green), MM (magenta), BL (blue) and DLBCL (black). Bar graphs represent mean ± SEM, with n=6.

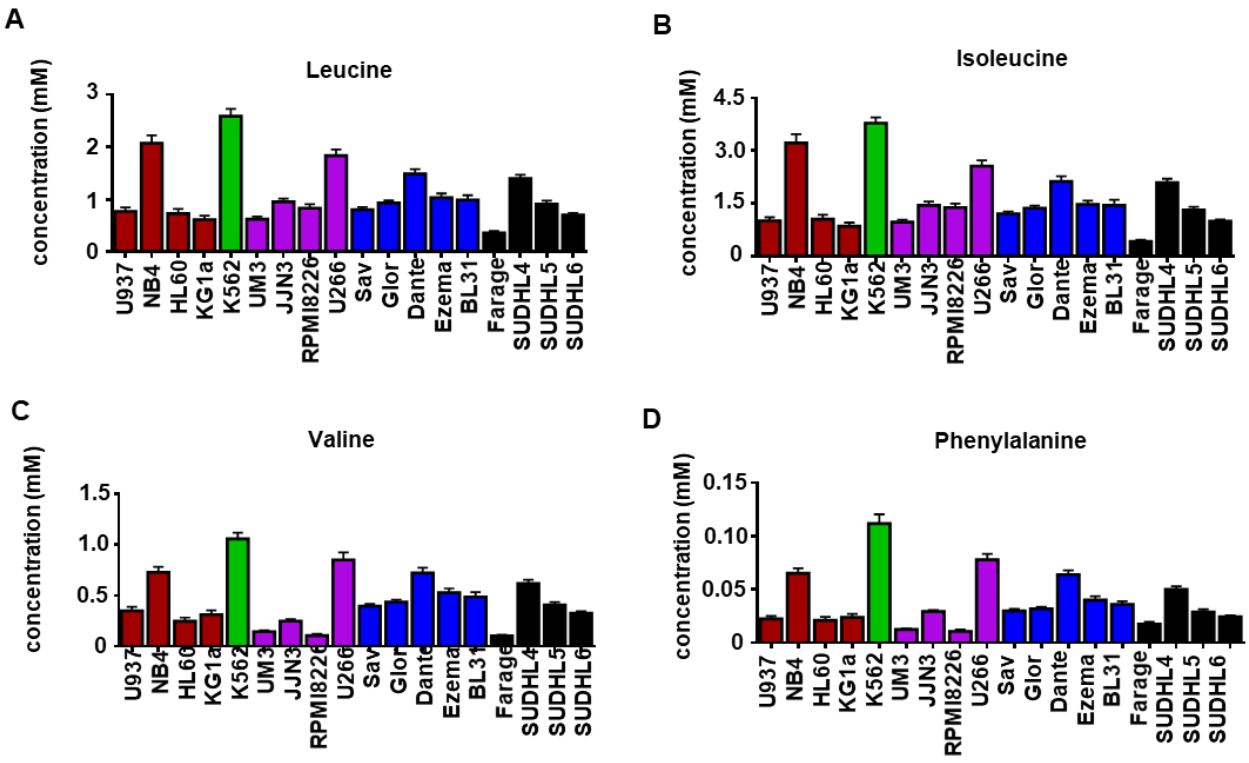

Figure 3.10 Illustration of the quantification of intracellular amino acids.

Signal intensities of leucine (A), isoleucine (B), valine (C) and phenylalanine (D) across the 18 haematological cancer cell lines which represent AML (red), CML (green), MM (magenta), BL (blue) and DLBCL (black). Bar graphs represent mean ± SEM, with n=6.

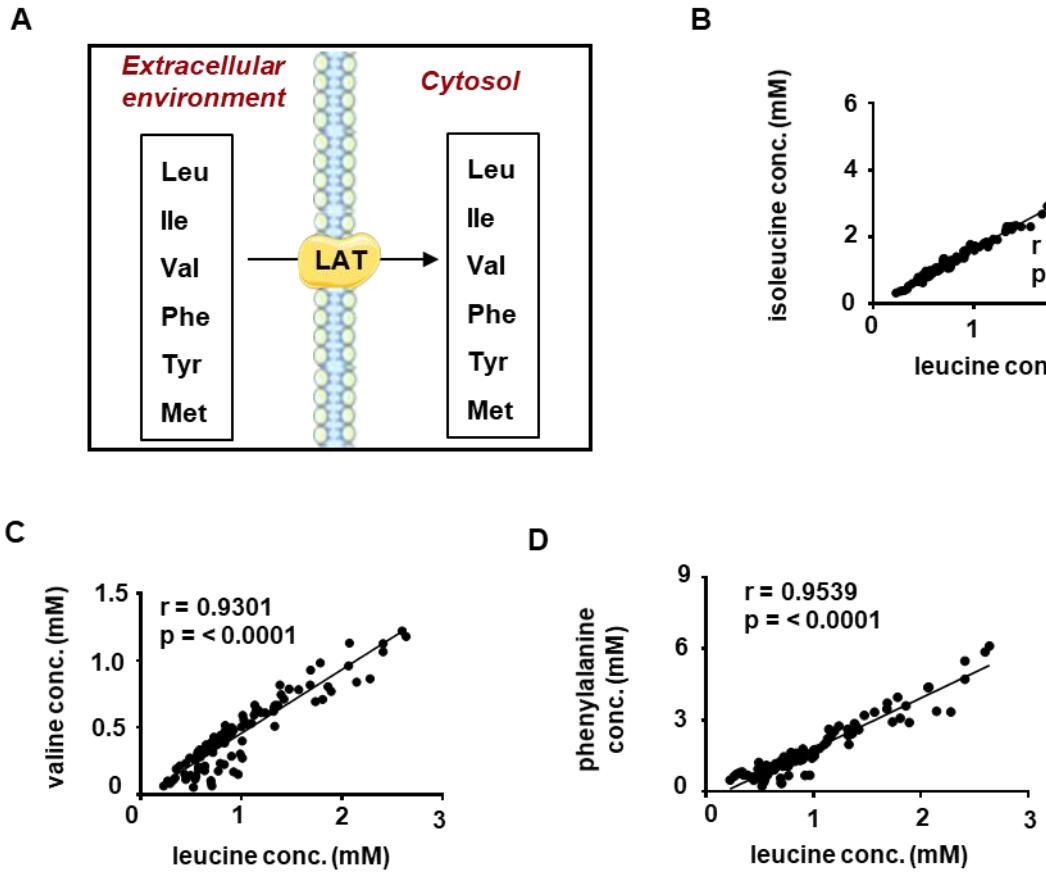

Figure 3.11 Relationships between the intracellular levels of metabolites.

Illustration of transport of BCAAs, phenylalanine, tyrosine and methionine by the LAT-1 transporter (A). Correlation between isoleucine and leucine(B). Correlation between valine and leucine (C). Correlation between phenylalanine and leucine (D). Pearson rank correlation coefficient (r) was used to uncover associations between metabolites in AML, CML, MM, BL and DLBCL cells.

3.2.6 NMR spectroscopy monitors the production and consumption of metabolites

Analysis of spent culture media provides crucial information about metabolic components which cancer cells consume and produce. To further understand the metabolic profiles of haematological cancers, 1D ^{1}H-NMR spectra of the cell-free extracellular medium and the conditioned media from AML, CML, BL, DLBCL and MM were acquired and analysed.

Analysis of the lactate peak from 1D ^{1}H-NMR spectra of conditioned media revealed that AML and CML cells, with the exception of KG1a cells, secreted the largest amount of lactate to their environments compared to lactate levels in the media of MM, BL and DLBCL cells (see Figure 3.12.A). AML cells, U937, HL60 and KG1a were shown to harbour the highest level of alanine in their media (see Figure 3.12.B). The extracellular alanine level of MM cells was pretty high in comparison with the extracellular alanine level of CML, BL and DLBCL cells. However, the lowest extracellular alanine level was observed in the conditioned medium of K562 cells despite the observation of large amounts of lactate in K562 cells.

Whilst myoinostol and glycine levels in cell culture media noticeably varied across AML and MM cell line cells, the media of distinct BL cell line cells contained similar amounts of myoinositol and glycine (see Figures 3.12.C and 3.12.D). This was the case for extracellular myoinositol and glycine in DLBCL cells with the exception of Farage cells for which myoinositol levels were greater than for most other cells. Interestingly, the amount of glycine in the media of U937, KG1a, K562, RPMI8226 and U266 cells more than that of the original cell culture medium. This observation demonstrates that the secretion of intracellular glycine into extacellular environment exceeded the uptake of extracellular glycine for U937, KG1a, K562, RPMI8226 and U266 cells.

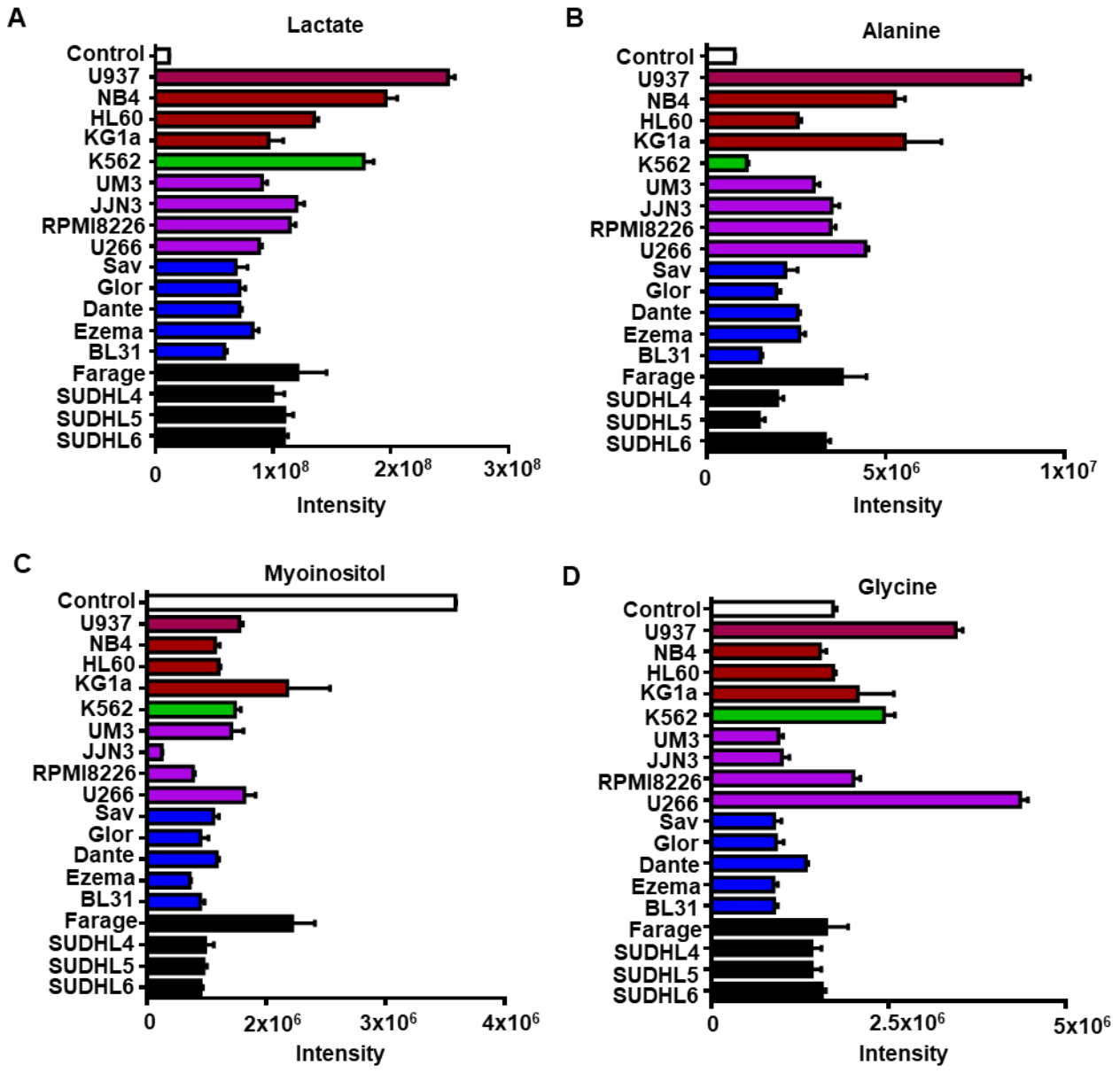

Figure 3.12 Graphical illustration of the comparison of extracellular metabolites related to glucose metabolism.

Comparison of the intensities of lactate (A), alanine (B), myoinositol (C), glycine (D) in the cell culture media of AML (red), CML (green), MM (magenta), BL (blue) and DLBCL (black) cell line cells. Bar graphs represent mean ± SEM, with n=3.

The spectral assignment of branched chain amino acids (BCAAs) was carried out to show how or to what extent haematological cancer cells are dependent on extracellular BCAAs. Comparison of the BCAAs in conditioned media from cell lines compared to standard defined cell culture medium revealed that MM and BL cells prominently relied on extracellular leucine, isoleucine and valine (see Figures 3.13.A - 3.13.C). AML and CML cells showed less dependence on extracellular BCAAs than BL and MM cells. Intriguingly, the isoleucine level in media of U937 cells was higher than that of the standard defined cell culture medium, suggesting that the amount of isoleucine that was exported from U937 cells to the medium was greater than the amount of the isoleucine that was imported into U937 cells from medium. Because LAT transporters are responsible for the transport of all BCAAs across the plasma membrane (Barollo et al., 2016), the relationship between the amount of leucine and isoleucine and also between the amount of valine and leucine was demonstrated by applying Pearson correlation tests. This correlation test revealed a positive correlation between the leucine and isoleucine and between the leucine and valine (see Figure 3.13.D).

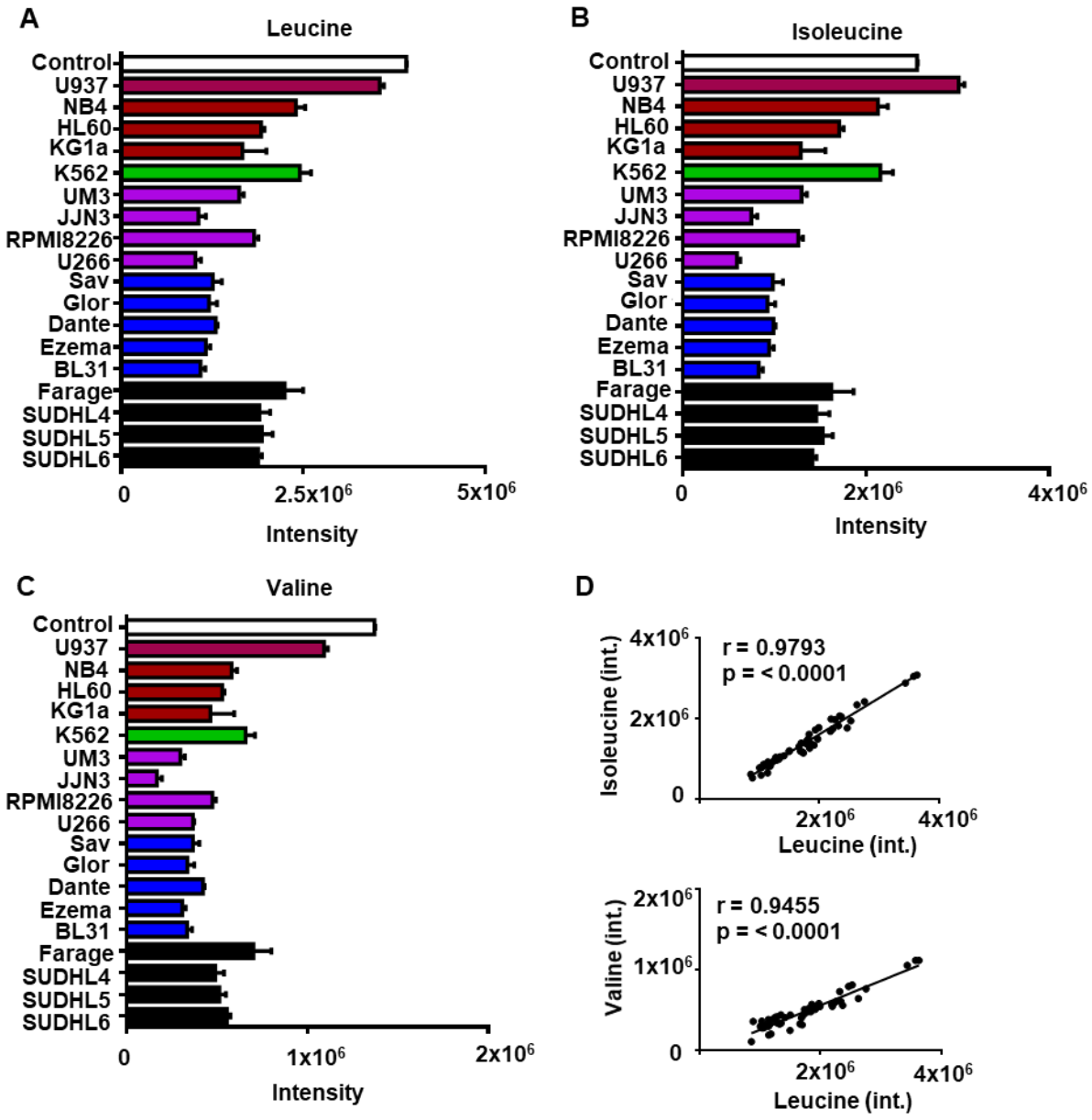

Figure 3.13 Graphical illustration of the comparison of extracellular BCAAs.

Comparison of the intensities of leucine (A), isoleucine (B), valine (C) in the cell culture media of AML (red), CML (green), MM (magenta), BL (blue) and DLBCL (black). Correlation analysis between leucine, isoleucine and valine in AML, CML, MM, BL and DLBCL cells using Pearson rank correlation coefficient (D). Bar graphs represent mean ± SEM, with n=3.

Furthermore, increases in the asparagine, aspartate and glutamate levels of the conditioned medium from U937 and K562 cells were observed (see Figures 3.14.A - 3.14.C). The glutamate level in conditioned media of AML, CML, MM and DLBCL was higher than the glutamate level in the cell-free cell culture medium, indicating that these cells, whilst potentially consuming glutamate, are releasing more into the media (see Figure 3.14.D). In contrast, the glutamate level in the conditioned media of BL cells was lower than the glutamate level in the cell-free cell culture medium (see Figure 3.14.D). This finding may suggest than BL cells consume a greater amount of glutamate than they release back into the media, hence the levels decrease in conditioned media.

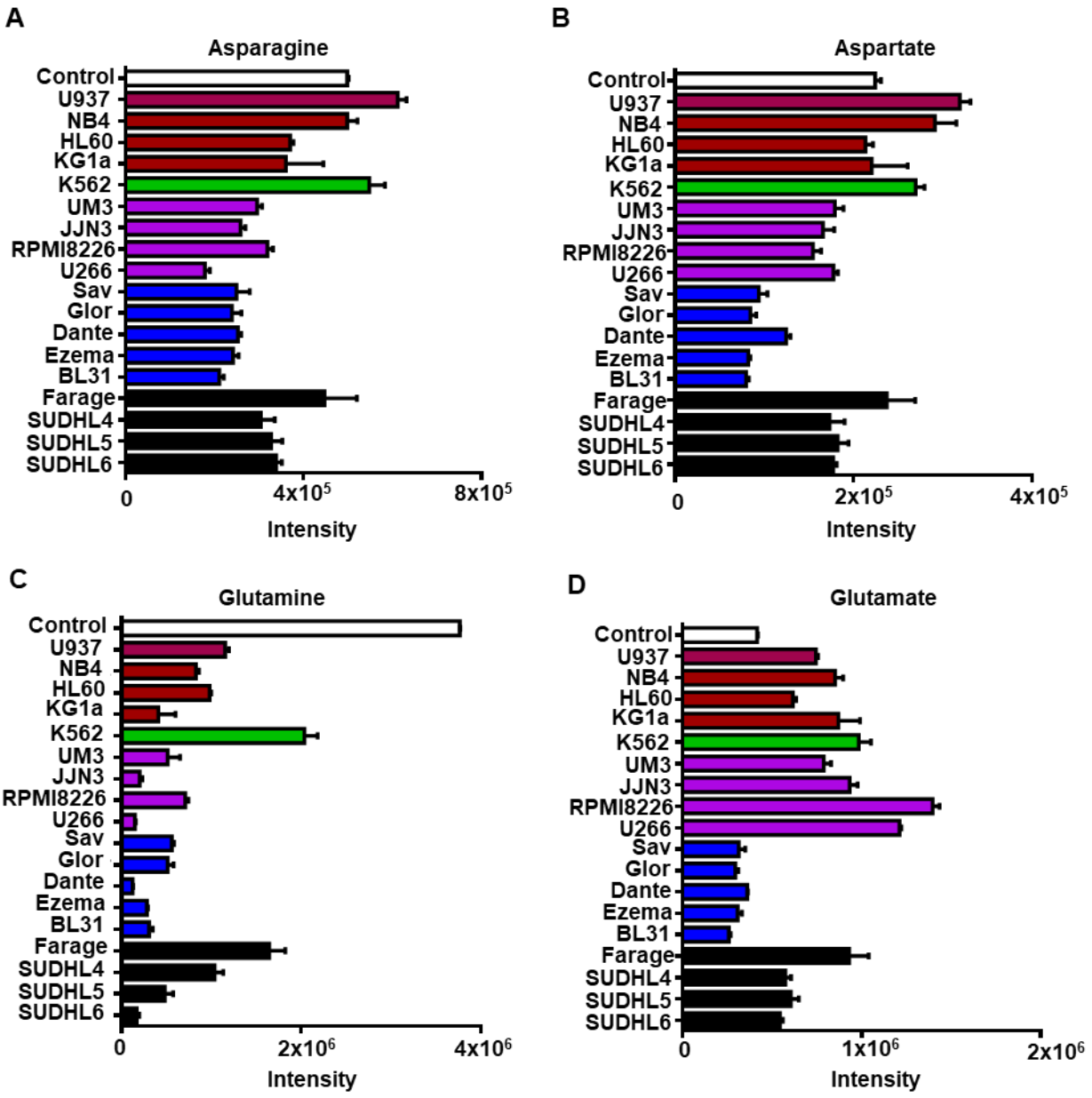

Figure 3.14 Graphical illustration of the comparison of extracellular amino acids.

Comparison of the intensities of asparagine (A), aspartate (B), glutamine (C) and glutamate (D) in the cell culture media of AML (red), CML (green), MM (magenta), BL (blue) and DLBCL (black). Bar graphs represent mean ± SEM, with n=3.

3.3 Discussion

3.3.1 1D ^{1}H-NMR spectroscopy to study metabolism in cells

Over the past two decades, 1D ^{1}H-NMR spectroscopy has emerged as one of the most useful tools to study metabolism in cells (Saborano et al., 2019). This is because every known organic compound has protons that resonate at a characteristic frequency. Because ^{1}H nuclei magnetically interact with neighbouring ^{1}H nuclei through scalar couplings, signals split with characteristic coupling constants; thereby providing additional information regarding the structure and environment (Dayrit & Dios, 2017).

In this study, 1D ^{1}H-NMR spectroscopy enabled us to identify and quantify complex multiple metabolites in cancer cells. However, narrow dispersion of ^{1}H chemical shifts and a large number of ^{1}H resonance signals inevitably create overlapped peaks with the different relative intensities on the NMR spectrum. Signal overlap in 1D ^{1}H-NMR spectrum complicates peak identification and metabolite quantification. For these reasons, only 22 intracellular and 13 extracellular metabolites were identified due to their distinctive signals in the relatively free-overlapping and uncrowded region in the ^{1}H-NMR spectrum using the NMRLab/MetaboLab software within Matlab. For example, citrate gives rise to multiplets at δ_H 2.5 ppm and δ_H 2.7 ppm (Dona et al., 2016). However, the citrate peaks at δ_H 2.5 and δ_H 2.7 ppm overlaps with glutathione and cystathionine respectively, i.e. this signal overlapping problem complicates obtaining quantitative information about the citrate amount. The other problem with the interpretation of 1D NMR spectrum was that ^{1}H protons from C-H units of the glucose backbone resonance between δ_H 3 - 5.5 ppm from the full range of δ_H 0- 10 ppm (A.-H. Emwas et al., 2019).

Hence, the occupation of the region δ_H 3 - 5.5 ppm by glucose peaks raises the probability of accidental overlaps. For instance, serine has signal multipltes at δ_H 3.8, δ_H 3.9 and δ_H 4.0 ppm (A.-H. Emwas et al., 2019). Nevertheless, some assigned metabolites still do not reflect the real cellular or extracellular amount of metabolites due to overlapping problem. For example, the lactate and threonine doublet peaks appear at δ_H 1.33 ppm, thus the measured lactate intensity in this study reflects the amount of lactate and threonine. However, this overlapping problem could be avoided by using Chenomx NMR Suite instead of NMRLab/MetaboLab software.

3.3.2 Differentiation between haematological cancers using PCA of ^{1}H-NMR spectroscopy

^{1}H-NMR spectroscopy detected a broad range of metabolites that allowed collection of a large data set for the haematological cancer cells in this study. PCA was carried out to reduce these big data sets in order to identify whether or to what extent any discrimination or similarity exists between haematological cancer cells and also between cancer cell lines from the same subtype of haematological cancers.

The PCA revealed a clear discrimination between AML, CML, BL and DLBCL cell lines. This could be reasoned by the subtype specific genetic mutations. For instance, PCA revealed a clear separation of K562 cells derived from a patient with CML in blast crisis, from AML cells (Pietarinen et al., 2015). Although CML cells in blast crisis present clinically like an acute leukaemia to a great extent, this sharp metabolic difference between AML cell lines and K562 cells was unexpected. This unexpected metabolic difference could be explained by the expression of the constitutively active tyrosine kinase oncoprotein BCR-

ABL in CML cells, since the BCR-ABL oncoprotein is reported to support proliferation, impaired transcriptional activity and survival (Cilloni & Saglio, 2012). As a result of oncogenic activity of BCR-ABL protein, CML cells could differently regulate metabolic pathways in comparison with AML cells.

Furthermore, the PCA score plot demonstrated that the biggest metabolic variation is present between different MM cell lines. This divergence in metabolic profiles of MM cells may reflect the existence of the widespread genetic heterogeneity in MM (Lohr et al., 2014). In contrast, the absence of separation of BL cell lines except for Dante, suggest that BL cells are metabolically highly similar. This remarkable overlap in metabolic features of BL cells may be a result of c-Myc overexpression (Scheller et al., 2010), which is the genetic hallmark of BL, as c-Myc regulates many aspects of metabolic processes such as glycolysis, glutaminolysis, and fatty acid oxidation (Chi V. Dang, 2013; Goetzman & Prochownik, 2018) leading to a typical Warburg effect signature.

3.3.3 Characterisation of the intracellular metabolic profile of haematological cancer cells

A semi-targeted NMR spectroscopy metabolomics approach was applied to identify intracellular metabolic profiles of different types of haematological cancers. This approach revealed the metabolic differences between AML, CML, MM, BL and DLBCL cells in this study.

This study revealed that lymphoma cells presented the most glycolytically oriented metabolic phenotype with a higher amount in intracellular lactate. The intracellular levels of lactate and aspartate are informative on the origin of the energy sources (Y.-J. Chen et

al., 2016), since the Warburg effect and the malate aspartate shuttle define cell's use of either glycolysis or OXPHOS to produce ATP. Thus, the levels of lactate and aspartate reflect how cancer cells rely on aerobic glycolysis and OXPHOS. For instance, a low level of aspartate was observed in BL cells while the highest amount of aspartate was found in MM cells that produced the lowest amount of lactate. These findings support that BL is the most glycolytic haematological cancer type while MM is the haematological cancer type that utilizes OXPHOS more than other types.

The elevated lactate in lymphoma cells relative to leukaemia and myeloma cells can be reasoned by the stabilisation of HIF-2α in normoxic conditions (Evens et al., 2008), c-Myc overexpression (Scheller et al., 2010, p.), gain-of-function mutations in EZH2 (Shen & Vakoc, 2015) or presence of tonic BCR signalling (survival of B cells in the absence of antigen) in lymphoma cells (Havranek et al., 2017). Limited O_2 supply stabilizes HIFs that develop numerous adaptive responses (Majmundar et al., 2010). In addition to genes related to hypoxia, HIFs were also found to directly promote aerobic glycolysis by activating the expression of LDHA, HK2, GLUT1 during hypoxia (Majmundar et al., 2010). However, lymphoma cells demonstrate normoxic HIF-2α stabilisation and a small amount of HIF-1α stabilisation (Evens et al., 2008). It can be speculated that the stabilisation of HIFs in lymphoma cells under normoxic conditions may be a driver of high lactate production in DLBCL and BL cells.

The other driver of aerobic glycolysis in the lymphoid cell is the B-cell antigen receptor (BCR), which is activated by antigen binding and not expressed by plasma cells which produce their secreted version, i.e., antibodies. BCR crosslinking following antigen encounter leads toa rapid increase in glucose uptake and glycolysis (Doughty et al., 2006).

However, DLBCL cells were found to display tonic BCR signalling which contributes to the survival of B cells in the absence of antigen stimulation activating multiple downstream effectors (Havranek et al., 2017). Since AML, CML and MM cells do not express BCR, which is massively expressed in GC cells, the observation of a high lactate level in lymphoma cells may be explained by the tonic BCR signalling in lymphoma cells in addition to other key drivers for aerobic glycolysis, such as c-Myc. Various types of c-Myc gene mutations, which induce over-expression and increased activity of LDH-A (Shim et al., 1997), are present in all BL patients and 5–15% of patients with DLBCL (Zhou et al., 2014).

The production of lactate through aerobic glycolysis indicates the rate of glucose metabolism in cells (Tiefenthaler et al., 2001). Even though lactate production was higher in BL and DLBCL, the level of UDP-glucose and myoinositol, which are produced from glucose 6-phosphate, was observed to be lower in BL and DLBCL cells compared to other haematological cancers. Myo-inositol inhibits the activity of PI3K (Kapral et al., 2017), and could thereby indirectly reduce aerobic glycolysis in cells as the PI3K pathway promotes the metabolic switch to aerobic glycolysis (L. Yu et al., 2017). From this point of view, we could explain why less glycolytic haematological cancer types, AML, CML and MM, were observed to have more myo-inositol.

One carbon metabolism is required for cells to support nucleotide synthesis thus benefits cancer cell survival (Newman & Maddocks, 2017). One carbon metabolism occurs both in mitochondria and cytosol. Formate is the key one-carbon unit for cells because of being transported between mitochondria and cytosol. For example, formate derived in mitochondria is exported to the cytosol to support the generation of serine from glycine

(Ducker & Rabinowitz, 2017). In this study, we observed that there is a significant negative correlation between glycine and formate in AML and MM cells. This negative association was unexpected, suggesting that this negative relationship between glycine and formate for AML and MM may have resulted from the translocation of mitochondrial formate to the cytoplasm and subsequent conversion of glycine to serine.

One of the most common metabolic alterations in cancer cells is the enhanced usage of glutamine (Cluntun et al., 2017). Besides being a constituent of proteins, glutamine acts as both an anaplerotic substrate for the TCA cycle and a nitrogen donor for the biosynthesis of nucleotides. As an anaplerotic substrate, glutamine is first converted to glutamate by the function of glutaminase. The correlation test that we applied revealed that the intracellular glutamate level is positively associated with intracellular glutamine and succinate levels in AML, CML, MM, BL and DLBCL cells. This finding shows that haematological cancers use glutamine to feed the TCA cycle. Moreover, the glutamate level detected in BL cells was relatively high compared to glutamate levels in other cells. Many studies have demonstrated that c-Myc transcription factor increases expression of glutaminase enzyme (P. Gao et al., 2009; D. Xiao et al., 2015). This observation could be the result of overexpression of c-Myc protein, which increases the expression of glutaminase enzyme, as BL cells are characterised by the overexpression c-Myc.

The most striking result was the detection of high amounts of creatine in the CML cell line K562. Phosphorylated creatine, known as phosphocreatine, serves as a rapidly mobilisable energy donor for ATP formation. This high level of creatine in CML cells suggests that K562 can use creatine to recycle ATP. However, creatine and phosphocreatine give resonance signals nearly at the same frequency in 1D ^{1}H-NMR

spectrum (Dewar et al., 2010). Thus, distinguishing creatine from phosphocreatine requires the application of other techniques such as reverse phase high-performance liquid chromatography (HPLC).

The identification of intracellular metabolites by 1D NMR approach helped us to describe the general metabolic profile of AML, CML, MM, BL and CML. However, an extended genome-wide association study is necessary to better understand metabolic traits quantified by 1D-NMR. In addition, the application of other techniques is required to better explore the altered metabolic pathways**.**

3.3.4 ^{1}H NMR metabolic profile of media samples

Another objective of this study was to investigate the differences between the extracellular metabolic profile of haematological cancer cells, i.e. the levels of metabolites in the media of cells. I used metabolomics data from 1D NMR spectroscopy to study nutrient consumption and metabolite accumulation within the media of AML, CML, MM, BL and DLBCL.

Lactate has often been seen as an useless by-product of anaerobic metabolism, needed to produce NAD^{+} during its formation from pyruvate to drive the productive phase of glycolysis. However, lactate has also been suggested as a metabolite serving as an alternate source of energy. For instance, lactate was found to be imported into cells and oxidised in mitochondria by cancer cells (Y.-J. Chen et al., 2016). In this study, I showed that AML and CML cells secreted high levels of lactate and alanine into their environment whereas their intracellular lactate level was quite low. I also demonstrated that BL cells produced more lactate and alanine but exported these metabolites less than AML and

CML cells. These findings could be explained by the activity of the lactate shuttle theory (Brooks, 2018) which suggests that the secreted lactate is imported into cells to be oxidised in the mitochondria for ATP production. It could be proposed that BL cells might actively use the lactate shuttle to maintain the TCA cycle.

The other key finding is the consumption of BCAAs by MM cells. I observed that there was a remarkable uptake of BCAAs from the extracellular environment MM cells. This addiction of BCAAs might have developed so that MM cells can meet demand for producing proteins and immunoglobulin light chains in large amounts, considering that MM are characterised by large amounts of abnormal proteins (Fairfield et al., 2016).

CHAPTER 4

BCAA METABOLISM IN MULTIPLE MYELOMA

4.1 Introduction

Cancer cells alter their metabolism in order to support their rapid cellular proliferation (Hsu & Sabatini, 2008). The increased glucose uptake in cancer cells is shown as a major characteristic of metabolic alteration. Apart from glucose, branched-chain amino acids (BCAAs; leucine, isoleucine, and valine) were described to be important for cancer cell proliferation and growth (Selwan & Edinger, 2017).

BCAAs are essential amino acids that must be provided by the diet. BCAAs are primarily oxidised in skeletal muscle and adipose tissue, whereas the other amino acids are mainly catabolised in the liver (Dewar et al., 2010). BCAAs are not only used for protein synthesis but also have unique properties with diverse physiological and metabolic roles. BCAAs were documented to participate in lipolysis, lipogenesis and glucose metabolism (Doi et al., 2003; Nishimura et al., 2010). For example, BCAAs were shown to promote the secretion of insulin (Nair & Short, 2005). In addition, leucine acts as a nonspecific carbon source of oxidation for production of energy in muscle cells, producing more energy than complete oxidation of glucose (Monirujjaman & Ferdouse, 2014). Besides playing a vital role in lipid and glucose metabolism in specific tissues, BCAAs were reported to participate in several signalling pathways, the most classic of which is the activation of the mTORC1 signalling pathway. mTORC1 plays a key role in regulating many fundamental cell processes. For instance, mTORC1 enhances protein synthesis, *de novo* lipid synthesis and glycolysis whilst it inhibits autophagy (Saxton & Sabatini, 2017). Among the three BCAAs, leucine has gained the greatest reputation for its role in the recruitment of mTORC1 to the lysosome (see Figure 4.1) (Yao et al., 2017).

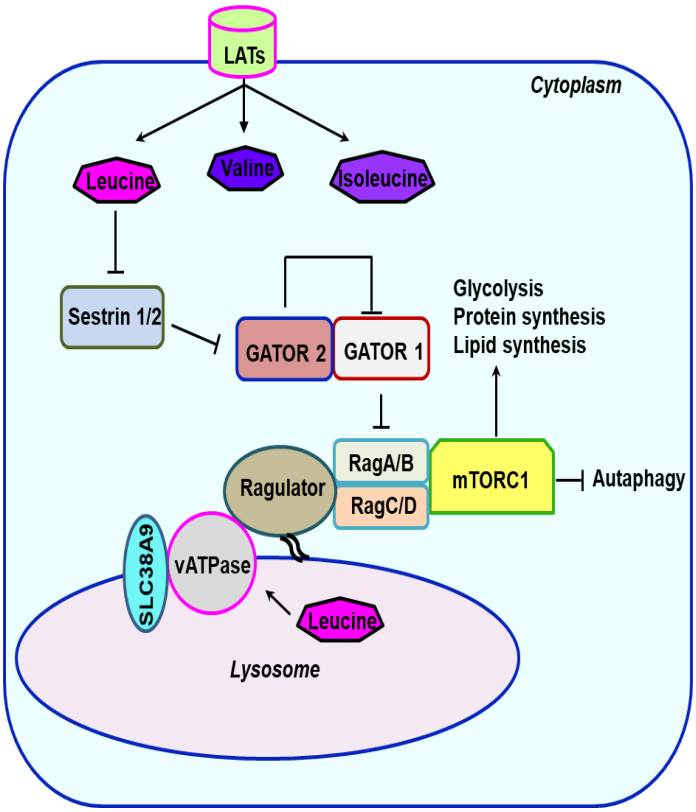

Figure 4.1 Schematic model of BCAAs uptake and leucine signalling to mTORC1.

Leucine, isoleucine and valine enter cells via the L-type amino acid transporters (LATs). Cytosolic leucine inhibits Sestrin1/2, leading to the activation of GATOR2 that inhibits GATOR1. Lysosomal luminal leucine activates vATPase. Then vATPase stimulates the activation of Ragulator, the guanine exchange factor (GEF) for RagA/B. The activation of the Rag heterodimer leads to the recruitment of mTORC1 to the lysosomal surface.

In recent years, many cancer cells have been shown to overexpress branched-chain amino acid aminotransferase 1 (BCAT1) enzyme, which catalyses a transamination reaction between glutamate and BCAAs in both directions (Selwan & Edinger, 2017; Tönjes et al., 2013; Zheng et al., 2016). In human gliomas, BCAT1 enhances glutamate excretion and promotes cell proliferation (Tönjes et al., 2013). The chemoresistance-inducing function of BCAT1 has been described in hepatocellular carcinoma (Zheng et al., 2016).

The critical requirement of extracellular BCAAs is reflected in the overexpression of L-type amino acid transporters (LATs) in many cancer cells (see Figure 4.1). LATs mainly transport neutral amino acids in a sodium independent manner. So far, LAT1, LAT2, LAT3

and LAT4 have been identified in different tissues. LAT1 transcripts are expressed in brain, spleen, testis, activated lymphocytes, pancreatic islet cells and blood-brain barrier cells while LAT2 mRNA is expressed in skeletal muscle, kidney, jejunum, ileum, fetal liver, prostate and ovaries (Q. Wang & Holst, 2015). LAT1 and LAT2 both interact with CD98 (4F2hc) through a conserved disulphide bridge and thus form a heterodimer (see Figure 4.2). CD98 is responsible for the plasma membrane localisation of LAT1 and LAT2 to transport BCAAs, phenylalanine, tyrosine, tryptophan and methionine in exchange for the intracellular glutamine (Kanai et al., 1998; Segawa et al., 1999). Conversely, LAT3 and LAT4 are monomeric amino acid transporters and display a narrow substrate selectivity (Q. Wang & Holst, 2015a). Expression of LAT3 is limited to skin, liver, muscle, prostate and pancreas whilst the expression of LAT4 is restricted to the placenta, kidney and peripheral blood leukocytes (Q. Wang & Holst, 2015a). A variety of cancer cells have been shown to predominantly overexpress LAT1 such as lung cancer and breast cancer and even though LAT2 has sequence similarity to LAT1 (Furuya et al., 2012; KAIRA et al., 2010; Kobayashi et al., 2005).

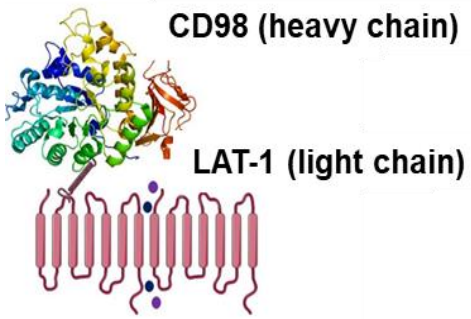

Figure 4.2 Schematic illustration of the structure of LAT1/CD98 heterodimeric transporter.
LAT1/CD98 heterodimeric transporter is a member of the SLC7 solute carrier family, which comprises CD98hc, also known as 4F2 antigen heavy chain, covalently links to LAT1 light chain (Singh & Ecker, 2018).

MM is characterised by the production of a high amount of non-functional immunoglobulins or immunoglobulin chains. Since MM cells need more amino acids to

produce immunoglobulins compared to other haematological cancer cells, they might be dependent on extracellular amino acids more than other cancer cells. In the previous chapter, MM cells were shown to take up more BCAAs than AML, CML, BL and DLBCL cells do. Given that leucine is required for the activity of mTORC1 that stimulates protein synthesis, MM cells might be dependent on extracellular leucine to support protein synthesis by enhancing mTORC1 activation. In addition, leucine is a ketogenic amino acid whose carbon skeleton can be catabolised for energy in the TCA cycle.

Based on these findings and observations, I aimed to further investigate the role of leucine in MM cells. In this chapter, BCAAs metabolism and expression level of LAT1/CD98 were studied in MM cells. The effects of inhibition of LATs by using specific inhibitors were explored using NMR spectroscopy and Celltiter Blue (CtB) assay.

4.2 Results

4.2.1 Multiple myeloma cells express CD98 more than other blood cancer cells

High quality ^{1}H NMR spectra from conditioned media samples of AML, CML, MM, BL and DLBCL revealed that MM cells take up more BCAAs than AML, CML, BL and DLBCL cells (see Figures 4.3.A - 4.3.C).

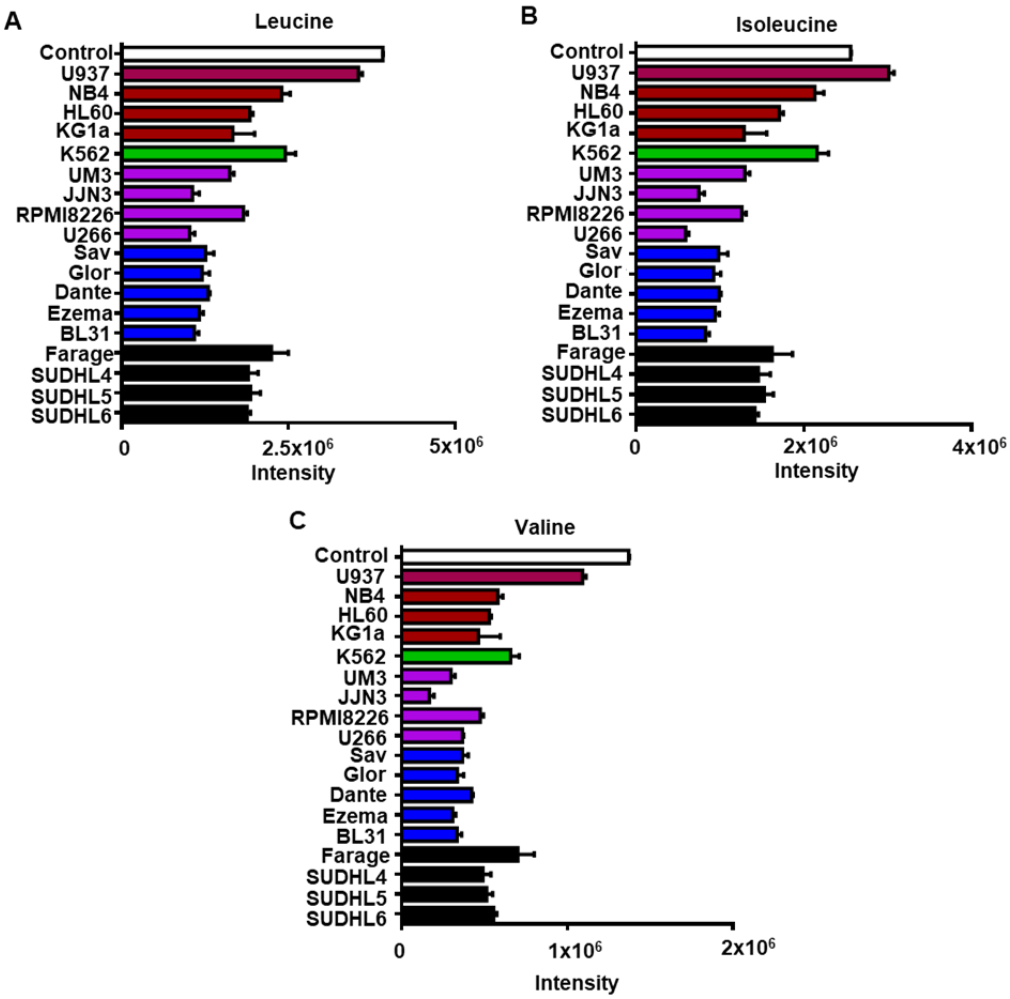

Figure 4.3 Graphical illustration of the comparison of extracellular BCAAs.

Comparison of the intensities of leucine (A), isoleucine (B), valine (C) in the cell culture media of AML, CML, MM, BL and DLBCL cell line cells.

To test whether MM cells express the LAT1 transporter on their cell surface to facilitate a high level of BCAAs uptake compared to AML, CML, BL and DLBCL cells, surface expression of LAT1/CD98 was examined by flow cytometry in AML cell line KG1a, CML cell line K562, MM cell lines U266 and JJN3, BL cell line Glor and DLBCL cell line Farage. Surprisingly, LAT1 surface level was found to be at the lowest level in MM cells and at the highest level in Farage and K562 cells (see Figure 4.4.A). However, flow cytometry analysis revealed that CD98 heavy chain was mostly present on the plasma membrane of MM cells (see Figure 4.4.B). The lowest level of CD98 surface staining was observed in K562 and Farage cells that exhibited the lowest BCAAs uptake compared to other cells. Then, I investigated whether or to what extent, an association between leucine uptake and the surface levels of CD98 and LAT1 is present. The Pearson correlation test analysis revealed that the amount of leucine left in the cell culture medium of U266, JJN3, Glor, SUDHL6, Farage, KG1a and K562 was negatively correlated with CD98 and positively correlated with LAT1 (see Figures 4.4.C and 4.4.D). These findings suggest that although the LAT1/CD98 transporter is comprised of CD98 heavy chain and LAT1 light chain the surface level of CD98 determines the level of BCAAs uptake from the extracellular environment in haematological cancer cells.

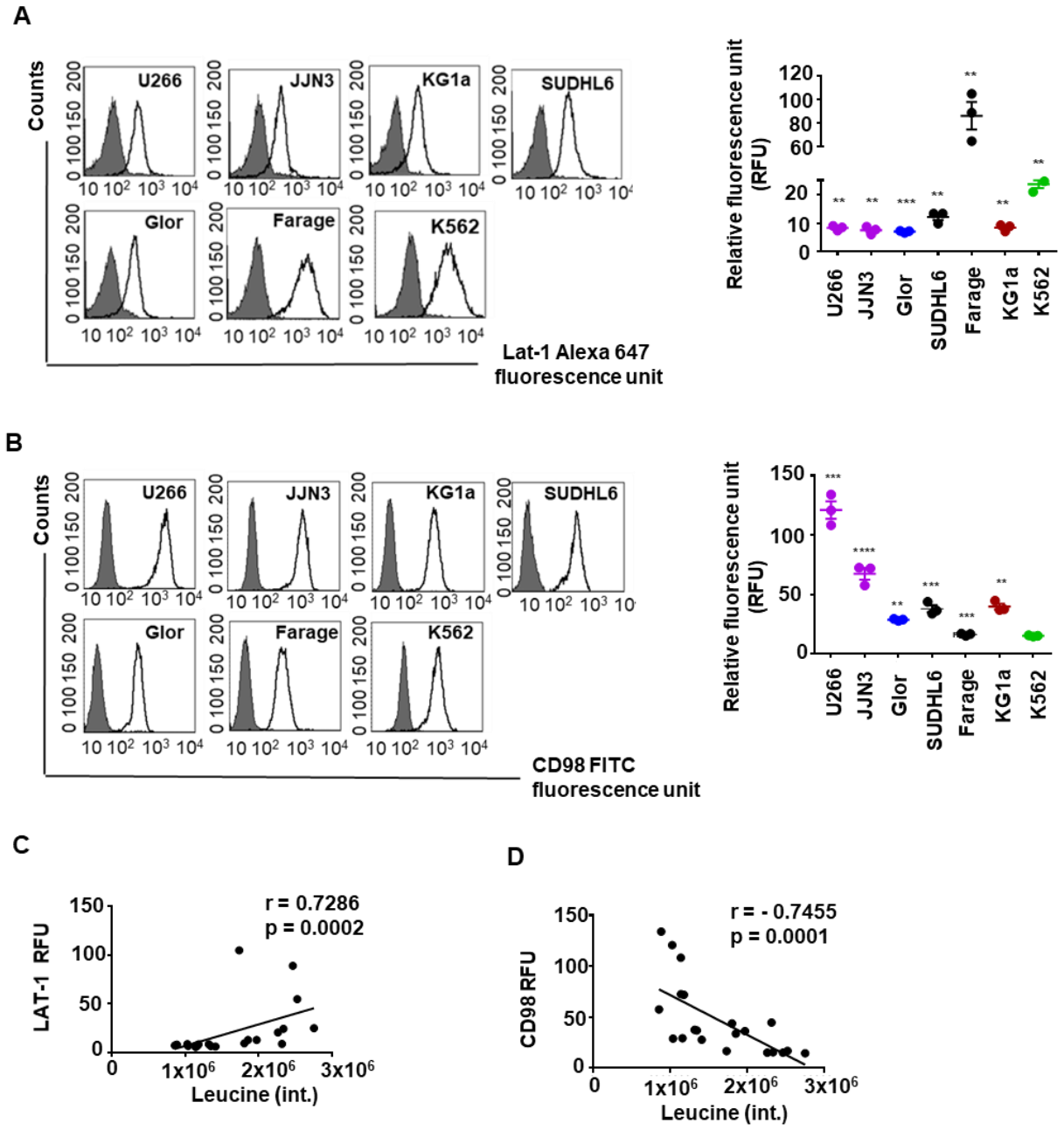

Figure 4.4 Cell surface expression of CD98 and LAT1.

Flow cytometry analysis showing the relative fluorescence units (RFU) of LAT1 (A) and CD98 (B). Black and white peaks represent isotype control and stained samples respectively. Bar graphs display the geometric mean of fluorescence intensities of CD98 and LAT1 divided by geometric mean of fluorescence intensities of unstained samples. Correlation analysis between leucine and CD98 (C) and between leucine and LAT1 (D) using Pearson rank correlation coefficient.

4.2.2 Catabolism of leucine in multiple myeloma cells

To find out whether leucine is metabolised in MM cells, $40x10^6$ U266, JJN3 and Farage cells were cultured with [U-^{13}C]-leucine for 48 hours. After metabolite extraction, 2D ^{1}H-^{13}C HSQC NMR spectroscopy was performed to analyse the metabolites derived from [U-^{13}C]-leucine (see Figure 4.5.A). Farage cell line was chosen to see how cancer cells less dependent on extracellular leucine metabolise the ^{13}C enriched leucine.

The production of [3-^{13}C]-glutamate and [3-^{13}C]-glutamine was detected in U266 and JJN3 cells (see Figures 4.5.B and 4.5.C). The ^{13}C incorporation into glutamate and glutamine shows that leucine is metabolised to produce acetyl-CoA in MM cells. As shown in Figure 4.5.A, leucine yields acetyl-CoA and acetyl-CoA derived intermediates. Briefly, acetyl-CoA molecules originating from [U-^{13}C]-leucine enters the TCA cycle. The entry of [1,2-^{13}C]-acetyl-CoA into TCA cycle results in ^{13}C carbons in citrate, isocitrate and α-KG. Thus, the detection of glutamate ^{13}C labelled at position 3 and 4 in U266 and JJN3 cells shows that glutamate was synthesised by transamination of α-ketoglutarate derived from leucine. In addition to ^{13}C labelled glutamate, ^{13}C enrichment in glutamine was also observed in U266 cells. The ^{13}C labelled glutamine could be produced from ^{13}C labelled glutamate by the activity of glutamine synthetase. The ^{13}C incorporation into glutamine was around 10% in U266 cells while the [U-^{13}C]-leucine was not metabolised to glutamine in JJN3 cells. Interestingly, I also identified large amounts of [11-^{13}C]-N-acetylneuraminic acid (Neu5Ac) originating from [U-^{13}C]-leucine in U266 and JJN3 cells (see Figures 4.5.B and 4.5.C). By contrast, ^{13}C enrichment in glutamine and Neu5Ac was not observed in Farage cells (see Figure 4.5.D).

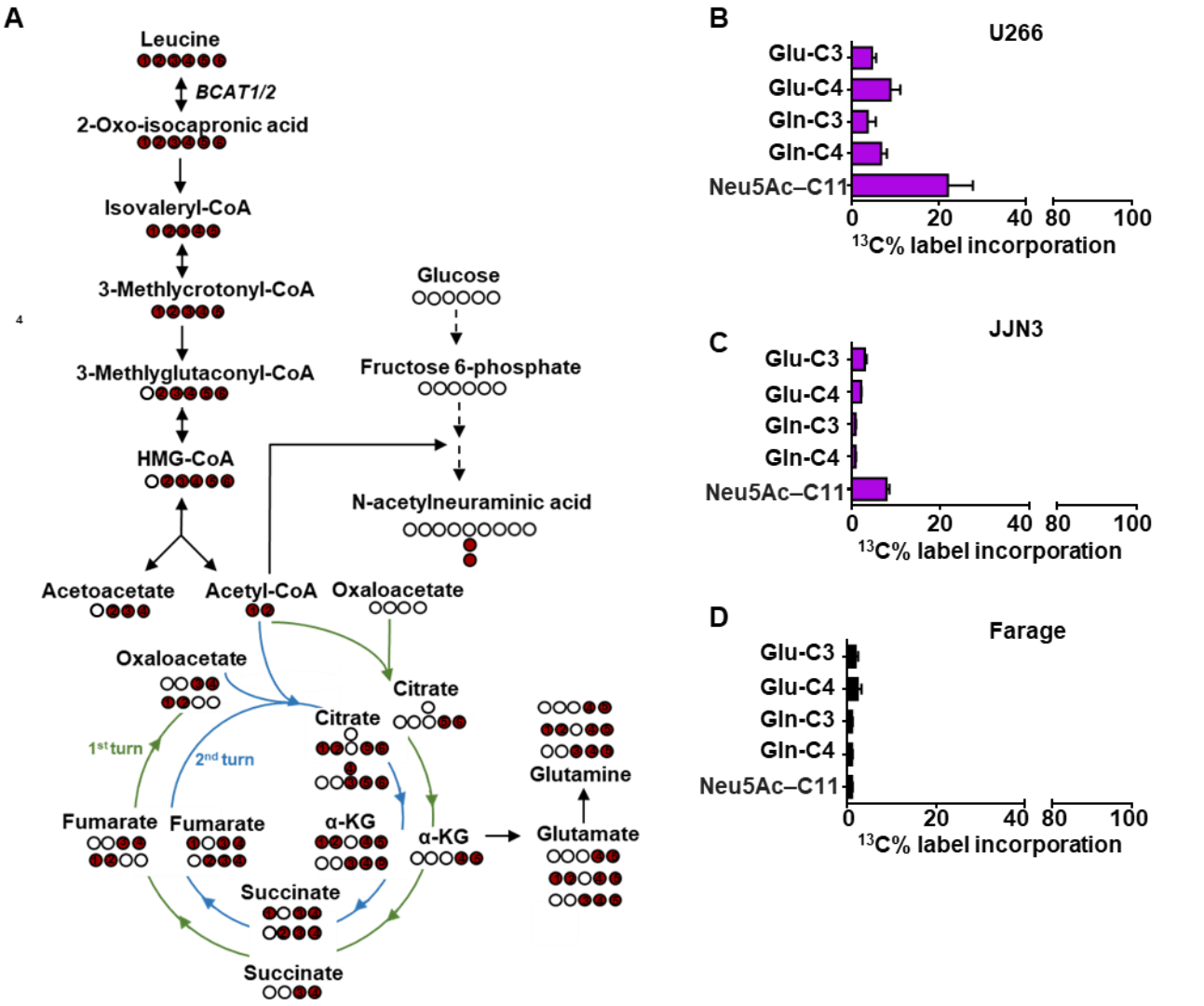

Figure 4.5 Catabolism of leucine in U266, JJN3 and Farage cells.

Schematic of labelling scheme using [U-^{13}C]-leucine showing the labelling of glutamate (Glu) and glutamine (Gln) via TCA cycle activity as well as production of N-acetylneuraminic acid from acetyl-CoA (A). Bar graphs represent the ^{13}C% label incorporation in U266 (B), JJN3 (C) and Farage (D) cells cultured for 48 hours in the presence of [U-^{13}C]-leucine. Data information: Data shown as mean SEM, n = 3.

4.2.3 LAT inhibitors reduce tumour cell viability

To understand whether the inhibition of LAT1/CD98 complex could affect the viability of MM cells, LAT1 inhibitors BCH and JPH203 were used (see Figures 4.6.A and 4.6.B). I first treated U266, JJN3 and K562 cells with BCH, a standard inhibitor of LATs (LAT1-4) at different concentration for 24 and 48 hours and then the Celltiter Blue assay was performed. K562 cell line was chosen as a cell line less dependent on exogenous BCAAs. BCH gradually decreased cell proliferation in a dose-dependent manner (see Figure 4.6.C). After 24 hours of exposure to BCH at 20 mM, the viability of three cell lines was decreased around 30%. However, the reduction in cell viability was similar in U266, JJN3 and K562 cells up to 48 hours of exposure to BCH with 24 hours of exposure to BCH. Furthermore, the similar gradual decrease in the viability of U266, JJN3 and K562 shows that BCH inhibits the cell proliferation regardless of exogenous BCAAs dependence of cells. To further test, whether a specific LAT1 inhibitor (JPH203) can result in a reduction in the viability of U266, JJN3, K562 and Farage cells, I assessed the effects of JPH203 on cell viability performing the Celltiter Blue assay. The inhibitory effect of JPH203 on U266, JJN3 and K562 cells was dose- and time-dependent as a moderate drop was observed in viable cells with an increasing JPH203 concentration and an increased exposure time (see Figure 4.6.D). U266, JJN3, K562 and Farage cells presented more than 50% cell viability after 24 and 48 hours of exposure to JPH203 at 50 μM. Comparison of 24 to 48 hours exposure data showed that Farage cell viability increased with increasing exposure time from 24 hours to 48 hours. The maximal reduction of viability was reached after 72 hours for all cells. However, this reduction was around only 50% for U266 and JJN3 even though these cells are most dependent on extracellular BCAAs.

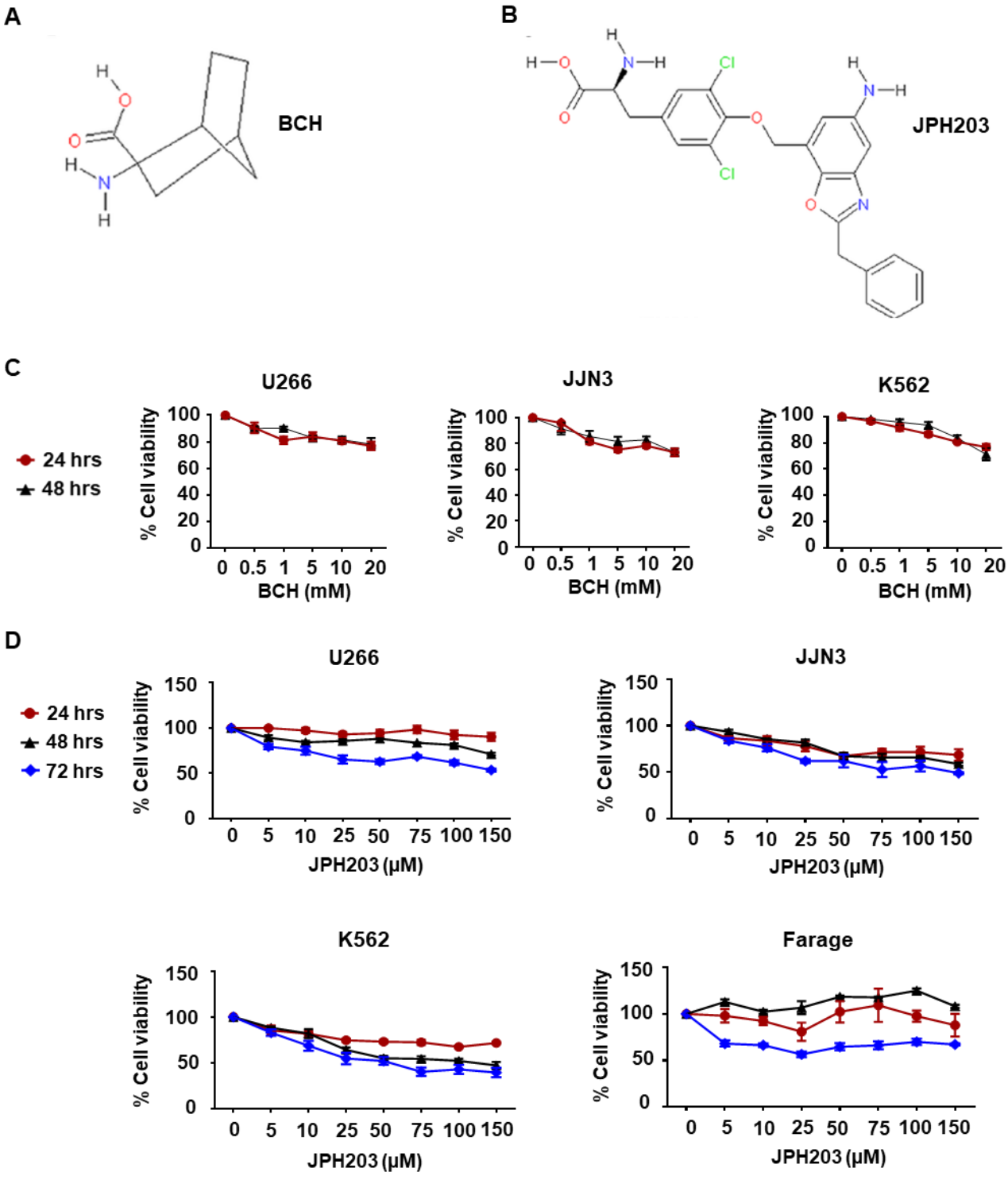
A
BCH
B
JPH203
C
24 hrs
48 hrs
U266
JJN3
K562
% Cell viability
BCH (mM)
0 0.5 1 5 10 20
D
24 hrs
48 hrs
72 hrs
U266
JJN3
K562
Farage
% Cell viability
JPH203 (μM)
0 5 10 25 50 75 100 150

Figure 4.6 Effect of BCH and JPH203 on cell proliferation.

Structure of BCH (A) and JH203 (B) (Q. Wang & Holst, 2015) Effect of BCH on cell viability in U266, JJN3 and K562 cells after treatment with increasing concentrations of BCH for 24 and 48 hours (C). Effect of JPH203 on cell viability in U266, JJN3, K562 and Farage cells after treatment with increasing concentrations of JPH203 for 24 ,48 and 72 hours (D). Cell viability was measured by Celltiter Blue assay. Each data point was presented as the mean ± SEM of three experiments.

4.2.4 Inhibition of LATs results in a decrease of cellular BCAAs in multiple myeloma cells

To explore the effects of inhibition of LATs in MM cells, I treated U266, JJN3 and K562 cells with 5 mM and 10 mM BCH for 48 hours. The effects of BCH on intracellular cell metabolism was investigated using NMR spectroscopy. The resonances of lactate, alanine, arginine, acetate, proline and succinate between 1.35 and 2.5 ppm in 1D ^{1}H-NMR spectra from cell extracts were not measured due to spectral overlap with peaks from BCH (see Figure 4.7.A). Thus, metabolites that do not overlap with BCH, were quantified. BCH potently reduced BCAA uptake in U266 cells (see Figure 4.7.B). Intracellular leucine, isoleucine and valine significantly decreased in both U266 and K562 cells in a dose-dependent manner whereas a slight reduction was observed in JJN3 cells (see Figures 4.8.A - 4.8.C). Although, LAT1 is also responsible for transporting phenylalanine across the plasma membrane, BCH at 5 mM did not decrease the intracellular phenylalanine level in U266 cells whereas 10mM BCH did (see Figure 4.6.D). BCH at 10 mM decreased less intracellular phenylalanine in K562 cells than 5 mM BCH did (see Figure 4.8.D). The BCH treatment dose-dependently reduced the intracellular phenylalanine in JJN3 cells (see Figure 4.8.D). A slight decrease in intracellular glycine was observed in U266 cells

treated with BCH at 10 mM while intracellular myoinositol, choline and creatine seemed not to be affected by BCH treatment. Interestingly, a small dose-dependent reduction in myoinositol and choline levels was observed in JJN3 cells (see Figures 4.8.E - 4.8.H).

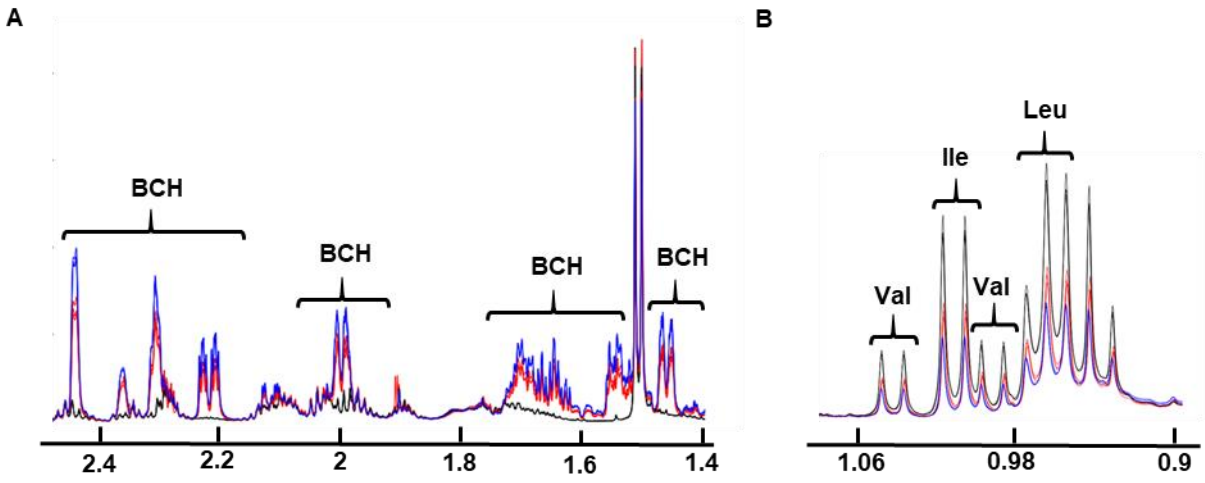

Figure 4.7 1D NMR spectra of U266 cells treated with BCH.

Representative 1D ^{1}H-NMR spectra of U266 cells indicating BCH (A) and BCAAs (B). Leu, leucine; Ile, isoleucine; Val, valine. Metabolites were extracted from intracellular samples of U266 cells treated with 5 mM and 10 mM BCH for 48 hours. Key: black line, untreated sample; red line, sample treated with 5 mM BCH; blue line, sample treated with 10 mM BCH. n=3

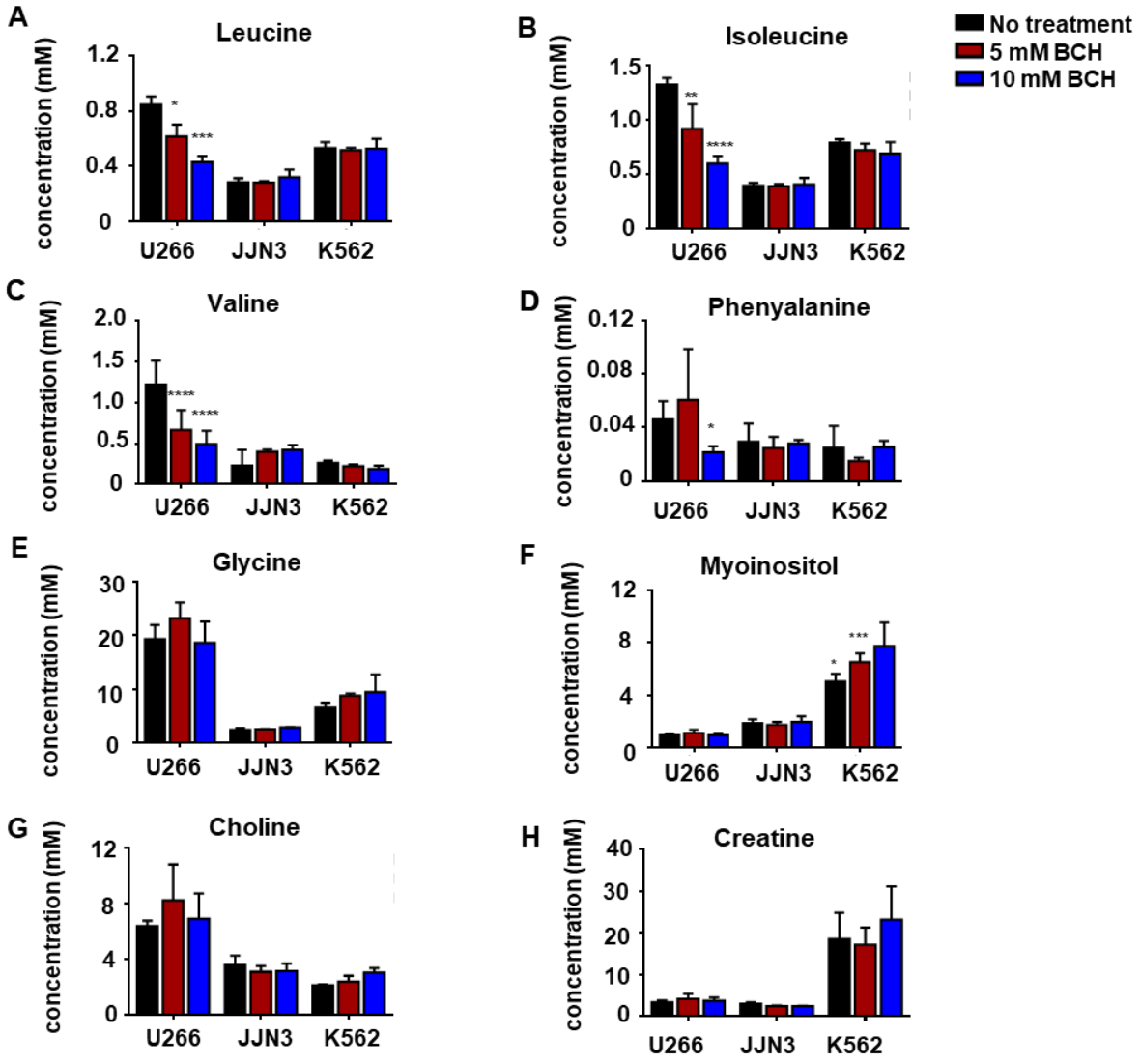

Figure 4.8 Effect of BCH on intracellular metabolism.

*Bar graphs show the relative intensities of the intracellular metabolites including leucine (A), isoleucine (B), valine (C), phenylalanine (D), glycine (E), myoinositol (F), choline (G), creatine (H) in U266, JJN3 and K562 cells treated with 5 mM and 10 mM BCH for 48 hours. Bar graphs represent mean ± SD with n=3. Two-way analysis of variance (ANOVA) was used to determine whether populations are statistically different from each other. * p<0.05, ** p<0.01, *** p<0.001, **** p<0.0001.*

To investigate the effect of blocking of LAT1, I used another supposedly more specific inhibitor JPH203 to treat U266 cells at 25 μM and 50 μM for 24 and 48 hours. In the 25 μM JPH203 treated U266 cells, LAT1 substrates including leucine, isoleucine, valine, phenylalanine and tyrosine levels were significantly lower than in non-treated cells (see Figures 4.9.A - 4.9.E). Interestingly, increasing JPH203 dose from 25 μM to 50 μM did not enhance the LAT1 inhibition. The inhibition of LAT1 with 25 μM JPH203 significantly increased the cellular glutamine, asparagine and glycine in U266 cells (see Figures 4.9.F - 4.9.H). In comparison with the increase in the level of these amino acids, cellular glutamate level was found to increase moderately after 24 hours 25 μM JPH203 treatment (see Figure 4.10.A). In contrast, 48 hours 50 μM JPH203 treatment resulted in an insignificant decrease in glutamate level in U266 cells. A slight change was observed in the levels of lactate, alanine, acetate and succinate in JPH203 treated U266 cells, while JPH203 treatment of U266 cells caused no alteration in the level myoinositol and arginine (see Figures 4.10.B - 4.10.G). Furthermore, 50 μM JP203 treatment of U266 cells for 24 hours and 48 hours reduced the intracellular aspartate level (see Figure 4.10.H).

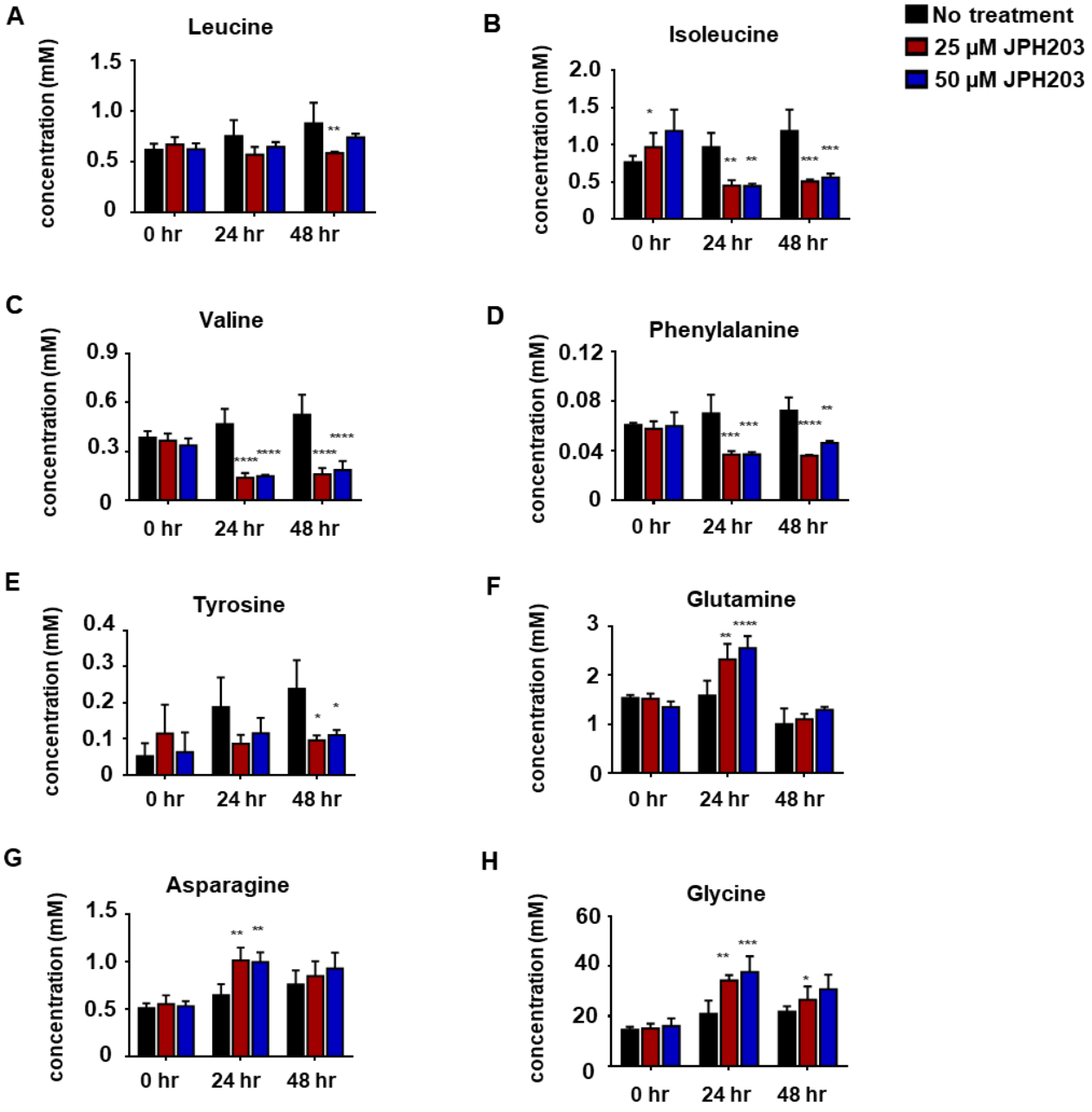

Figure 4.9 Effect of the LAT1 inhibitor JPH203 on intracellular metabolism.

*Bar graphs show the relative intensities of the metabolites including leucine (A), isoleucine (B), valine (C), phenylalanine (D), tyrosine (E), glutamine (F), asparagine (G), glycine (H) in U266 cells treated with 25 μM and 50 μM JPH203 for 24 and 48 hours. Bar graphs represent mean ± SD, with n=3. Two-way analysis of variance (ANOVA) was used to determine whether populations are statistically different from each other. * p<0.05, ** p<0.01, *** p<0.001, **** p<0.0001.*

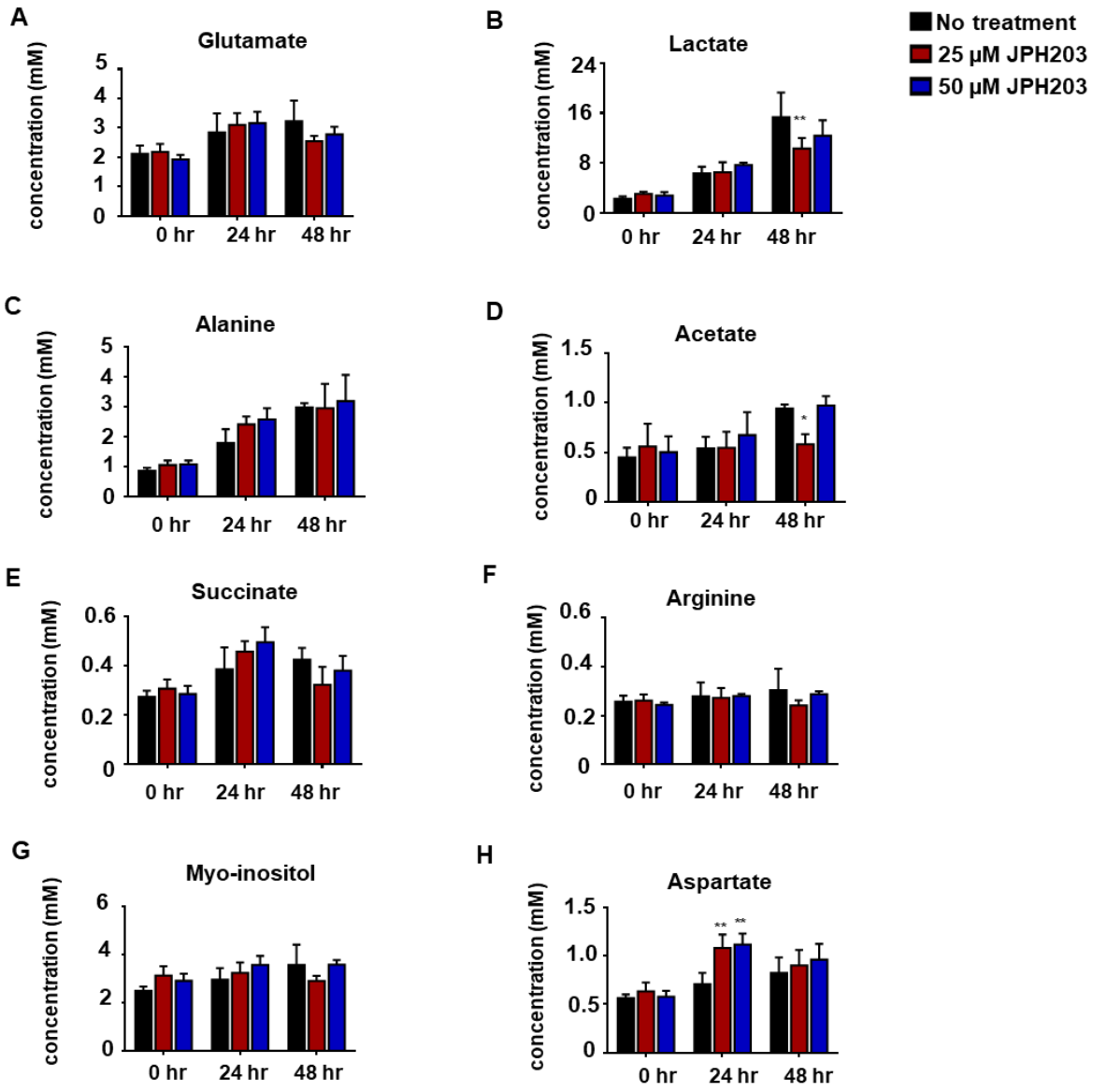

Figure 4.10 Effect of JPH203 on intracellular metabolism.

*Bar graphs show the relative intensities of the metabolites including glutamate (A), lactate (B), alanine (C), acetate (D), succinate (E), arginine (F), myoinositol (G), aspartate (H) in U266 cells treated with 25 μM and 50 μM JPH203 for 24 and 48 hour0s. Bar graphs represent mean ± SD, with n=3. Two-way analysis of variance (ANOVA) was used to determine whether populations are statistically different from each other. * p<0.05, ** p<0.01, *** p<0.001, **** p<0.0001.*

4.3 Discussion

4.3.1 Association of CD98 heavy chain with LAT1 and LAT2 light chains

This study demonstrated that MM cells express CD98 heavy chain at higher levels than cells from different subtypes of haematological cancers. However, flow cytometry analysis revealed that the level of LAT1 light chain on the surface of MM cells is less than the LAT1 surface level of other cells. Although CD98 is involved in the localisation of LAT1 light chain which is involved in the trafficking of the LAT1/CD98 heterodimer complex to the membrane (Bröer et al., 2001), the BCAA uptake was negatively correlated with surface level of LAT1 light chain in this study. This unexpected result can be explained by two potential scenarios. The first scenario relates to masking of LAT1 light chain by the CD98 heavy chain in the large extracellular domain of LAT1/CD98 heterodimer (Barollo et al., 2016). Briefly, the ~40 kDa LAT1 light chain penetrates the cellular membrane by forming disulfide-linkage with ~80–85 kDa CD98 heavy chain. Based on these facts, the LAT1 light chain may be masked by large extracellular CD98, therefore could not bind to the antibody that we used to measure the surface level of LAT1 light chain by flow cytometry. A second possible scenario is the association of CD98 with LAT2 instead of LAT1. Briefly, LAT2 light chain requires association with CD98 for stable localisation at the cellular membrane to have a function to transfer BCAAs. Although many studies have shown that LAT1 is upregulated in cancers (Furuya et al., 2012; Kobayashi et al., 2005; Q. Wang & Holst, 2015), LAT2 could be overexpressed in MM cells and result in presence of high level of CD98 on the cellular membrane of MM cells.

4.3.2 Catabolism of leucine in multiple myeloma cells

In past decades, MM has been shown to significantly alter glucose and glutamine metabolism like many cancers (Rizzieri et al., 2019). In the previous chapter, I showed that MM cells take up more BCAAs from their extracellular environment than other cancer cells. To shed new light into our understanding of BCAA metabolism in MM cells, leucine metabolism has been exploited in this chapter.

In this chapter, leucine was found to be fully oxidised in MM cells. Intriguingly, the contribution of carbon substrates to glutamate from leucine occurred in U266 cells. As the first step of leucine catabolism, leucine is transaminated to branched-chain α-keto acid (BCKA) by the activity of branched-chain amino acid aminotransferase 1 (BCAT1) (E. A. Ananieva & Wilkinson, 2018). In this reaction, the α-amino group of leucine is transferred to α-ketoglutarate to yield α-ketoisocaproate and glutamate. Thus, the glutamate that formed by transamination of leucine contains one nitrogen atom derived from leucine. However, the glutamate that we detected was ^{13}C labelled. Hence, the production of glutamate in U266 and JJN3 cells proves that α-ketoisocaproate derived from leucine is further metabolised to yield acetyl-CoA in MM cells (Moghei et al., 2016). The acetyl-CoA then enters the TCA cycle by condensation with oxaloacetate. Therefore, leucine is not only a building block in the polypeptide chain of proteins but also acts as an energetic molecule in MM cells. However, lipid and ketone bodies synthesis from leucine needs to be studied, since acetyl-CoA acts as a key precursor for the synthesis of fatty acid and ketone bodies in cells.N-acetylneuraminic acid (Neu5Ac), also known as sialic acid, is an important family of related 9-carbon sugars. Neu5Ac is positioned at the tip of glycans on cell-surface glycoproteins and glycolipids in a process called sialylation (Bork et al., 2009).

Cell surface sialylation is dynamic and often changes in response to cellular differentiation. In light of its important biological and pathological functions, the relationship between Neu5Ac and cancer has been drawing great attention. Increased expression of sialylated glycans represents one of the most important modifications of the glycome during tumour development, including MM, and often correlates with aggressive metastatic behaviour (Natoni et al., 2019; Teoh et al., 2018). Many studies have presented that the level of Neu5Ac increases in the serum of patients with MM (Cohen et al., 1989; Crook et al., 1996; Natoni et al., 2019). Here I demonstrated that the majority of acetyl-CoA derived from leucine participates in the production of Neu5Ac in U266 and JJN3 cells. This finding suggests that leucine supports sialic acid formation and sialylation more than acting as an energetic molecule in MM cells.

4.3.3 Treatment of cells with LAT inhibitors

Increased expression of LAT family members in several cancers has been reported (Häfliger & Charles, 2019; Q. Wang & Holst, 2015). I observed that MM cells consume more BCAAs than leukaemia and lymphoma cells. Although MM cells seemed not to express LAT1 more than AML, CML, BL and DLBCL cells, I found that they express CD98 more than other cells. In addition, the surface level of CD98 was found to be positively correlated with leucine uptake.

Due to the association of LAT1 with cancer patient's survival rates (Hayashi & Anzai, 2017), there have been efforts to synthesise LAT1 inhibitors. I investigated the effect of the L-type amino acid transporter inhibitor BCH and a LAT1 selective inhibitor JPH203 on viability and metabolism of MM cells. BCH differs from JPH203 since it cannot differentiate

LAT1 from other LAT transporters, thereby targeting all LATs on the plasma membrane. In this study, BCH did not cause a dramatic decrease in viability of cells when cells were treated even with 20 mM of BCH. Another study revealed that BCH at 100 mM is required to result in the death of 100% of the esophageal cancer cells (Ohshima et al., 2016). However, JPH203 applied in micromolar concentrations resulted in a better cytotoxic effect. These data suggested that blood cells could be either resistant to BCH or require high doses of BCH. Nevertheless, treatment of U266 cells with BCH at 10 mM decreased the intracellular BCAAs level as much as the treatment with JPH203 at 25 μM did. Although these inhibitors decreased the intracellular BCAAs approximately at the same level, they did not result in cell death in the same level. Thus, we could speculate that the reduction of intracellular BCAAs is not an effective way to decrease viability of MM cells even though MM cells seemed to consume extracellular BCAAs more than leukaemia and lymphoma cells. From this point of view, JPH203 might have shown its cytotoxic effect impairing with something else in cells rather than blocking LAT1 transporter. To test it, LAT1 knockdown is required to show whether JPH203 can lead to cell death in the absence of LAT1 protein.

CHAPTER 5

ASPARAGINE AND SERINE METABOLISM IN LYMPHOMA CELLS

5.1 Introduction

B-cell non-Hodgkin lymphomas (B-NHLs) encompass malignant tumours that results from the clonal growth of B cells at varying stages of development (Coso et al., 2015). Most B-NHL cells originate from the germinal centre (GC) reaction (Mlynarczyk et al., 2019). GCs are transient and dynamic structure that form within secondary lymphoid organs in response to T cell dependent antigens (see Figure 5.1).

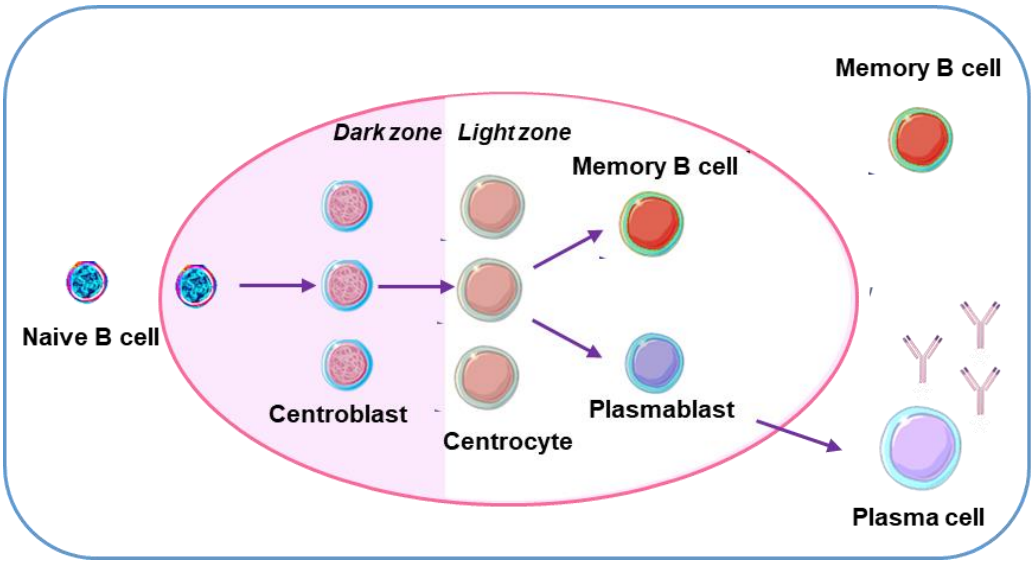

Figure 5.1 Structure of germinal centre.

Germinal centres (GCs) form in the secondary lymphoid organs (spleen, lymph nodes, tonsils, Peyer's patches, and mucosal tissues) in which B cells rapidly proliferate, differentiate and undergo affinity maturation. As the germinal centre matures, GCs are polarised into dark and light zones. Naive B cells initiate a germinal centre response when they encounter an antigen. The naive B cells turn into centroblasts and centrocytes within the GC. Centrocytes subsequently differentiate into memory B cells or into short-lived plasma cells called plasmablasts. Then plasmablasts leave the GC and terminally differentiate into long-lived plasma cells in the bone marrow.

GC B cells undergo intense clonal diversification and somatic hypermutation of their immunoglobulin variable genes encoding their B cell receptors. Although the GC reaction is tightly regulated to avoid emergence of autoreactive B cell clones, GC B cells are still at a considerably high risk for acquiring the properties of cancer because of attenuation of DNA damage and replication checkpoints (Mlynarczyk et al., 2019).

BL and DLBCL are subtypes of B-cell lymphomas that have been exposed to GC reaction (de Leval & Hasserjian, 2009). In the most recent WHO classification, a strict diagnostic criterion is defined for BL; presence of c-Myc rearrangement, positive for BCL6, negative for BCL2 and medium-sized cellular morphology (Swerdlow et al., 2016b). Despite having a characteristic gene expression profile, some BL cases morphologically resemble DLBCL, which could increase the risk of misdiagnosis. GEP of DLBCL has identified two main subtypes: germinal centre B-cells (GCB) or activated B-cells (ABC) (Devin et al., 2019). Morphologic features of BL and GCB-DLBCL overlap even though GCB DLBCL subtype harbours different oncogenic pathways to drive cellular transformation. Indeed, both lymphoma types are usually positive for CD19, CD20 and BCL-6 (Devin et al., 2019). Moreover, aberrant phenotypes are present in DLBCL and lead to confusion in diagnosis. For instance, Myc translocation that is characteristic to BL have been detected in a significant subset of DLBCL cases (Said, 2013). Nevertheless, there is an ongoing effort to separate these lymphoma types from each other to avoid undertreatment or overtreatment of patients.

Accurate diagnosis is required to treat BL and DLBCL patients properly since treatment regimens for these lymphoma types are remarkably different. The conventional regimen of four drugs known as CHOP which consists of cyclophosphamide, hydroxydaunorubicin

vincristine and prednisone is favoured for DLBCL whereas more intensive chemotherapy is preferred for BL (Sinha et al., 2012). For instance, BL patients usually have a poor outcome when they are treated with regimens for DLBCL as compared with those treated with more intensive regimens (Thomas et al., 2011). Therefore, a deep insight into the specific nature of BL and DLBCL is indispensable to accurately distinguish these cases and to develop new and emerging targeted therapies.

Amino acids play essential roles in the maintenance of cellular redox homoeostasis, replenishment (anaplerosis) of TCA cycle intermediates and synthesis of nucleosides besides their direct role as substrates for protein synthesis. Cancer cells usually rewire amino acid metabolism so that they can meet the biosynthetic demands of rapid replication. A number of cancers lose the ability to synthesise non-essential amino acids and then become dependent on exogenous sources. For instance, some melanoma and prostate cancers have been found auxotrophic for arginine due to lack of expression of argininosuccinate synthetase (ASS1) (Dillon et al., 2004). It has been shown that leukaemic lymphoblasts display little or no detectable asparagine synthetase (ASNS) that transfers the amide group from glutamine to aspartate yielding asparagine (Lomelino et al., 2017). Acute lymphoblastic leukaemia (ALL) cells were found to be sensitive to depletion of extracellular asparagine. Furthermore, these observations were used to develop targeted therapy for auxotrophic ALL cells. Asparaginase (ASNase) has been used to treat patients with ALL. ASNase catalyses the conversion of asparagine to aspartate, thereby depleting blood asparagine and starving leukaemic cells of asparagine and leading ultimately to cell death. Extensive clinical data have shown that the long-term outcome of ALL has improved dramatically due to the development of ASNase treatment

(Cecconello et al., 2020; Lomelino et al., 2017).

Asparagine as a versatile amino acid has a role in protein synthesis, serine uptake and mTORC1 activity (Krall et al., 2016). Depletion of asparagine reduces protein synthesis, amino acid uptake and mTORC1 activity in asparagine auxotrophic cells. In this chapter, the distinctive differences in asparagine metabolism between BL and DLBCL were studied to exploit new treatment strategies. I compared the effect of exogenous asparagine on serine metabolism for BL vs DLBCL. For this, I have investigated the effects of asparagine deprivation on serine uptake and production, as well as the inhibition of serine synthesis by targeting phosphoglycerate dehydrogenase (PHGDH).

5.2 Results

5.2.1 Extracellular metabolic differences between BL and DLBCL

To elucidate extracellular metabolic differences between BL and DLBCL, metabolites in cell culture were studied in the media of BL and DLBCL cell using NMR spectroscopy. 1D ^{1}H-NMR spectroscopy enabled assignment of 13 metabolites that have a unique peak pattern. A principal component analysis (PCA) was performed with a metabolite data matrix (13 metabolites versus samples) obtained from the media samples of Sav, Glor, Ezema, BL31, Farage, SUDHL4, SUDHL5 and SUDHL6 cells.

The PCA score plot of the 1D ^{1}H-NMR spectra is shown in Figure 5.2.A. The first principal component (PC1) describes 58% of the total variation while PC2 demonstrates 26% of the total variation. The PCA pronouncedly separated BL cells from the DLBCL cells, reflecting the differences in metabolite composition. The loading plot of the PCA analysis pointed out that the separation of BL from DLBCL was mainly based on differences in relative amounts of asparagine and glutamine and lactate (see Figure 5.2.B). This analysis revealed that BL cells consumed dramatically more extracellular asparagine, glutamine and lactate than the DLBCL cells (see Figures 5.2.C - 5.2.E).

To reveal genetic diversity between BL and DLBCL, transcripts abundances were quantified for 17048 genes in the dataset derived from 19 BL and 12 DLBCL patients. Differential expression analysis performed by Mr. Grigorios Papatzikas identified 6475 genes as statistically significant altered genes between the two diseases (Figure 5.2. F). Notably, 264 statistically significant metabolic genes were found. This strong signature has considerable potential to support differentiation between BL and DLBCL on a

diagnostic level.

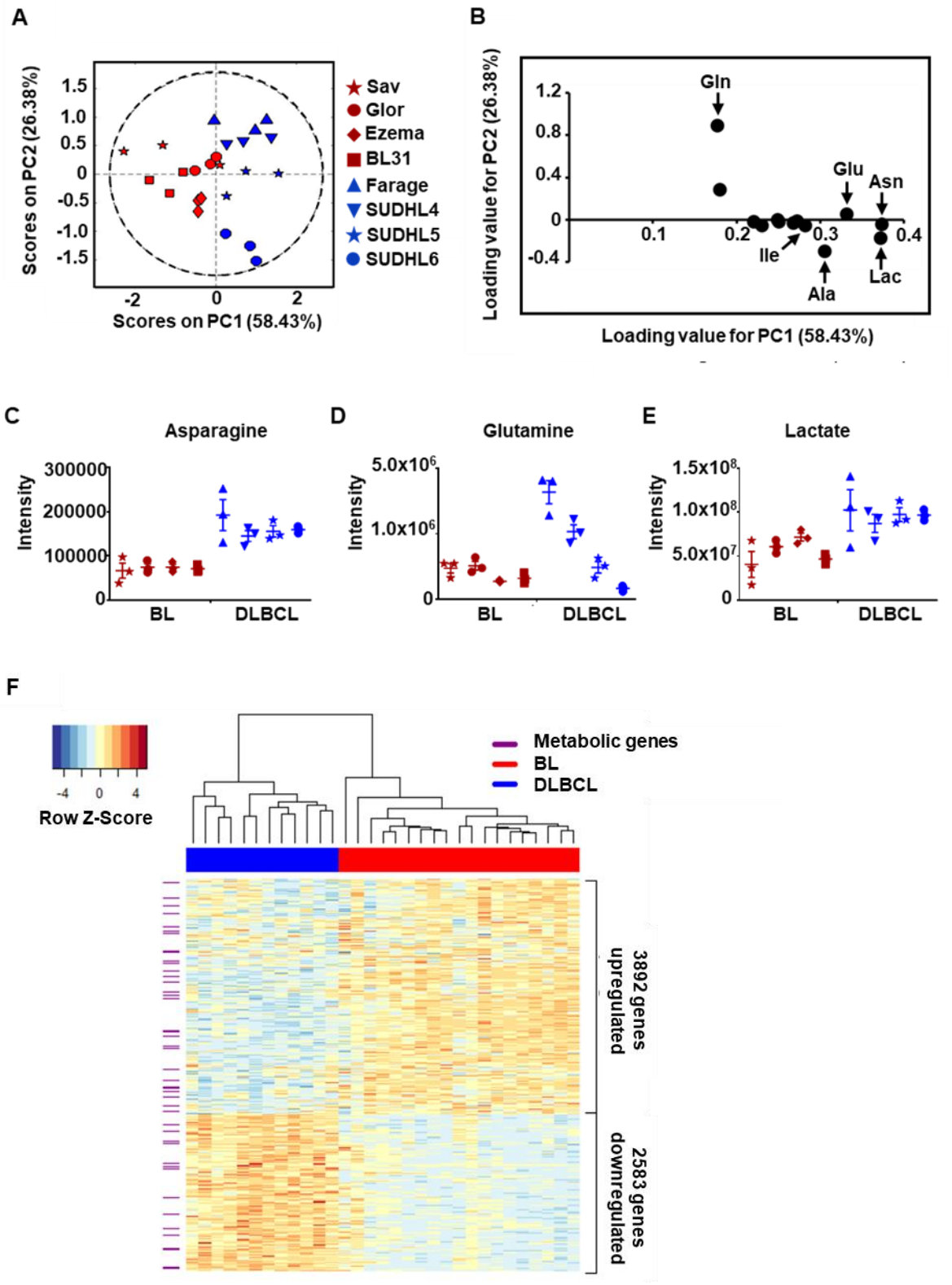

Figure 5.2 Metabolic differences between BL and DLBCL.

Principal Component Analysis (PCA) (A) and corresponding loadings plot (B) of a metabolite data matrix that consists of 13 metabolites in the spent media of four BL cell lines (red) and four DLBCL cell lines (blue). Comparison of 1D ^{1}H-NMR peak intensities of asparagine at 2.80 ppm (C), glutamine at 2.46 ppm (D), lactate at 1.33 ppm (E) in the cell culture media of BL and DLBCL cell line cells. Heatmap of 6475 statistically significant genes between DLBCL and BL. Purple colour indicates the rows of the 264 statistically significant metabolic genes (F). The confidence ellipse in A is based on with 95% confidence. Bar graphs represent mean ± SEM, with n=3. Gene expression values have been converted to a Z-score scale along the rows for case comparisons. Dendrogram in hierarchical clustering analysis was produced with Ward method and distance 1-Spearman's rank correlation.

5.2.2 Association between extracellular asparagine and serine metabolism

In consideration of the recent report showing the regulation of serine metabolism by asparagine (Krall et al., 2016), I aimed to further investigate the role of asparagine on metabolism in BL and DLBCL cells. To determine the influence of extracellular asparagine on glycolysis, serine uptake and glutaminolysis, BL and DLBCL cells were cultured in a medium with or no asparagine containing ^{13}C-stable-isotope labelled tracers for the 2D HSQC NMR experiments. As tracers, I used [U-^{13}C]-glucose, [U-^{13}C]-serine and [3-^{13}C]-glutamine (see Figure 5.3.A). Glor and Farage cell lines were chosen to represent BL and DLBCL respectively.

Firstly, to assess the effect of asparagine on glycolysis, 20 x10^{6} BL and DLBCL cells were cultured in asparagine depleted or in complete media containing [U-^{13}C]-glucose for 24 hours. HSQC analysis of tracer-based experiments revealed that asparagine deprivation increased the formation of serine from [U-^{13}C]-glucose in Glor and in Farage cells (see Figure 5.3.B). However, glycine production from [U-^{13}C]-glucose remained steady in both

cell lines (see Figure 5.3.C). When deprived of asparagine, divergent changes in lactate production were observed in Glor and Farage cells. Compared to lactate production in cells grown in cell culture media with asparagine, a dramatic increase in production of lactate from glucose was observed in Glor cells, while a significant decrease was found in lactate production in Farage cells (see Figure 5.3.D). However, asparagine deprivation resulted in an enhancement in alanine production in DLBCL Farage cells (see Figure 5.3.E). Furthermore, asparagine starvation led to a pronounced increase in AMP production in Glor cells (see Figure 5.3.F).

To determine the influence of asparagine on serine uptake and glutaminolysis, 10 x10^6 BL and DLBCL cells were cultured in asparagine depleted or complete media containing [U-^{13}C]-serine and [3-^{13}C]-glutamine for 24 hours. The analysis of HSQC spectra of Glor and Farage cells revealed that the influx of serine reduced in both Glor cells and Farage cells in asparagine depleted media (see Figures 5.4.A and 5.4.B). I also observed no change in the level of glycine originating from extracellular [U-^{13}C]-serine (see Figure 5.4.C). The use of [3-^{13}C]-glutamine to trace the catabolism of glutamine carbons in the TCA cycle revealed that the absence of asparagine slightly raised the intracellular level of ^{13}C-glutamate and ^{13}C-glutamine levels (see Figures 5.4.C - 5.4.F). However, I could not observe any changes in the level of TCA intermediates derived from [3-^{13}C]-glutamine in Glor cells (see Figures 5.4.F - 5.4.H). Farage cells cultured in the media without asparagine produced more succinate and malate originating from [3-^{13}C]-glutamine compared to control cells (see Figures 5.4.F - 5.4.H). These results suggest that asparagine regulates glucose and serine metabolism in BL and DLBCL cells.

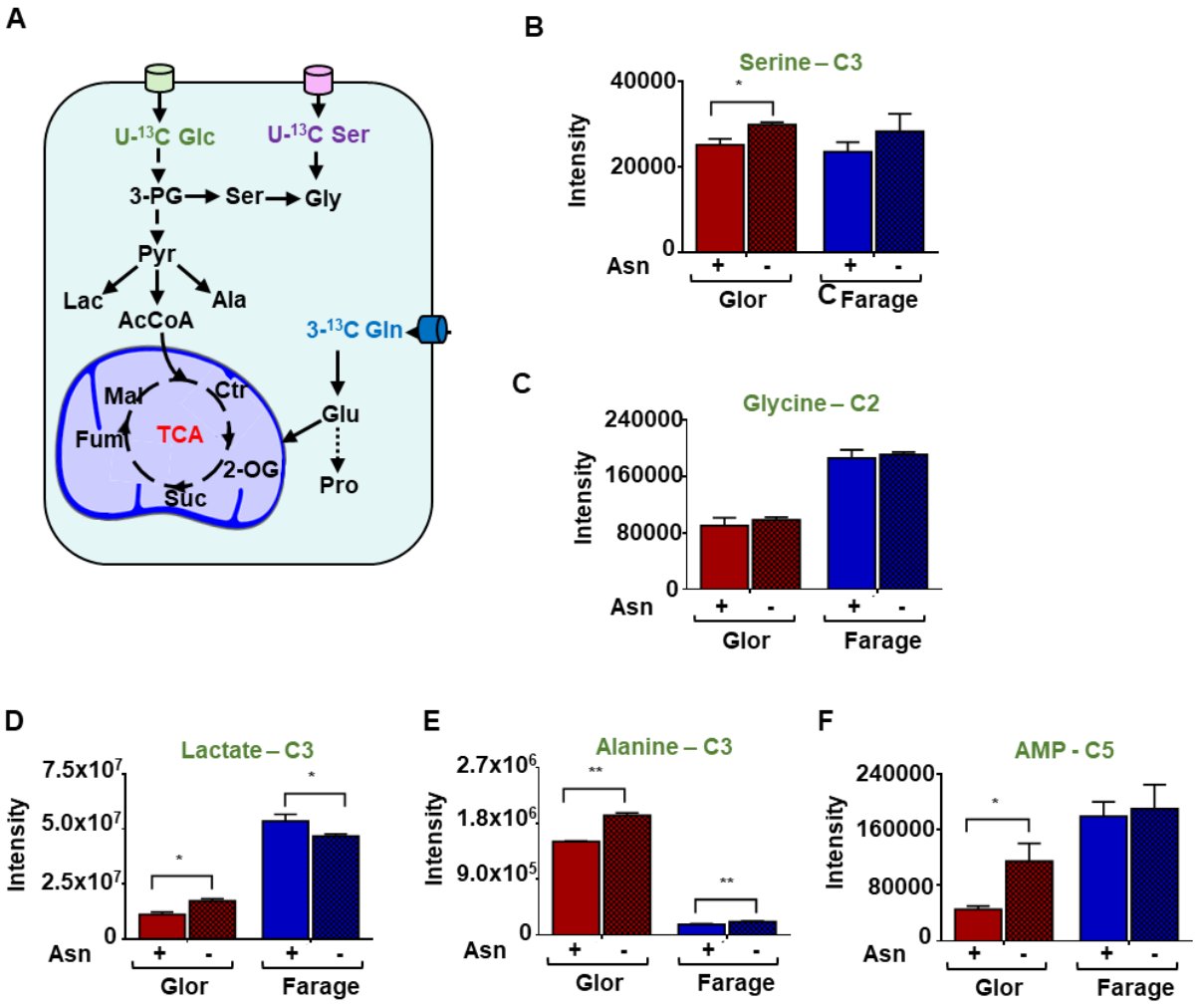

Figure 5.3 Asparagine alters glucose metabolism.

*^{1}H-^{13}C HSQC analysis of the cell extraction of Glor and Farage cells cultured in a medium containing [U-^{13}C]-glucose in the absence or presence of asparagine for 24 hours. Illustration of metabolism of [U-^{13}C]-glucose, [U-^{13}C]-serine and [3-^{13}C]-glutamine in a cell (A). ^{13}C peak intensity of [3-^{13}C]-serine (B), [2-^{13}C]- glycine (C), [3-^{13}C]- lactate (D), [3-^{13}C]-alanine (E) and [5-^{13}C]-AMP (F) derived from [U-^{13}C]-glucose. Data is shown as mean ± SEM expression. *p < 0.05; **p < 0.01; ***p < 0.001.*

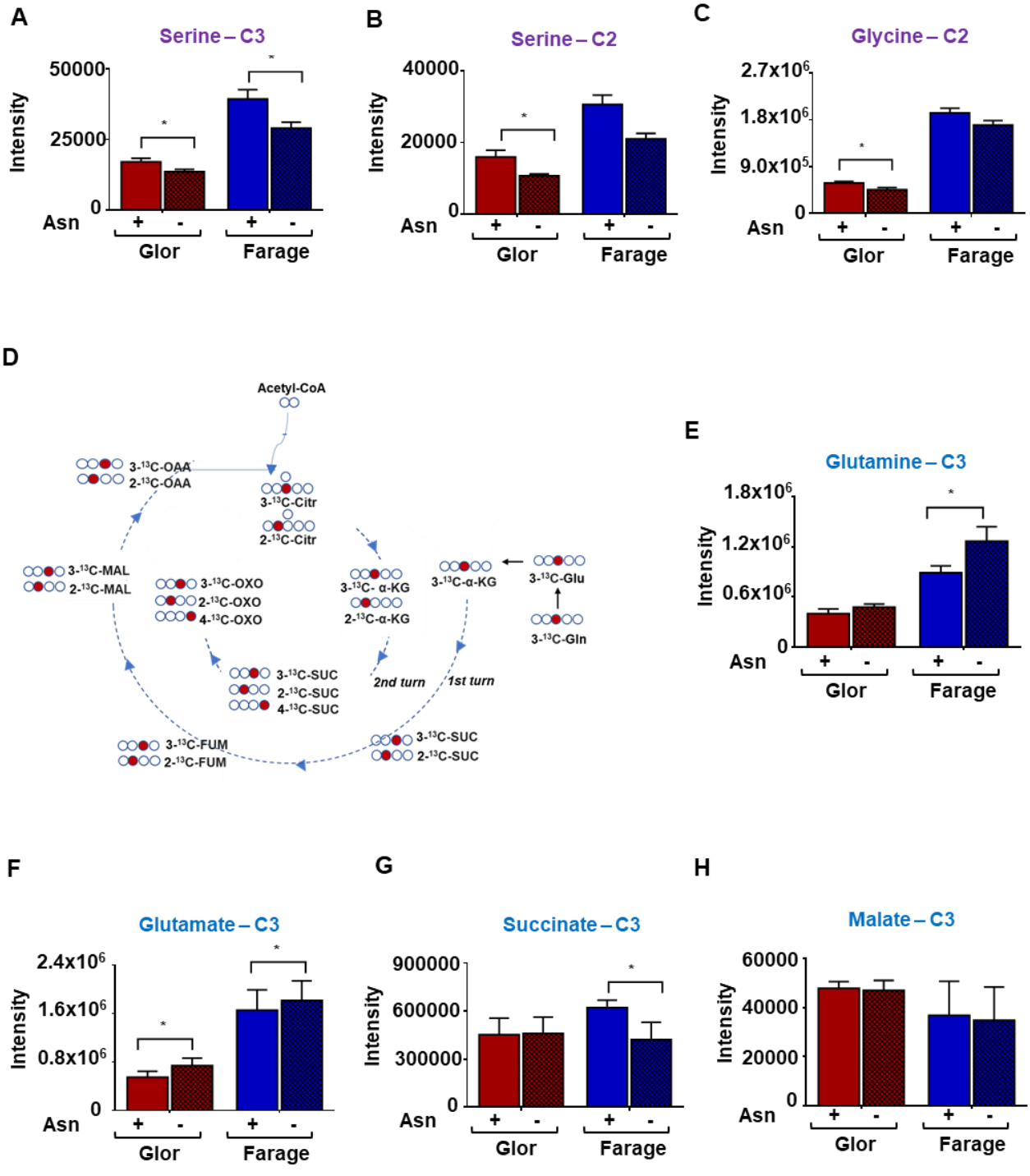
A
Serine – C3
Intensity
50000
25000
0
Asn
+ -
Glor
+ -
Farage
B
Serine – C2
40000
20000
C
Glycine – C2
2.7x10^6
1.8x10^6
9.0x10^5
D
Acetyl-CoA
3-13C-OAA
2-13C-OAA
3-13C-Citr
2-13C-Citr
3-13C-MAL
2-13C-MAL
3-13C-OXO
2-13C-OXO
4-13C-OXO
3-13C- α-KG
2-13C-α-KG
3-13C-α-KG
3-13C-Glu
3-13C-Gln
3-13C-SUC
2-13C-SUC
4-13C-SUC
2nd turn
1st turn
3-13C-FUM
2-13C-FUM
E
Glutamine – C3
1.8x10^6
1.2x10^6
0.6x10^6
F
Glutamate – C3
2.4x10^6
1.6x10^6
0.8x10^6
G
Succinate – C3
900000
600000
300000
H
Malate – C3
60000
40000
20000

Figure 5.4 Extracellular asparagine regulates glutamine metabolism of DLBCL cells.
*Analysis of 2D ^{1}H-^{13}C HSQC spectra of the cell extraction of Glor and Farage cells cultured in a medium containing [U-^{13}C]-serine and [3-^{13}C] glutamine in the absence or presence of asparagine for 24 hours . ^{13}C peak intensity of [3-^{13}C]-serine (A), [2-^{13}C]-serine (B), [2-^{13}C]-glycine (C) derived from [U-^{13}C]-serine. Metabolic fates of [3-^{13}C]-glutamine in a cell (D). ^{13}C peak intensity of [3-^{13}C]-glutamine (E), [3-^{13}C]-glutamate (F), [3-^{13}C]-succinate (G) and [3-^{13}C]-malate derived from [U-^{13}C]-glutamine. Data is shown as mean ± SEM expression.Data are shown as *p < 0.05; **p < 0.01; ***p < 0.001.*

5.2.3 Metabolic effects of asparaginase and NCT503

The use of the asparagine-free medium is not enough to completely eliminate extracellular asparagine as cells can synthesize aspragine from aspartate and can secrete asparagine into their environment. Asparaginase (ASNase), which catalyzes the hydrolysis of asparagine to aspartate, has been used as a medication to decrease extracellular asparagine in asparagine dependent cancers (Cecconello et al., 2020). Thus, to test whether and to what extent ASNase can completely diminish the extracellular asparagine, ASNase at different doses was added into fresh complete media. After supplementation of fresh media with ASNase at 0.1 U/ml, 0.25 U/ml and 0.5 U/ml for 24 hours, the 1D ^{1}H-NMR measurement was performed. ASNase at 0.1 U/ml was found to be enough to completely diminish asparagine which was proven by a 4-fold increase in the aspartate level in comparison with the control media cells (see Figures 5.5.A and 5.5.B). Moreover, ASNase also broke down a significant amount of glutamine into glutamate in a dose-dependent manner cells (see Figures 5.5.A and 5.5.B). Although ASNase at 0.1 U/ml depleted almost all asparagine, it reduced glutamine levels by 14%. However, ASNase at 0.5 U/ml significantly reduced glutamine level by 88%. Consistent with the decrease in

glutamine level, media containing ASNase at 0.5 U/ml had the highest level of glutamate. Hence, 0.1 U/mL ASNase was used for experiments with cells.

As shown earlier, asparagine regulates serine metabolism by increasing serine production from glucose and decreasing serine uptake. This observation encouraged me to ask if the expression level of PHGDH, an enzyme that catalyses the first rate-limiting step of serine synthesis from glucose, can be increased by reducing extracellular asparagine with ASNase. To answer this question, BL (Glor, Sav, BL31) cells and DLBCL (Farage, SUDHL4, SUDHL6) cells were exposed to 0.1 U/ml ASNase for 24 hours. Western blot was used to evaluate the relative concentration of PHGDH in treated and non-treated cells. Western blot analysis showed that ASNase treatment increased the protein levels of PHGDH in BL cells while no alteration in the protein level of PHGDH occurred in DLBCL cells in response to ASNase cells (see Figure 5.5.C).

To further understand the role of amino acids biosynthesis in BL and DLBCL, Mr. Grigorios Papatzikas analysed 980 gene sets which represent the majority of biological processes and pathways derived from 19 BL and 12 DLBCL patients. Mr. Grigorios Papatzikas performed GSEA with SetRank, which reduces the risk of false positive hits. Mr. Grigorios Papatzikas then constructed gene interaction networks, using STRING database (Szklarczyk et al., 2019) for all the statistically significant gene sets that are associated with serine metabolism. We found that genes associated with serine biosynthesis pathway are upregulated in BL cases (see Figure 5.5.D).

After I observed that glutamine and asparagine depletion mediated by ASNase increases the expression level of PHGDH in BL cells, I examined whether inhibition of PHGDH by a spesific inhibitor would decrease cell viability (see Figure 5.5.E).To answer that I evaluated

anti-cancer effects of PHGDH inhibition on proliferation of BL (Glor, Sav, BL31) cells and DLBCL (Farage, SUDHL4, SUDHL6) cells through using a PHGDH inhibitor, NCT503 (Pacold et al., 2016) for 72 hours. The effects of NCT503 on viability were measured by Celltiter Blue assay at different concentrations. NCT503 inhibited cell proliferation in all cell lines with IC50 values between 6.65 μM and 52.71 μM (see Figures 5.6.A and 5.6.B). BL cells (IC50 6.55–20.91 μM) were found to be more sensitive to PHGDH inhibition than DLBCL cells (IC50 12.21–52.71 μM). Next, I tested how effectively NCT503 inhibits serine production from glucose. To study the effect of NCT503 on serine production from glucose, DLBCL (Farage, SUDHL6) and BL (Glor, BL31) cells were cultured with [U-^{13}C]-glucose and NCT-503 at 10 μM for 24 hours. BL and DLBCL cells exhibited a marked attenuation in the amounts of [U-^{13}C]-glucose derived [3-^{13}C]-serine and [2-^{13}C]-glycine compared to untreated cells (see Figures 5.7.A and 5.7.B). Strikingly, lactate production from glucose was enhanced by the inactivation of PHGDH in all cells (see Figure 5.7.C). Conversely, NCT503 reduced alanine production in BL cells (see Figure 5.7.D). AMP production was found to increase in DLBCL cells by the inhibition of PHGDH in DLBCL cells (see Figure 5.7.E).

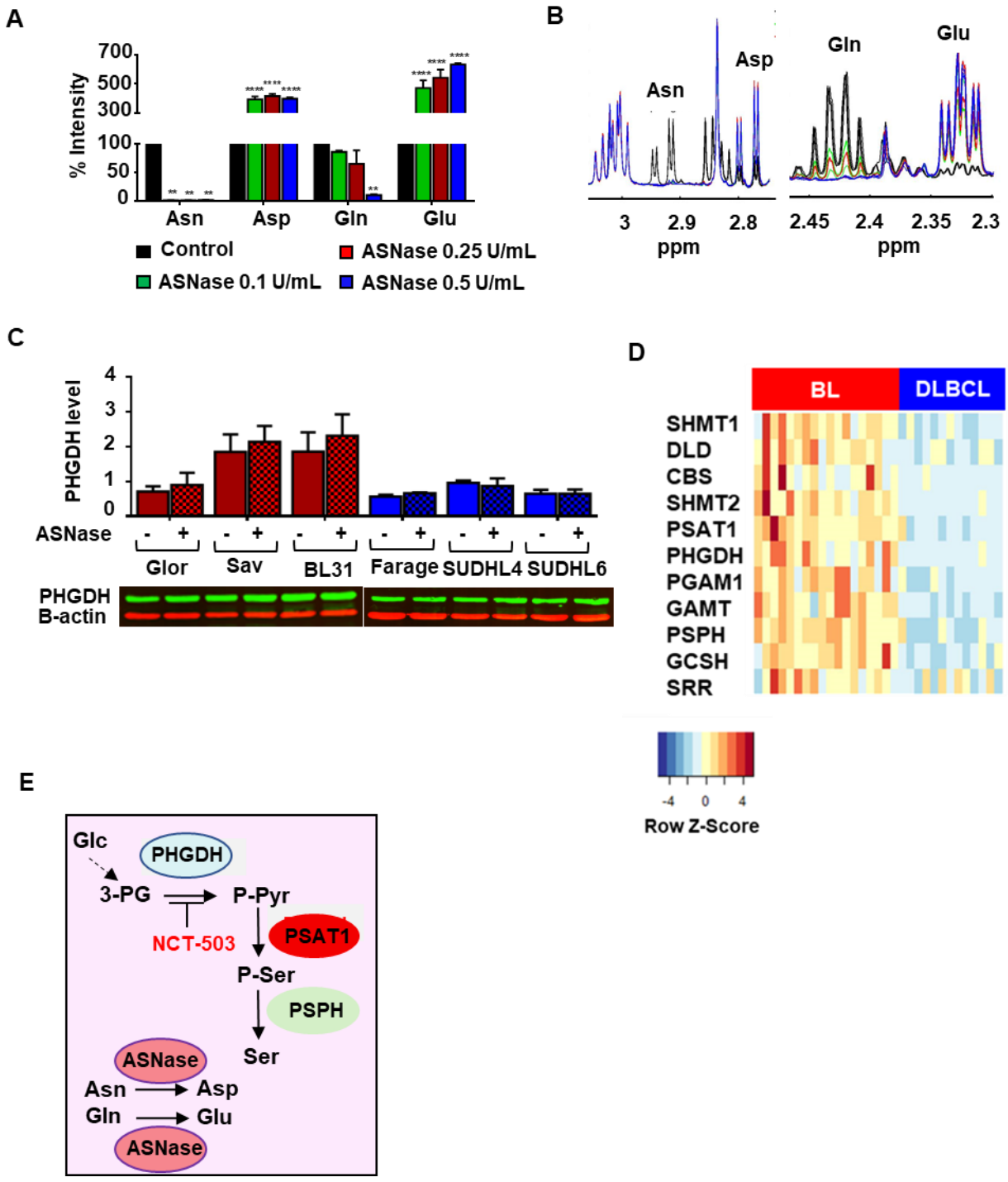

Figure 5.5 The effect of ASNase on asparagine, glutamine and synthesis of serine.

Relative 1D ^{1}H-NMR peak intensity of asparagine, aspartate, glutamine and glutamate in the fresh medium supplemented without or with asparaginase (ASNase) at 0.1 U/ml, 0.25 U/ml and 0.5

*U/ml for 24 hours (A). Representative 1D NMR spectra demonstrating the alteration in the level of asparagine, aspartate, glutamine and glutamate in the medium supplemented with no ASNase, ASNase at 0.1 U/ml (green line), 0.25 U/ml (red line), 0.5 U/ml (blue line) for 24 hours (B). Western blot analysis shows the expression of PHGDH in Glor, Sav, BL31, Farage, SUDHL4 and SUDHL6 cell lines after treatment without or with 0.1 U/ml ASNase for 24 hours.. The graph presents the relative abundances of PHGDH after normalisation with B-actin (C). Heatmap of statistically significant genes associated with serine metabolism in DLBCL and BL. (D) Illustration of the mechanism of action of ASNase and NCT503 (E). Bar graphs represent mean ± SEM, with n=3;*p < 0.05; **p < 0.01; ***p < 0.001. Abbreviations: SHMT1: serine hydroxymethyltransferase 1; DLD: dihydrolipoamide dehydrogenase; CBS: cystathionine beta-synthase; SHMT2: serine hydroxymethyltransferase 2; PSAT1: phosphohydroxythreonine aminotransferase; PHGDH: phosphoglycerate dehydrogenase; PGAM1: phosphoglycerate mutase 1; GAMT: guanidinoacetate methyltransferase; PSPH: phosphoserine phosphatase; GCSH: glycine cleavage system protein H; SRR: serine racemase. Dendrogram in hierarchical clustering analysis was produced with Ward method and distance 1- Spearman's rank correlation.*

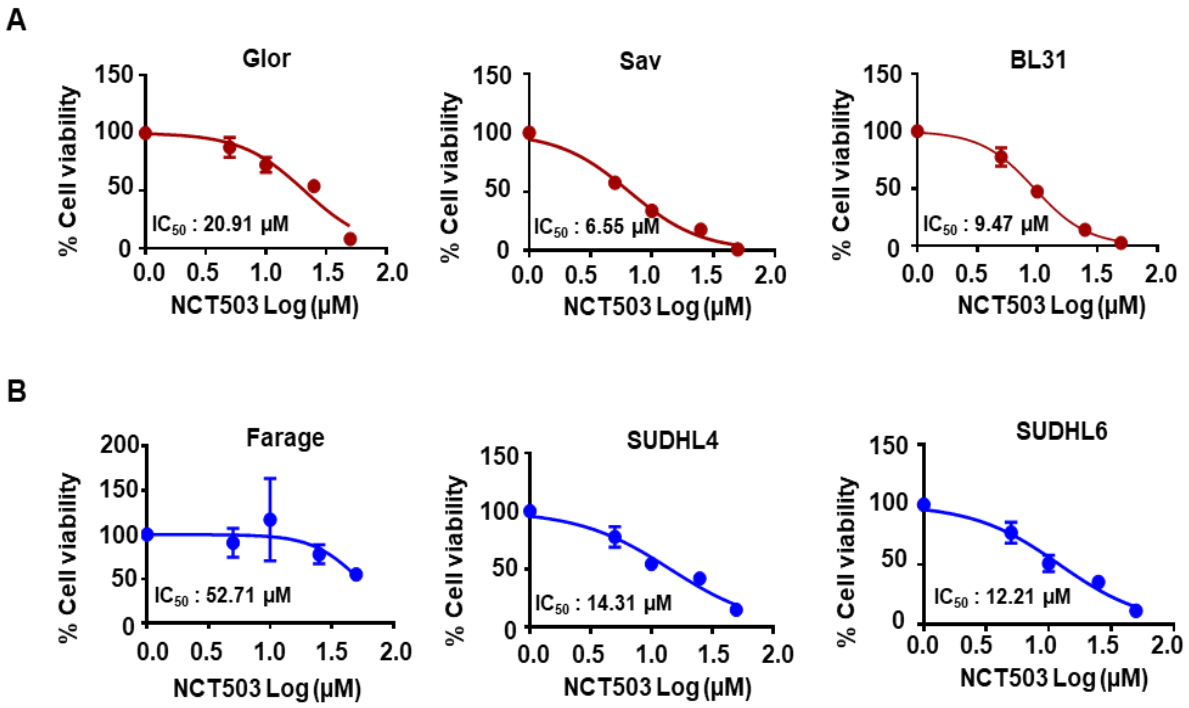

Figure 5.6 NCT503 decreases cell viability.

Effect of NC503 on BL and DLBCL on cell viability. Cell viability was measured by Celltiter Blue assay in BL (Glor, Sav, BL31) (A) and DLBCL (Farage, SUDHL4, SUDHL6) (B) cells treated with increasing doses of NCT503 for 72 hours. Cytotoxicity curves represent the mean of 3 independent experiments ± SD performed in 3 replicates per drug concentration.

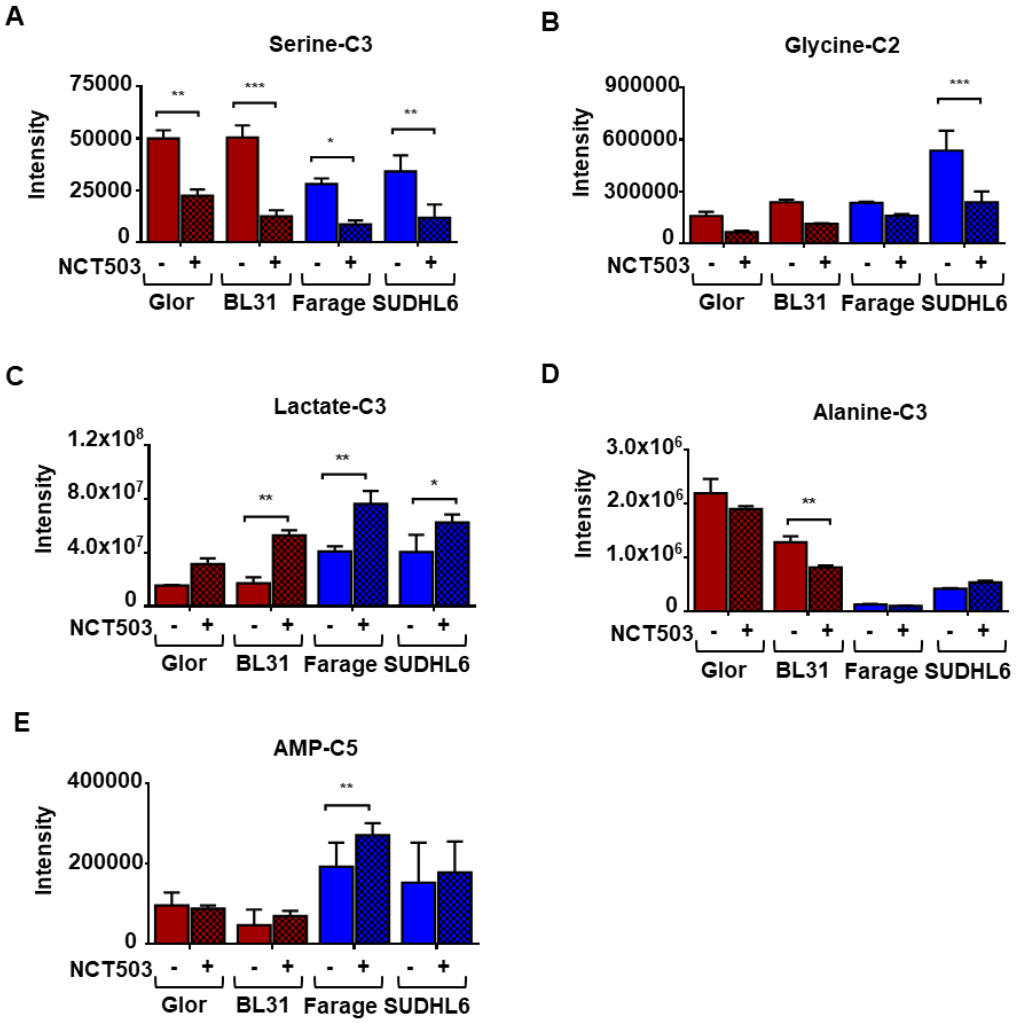

Figure 5.7 Effects of NCT503 treatment on glucose metabolism.

*Analysis of 2D ^{1}H-^{13}C HSQC spectra of metabolites extracted from Glor, BL31, Farage and BL31 cells incubated with [3-^{13}C] glutamine in the presence and absence of NCT503 at 10 μM for 24 hours. Graphs represent ^{13}C labelled serine (A), glycine (B), lactate (C), alanine (D) and AMP (E). Data is shown as mean ± SEM. *p < 0.05; **p < 0.01; ***p < 0.001.*

5.2.4 The synergistic effect of asparaginase and NCT503

Asparagine deprivation and PHGDH inhibition were shown to alter cell metabolism (see Figure 5.8.A). However, the effect of extracellular asparagine and serine deprivation on viability of BL and DLBCL cells was not evaulated. To get an insight into the effect of asparagine and serine on cell viability, BL Glor cells and DLBCL Farage cells were cultured in the absence of extracellular asparagine or serine, and also in media supplemented with ASNase at 0.1 U/mL or NCT503 at 10 μM for 72 hours. Then Celltiter Blue assay was performed. The asparagine deprivation and treatment of ASNase at 0.1 U/ml exhibited a similar reduction in the viability of Glor and Farage cells (see Figure 5.8.B). Glor cells appeared to be more sensitive to serine starvation than inhibition of PHGDH enzyme, as deprivation of serine resulted in a ~50% decrease in cell viability. Nevertheless, NCT503 treatment of Glor cells caused a ~25% reduction in cell proliferation. Moreover, Farage cells were found not to be affected by the inhibition of PHGDH enzyme by NCT503 compared to cells cultured in complete media. The extent of reduction in viability was almost similar for both lymphoma cells grown in asparagine and serine free media. These results suggested that BL cells are much more sensitive to the maintenance of the serine pool than DLBCL cells. BL cells were found to be sensitive to inhibition of serine uptake and serine production from glucose opposite to Farage cells.

Previously asparagine starvation was shown to decrease serine uptake and to increase serine production from glucose. NCT503 was found to decrease production of serine from glucose. In light of these findings, combination of ASNase with NCT503 may decrease more intracellular serine, thereby leading to more reduction in the viability of cells. Thus, I aimed to test if the combination of NCT503 with ASNase could decrease the sensitivity

of BL cells to ASNase, since BL cells were found to be more dependent on extracellular asparagine and also produce more serine from glucose compared to DLBCL cells. To answer that BL (Glor, Sav, BL31) and DLBCL (Farage, SUDHL4, SUDHL6) cells were treated with ASNase at 0.1 U/ml or combination of ASNase at 0.1 U/ml with NCT503 at 10 μM for 24, 48 and 72 hours. ASNase alone reduced the viability of BL and DLBCL cells to around 50% after 72 hours of treatment (see Figure 5.8.C). Treatment of BL and DLBCL cells with ASNase at 0.1 U/ml resulted in a time-dependent decrease in cell viability of those cells. 72 hour exposure of ASNase at 0.1 U/ml to BL and DLBCL cells caused approximately 50% cell loss in both lymphoma types. Moreover, the combination of ASNase with NCT503 had a synergistic effect on cell viability in BL cells, exhibiting more decrease in cell viability as compared to those obtained from treatment of ASNase alone. Conversely, the combination of ASNase with NCT503 showed no synergistic effect on the viability of DLBCL cells, suggesting that the combination of ASNase with NCT503 is solely synergistic for BL.

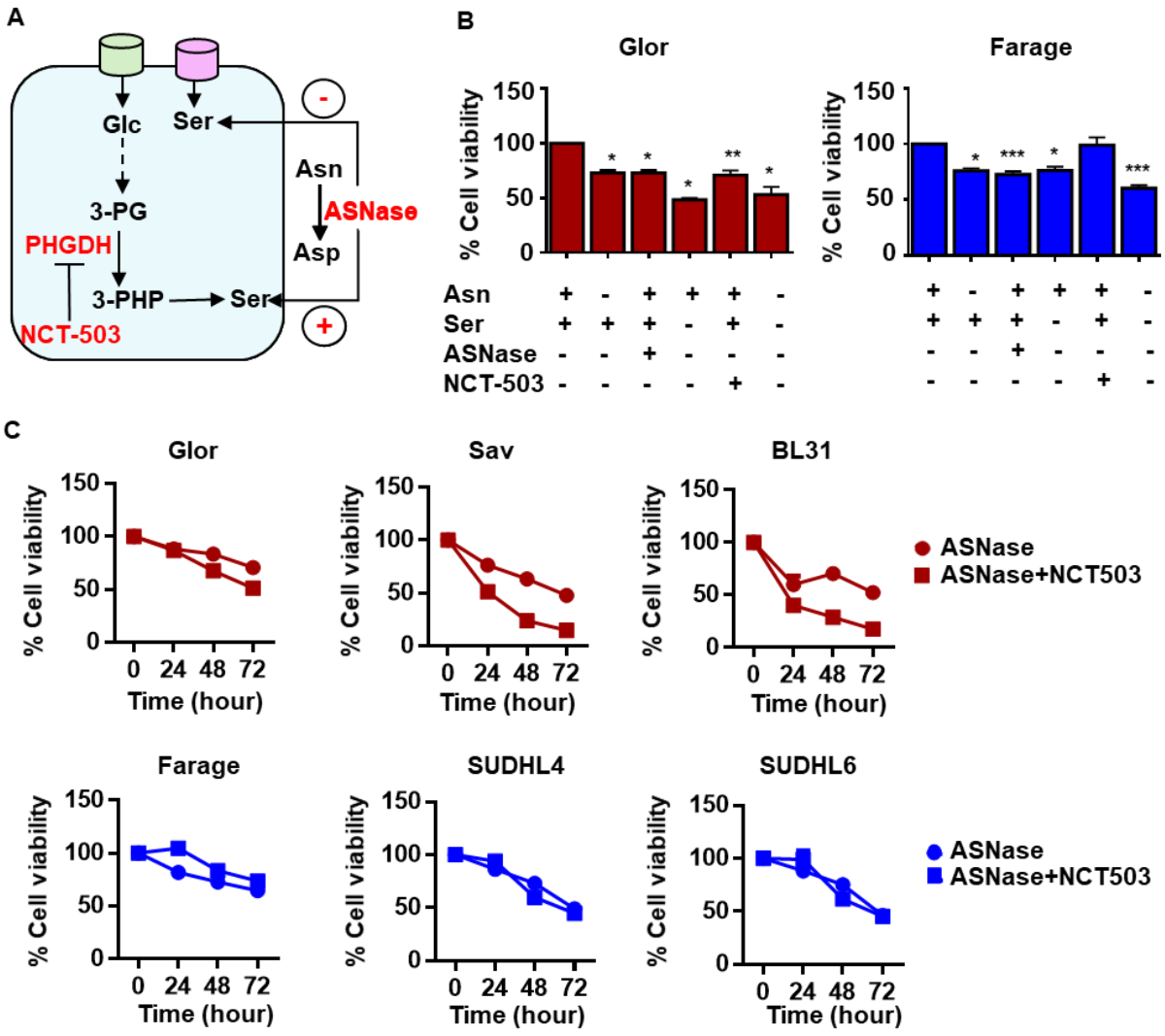

Figure 5.8 Combined effects of asparaginase and NCT503.

*Illustration of combined effects of asparaginase (ASNase) and NCT503 on serine and asparagine metabolism (A). The viability of Glor and Farage cells in a complete medium, in asparagine-free medium, in serine free medium, in the medium with ASNase at 0.1 U/ml, in the medium with NCT503 at 10 uM and in the serine and asparagine free medium after 72 hours (B). Treatment of Glor, Sav, BL31, Farage, SUDHL4, SUDHL6 with ASNase at 0.1 U/ml and ASNase at 0.1 U/ml plus NCT-503 at 10 μM for 24, 48 and 72 hours. Cell viability was assessed by the Celltiter Blue assay. Data is shown as mean ± SEM. *p < 0.05; **p < 0.01; ***p < 0.001.*

5.3 Discussion

5.3.1 Dependence of BL cells on extracellular asparagine

Although daily practise shows that BL and DLBCL display some intermediate and unclassifiable genetic features, which could increase the risk of misdiagnosis, we showed that distinctive differences in metabolism between BL and DLBCL using both metabolomics and transcriptomics. Gene expression profiling has revealed 264 altered metabolic genes between the two diseases.

In this study, I demonstrated that BL cells are more dependent on extracellular asparagine than DLBCL cells. This result can suggest that BL cells may either have more impaired capacity to synthesise adequate amounts of asparagine than DLBCL cells or need more asparagine than DLBCL cells need. Previous studies have shown that ALL cells have reduced or complete loss of expression of asparagine synthetase (ASNS) that synthesise asparagine from aspartate (Beard et al., 1970; Jiang et al., 2019). In the light of this finding, it could be proposed that BL cells may express ASNS less than DLBCL cells; thereby being more dependent on extracellular asparagine. However, most healthy cells increase transcription of ASNS and synthesis of asparagine when exposed to asparagine starvation (Balasubramanian et al., 2013). Indeed, ASNase resistant ALL cells were shown to have elevated ASNS protein expression. Conversely, when BL and DLBCL cells were treated with ASNase at 0.1 U/ml for 72 hours, this treatment resulted in 50% of cell loss. From this observation, it could be speculated that BL and DLBCL cells may not be able to regulate ASNS expression as much as normal healthy cells do.

Another possible reason behind the cell loss in response to ASNase treatment of BL and

DLBCL cells could be the role of asparagine in protein synthesis and in the regulation of uptake of other amino acids. Asparagine is a building block to produce protein and found to be a regulator of amino acid uptake and mTORC1 activity (Krall et al., 2016). Hence, asparagine starvation could impair protein synthesis and trigger apoptosis.

5.3.2 The metabolic consequences of asparagine starvation

Here, I examined the role of extracellular asparagine on cell metabolism. Particularly, the deprivation of extracellular asparagine resulted in an increase in serine, lactate, alanine and AMP production from glucose in BL cells. Asparagine starvation could enhance glucose uptake and thereby promoting glycolysis in BL cells to overcome the stress arising from the absence of extracellular asparagine Furthermore, loss of mitochondrial function and a compensatory increase in glycolysis occur during apoptosis of human leukaemia cells (Tiefenthaler et al., 2001). In this study, I showed that asparagine deprivation mediated by ASNase induced cell death in both BL and DLBCL. Taken together, the enhancement in the level of metabolites derived from glucose in BL cells could be explained by loss of mitochondrial function due to apoptosis. Another possible scenario to explain the increase in glycolytic intermediates in BL cells could be activation of PPP during asparagine starvation. The PPP supports cancer cell survival by directing glucose flux to its oxidative branch for nucleic acid synthesis and NADPH generation under stress condition (Jin & Zhou, 2019). In this regard, the increase in AMP level and other metabolites derived from glucose in BL cells might be associated with the activation of PPP to support cell growth and proliferation during nutrient deficiency. In contrast to the role of exogenous asparagine on the metabolism of BL cells, DLBCL cells significantly

decreased the lactate production from glucose in the absence of asparagine and show a slight increase in alanine and AMP production from glucose. These findings demonstrate that exogenous asparagine affects glucose metabolism differently in distinct cancer types. However, serine metabolism was affected in a similar manner in both lymphoma types by asparagine starvation.

Serine is a central node for the synthesis of glycine, cysteine and sphingolipids (X. Gao et al., 2018). Particularly, the conversion of serine to glycine is involved in the generation of one-carbon units that contribute to purine synthesis. Thus, the requirement of serine for the biosynthesis of purine bases makes serine a master regulator of nucleotide synthesis in cells (Lane & Fan, 2015). A recent study demonstrated that intracellular asparagine deprivation mediated by ASNS knockdown elevated the expression of enzymes involved in serine synthesis from glucose (Krall et al., 2016). Indeed, the same study revealed that intracellular asparagine regulates uptake of serine. Here, I showed that extracellular asparagine is involved in the regulation of serine metabolism. Although I did not quantify ASNS expression level in both lymphoma types, inadequate expression of ASNS in BL could be present in BL cell; thus, exogenous asparagine may regulate serine synthesis and serine uptake in lymphoma cells.

The data shown in this chapter support that extracellular asparagine is an important contributor to the regulation of glucose and serine metabolism. These findings can support that extracellular asparagine controls serine uptake and serine synthesis; thereby modulating the nucleotide biosynthesis in exogenous asparagine dependent cells due to the importance of serine in purine nucleotide biosynthesis.

5.3.3 The combination of a PHGDH inhibitor with asparaginase

In this chapter BL cells were found to express the PGHDH more than DLBCL cells. In the light of the effect of extracellular asparagine on serine synthesis, I combined the ASNase with NCT503 so that the intracellular serine amount could be further decreased, thereby leading to an additional reduction in the viability of BL cells. As shown, this combination induced a synergistic effect in terms of cytotoxic activity in BL cells. NCT503 enhanced the efficacy and sensitivity of ASNase to BL cells. However, this synergistic effect was not observed in DLBCL cells.

A recent study uncovered that PHGDH directly enhances the initiation of translation by interacting with translation initiation factors (Ma et al., 2019). Several studies also reported that PHGDH promotes cancer cell growth by upregulating the expression of cancer-promoting genes, such as cyclin B and cyclin D (J. Liu et al., 2013; Ma et al., 2019). Taken together, it could be speculated that the inhibition of PHGDH by NCT503 is more harmful to BL cells since BL cells express more PGHDH than DLBCL cells. Thus, the combination of ASNase with NCT503 might have exhibited synergistic inhibitory effects on BL cell growth in all three cell lines due to the role of PHGDH in non-metabolic pathways.

Combination approaches are designed to reduce the overall dose of drugs. Here, the combination of NCT503 with ASNase resulted in an increased cell loss owing to the sensitivity of BL cells to PHGDH inhibition in comparison with DLBCL cells. Thus, this work revealed that BL could be effectively treated by ASNase at a low dose along with a PHGDH inhibitor.

CHAPTER 6

GENERAL DISCUSSION

6.1 General discussion

Cancer cells exhibit altered metabolism compared to normal cells, utilising nutrients in a different manner in order to fulfil their energy demands (Hsu & Sabatini, 2008). This was first observed by Otto Warburg in 1924 who demonstrated that tumour cells shift their metabolism towards aerobic glycolysis even under high oxygen condition (Warburg et al., 1927). This switch from oxidative metabolism to aerobic glycolysis is called the Warburg effect, and promotes tumourigenesis and malignancy progression. Given the capacity of cancer cells to adjust their metabolism in response to challenging conditions, the evaluation of metabolites present in cancer cells and their microenvironment has gained significant importance. In this study, I focused on characterisation of metabolic differences in haematological cancer subtypes using NMR spectroscopy.

1D ^{1}H-NMR spectroscopy has emerged as one of the useful tools to study metabolism in cells. However, narrow dispersion of ^{1}H chemical shifts and a large number of ^{1}H resonance signals inevitably generate overlapping peaks in the NMR spectrum. Hence, the signal overlaps in 1D NMR spectra complicates peak identification and metabolite quantification (Dona et al., 2016). Nevertheless, 1D NMR spectroscopy enabled me to identify and quantify 22 intracellular and 13 extracellular metabolites that have a unique peak pattern. Identification of intracellular and extracellular metabolites highlighted substantial variation in the general metabolic profile of AML, CML, BL DLBCL and MM cell lines. Indeed, the PCA analysis displayed a clear separation between these haematological cancer subtypes. One of the major separations was observed between AML (HL60, NB4, KG1a, U937) and the CML cell line K562. K562 cells were derived from a CML patient in blast crisis (A et al., 2010); therefore they behave like an AML. The K562

cells were sharply discriminated from all AML cell lines, suggesting that presence of the BCR-ABL protein could affect cellular metabolism. BCR-ABL protein contributes to glycolytic metabolism, promoting the Warburg effect (Shanmugam et al., 2009). Despite the presence of BCR-ABL protein in K562 cells, AML cells were found to be more glycolytic than CML cells with a higher amount of lactate production in this study.

From my data and analysis of cell extracts, a great amount of creatine in K562 cells is the most distinguishing feature. Over the years, countless studies have exhibited that the creatine/phosphocreatine system is a shuttle for energy-rich phosphates between cellular sites of ATP utilisation (Brosnan & Brosnan, 2010; M & R, 2000; Taegtmeyer & Ingwall, 2013). However, key enzymes required for *de novo* creatine synthesis are expressed in skeletal muscle, liver and kidney (M & R, 2000), thus making *de novo* creatine synthesis in leukaemia cells unlikely. Despite this fact, the large amount of creatine found in K562 cells shows that the enzymes involved in *de novo* creatine synthesis are highly expressed in K562 cells. Other studies have also observed increased intracellular levels of creatine in imatinib-resistant CML cells and drug-resistant human breast cancer cells (Dewar et al., 2010; Kurmi et al., 2018). These findings can suggest that creatine may contribute to drug resistance besides acting as an intermediary of energy transfer.

A wide metabolic heterogeneity was observed between MM cell lines in this study. A significant heterogeneity in MM patients exists at both genetic and the clonal levels (Rasche et al., 2019). Several studies have reported the genomic landscape of MM patients pointing out the recurrently mutated genes that are likely causal drivers of the MM, such as KRAS, NRAS and BRAF (Hideshima et al., 2004; Rasche et al., 2019; Weaver & Tariman, 2017). However, although KRAS mutations are known as the most

common putative oncogenic mutations in MM, these mutations are just present in 16% of patients with MM (Kazandjian et al., 2019). Furthermore, multiple layers of heterogeneity were also revealed in MM. Thus, the large metabolic heterogeneity observed in PCA plots of MM cell lines might be result of the molecular heterogeneity in the MM cells.

I revealed that lactate production was greater in DLBCL and BL cells than AML, CML and MM cells. Lymphoma cells were found to be more glycolysis-oriented in comparison with leukaemia cells. The high levels of lactate in lymphoma cells relative to leukaemia and MM cells can be reasoned by the stabilisation of HIF-2α in normoxic conditions, c-Myc overexpression, gain-of-function mutations in EZH2 or presence of tonic BCR signalling in lymphoma cells. However, BL and DLBCL cells demonstrate HIF-2α stabilization even under normoxic condition (Evens et al., 2008). It can be suggested that the stabilisation of HIFs in lymphoma cells under normoxic conditions may be a driver of high lactate production in DLBCL and BL cells. The other potential driver of aerobic glycolysis in the lymphoid cells is the BCR signalling (Doughty et al., 2006). BCR crosslinking following antigen encounter leads to induce a rapid increase in glucose uptake and glycolysis. However, DLBCL cells were found to display tonic BCR signalling which activates multiple downstream effectors without BCR crosslinking (Havranek et al., 2017). Since AML, CML and MM cells do not express BCR ,which is massively expressed in GC cells, the observation of high lactate level in lymphoma cells may be a result of the tonic BCR signalling, in addition to other key drivers for aerobic glycolysis, such as c-Myc. Various types of c-Myc gene mutations, which induce over-expression or increased activity of LDHA, are present in all BL patients and 5–15% of patients with DLBCL (Nguyen et al., 2017).

I also showed that there was considerable uptake of leucine, isoleucine and valine from the extracellular environment in MM cells. MM cells are likely to upregulate BCAAs uptake to meet demand for production of immunoglobulin light or heavy chains. BCAAs are transported by LAT (LAT1, LAT2, LAT3, LAT4) transporters (Hayashi & Anzai, 2017). LAT1 interacts with CD98 to localize to plasma membrane (Bröer et al., 2001). I demonstrated that that CD98 was mostly present in MM cells that had showed the highest BCAAs uptake. One of the characteristics of MM is the excessive production of monoclonal protein. The excessive accumulation of unfolded proteins in their endoplasmic reticulum initiates the integrated stress response which results in inhibition of protein synthesis while promoting the expression of ATF4 protein. ATF4 protein has been found to regulate CD98/SLC3A2 (Drummond et al., 2011). Thus, the high level of the surface CD98 could be resulted from the expression of ATF4 due to the accumulation of unfolded proteins.

Conversely, LAT1 surface level was found to be at the lowest level in MM cells. The detection of low level LAT1 on MM cell by flow cytometry may be due to technical issues. As CD98 is much larger than LAT1, LAT1 could be physically masked by CD98 at the cell surface and therefore not easily accessible for antibody staining, hence giving low LAT1 signal intensities by flow cytometry analysis. To address this, western blotting could be performed. Another possible scenario to explain the detection of low level of LAT1 on MM cells may be the association of CD98 with LAT2 instead of LAT1 in MM cells. Just like LAT1, LAT2 forms a heterodimer with CD98 (Bröer et al., 2001).

I investigated the metabolic role of leucine in MM cells. I found that leucine is broken down to acetyl-CoA by MM cells to promote the TCA cycle. I also showed that leucine acts as an energetic molecule in MM cells. Furthermore, acetyl-CoA derived from leucine was

showed to be involved in sialic acid formation in MM cells. Hypersialylation has been previously implicated in cancer malignancy and metastatic potential (Rodrigues & Macauley, 2018). Sialic acid production increases in MM cells (J. Chen et al., 2015). Thus, it could be suggested that MM cells break down leucine to acetyl-CoA to support aberrant glycolysation.

BL cells were found to be more dependent on extracellular asparagine than DLBCL cells. BL cells may have more impaired capacity to synthesise asparagine than DLBCL cells due to inadequate expression of asparagine synthetase (ASNS). Many studies demonstrated that ALL cells are dependent upon extracellular asparagine as they are unable to *de nova* synthesise asparagine from aspartate owing to reduced or complete loss of expression of ASNS (Balasubramanian et al., 2013; Beard et al., 1970). Consequently, the clinical use of ASNase, which converts asparagine into aspartate, was approved to treat patients with ALL (Beard et al., 1970). Thus, asparagine dependency of BL cells directed me to investigate the asparagine metabolism in BL cells. Particularly, starvation of extracellular asparagine caused an increase in lactate, alanine and AMP production from glucose in BL cells. In light of this finding, BL cells seemed to enhance glucose uptake thereby promoting glycolysis to overcome the cellular stress arising from the absence of extracellular asparagine. In contrast, DLBCL cells were observed to decrease lactate production when exposed to asparagine starvation. Taken together, exogenous asparagine affects different cell types in different ways with regard to the glycolysis. However, exogenous asparagine affected serine metabolism in a similar manner in both lymphoma types. Asparagine starvation increased serine production from glucose and decreased serine uptake in BL and DLBCL cells. In addition, asparagine

deprivation mediated by ASNase elevated the expression of PHGDH that is involved in serine synthesis from glucose. My findings show that exogenous asparagine is an important contributor to the regulation of glucose and serine metabolism.

BL cells were found to be more sensitive to PHGDH inhibition by NCT503 than DLBCL cells. The combination of NCT503 with ASNase resulted in a more decrease in viability of BL cells compared to the reduction in the viability of DLBCL cells. Thus, I revealed that BL could be effectively treated by ASNase at a low dose with a PHGDH inhibitor.

6.2 Future work

Even though I have studied the metabolic phenotype of five distinct haematological cancers which represent AML, CML, BL, DLBCL and MM, metabolic phenotypes of many haematological cancer types still remain to be elucidated. To further understand the metabolic diversity of haematological cancers, more cell lines from different haematological cancer subtypes could be studied using NMR spectroscopy. More importantly, many conclusions are drawn from *in vitro* experiments of cancer cells in this thesis. Given that many studies have revealed that the metabolism of cancer cells can differ from that of primary tumours, *in vivo* studies would provide crucial data for proof-concept determination of the metabolic underpinnings in haematological cancer cells.

To elucidate altered metabolic pathways of AML, CML, BL, DLBCL and MM, different isotopically labelled precursors would need to be used as starting points to determine the intermediates and products of metabolism across 18 cell lines. For instance, 2D NMR examination of cells which are grown in a medium containing [1,2-^{13}C]-glucose and [3-^{13}C]-glutamine would present the balance between glycolysis and glutaminolysis in supplying the TCA cycle. Thus, the use of different isotopically labelled precursors would shed more light on the metabolic phenotypes of AML, CML, BL, DLBCL and MM cells.

To understand creatine metabolism in CML cells, the creatine synthetic pathway (AGAT and GAMT enzymes) would be investigated at the protein and the mRNA level. To test whether creatine synthesis is associated with the drug resistance, ^{1}H NMR spectroscopy would be carried out on cell extracts of imatinib-sensitive CML cells and imatinib-resistant CML cells. Given that many studies have revealed that creatine/phosphocreatine system functions as an energy buffer, the effect of the knockdown of AGAT and GAMT genes on

the viability of CML cells would be studied.

To further investigate the BCAA metabolism in MM cells, the expression level of LAT2, LAT3 and LAT4 could be studied. The expression level of intracellular LAT1 light chain and CD98 heavy chain would be assessed by western blot in order to test whether their intracellular expressions are correlated with their cell surface levels. Furthermore, knockdown of CD98 would be performed to understand the role of CD98 in BCAA uptake. To understand whether or to what extend MM cells rely on BCAAs for the production of monoclonal free κ and λ immunoglobulin light chains, the effect of inhibition of LAT1/CD98 transporter by BCH or JPH203 on the production of kappa and lambda light chains could be studied. The importance of LAT1 on BCAAs uptake would be investigated using LAT1 knockout cells.

To deepen understanding of the level of asparagine dependency of lymphoma cells, the use of more BL and DLBCL cell lines could validate the observations related to extracellular asparagine dependency of BL cells. The measurement of expression level of asparagine synthetase (ASNS) in cell samples from patients with BL and DLBCL could show the extracellular asparagine dependencies of primary cells. Gene expression profiling of samples from BL and DLBCL patients and cell lines would allow simultaneous monitoring of the transcriptional behaviour of genes involved in asparagine and serine metabolism. In this thesis, asparagine deprivation mediated by ASNase was shown to induce cell death. Future investigations may address which cell death mechanism is activated by asparagine deprivation. ASNS and PHGDH knockdown mouse would be used to study the biological effects of ASNase.

6.3 Final remark

Cancer cells exhibit altered metabolism, regulating the dynamics of the central metabolic pathways in a different manner (Hsu & Sabatini, 2008). The metabolic alterations of haematological cancers and characterisations of metabolic differences in cancer subtypes have not been well-focused so far.

Using NMR-based metabolite profiling, I revealed how haematological cancer cells converge multiple biochemical pathways. I have also expanded the scope of metabolic dependencies beyond the classical pathways that are known in cancer cells. From a therapeutic perspective, my work has also presented potential metabolic vulnerabilities that might be targeted for therapies of BL and MM. Future research should bring further light to these emerging vulnerabilities and dependencies and conceive ways to use them for diagnosis and therapy. This will require the use of *in vivo* models and integration of NMR based metabolomics with other methods.

Briefly, I believe my findings provide deep insights into metabolism in haematological cancer cells and aid to tailor therapeutic strategies by researchers.

APPENDICIES

Appendix A: Recipes and buffers

A.1 Protein extraction

Ripa buffer

- 1ml of NP40 (IGEPAL)
- 0.5g sodium deoxycholate
- 1ml 10% SDS
- Adjust volume to 100ml with dH20.

A.2.Western blotting

10 x SDS running buffer

- 30g Tris (250mM)
- 144g glycine (1.92M)
- 10g SDS (1%)
- Adjust volume to 1 litre with dH20.
- Dilute 1:10 to make 1x SDS Running Buffer

4 x SDS gel loading buffer

- 2.0ml 1M Tris-HCl, pH 6.8
- 0.8g SDS
- 4.0ml 100% glycerol
- 0.4Ml 14.7M β-mercaptoethanol
- 1.0ml 0.5M EDTA

- 8.0mg bromophenol blue
- 2.6ml dH_2O
- Dilute 1:4 to make 1x SDS gel loading buffer.

1.5M Tris (pH 8.8)

- Dissolve 90.8g Tris in 400ml dH_20 and adjust pH to 8.8
- Make up to 500ml in dH_20
- 0.5M Tris (pH 6.8)
- Dissolve 30.3g Tris in 400ml dH20 and adjust pH to 6.8
- Make up to 500ml with dH20

Transfer Buffer

- Dissolve 7.575g Tris and 36g glycine in 500ml methanol
- Make up the volume to 2.5 litres with dH_20

TBTS-T

- Dissolve 16g Nacl and 2ml Tween 20 in 40ml 1M Tris HCL pH7.6
- Make up the volume to 2 litres with dH_20

TBS

- Add:20mM Tris HCl, pH 7.5
- 0.8% w/v NaCl
- Make up the volume to 1L with dH_2O

LIST OF REFERENCES

A, J., Qian, S., Wang, G., Yan, B., Zhang, S., Huang, Q., Ni, L., Zha, W., Liu, L., Cao, B., Hong, M., Wu, H., Lu, H., Shi, J., Li, M., & Li, J. (2010). Chronic Myeloid Leukemia Patients Sensitive and Resistant to Imatinib Treatment Show Different Metabolic Responses. *PLoS ONE*, *5*(10). https://doi.org/10.1371/journal.pone.0013186

Abate, F., Ambrosio, M. R., Mundo, L., Laginestra, M. A., Fuligni, F., Rossi, M., Zairis, S., Gazaneo, S., De Falco, G., Lazzi, S., Bellan, C., Rocca, B. J., Amato, T., Marasco, E., Etebari, M., Ogwang, M., Calbi, V., Ndede, I., Patel, K., … Rabadan, R. (2015). Distinct Viral and Mutational Spectrum of Endemic Burkitt Lymphoma. *PLoS Pathogens*, *11*(10), e1005158. https://doi.org/10.1371/journal.ppat.1005158

Adams, J., & Nassiri, M. (2015). Acute Promyelocytic Leukemia: A Review and Discussion of Variant Translocations. *Archives of Pathology & Laboratory Medicine*, *139*(10), 1308–1313. https://doi.org/10.5858/arpa.2013-0345-RS

Alabduladhem, T. O., & Bordoni, B. (2020). Physiology, Krebs Cycle. In *StatPearls*. StatPearls Publishing. http://www.ncbi.nlm.nih.gov/books/NBK556032/

Alizadeh, A. A., Eisen, M. B., Davis, R. E., Ma, C., Lossos, I. S., Rosenwald, A., Boldrick, J. C., Sabet, H., Tran, T., Yu, X., Powell, J. I., Yang, L., Marti, G. E., Moore, T., Hudson, J., Lu, L., Lewis, D. B., Tibshirani, R., Sherlock, G., … Staudt, L. M. (2000). Distinct types of diffuse large B-cell lymphoma identified by gene expression profiling. *Nature*, *403*(6769), 503–511. https://doi.org/10.1038/35000501

Alsous, M., Abu Farha, R., Alefishat, E., Al Omar, S., Momani, D., Gharabli, A., McElnay, J., Horne, R., & Rihani, R. (2017). Adherence to 6-Mercaptopurine in children and adolescents with Acute Lymphoblastic Leukemia. *PLoS ONE*, *12*(9). https://doi.org/10.1371/journal.pone.0183119

Anderson, N. M., Mucka, P., Kern, J. G., & Feng, H. (2018). The emerging role and targetability of the TCA cycle in cancer metabolism. *Protein & Cell*, *9*(2), 216–237. https://doi.org/10.1007/s13238-017-0451-1

Apperley, J. F. (2015). Chronic myeloid leukaemia. *Lancet (London, England)*, *385*(9976), 1447–1459. https://doi.org/10.1016/S0140-6736(13)62120-0

Arber, D. A., Orazi, A., Hasserjian, R., Thiele, J., Borowitz, M. J., Le Beau, M. M., Bloomfield, C. D., Cazzola, M., & Vardiman, J. W. (2016). The 2016 revision to the World Health Organization classification of myeloid neoplasms and acute leukemia. *Blood*, *127*(20), 2391–2405. https://doi.org/10.1182/blood-2016-03-643544

Aretz, I., & Meierhofer, D. (2016). Advantages and Pitfalls of Mass Spectrometry Based Metabolome Profiling in Systems Biology. *International Journal of Molecular Sciences*, *17*(5). https://doi.org/10.3390/ijms17050632

Ata, R., & Antonescu, C. N. (2017). Integrins and Cell Metabolism: An Intimate Relationship Impacting Cancer. *International Journal of Molecular Sciences*, *18*(1). https://doi.org/10.3390/ijms18010189

Balasubramanian, M. N., Butterworth, E. A., & Kilberg, M. S. (2013). Asparagine synthetase: Regulation by cell stress and involvement in tumor biology. *American Journal of Physiology - Endocrinology and Metabolism*, *304*(8), E789–E799. https://doi.org/10.1152/ajpendo.00015.2013

Barnes, K., McIntosh, E., Whetton, A. D., Daley, G. Q., Bentley, J., & Baldwin, S. A. (2005). Chronic myeloid leukaemia: An investigation into the role of Bcr-Abl-induced abnormalities in glucose transport regulation. *Oncogene*, *24*(20), 3257–3267. https://doi.org/10.1038/sj.onc.1208461

Barollo, S., Bertazza, L., Watutantrige-Fernando, S., Censi, S., Cavedon, E., Galuppini, F., Pennelli, G., Fassina, A., Citton, M., Rubin, B., Pezzani, R., Benna, C., Opocher, G., Iacobone, M., & Mian, C. (2016). Overexpression of L-Type Amino Acid Transporter 1 (LAT1) and 2 (LAT2): Novel Markers of Neuroendocrine Tumors. *PLOS ONE*, *11*(5), e0156044. https://doi.org/10.1371/journal.pone.0156044

Beard, M. E., Crowther, D., Galton, D. A., Guyer, R. J., Fairley, G. H., Kay, H. E., Knapton, P. J., Malpas, J. S., & Scott, R. B. (1970). L-asparaginase in treatment of acute leukaemia and lymphosarcoma. *British Medical Journal*, *1*(5690), 191–195. https://doi.org/10.1136/bmj.1.5690.191

Béguelin, W., Popovic, R., Teater, M., Jiang, Y., Bunting, K. L., Rosen, M., Shen, H., Yang, S. N., Wang, L., Ezponda, T., Martinez-Garcia, E., Zhang, H., Zheng, Y., Verma, S. K., McCabe, M. T., Ott, H. M., Van Aller, G. S., Kruger, R. G., Liu, Y., … Melnick, A. M. (2013). EZH2 is required for germinal center formation and somatic EZH2 mutations promote lymphoid transformation. *Cancer Cell*, *23*(5), 677–692. https://doi.org/10.1016/j.ccr.2013.04.011

Beloribi-Djefaflia, S., Vasseur, S., & Guillaumond, F. (2016). Lipid metabolic reprogramming in cancer cells. *Oncogenesis*, *5*(1), e189–e189. https://doi.org/10.1038/oncsis.2015.49

Berg, J. M., Tymoczko, J. L., & Stryer, L. (2002). Fatty Acid Metabolism. *Biochemistry. 5th Edition*. https://www.ncbi.nlm.nih.gov/books/NBK21173/

Bhattacharya, B., Mohd Omar, M. F., & Soong, R. (2016). The Warburg effect and drug resistance. *British Journal of Pharmacology*, *173*(6), 970–979. https://doi.org/10.1111/bph.13422

Bolzoni, M., Chiu, M., Accardi, F., Vescovini, R., Airoldi, I., Storti, P., Todoerti, K., Agnelli, L.,

Missale, G., Andreoli, R., Bianchi, M. G., Allegri, M., Barilli, A., Nicolini, F., Cavalli, A., Costa, F., Marchica, V., Toscani, D., Mancini, C., … Giuliani, N. (2016). Dependence on glutamine uptake and glutamine addiction characterize myeloma cells: A new attractive target. *Blood*, *128*(5), 667–679. https://doi.org/10.1182/blood-2016-01-690743

Bork, K., Horstkorte, R., & Weidemann, W. (2009). Increasing the sialylation of therapeutic glycoproteins: The potential of the sialic acid biosynthetic pathway. *Journal of Pharmaceutical Sciences*, *98*(10), 3499–3508. https://doi.org/10.1002/jps.21684

Boroughs, L. K., & DeBerardinis, R. J. (2015). Metabolic pathways promoting cancer cell survival and growth. *Nature Cell Biology*, *17*(4), 351–359. https://doi.org/10.1038/ncb3124

Bott, A. J., Peng, I.-C., Fan, Y., Faubert, B., Zhao, L., Li, J., Neidler, S., Sun, Y., Jaber, N., Krokowski, D., Lu, W., Pan, J.-A., Powers, S., Rabinowitz, J., Hatzoglou, M., Murphy, D. J., Jones, R., Wu, S., Girnun, G., & Zong, W.-X. (2015). Oncogenic Myc induces expression of glutamine synthetase through promoter demethylation. *Cell Metabolism*, *22*(6), 1068–1077. https://doi.org/10.1016/j.cmet.2015.09.025

Bray, N. L., Pimentel, H., Melsted, P., & Pachter, L. (2016). Near-optimal probabilistic RNA-seq quantification. *Nature Biotechnology*, *34*(5), 525–527. https://doi.org/10.1038/nbt.3519

Brigle, K., & Rogers, B. (2017). Pathobiology and Diagnosis of Multiple Myeloma. *Seminars in Oncology Nursing*, *33*(3), 225–236. https://doi.org/10.1016/j.soncn.2017.05.012

Bröer, A., Friedrich, B., Wagner, C. A., Fillon, S., Ganapathy, V., Lang, F., & Bröer, S. (2001). Association of 4F2hc with light chains LAT1, LAT2 or y+LAT2 requires different domains. *Biochemical Journal*, *355*(Pt 3), 725–731.

Brooks, G. A. (2018). The Science and Translation of Lactate Shuttle Theory. *Cell Metabolism*,

27(4), 757–785. https://doi.org/10.1016/j.cmet.2018.03.008

Brosnan, J. T., & Brosnan, M. E. (2010). Creatine metabolism and the urea cycle. *Molecular Genetics and Metabolism*, *100*, S49–S52. https://doi.org/10.1016/j.ymgme.2010.02.020

Bruntz, R. C., Lane, A. N., Higashi, R. M., & Fan, T. W.-M. (2017). Exploring cancer metabolism using stable isotope-resolved metabolomics (SIRM). *The Journal of Biological Chemistry*, *292*(28), 11601–11609. https://doi.org/10.1074/jbc.R117.776054

Bryant, K. L., Mancias, J. D., Kimmelman, A. C., & Der, C. J. (2014). KRAS: Feeding pancreatic cancer proliferation. *Trends in Biochemical Sciences*, *39*(2), 91–100. https://doi.org/10.1016/j.tibs.2013.12.004

Burkitt, D. (1958). A sarcoma involving the jaws in African children. *The British Journal of Surgery*, *46*(197), 218–223. https://doi.org/10.1002/bjs.18004619704

Burns, J. S., & Manda, G. (2017). Metabolic Pathways of the Warburg Effect in Health and Disease: Perspectives of Choice, Chain or Chance. *International Journal of Molecular Sciences*, *18*(12). https://doi.org/10.3390/ijms18122755

Campo, E., Swerdlow, S. H., Harris, N. L., Pileri, S., Stein, H., & Jaffe, E. S. (2011). The 2008 WHO classification of lymphoid neoplasms and beyond: Evolving concepts and practical applications. *Blood*, *117*(19), 5019–5032. https://doi.org/10.1182/blood-2011-01-293050

Cao, K., Li, J., Chen, J., Qian, L., Wang, A., Chen, X., Xiong, W., Tang, J., Tang, S., Chen, Y., Chen, Y., Cheng, Y., & Zhou, J. (2017). MicroRNA-33a-5p increases radiosensitivity by inhibiting glycolysis in melanoma. *Oncotarget*, *8*(48), 83660–83672. https://doi.org/10.18632/oncotarget.19014

Caro, P., Kishan, A. U., Norberg, E., Stanley, I. A., Chapuy, B., Ficarro, S. B., Polak, K., Tondera, D., Gounarides, J., Yin, H., Zhou, F., Green, M. R., Chen, L., Monti, S., Marto, J. A.,

Shipp, M. A., & Danial, N. N. (2012). Metabolic signatures uncover distinct targets in molecular subsets of diffuse large B cell lymphoma. *Cancer Cell*, *22*(4), 547–560. https://doi.org/10.1016/j.ccr.2012.08.014

Cavanagh, J. (1995). *Protein NMR Spectroscopy: Principles and Practice*.

Cecconello, D. K., Magalhães, M. R. de, Werlang, I. C. R., Lee, M. L. de M., Michalowski, M. B., & Daudt, L. E. (2020). Asparaginase: An old drug with new questions. *Hematology, Transfusion and Cell Therapy*, *42*(3), 275–282. https://doi.org/10.1016/j.htct.2019.07.010

Chapman, J., & Zhang, Y. (2020). Histology, Hematopoiesis. In *StatPearls*. StatPearls Publishing. http://www.ncbi.nlm.nih.gov/books/NBK534246/

Chapuis, N., Poulain, L., Birsen, R., Tamburini, J., & Bouscary, D. (2019). Rationale for Targeting Deregulated Metabolic Pathways as a Therapeutic Strategy in Acute Myeloid Leukemia. *Frontiers in Oncology*, *9*. https://doi.org/10.3389/fonc.2019.00405

Chapuy, B., Cheng, H., Watahiki, A., Ducar, M. D., Tan, Y., Chen, L., Roemer, M. G. M., Ouyang, J., Christie, A. L., Zhang, L., Gusenleitner, D., Abo, R. P., Farinha, P., von Bonin, F., Thorner, A. R., Sun, H. H., Gascoyne, R. D., Pinkus, G. S., van Hummelen, P., … Shipp, M. A. (2016). Diffuse large B-cell lymphoma patient-derived xenograft models capture the molecular and biological heterogeneity of the disease. *Blood*, *127*(18), 2203–2213. https://doi.org/10.1182/blood-2015-09-672352

Chaudhry, R., & Varacallo, M. (2020). Biochemistry, Glycolysis. In *StatPearls*. StatPearls Publishing. http://www.ncbi.nlm.nih.gov/books/NBK482303/

Chen, J., Fang, M., Zhao, Y.-P., Yi, C.-H., Ji, J., Cheng, C., Wang, M.-M., Gu, X., Sun, Q.-S., Chen, X.-L., & Gao, C.-F. (2015). Serum N-Glycans: A New Diagnostic Biomarker for Light Chain Multiple Myeloma. *PloS One*, *10*(6), e0127022.

https://doi.org/10.1371/journal.pone.0127022

Chen, Y., Peng, C., Li, D., & Li, S. (2010). Molecular and cellular bases of chronic myeloid leukemia. *Protein & Cell*, *1*(2), 124–132. https://doi.org/10.1007/s13238-010-0016-z

Chen, Y.-J., Mahieu, N. G., Huang, X., Singh, M., Crawford, P. A., Johnson, S. L., Gross, R. W., Schaefer, J., & Patti, G. J. (2016). Lactate metabolism is associated with mammalian mitochondria. *Nature Chemical Biology*, *12*(11), 937–943. https://doi.org/10.1038/nchembio.2172

Cheng, C., Wang, Z., & Chen, J. (2014). Targeting FASN in Breast Cancer and the Discovery of Promising Inhibitors from Natural Products Derived from Traditional Chinese Medicine. *Evidence-Based Complementary and Alternative Medicine : ECAM*, *2014*. https://doi.org/10.1155/2014/232946

Chin, K., DeVries, S., Fridlyand, J., Spellman, P. T., Roydasgupta, R., Kuo, W.-L., Lapuk, A., Neve, R. M., Qian, Z., Ryder, T., Chen, F., Feiler, H., Tokuyasu, T., Kingsley, C., Dairkee, S., Meng, Z., Chew, K., Pinkel, D., Jain, A., … Gray, J. W. (2006). Genomic and transcriptional aberrations linked to breast cancer pathophysiologies. *Cancer Cell*, *10*(6), 529–541. https://doi.org/10.1016/j.ccr.2006.10.009

Cho, E. S., Cha, Y. H., Kim, H. S., Kim, N. H., & Yook, J. I. (2018). The Pentose Phosphate Pathway as a Potential Target for Cancer Therapy. *Biomolecules & Therapeutics*, *26*(1), 29–38. https://doi.org/10.4062/biomolther.2017.179

Chong, M., Jayaraman, A., Marin, S., Selivanov, V., de Atauri Carulla, P. R., Tennant, D. A., Cascante, M., Günther, U. L., & Ludwig, C. (2017). Combined Analysis of NMR and MS Spectra (CANMS). *Angewandte Chemie International Edition*, *56*(15), 4140–4144. https://doi.org/10.1002/anie.201611634

Cilloni, D., & Saglio, G. (2012). Molecular Pathways: BCR-ABL. *Clinical Cancer Research*, *18*(4), 930–937. https://doi.org/10.1158/1078-0432.CCR-10-1613

Cluntun, A. A., Lukey, M. J., Cerione, R. A., & Locasale, J. W. (2017). Glutamine Metabolism in Cancer: Understanding the Heterogeneity. *Trends in Cancer*, *3*(3), 169–180. https://doi.org/10.1016/j.trecan.2017.01.005

Cochrane, G., Karsch-Mizrachi, I., Nakamura, Y., & on behalf of the International Nucleotide Sequence Database Collaboration. (2011). The International Nucleotide Sequence Database Collaboration. *Nucleic Acids Research*, *39*(Database), D15–D18. https://doi.org/10.1093/nar/gkq1150

Cohen, A. M., Allalouf, D., Bessler, H., Djaldetti, M., Malachi, T., & Levinsky, H. (1989). Sialyltransferase activity and sialic acid levels in multiple myeloma and monoclonal gammopathy. *European Journal of Haematology*, *42*(3), 289–292. https://doi.org/10.1111/j.1600-0609.1989.tb00114.x

Collart, F. R., Chubb, C. B., Mirkin, B. L., & Huberman, E. (1992). Increased inosine-5'-phosphate dehydrogenase gene expression in solid tumor tissues and tumor cell lines. *Cancer Research*, *52*(20), 5826–5828. https://doi.org/10.2172/10148922

Conrad, M., & Sato, H. (2012). The oxidative stress-inducible cystine/glutamate antiporter, system x (c) (-): Cystine supplier and beyond. *Amino Acids*, *42*(1), 231–246. https://doi.org/10.1007/s00726-011-0867-5

Coso, D., Garciaz, S., & Bouabdallah, R. (2015, November 30). *Clinical and biological aspects of aggressive B-cell non-Hodgkin lymphoma in adolescents and young adults*. Clinical Oncology in Adolescents and Young Adults. https://doi.org/10.2147/COAYA.S70365

Cowan, A. J., Allen, C., Barac, A., Basaleem, H., Bensenor, I., Curado, M. P., Foreman, K.,

Gupta, R., Harvey, J., Hosgood, H. D., Jakovljevic, M., Khader, Y., Linn, S., Lad, D., Mantovani, L., Nong, V. M., Mokdad, A., Naghavi, M., Postma, M., … Fitzmaurice, C. (2018). Global Burden of Multiple Myeloma. *JAMA Oncology*, *4*(9), 1221–1227. https://doi.org/10.1001/jamaoncol.2018.2128

Crook, M. A., Couchman, S., & Tutt, P. (1996). Serum sialic acid in patients with multiple myeloma. *British Journal of Biomedical Science*, *53*(3), 185–186.

Csibi, A., Lee, G., Yoon, S.-O., Tong, H., Ilter, D., Elia, I., Fendt, S.-M., Roberts, T. M., & Blenis, J. (2014). The mTORC1/S6K1 pathway regulates glutamine metabolism through the eIF4B-dependent control of c-Myc translation. *Current Biology: CB*, *24*(19), 2274–2280. https://doi.org/10.1016/j.cub.2014.08.007

Dalla-Favera, R., Bregni, M., Erikson, J., Patterson, D., Gallo, R. C., & Croce, C. M. (1982). Human c-myc onc gene is located on the region of chromosome 8 that is translocated in Burkitt lymphoma cells. *Proceedings of the National Academy of Sciences of the United States of America*, *79*(24), 7824–7827.

Dalva-Aydemir, S., Bajpai, R., Martinez, M., Adekola, K. U. A., Kandela, I., Wei, C., Singhal, S., Koblinski, J. E., Raje, N. S., Rosen, S. T., & Shanmugam, M. (2015). Targeting the metabolic plasticity of multiple myeloma with FDA-approved ritonavir and metformin. *Clinical Cancer Research: An Official Journal of the American Association for Cancer Research*, *21*(5), 1161–1171. https://doi.org/10.1158/1078-0432.CCR-14-1088

Dang, C. V. (2011). Therapeutic targeting of Myc-reprogrammed cancer cell metabolism. *Cold Spring Harbor Symposia on Quantitative Biology*, *76*, 369–374. https://doi.org/10.1101/sqb.2011.76.011296

Dang, Chi V. (2013). MYC, Metabolism, Cell Growth, and Tumorigenesis. *Cold Spring Harbor*

Perspectives in Medicine, *3*(8). https://doi.org/10.1101/cshperspect.a014217

Dang, L., White, D. W., Gross, S., Bennett, B. D., Bittinger, M. A., Driggers, E. M., Fantin, V. R., Jang, H. G., Jin, S., Keenan, M. C., Marks, K. M., Prins, R. M., Ward, P. S., Yen, K. E., Liau, L. M., Rabinowitz, J. D., Cantley, L. C., Thompson, C. B., Vander Heiden, M. G., & Su, S. M. (2009). Cancer-associated IDH1 mutations produce 2-hydroxyglutarate. *Nature*, *462*(7274), 739. https://doi.org/10.1038/nature08617

Dayrit, F. M., & Dios, A. C. de. (2017). 1H and 13C NMR for the Profiling of Natural Product Extracts: Theory and Applications. In E. Sharmin & F. Zafar (Eds.), *Spectroscopic Analyses—Developments and Applications*. InTech. https://doi.org/10.5772/intechopen.71040

de Leval, L., & Hasserjian, R. P. (2009). Diffuse Large B-Cell Lymphomas and Burkitt Lymphoma. *Hematology/Oncology Clinics of North America*, *23*(4), 791–827. https://doi.org/10.1016/j.hoc.2009.04.004

DeBerardinis, R. J., & Chandel, N. S. (2016). Fundamentals of cancer metabolism. *Science Advances*, *2*(5), e1600200. https://doi.org/10.1126/sciadv.1600200

DeBerardinis, R. J., Mancuso, A., Daikhin, E., Nissim, I., Yudkoff, M., Wehrli, S., & Thompson, C. B. (2007). Beyond aerobic glycolysis: Transformed cells can engage in glutamine metabolism that exceeds the requirement for protein and nucleotide synthesis. *Proceedings of the National Academy of Sciences of the United States of America*, *104*(49), 19345–19350. https://doi.org/10.1073/pnas.0709747104

Delaglio, F., Grzesiek, S., Vuister, G. W., Zhu, G., Pfeifer, J., & Bax, A. (1995). NMRPipe: A multidimensional spectral processing system based on UNIX pipes. *Journal of Biomolecular NMR*, *6*(3), 277–293. https://doi.org/10.1007/BF00197809

Devin, J., Kassambara, A., Bruyer, A., Moreaux, J., & Bret, C. (2019). Phenotypic Characterization of Diffuse Large B-Cell Lymphoma Cells and Prognostic Impact. *Journal of Clinical Medicine*, *8*(7). https://doi.org/10.3390/jcm8071074

Dewar, B. J., Keshari, K., Jeffries, R., Dzeja, P., Graves, L. M., & Macdonald, J. M. (2010). Metabolic assessment of a novel chronic myelogenous leukemic cell line and an imatinib resistant subline by 1H NMR spectroscopy. *Metabolomics*, *6*(3), 439–450. https://doi.org/10.1007/s11306-010-0204-0

Dillon, B. J., Prieto, V. G., Curley, S. A., Ensor, C. M., Holtsberg, F. W., Bomalaski, J. S., & Clark, M. A. (2004). Incidence and distribution of argininosuccinate synthetase deficiency in human cancers. *Cancer*, *100*(4), 826–833. https://doi.org/10.1002/cncr.20057

Doi, M., Yamaoka, I., Fukunaga, T., & Nakayama, M. (2003). Isoleucine, a potent plasma glucose-lowering amino acid, stimulates glucose uptake in C2C12 myotubes. *Biochemical and Biophysical Research Communications*, *312*(4), 1111–1117. https://doi.org/10.1016/j.bbrc.2003.11.039

Dona, A. C., Kyriakides, M., Scott, F., Shephard, E. A., Varshavi, D., Veselkov, K., & Everett, J. R. (2016). A guide to the identification of metabolites in NMR-based metabonomics/metabolomics experiments. *Computational and Structural Biotechnology Journal*, *14*, 135–153. https://doi.org/10.1016/j.csbj.2016.02.005

Doughty, C. A., Bleiman, B. F., Wagner, D. J., Dufort, F. J., Mataraza, J. M., Roberts, M. F., & Chiles, T. C. (2006). Antigen receptor–mediated changes in glucose metabolism in B lymphocytes: Role of phosphatidylinositol 3-kinase signaling in the glycolytic control of growth. *Blood*, *107*(11), 4458–4465. https://doi.org/10.1182/blood-2005-12-4788

Dozzo, M., Carobolante, F., Donisi, P. M., Scattolin, A., Maino, E., Sancetta, R., Viero, P., &

Bassan, R. (2016). Burkitt lymphoma in adolescents and young adults: Management challenges. *Adolescent Health, Medicine and Therapeutics*, *8*, 11–29. https://doi.org/10.2147/AHMT.S94170

Drummond, M. J., Fry, C. S., Glynn, E. L., Timmerman, K. L., Dickinson, J. M., Walker, D. K., Gundermann, D. M., Volpi, E., & Rasmussen, B. B. (2011). Skeletal muscle amino acid transporter expression is increased in young and older adults following resistance exercise. *Journal of Applied Physiology*, *111*(1), 135–142. https://doi.org/10.1152/japplphysiol.01408.2010

Duan, S., Huang, W., Liu, X., Liu, X., Chen, N., Xu, Q., Hu, Y., Song, W., & Zhou, J. (2018). IMPDH2 promotes colorectal cancer progression through activation of the PI3K/AKT/mTOR and PI3K/AKT/FOXO1 signaling pathways. *Journal of Experimental & Clinical Cancer Research: CR*, *37*(1), 304. https://doi.org/10.1186/s13046-018-0980-3

Ducker, G. S., & Rabinowitz, J. D. (2017). One-Carbon Metabolism in Health and Disease. *Cell Metabolism*, *25*(1), 27–42. https://doi.org/10.1016/j.cmet.2016.08.009

Dudek, C.-A., Schlicker, L., & Hiller, K. (2020). Non-Targeted Mass Isotopolome Analysis Using Stable Isotope Patterns to Identify Metabolic Changes. *Methods in Molecular Biology (Clifton, N.J.)*, *2088*, 17–32. https://doi.org/10.1007/978-1-0716-0159-4_2

El Arfani, C., De Veirman, K., Maes, K., De Bruyne, E., & Menu, E. (2018). Metabolic Features of Multiple Myeloma. *International Journal of Molecular Sciences*, *19*(4). https://doi.org/10.3390/ijms19041200

Emadi, A., Jun, S. A., Tsukamoto, T., Fathi, A. T., Minden, M. D., & Dang, C. V. (2014). Inhibition of glutaminase selectively suppresses the growth of primary acute myeloid leukemia cells with IDH mutations. *Experimental Hematology*, *42*(4), 247–251.

https://doi.org/10.1016/j.exphem.2013.12.001

Emwas, A.-H. M. (2015). The strengths and weaknesses of NMR spectroscopy and mass spectrometry with particular focus on metabolomics research. *Methods in Molecular Biology (Clifton, N.J.)*, *1277*, 161–193. https://doi.org/10.1007/978-1-4939-2377-9_13

Emwas, A.-H., Roy, R., McKay, R. T., Tenori, L., Saccenti, E., Gowda, G. A. N., Raftery, D., Alahmari, F., Jaremko, L., Jaremko, M., & Wishart, D. S. (2019). NMR Spectroscopy for Metabolomics Research. *Metabolites*, *9*(7), 123. https://doi.org/10.3390/metabo9070123

Erra Díaz, F., Dantas, E., & Geffner, J. (2018, December 30). *Unravelling the Interplay between Extracellular Acidosis and Immune Cells* [Review Article]. Mediators of Inflammation; Hindawi. https://doi.org/10.1155/2018/1218297

Evens, A. M., Schumacker, P. T., Helenowski, I. B., Singh, A. T. K., Dokic, D., Keswani, A., Kordeluk, E., Raji, A., Winter, J. N., Jovanovic, B. D., Holmgren, A., Nelson, B. P., & Gordon, L. I. (2008). Hypoxia-Inducible Factor-Alpha Activation in Lymphoma and Relationship to the Thioredoxin Family. *British Journal of Haematology*, *141*(5), 676–680. https://doi.org/10.1111/j.1365-2141.2008.07093.x

Fairfield, H., Falank, C., Avery, L., & Reagan, M. R. (2016). Multiple myeloma in the marrow: Pathogenesis and treatments. *Annals of the New York Academy of Sciences*, *1364*(1), 32–51. https://doi.org/10.1111/nyas.13038

Fan, T. W.-M., & Lane, A. N. (2016). Applications of NMR spectroscopy to systems biochemistry. *Progress in Nuclear Magnetic Resonance Spectroscopy*, *92–93*, 18–53. https://doi.org/10.1016/j.pnmrs.2016.01.005

Fang, S., & Fang, X. (2016). Advances in glucose metabolism research in colorectal cancer. *Biomedical Reports*, *5*(3), 289–295. https://doi.org/10.3892/br.2016.719

Fischer, K., Hoffmann, P., Voelkl, S., Meidenbauer, N., Ammer, J., Edinger, M., Gottfried, E., Schwarz, S., Rothe, G., Hoves, S., Renner, K., Timischl, B., Mackensen, A., Kunz-Schughart, L., Andreesen, R., Krause, S. W., & Kreutz, M. (2007). Inhibitory effect of tumor cell-derived lactic acid on human T cells. *Blood*, *109*(9), 3812–3819. https://doi.org/10.1182/blood-2006-07-035972

Flavin, R., Peluso, S., Nguyen, P. L., & Loda, M. (2010). Fatty acid synthase as a potential therapeutic target in cancer. *Future Oncology (London, England)*, *6*(4), 551–562. https://doi.org/10.2217/fon.10.11

Fritz, V., & Fajas, L. (2010). Metabolism and proliferation share common regulatory pathways in cancer cells. *Oncogene*, *29*(31), 4369–4377. https://doi.org/10.1038/onc.2010.182

Furuya, M., Horiguchi, J., Nakajima, H., Kanai, Y., & Oyama, T. (2012). Correlation of L-type amino acid transporter 1 and CD98 expression with triple negative breast cancer prognosis. *Cancer Science*, *103*(2), 382–389. https://doi.org/10.1111/j.1349-7006.2011.02151.x

Fuss, T. L., & Cheng, L. L. (2016). Metabolic Imaging in Humans. *Topics in Magnetic Resonance Imaging: TMRI*, *25*(5), 223–235. https://doi.org/10.1097/RMR.0000000000000100

G, L., J, Z., M, Y., C, C., Y, Z., Z, F., Y, G., B, Y., Y, L., Q, Z., Q, L., H, Y., L, Y., X, Z., Z, L., R, C., F, H., C, T., & B, Z. (2015). Glutamate dehydrogenase is a novel prognostic marker and predicts metastases in colorectal cancer patients. *Journal of Translational Medicine*, *13*, 144–144. https://doi.org/10.1186/s12967-015-0500-6

Gaglio, D., Metallo, C. M., Gameiro, P. A., Hiller, K., Danna, L. S., Balestrieri, C., Alberghina, L., Stephanopoulos, G., & Chiaradonna, F. (2011). Oncogenic K-Ras decouples glucose

and glutamine metabolism to support cancer cell growth. *Molecular Systems Biology*, *7*, 523. https://doi.org/10.1038/msb.2011.56

Gallagher, S. M., Castorino, J. J., & Philp, N. J. (2009). Interaction of monocarboxylate transporter 4 with β1-integrin and its role in cell migration. *American Journal of Physiology - Cell Physiology*, *296*(3), C414–C421. https://doi.org/10.1152/ajpcell.00430.2008

Gandhi, N., & Das, G. M. (2019). Metabolic Reprogramming in Breast Cancer and Its Therapeutic Implications. *Cells*, *8*(2). https://doi.org/10.3390/cells8020089

Gao, P., Tchernyshyov, I., Chang, T.-C., Lee, Y.-S., Kita, K., Ochi, T., Zeller, K. I., De Marzo, A. M., Van Eyk, J. E., Mendell, J. T., & Dang, C. V. (2009). C-Myc suppression of miR-23a/b enhances mitochondrial glutaminase expression and glutamine metabolism. *Nature*, *458*(7239), 762–765. https://doi.org/10.1038/nature07823

Gao, X., Lee, K., Reid, M. A., Sanderson, S. M., Qiu, C., Li, S., Liu, J., & Locasale, J. W. (2018). Serine Availability Influences Mitochondrial Dynamics and Function through Lipid Metabolism. *Cell Reports*, *22*(13), 3507–3520. https://doi.org/10.1016/j.celrep.2018.03.017

Gerecke, C., Fuhrmann, S., Strifler, S., Schmidt-Hieber, M., Einsele, H., & Knop, S. (2016). The Diagnosis and Treatment of Multiple Myeloma. *Deutsches Ärzteblatt International*, *113*(27–28), 470–476. https://doi.org/10.3238/arztebl.2016.0470

Glasheen, J. J., & Sorensen, M. D. (2005). Burkitt's lymphoma presenting with lactic acidosis and hypoglycemia—A case presentation. *Leukemia & Lymphoma*, *46*(2), 281–283. https://doi.org/10.1080/10428190400016723

Goetzman, E. S., & Prochownik, E. V. (2018). The Role for Myc in Coordinating Glycolysis,

Oxidative Phosphorylation, Glutaminolysis, and Fatty Acid Metabolism in Normal and Neoplastic Tissues. *Frontiers in Endocrinology*, *9*, 129. https://doi.org/10.3389/fendo.2018.00129

Gooptu, M., Whitaker-Menezes, D., Sprandio, J., Domingo-Vidal, M., Lin, Z., Uppal, G., Gong, J., Fratamico, R., Leiby, B., Dulau-Florea, A., Caro, J., & Martinez-Outschoorn, U. (2017). Mitochondrial and glycolytic metabolic compartmentalization in diffuse large B-cell lymphoma. *Seminars in Oncology*, *44*(3), 204–217. https://doi.org/10.1053/j.seminoncol.2017.10.002

Günther, U. L., Ludwig, C., & Rüterjans, H. (2000). NMRLAB—Advanced NMR Data Processing in Matlab. *Journal of Magnetic Resonance*, *145*(2), 201–208. https://doi.org/10.1006/jmre.2000.2071

Gurina, T. S., & Mohiuddin, S. S. (2020). Biochemistry, Protein Catabolism. In *StatPearls*. StatPearls Publishing. http://www.ncbi.nlm.nih.gov/books/NBK556047/

Haddad, A., & Mohiuddin, S. S. (2020). Biochemistry, Citric Acid Cycle. In *StatPearls*. StatPearls Publishing. http://www.ncbi.nlm.nih.gov/books/NBK541072/

Häfliger, P., & Charles, R.-P. (2019). The L-Type Amino Acid Transporter LAT1—An Emerging Target in Cancer. *International Journal of Molecular Sciences*, *20*(10). https://doi.org/10.3390/ijms20102428

Hallek, M., Bergsagel, P. L., & Anderson, K. C. (1998). Multiple myeloma: Increasing evidence for a multistep transformation process. *Blood*, *91*(1), 3–21.

Hammoudi, N., Riaz Ahmed, K. B., Garcia-Prieto, C., & Huang, P. (2011). Metabolic alterations in cancer cells and therapeutic implications. *Chinese Journal of Cancer*, *30*(8), 508–525. https://doi.org/10.5732/cjc.011.10267

Hanahan, D., & Weinberg, R. A. (2011). Hallmarks of cancer: The next generation. *Cell*, *144*(5), 646–674. https://doi.org/10.1016/j.cell.2011.02.013

Hattori, A., Tsunoda, M., Konuma, T., Kobayashi, M., Nagy, T., Glushka, J., Tayyari, F., McSkimming, D., Kannan, N., Tojo, A., Edison, A. S., & Ito, T. (2017). Cancer progression by reprogrammed BCAA metabolism in myeloid leukaemia. *Nature*, *545*(7655), 500–504. https://doi.org/10.1038/nature22314

Havranek, O., Xu, J., Köhrer, S., Wang, Z., Becker, L., Comer, J. M., Henderson, J., Ma, W., Man Chun Ma, J., Westin, J. R., Ghosh, D., Shinners, N., Sun, L., Yi, A. F., Karri, A. R., Burger, J. A., Zal, T., & Davis, R. E. (2017). Tonic B-cell receptor signaling in diffuse large B-cell lymphoma. *Blood*, *130*(8), 995–1006. https://doi.org/10.1182/blood-2016-10-747303

Hayashi, K., & Anzai, N. (2017). Novel therapeutic approaches targeting L-type amino acid transporters for cancer treatment. *World Journal of Gastrointestinal Oncology*, *9*(1), 21–29. https://doi.org/10.4251/wjgo.v9.i1.21

He, Ying, Zheng, Z., Xu, Y., Weng, H., Gao, Y., Qin, K., Rong, J., Chen, C., Yun, M., Zhang, J., & Ye, S. (2018). Over-expression of IMPDH2 is associated with tumor progression and poor prognosis in hepatocellular carcinoma. *American Journal of Cancer Research*, *8*(8), 1604–1614.

He, Yunhua, Wang, Y., Liu, H., Xu, X., He, S., Tang, J., Huang, Y., Miao, X., Wu, Y., Wang, Q., & Cheng, C. (2015). Pyruvate kinase isoform M2 (PKM2) participates in multiple myeloma cell proliferation, adhesion and chemoresistance. *Leukemia Research*, *39*(12), 1428–1436. https://doi.org/10.1016/j.leukres.2015.09.019

Hideshima, T., Bergsagel, P. L., Kuehl, W. M., & Anderson, K. C. (2004). Advances in biology of

multiple myeloma: Clinical applications. *Blood*, *104*(3), 607–618. https://doi.org/10.1182/blood-2004-01-0037

Hitosugi, T., Kang, S., Vander Heiden, M. G., Chung, T.-W., Elf, S., Lythgoe, K., Dong, S., Lonial, S., Wang, X., Chen, G. Z., Xie, J., Gu, T.-L., Polakiewicz, R. D., Roesel, J. L., Boggon, T. J., Khuri, F. R., Gilliland, D. G., Cantley, L. C., Kaufman, J., & Chen, J. (2009). Tyrosine phosphorylation inhibits PKM2 to promote the Warburg effect and tumor growth. *Science Signaling*, *2*(97), ra73. https://doi.org/10.1126/scisignal.2000431

Hodgkin. (1832). On some Morbid Appearances of the Absorbent Glands and Spleen. *Medico-Chirurgical Transactions*, *17*, 68–114.

Hollinshead, K. E. R., Williams, D. S., Tennant, D. A., & Ludwig, C. (2016). Probing Cancer Cell Metabolism Using NMR Spectroscopy. *Advances in Experimental Medicine and Biology*, *899*, 89–111. https://doi.org/10.1007/978-3-319-26666-4_6

Hsu, P. P., & Sabatini, D. M. (2008). Cancer Cell Metabolism: Warburg and Beyond. *Cell*, *134*(5), 703–707. https://doi.org/10.1016/j.cell.2008.08.021

Huang, C., & Freter, C. (2015). Lipid Metabolism, Apoptosis and Cancer Therapy. *International Journal of Molecular Sciences*, *16*(1), 924–949. https://doi.org/10.3390/ijms16010924

Hyberts, S. G., Arthanari, H., Robson, S. A., & Wagner, G. (2014). Perspectives in magnetic resonance: NMR in the post-FFT era. *Journal of Magnetic Resonance (San Diego, Calif.: 1997)*, *241*, 60–73. https://doi.org/10.1016/j.jmr.2013.11.014

Hyberts, S. G., Milbradt, A. G., Wagner, A. B., Arthanari, H., & Wagner, G. (2012). Application of iterative soft thresholding for fast reconstruction of NMR data non-uniformly sampled with multidimensional Poisson Gap scheduling. *Journal of Biomolecular NMR*, *52*(4), 315–327. https://doi.org/10.1007/s10858-012-9611-z

Jiang, J., Srivastava, S., Seim, G., Pavlova, N. N., King, B., Zou, L., Zhang, C., Zhong, M., Feng, H., Kapur, R., Wek, R. C., Fan, J., & Zhang, J. (2019). Promoter demethylation of the asparagine synthetase gene is required for an ATF4-dependent adaptation to asparagine depletion. *Journal of Biological Chemistry*, jbc.RA119.010447. https://doi.org/10.1074/jbc.RA119.010447

Jin, L., & Zhou, Y. (2019). Crucial role of the pentose phosphate pathway in malignant tumors. *Oncology Letters*, *17*(5), 4213–4221. https://doi.org/10.3892/ol.2019.10112

KAIRA, K., ORIUCHI, N., IMAI, H., SHIMIZU, K., YANAGITANI, N., SUNAGA, N., HISADA, T., KAWASHIMA, O., KAMIDE, Y., ISHIZUKA, T., KANAI, Y., NAKAJIMA, T., & MORI, M. (2010). Prognostic significance of L-type amino acid transporter 1 (LAT1) and 4F2 heavy chain (CD98) expression in surgically resectable stage III non-small cell lung cancer. *Experimental and Therapeutic Medicine*, *1*(5), 799–808. https://doi.org/10.3892/etm.2010.117

Kanai, Y., Segawa, H., Miyamoto, K. i, Uchino, H., Takeda, E., & Endou, H. (1998). Expression cloning and characterization of a transporter for large neutral amino acids activated by the heavy chain of 4F2 antigen (CD98). *The Journal of Biological Chemistry*, *273*(37), 23629–23632. https://doi.org/10.1074/jbc.273.37.23629

Kanehisa, M., Sato, Y., Furumichi, M., Morishima, K., & Tanabe, M. (2019). New approach for understanding genome variations in KEGG. *Nucleic Acids Research*, *47*(D1), D590–D595. https://doi.org/10.1093/nar/gky962

Kang, Z.-J., Liu, Y.-F., Xu, L.-Z., Long, Z.-J., Huang, D., Yang, Y., Liu, B., Feng, J.-X., Pan, Y.-J., Yan, J.-S., & Liu, Q. (2016). The Philadelphia chromosome in leukemogenesis. *Chinese Journal of Cancer*, *35*, 48. https://doi.org/10.1186/s40880-016-0108-0

Karlíková, R., Široká, J., Friedecký, D., Faber, E., Hrdá, M., Mičová, K., Fikarová, I., Gardlo, A., Janečková, H., Vrobel, I., & Adam, T. (2016). Metabolite Profiling of the Plasma and Leukocytes of Chronic Myeloid Leukemia Patients. *Journal of Proteome Research*, *15*(9), 3158–3166. https://doi.org/10.1021/acs.jproteome.6b00356

Kazandjian, D., Hill, E., Hultcrantz, M., Rustad, E. H., Yellapantula, V., Akhlaghi, T., Korde, N., Mailankody, S., Dew, A., Papaemmanuil, E., Maric, I., Kwok, M., & Landgren, O. (2019). Molecular underpinnings of clinical disparity patterns in African American vs. Caucasian American multiple myeloma patients. *Blood Cancer Journal*, *9*(2), 1–8. https://doi.org/10.1038/s41408-019-0177-9

Kihara, R., Nagata, Y., Kiyoi, H., Kato, T., Yamamoto, E., Suzuki, K., Chen, F., Asou, N., Ohtake, S., Miyawaki, S., Miyazaki, Y., Sakura, T., Ozawa, Y., Usui, N., Kanamori, H., Kiguchi, T., Imai, K., Uike, N., Kimura, F., … Naoe, T. (2014). Comprehensive analysis of genetic alterations and their prognostic impacts in adult acute myeloid leukemia patients. *Leukemia*, *28*(8), 1586–1595. https://doi.org/10.1038/leu.2014.55

Klein, G. (2009). Burkitt lymphoma—A stalking horse for cancer research? *Seminars in Cancer Biology*, *19*(6), 347–350. https://doi.org/10.1016/j.semcancer.2009.07.001

Kobayashi, H., Ishii, Y., & Takayama, T. (2005). Expression of L-type amino acid transporter 1 (LAT1) in esophageal carcinoma. *Journal of Surgical Oncology*, *90*(4), 233–238. https://doi.org/10.1002/jso.20257

Koppenol, W. H., Bounds, P. L., & Dang, C. V. (2011). Otto Warburg's contributions to current concepts of cancer metabolism. *Nature Reviews. Cancer*, *11*(5), 325–337. https://doi.org/10.1038/nrc3038

Krall, A. S., Xu, S., Graeber, T. G., Braas, D., & Christofk, H. R. (2016). Asparagine promotes

cancer cell proliferation through use as an amino acid exchange factor. *Nature Communications*, *7*(1), 1–13. https://doi.org/10.1038/ncomms11457

Kurhanewicz, J., Vigneron, D. B., Ardenkjaer-Larsen, J. H., Bankson, J. A., Brindle, K., Cunningham, C. H., Gallagher, F. A., Keshari, K. R., Kjaer, A., Laustsen, C., Mankoff, D. A., Merritt, M. E., Nelson, S. J., Pauly, J. M., Lee, P., Ronen, S., Tyler, D. J., Rajan, S. S., Spielman, D. M., … Rizi, R. (2019). Hyperpolarized 13C MRI: Path to Clinical Translation in Oncology. *Neoplasia (New York, N.Y.)*, *21*(1), 1–16. https://doi.org/10.1016/j.neo.2018.09.006

Kurmi, K., Hitosugi, S., Yu, J., Boakye-Agyeman, F., Wiese, E. K., Larson, T. R., Dai, Q., Machida, Y. J., Lou, Z., Wang, L., Boughey, J. C., Kaufmann, S. H., Goetz, M. P., Karnitz, L. M., & Hitosugi, T. (2018). Tyrosine Phosphorylation of Mitochondrial Creatine Kinase 1 Enhances a Druggable Tumor Energy Shuttle Pathway. *Cell Metabolism*, *28*(6), 833-847.e8. https://doi.org/10.1016/j.cmet.2018.08.008

Kwon, O.-H., Kang, T.-W., Kim, J.-H., Kim, M., Noh, S.-M., Song, K.-S., Yoo, H.-S., Kim, W.-H., Xie, Z., Pocalyko, D., Kim, S.-Y., & Kim, Y. S. (2012). Pyruvate kinase M2 promotes the growth of gastric cancer cells via regulation of Bcl-xL expression at transcriptional level. *Biochemical and Biophysical Research Communications*, *423*(1), 38–44. https://doi.org/10.1016/j.bbrc.2012.05.063

L, Z., U, H., K, N., & G, K. (1976). Characteristic chromosomal abnormalities in biopsies and lymphoid-cell lines from patients with Burkitt and non-Burkitt lymphomas. *International Journal of Cancer*, *17*(1), 47–56. https://doi.org/10.1002/ijc.2910170108

Lane, A. N., & Fan, T. W.-M. (2015). Regulation of mammalian nucleotide metabolism and biosynthesis. *Nucleic Acids Research*, *43*(4), 2466–2485.

https://doi.org/10.1093/nar/gkv047

Lane, A. N., & Fan, T. W.-M. (2017). NMR-based Stable Isotope Resolved Metabolomics in systems biochemistry. *Archives of Biochemistry and Biophysics*, *628*, 123–131. https://doi.org/10.1016/j.abb.2017.02.009

Li, C., Yan, Z., Cao, X., Zhang, X., & Yang, L. (2016). Phosphoribosylpyrophosphate Synthetase 1 Knockdown Suppresses Tumor Formation of Glioma CD133+ Cells Through Upregulating Cell Apoptosis. *Journal of Molecular Neuroscience*, *60*(2), 145–156. https://doi.org/10.1007/s12031-016-0783-y

Lien, E. C., Lyssiotis, C. A., Juvekar, A., Hu, H., Asara, J. M., Cantley, L. C., & Toker, A. (2016). Glutathione biosynthesis is a metabolic vulnerability in PI3K/Akt-driven breast cancer. *Nature Cell Biology*, *18*(5), 572–578. https://doi.org/10.1038/ncb3341

Lin, P., Chen, L., Luthra, R., Konoplev, S. N., Wang, X., & Medeiros, L. J. (2008). Acute myeloid leukemia harboring t(8;21)(q22;q22): A heterogeneous disease with poor outcome in a subset of patients unrelated to secondary cytogenetic aberrations. *Modern Pathology*, *21*(8), 1029–1036. https://doi.org/10.1038/modpathol.2008.92

Lin, P., & Falini, B. (2015). Acute Myeloid Leukemia With Recurrent Genetic Abnormalities Other Than Translocations. *American Journal of Clinical Pathology*, *144*(1), 19–28. https://doi.org/10.1309/AJCP97BJBEVZEUIN

Liu, J., Guo, S., Li, Q., Yang, L., Xia, Z., Zhang, L., Huang, Z., & Zhang, N. (2013). Phosphoglycerate dehydrogenase induces glioma cells proliferation and invasion by stabilizing forkhead box M1. *Journal of Neuro-Oncology*, *111*(3), 245–255. https://doi.org/10.1007/s11060-012-1018-x

Liu, W., Fang, Y., Wang, X.-T., Liu, J., Dan, X., & Sun, L.-L. (2014). Overcoming 5-Fu

resistance of colon cells through inhibition of Glut1 by the specific inhibitor WZB117. *Asian Pacific Journal of Cancer Prevention: APJCP*, *15*(17), 7037–7041. https://doi.org/10.7314/apjcp.2014.15.17.7037

Lohr, J. G., Stojanov, P., Carter, S. L., Cruz-Gordillo, P., Lawrence, M. S., Auclair, D., Sougnez, C., Knoechel, B., Gould, J., Saksena, G., Cibulskis, K., McKenna, A., Chapman, M. A., Straussman, R., Levy, J., Perkins, L. M., Keats, J. J., Schumacher, S. E., Rosenberg, M., … Stockerl-Goldstein, K. (2014). Widespread Genetic Heterogeneity in Multiple Myeloma: Implications for Targeted Therapy. *Cancer Cell*, *25*(1), 91–101. https://doi.org/10.1016/j.ccr.2013.12.015

Lomelino, C. L., Andring, J. T., McKenna, R., & Kilberg, M. S. (2017). Asparagine synthetase: Function, structure, and role in disease. *The Journal of Biological Chemistry*, *292*(49), 19952–19958. https://doi.org/10.1074/jbc.R117.819060

Ludwig, C., & Günther, U. L. (2011). MetaboLab—Advanced NMR data processing and analysis for metabolomics. *BMC Bioinformatics*, *12*(1), 366. https://doi.org/10.1186/1471-2105-12-366

Luengo, A., Gui, D. Y., & Vander Heiden, M. G. (2017). Targeting Metabolism for Cancer Therapy. *Cell Chemical Biology*, *24*(9), 1161–1180. https://doi.org/10.1016/j.chembiol.2017.08.028

Lz, M., La, W., Gr, P., & Fp, K. (1997). Enzymes of the fatty acid synthesis pathway are highly expressed in in situ breast carcinoma. *Clinical Cancer Research : An Official Journal of the American Association for Cancer Research*, *3*(11), 2115–2120.

M, W., & R, K.-D. (2000, July). *Creatine and creatinine metabolism*. Physiological Reviews; Physiol Rev. https://doi.org/10.1152/physrev.2000.80.3.1107

Ma, X., Li, B., Liu, J., Fu, Y., & Luo, Y. (2019). Phosphoglycerate dehydrogenase promotes pancreatic cancer development by interacting with eIF4A1 and eIF4E. *Journal of Experimental & Clinical Cancer Research : CR*, *38*. https://doi.org/10.1186/s13046-019-1053-y

Majewski, N., Nogueira, V., Bhaskar, P., Coy, P. E., Skeen, J. E., Gottlob, K., Chandel, N. S., Thompson, C. B., Robey, R. B., & Hay, N. (2004). Hexokinase-mitochondria interaction mediated by Akt is required to inhibit apoptosis in the presence or absence of Bax and Bak. *Molecular Cell*, *16*(5), 819–830. https://doi.org/10.1016/j.molcel.2004.11.014

Majmundar, A. J., Wong, W. J., & Simon, M. C. (2010). Hypoxia-Inducible Factors and the Response to Hypoxic Stress. *Molecular Cell*, *40*(2), 294–309. https://doi.org/10.1016/j.molcel.2010.09.022

Marbaniang, C., & Kma, L. (2018). Dysregulation of Glucose Metabolism by Oncogenes and Tumor Suppressors in Cancer Cells. *Asian Pacific Journal of Cancer Prevention: APJCP*, *19*(9), 2377–2390. https://doi.org/10.22034/APJCP.2018.19.9.2377

Mardis, E. R., Ding, L., Dooling, D. J., Larson, D. E., McLellan, M. D., Chen, K., Koboldt, D. C., Fulton, R. S., Delehaunty, K. D., McGrath, S. D., Fulton, L. A., Locke, D. P., Magrini, V. J., Abbott, R. M., Vickery, T. L., Reed, J. S., Robinson, J. S., Wylie, T., Smith, S. M., … Ley, T. J. (2009). Recurring Mutations Found by Sequencing an Acute Myeloid Leukemia Genome. *The New England Journal of Medicine*, *361*(11), 1058–1066. https://doi.org/10.1056/NEJMoa0903840

Markley, J. L., Brüschweiler, R., Edison, A. S., Eghbalnia, H. R., Powers, R., Raftery, D., & Wishart, D. S. (2017). The future of NMR-based metabolomics. *Current Opinion in Biotechnology*, *43*, 34–40. https://doi.org/10.1016/j.copbio.2016.08.001

Mawson, A. R., & Majumdar, S. (2017). Malaria, Epstein-Barr virus infection and the pathogenesis of Burkitt's lymphoma. *International Journal of Cancer*, *141*(9), 1849–1855. https://doi.org/10.1002/ijc.30885

McConkey, D. J. (2017). The integrated stress response and proteotoxicity in cancer therapy. *Biochemical and Biophysical Research Communications*, *482*(3), 450–453. https://doi.org/10.1016/j.bbrc.2016.11.047

Mckay, R. T. (2011). How the 1D-NOESY suppresses solvent signal in metabonomics NMR spectroscopy: An examination of the pulse sequence components and evolution. *Concepts in Magnetic Resonance Part A*, *38A*(5), 197–220. https://doi.org/10.1002/cmr.a.20223

Meyer-Bahlburg, A., Bandaranayake, A. D., Andrews, S. F., & Rawlings, D. J. (2009). Reduced c-myc expression levels limit follicular mature B cell cycling in response to TLR signals. *Journal of Immunology (Baltimore, Md. : 1950)*, *182*(7), 4065–4075. https://doi.org/10.4049/jimmunol.0802961

Miller, A., Nagy, C., Knapp, B., Laengle, J., Ponweiser, E., Groeger, M., Starkl, P., Bergmann, M., Wagner, O., & Haschemi, A. (2017). Exploring Metabolic Configurations of Single Cells within Complex Tissue Microenvironments. *Cell Metabolism*, *26*(5), 788-800.e6. https://doi.org/10.1016/j.cmet.2017.08.014

Miller, M. S., & Miller, L. D. (2011). RAS Mutations and Oncogenesis: Not all RAS Mutations are Created Equally. *Frontiers in Genetics*, *2*, 100. https://doi.org/10.3389/fgene.2011.00100

Mlynarczyk, C., Fontán, L., & Melnick, A. (2019). Germinal center-derived lymphomas: The darkest side of humoral immunity. *Immunological Reviews*, *288*(1), 214–239. https://doi.org/10.1111/imr.12755

Moghei, M., Tavajohi-Fini, P., Beatty, B., & Adegoke, O. A. J. (2016). Ketoisocaproic acid, a metabolite of leucine, suppresses insulin-stimulated glucose transport in skeletal muscle cells in a BCAT2-dependent manner. *American Journal of Physiology - Cell Physiology*, *311*(3), C518–C527. https://doi.org/10.1152/ajpcell.00062.2016

Monirujjaman, M., & Ferdouse, A. (2014, August 19). *Metabolic and Physiological Roles of Branched-Chain Amino Acids* [Review Article]. Advances in Molecular Biology; Hindawi. https://doi.org/10.1155/2014/364976

Monti, S., Savage, K. J., Kutok, J. L., Feuerhake, F., Kurtin, P., Mihm, M., Wu, B., Pasqualucci, L., Neuberg, D., Aguiar, R. C. T., Dal Cin, P., Ladd, C., Pinkus, G. S., Salles, G., Harris, N. L., Dalla-Favera, R., Habermann, T. M., Aster, J. C., Golub, T. R., & Shipp, M. A. (2005). Molecular profiling of diffuse large B-cell lymphoma identifies robust subtypes including one characterized by host inflammatory response. *Blood*, *105*(5), 1851–1861. https://doi.org/10.1182/blood-2004-07-2947

Moore, G. E., Gerner, R. E., & Franklin, H. A. (1967). Culture of Normal Human Leukocytes. *JAMA*, *199*(8), 519–524. https://doi.org/10.1001/jama.1967.03120080053007

Moschoi, R., Imbert, V., Nebout, M., Chiche, J., Mary, D., Prebet, T., Saland, E., Castellano, R., Pouyet, L., Collette, Y., Vey, N., Chabannon, C., Recher, C., Sarry, J.-E., Alcor, D., Peyron, J.-F., & Griessinger, E. (2016). Protective mitochondrial transfer from bone marrow stromal cells to acute myeloid leukemic cells during chemotherapy. *Blood*, *128*(2), 253–264. https://doi.org/10.1182/blood-2015-07-655860

Mounier, C., Bouraoui, L., & Rassart, E. (2014). Lipogenesis in cancer progression (review). *International Journal of Oncology*, *45*(2), 485–492. https://doi.org/10.3892/ijo.2014.2441

Munir, R., Lisec, J., Swinnen, J. V., & Zaidi, N. (2019). Lipid metabolism in cancer cells under

metabolic stress. *British Journal of Cancer*, *120*(12), 1090–1098. https://doi.org/10.1038/s41416-019-0451-4

Mushtaq, M., Darekar, S., Klein, G., & Kashuba, E. (2015). Different Mechanisms of Regulation of the Warburg Effect in Lymphoblastoid and Burkitt Lymphoma Cells. *PloS One*, *10*(8), e0136142. https://doi.org/10.1371/journal.pone.0136142

Nair, K. S., & Short, K. R. (2005). Hormonal and signaling role of branched-chain amino acids. *The Journal of Nutrition*, *135*(6 Suppl), 1547S-52S. https://doi.org/10.1093/jn/135.6.1547S

Nakano, A., Miki, H., Nakamura, S., Harada, T., Oda, A., Amou, H., Fujii, S., Kagawa, K., Takeuchi, K., Ozaki, S., Matsumoto, T., & Abe, M. (2012). Up-regulation of hexokinaseII in myeloma cells: Targeting myeloma cells with 3-bromopyruvate. *Journal of Bioenergetics and Biomembranes*, *44*(1), 31–38. https://doi.org/10.1007/s10863-012-9412-9

Natoni, A., Bohara, R., Pandit, A., & O'Dwyer, M. (2019). Targeted Approaches to Inhibit Sialylation of Multiple Myeloma in the Bone Marrow Microenvironment. *Frontiers in Bioengineering and Biotechnology*, *7*. https://doi.org/10.3389/fbioe.2019.00252

Newman, A. C., & Maddocks, O. D. K. (2017). One-carbon metabolism in cancer. *British Journal of Cancer*, *116*(12), 1499–1504. https://doi.org/10.1038/bjc.2017.118

Nguyen, L., Papenhausen, P., & Shao, H. (2017). The Role of c-MYC in B-Cell Lymphomas: Diagnostic and Molecular Aspects. *Genes*, *8*(4). https://doi.org/10.3390/genes8040116

Nicholson, J. K., & Lindon, J. C. (2008). Metabonomics. *Nature*, *455*(7216), 1054–1056. https://doi.org/10.1038/4551054a

Nicklin, P., Bergman, P., Zhang, B., Triantafellow, E., Wang, H., Nyfeler, B., Yang, H., Hild, M.,

Kung, C., Wilson, C., Myer, V. E., MacKeigan, J. P., Porter, J. A., Wang, Y. K., Cantley, L. C., Finan, P. M., & Murphy, L. O. (2009). Bidirectional Transport of Amino Acids Regulates mTOR and Autophagy. *Cell*, *136*(3), 521–534. https://doi.org/10.1016/j.cell.2008.11.044

Nie, C., He, T., Zhang, W., Zhang, G., & Ma, X. (2018). Branched Chain Amino Acids: Beyond Nutrition Metabolism. *International Journal of Molecular Sciences*, *19*(4). https://doi.org/10.3390/ijms19040954

Nishimura, J., Masaki, T., Arakawa, M., Seike, M., & Yoshimatsu, H. (2010). Isoleucine Prevents the Accumulation of Tissue Triglycerides and Upregulates the Expression of PPARα and Uncoupling Protein in Diet-Induced Obese Mice. *The Journal of Nutrition*, *140*(3), 496–500. https://doi.org/10.3945/jn.109.108977

Norris, R. E., & Adamson, P. C. (2010). Clinical potency of methotrexate, aminopterin, talotrexin and pemetrexed in childhood leukemias. *Cancer Chemotherapy and Pharmacology*, *65*(6), 1125–1130. https://doi.org/10.1007/s00280-009-1120-8

Ohshima, Y., Kaira, K., Yamaguchi, A., Oriuchi, N., Tominaga, H., Nagamori, S., Kanai, Y., Yokobori, T., Miyazaki, T., Asao, T., Tsushima, Y., Kuwano, H., & Ishioka, N. S. (2016). Efficacy of system l amino acid transporter 1 inhibition as a therapeutic target in esophageal squamous cell carcinoma. *Cancer Science*, *107*(10), 1499–1505. https://doi.org/10.1111/cas.13021

Ok, C. Y., Loghavi, S., Sui, D., Wei, P., Kanagal-Shamanna, R., Yin, C. C., Zuo, Z., Routbort, M. J., Tang, G., Tang, Z., Jorgensen, J. L., Luthra, R., Ravandi, F., Kantarjian, H. M., DiNardo, C. D., Medeiros, L. J., Wang, S. A., & Patel, K. P. (2019). Persistent IDH1/2 mutations in remission can predict relapse in patients with acute myeloid leukemia.

Haematologica, *104*(2), 305–311. https://doi.org/10.3324/haematol.2018.191148

Öman, T., Tessem, M.-B., Bathen, T. F., Bertilsson, H., Angelsen, A., Hedenström, M., & Andreassen, T. (2014). Identification of metabolites from 2D 1H-13C HSQC NMR using peak correlation plots. *BMC Bioinformatics*, *15*(1). https://doi.org/10.1186/s12859-014-0413-z

Pacold, M. E., Brimacombe, K. R., Chan, S. H., Rohde, J. M., Lewis, C. A., Swier, L. J. Y. M., Possemato, R., Chen, W. W., Sullivan, L. B., Fiske, B. P., Cho, S. W., Freinkman, E., Birsoy, K., Abu-Remaileh, M., Shaul, Y. D., Liu, C. M., Zhou, M., Koh, M. J., Chung, H., … Sabatini, D. M. (2016). A PHGDH inhibitor reveals coordination of serine synthesis and 1-carbon unit fate. *Nature Chemical Biology*, *12*(6), 452–458. https://doi.org/10.1038/nchembio.2070

Papaemmanuil, E., Gerstung, M., Bullinger, L., Gaidzik, V. I., Paschka, P., Roberts, N. D., Potter, N. E., Heuser, M., Thol, F., Bolli, N., Gundem, G., Van Loo, P., Martincorena, I., Ganly, P., Mudie, L., McLaren, S., O'Meara, S., Raine, K., Jones, D. R., … Campbell, P. J. (2016). Genomic Classification and Prognosis in Acute Myeloid Leukemia. *The New England Journal of Medicine*, *374*(23), 2209–2221. https://doi.org/10.1056/NEJMoa1516192

Paplomata, E., & O'Regan, R. (2014). The PI3K/AKT/mTOR pathway in breast cancer: Targets, trials and biomarkers. *Therapeutic Advances in Medical Oncology*, *6*(4), 154–166. https://doi.org/10.1177/1758834014530023

Patil, M., Bhaumik, J., Babykutty, S., Banerjee, U., & Fukumura, D. (2016). Arginine dependence of tumor cells: Targeting a chink in cancer's armor. *Oncogene*, *35*(38), 4957–4972. https://doi.org/10.1038/onc.2016.37

Patra, K. C., Wang, Q., Bhaskar, P. T., Miller, L., Wang, Z., Wheaton, W., Chandel, N., Laakso, M., Muller, W. J., Allen, E. L., Jha, A. K., Smolen, G. A., Clasquin, M. F., Robey, B., & Hay, N. (2013). Hexokinase 2 is required for tumor initiation and maintenance and its systemic deletion is therapeutic in mouse models of cancer. *Cancer Cell*, *24*(2), 213–228. https://doi.org/10.1016/j.ccr.2013.06.014

Pavlides, S., Whitaker-Menezes, D., Castello-Cros, R., Flomenberg, N., Witkiewicz, A. K., Frank, P. G., Casimiro, M. C., Wang, C., Fortina, P., Addya, S., Pestell, R. G., Martinez-Outschoorn, U. E., Sotgia, F., & Lisanti, M. P. (2009). The reverse Warburg effect: Aerobic glycolysis in cancer associated fibroblasts and the tumor stroma. *Cell Cycle (Georgetown, Tex.)*, *8*(23), 3984–4001. https://doi.org/10.4161/cc.8.23.10238

Pavlova, N. N., & Thompson, C. B. (2016). The Emerging Hallmarks of Cancer Metabolism. *Cell Metabolism*, *23*(1), 27–47. https://doi.org/10.1016/j.cmet.2015.12.006

Peñuelas, S., Noé, V., & Ciudad, C. J. (2005). Modulation of IMPDH2, survivin, topoisomerase I and vimentin increases sensitivity to methotrexate in HT29 human colon cancer cells. *The FEBS Journal*, *272*(3), 696–710. https://doi.org/10.1111/j.1742-4658.2004.04504.x

Phan, L. M., Yeung, S.-C. J., & Lee, M.-H. (2014). Cancer metabolic reprogramming: Importance, main features, and potentials for precise targeted anti-cancer therapies. *Cancer Biology & Medicine*, *11*(1), 1–19. https://doi.org/10.7497/j.issn.2095-3941.2014.01.001

Pickup, M. W., Mouw, J. K., & Weaver, V. M. (2014). The extracellular matrix modulates the hallmarks of cancer. *EMBO Reports*, *15*(12), 1243–1253. https://doi.org/10.15252/embr.201439246

Pietarinen, P. O., Pemovska, T., Kontro, M., Yadav, B., Mpindi, J. P., Andersson, E. I., Majumder,

M. M., Kuusanmäki, H., Koskenvesa, P., Kallioniemi, O., Wennerberg, K., Heckman, C. A., Mustjoki, S., & Porkka, K. (2015). Novel drug candidates for blast phase chronic myeloid leukemia from high-throughput drug sensitivity and resistance testing. *Blood Cancer Journal*, *5*(5), e309–e309. https://doi.org/10.1038/bcj.2015.30

Plathow, C., & Weber, W. A. (2008). Tumor cell metabolism imaging. *Journal of Nuclear Medicine: Official Publication, Society of Nuclear Medicine*, *49 Suppl 2*, 43S-63S. https://doi.org/10.2967/jnumed.107.045930

Porta, C., Paglino, C., & Mosca, A. (2014). Targeting PI3K/Akt/mTOR Signaling in Cancer. *Frontiers in Oncology*, *4*. https://doi.org/10.3389/fonc.2014.00064

Puchades-Carrasco, L., Lecumberri, R., Martínez-López, J., Lahuerta, J.-J., Mateos, M.-V., Prósper, F., San-Miguel, J. F., & Pineda-Lucena, A. (2013). Multiple myeloma patients have a specific serum metabolomic profile that changes after achieving complete remission. *Clinical Cancer Research: An Official Journal of the American Association for Cancer Research*, *19*(17), 4770–4779. https://doi.org/10.1158/1078-0432.CCR-12-2917

Qiao, H., Tan, X., Lv, D., Xing, R., Shu, F., Zhong, C., Li, C., Zou, Y., & Mao, X. (2020). Phosphoribosyl pyrophosphate synthetases 2 knockdown inhibits prostate cancer progression by suppressing cell cycle and inducing cell apoptosis. *Journal of Cancer*, *11*(5), 1027–1037. https://doi.org/10.7150/jca.37401

Qiu, Z., Guo, W., Wang, Q., Chen, Z., Huang, S., Zhao, F., Yao, M., Zhao, Y., & He, X. (2015). MicroRNA-124 reduces the pentose phosphate pathway and proliferation by targeting PRPS1 and RPIA mRNAs in human colorectal cancer cells. *Gastroenterology*, *149*(6), 1587-1598.e11. https://doi.org/10.1053/j.gastro.2015.07.050

Radich, J. P., Dai, H., Mao, M., Oehler, V., Schelter, J., Druker, B., Sawyers, C., Shah, N., Stock,

W., Willman, C. L., Friend, S., & Linsley, P. S. (2006). Gene expression changes associated with progression and response in chronic myeloid leukemia. *Proceedings of the National Academy of Sciences of the United States of America*, *103*(8), 2794–2799. https://doi.org/10.1073/pnas.0510423103

Rajkumar, S. V. (2005). MGUS and Smoldering Multiple Myeloma: Update on Pathogenesis, Natural History, and Management. *Hematology*, *2005*(1), 340–345. https://doi.org/10.1182/asheducation-2005.1.340

Rajkumar, S. V. (2018). Multiple myeloma: 2018 update on diagnosis, risk-stratification, and management. *American Journal of Hematology*, *93*(8), 1091–1110. https://doi.org/10.1002/ajh.25117

Rasche, L., Kortüm, K. M., Raab, M. S., & Weinhold, N. (2019). The Impact of Tumor Heterogeneity on Diagnostics and Novel Therapeutic Strategies in Multiple Myeloma. *International Journal of Molecular Sciences*, *20*(5). https://doi.org/10.3390/ijms20051248

Rasmussen, B. B., & Adams, C. M. (2020). ATF4 Is a Fundamental Regulator of Nutrient Sensing and Protein Turnover. *The Journal of Nutrition*, *150*(5), 979–980. https://doi.org/10.1093/jn/nxaa067

Ray, U., & Roy, S. S. (2018). Aberrant lipid metabolism in cancer cells—The role of oncolipid-activated signaling. *The FEBS Journal*, *285*(3), 432–443. https://doi.org/10.1111/febs.14281

Reiter-Brennan, C., Semmler, L., & Klein, A. (2018). The effects of 2-hydroxyglutarate on the tumorigenesis of gliomas. *Contemporary Oncology*, *22*(4), 215–222. https://doi.org/10.5114/wo.2018.82642

Reitzer, L. J., Wice, B. M., & Kennell, D. (1979). Evidence that glutamine, not sugar, is the major

energy source for cultured HeLa cells. *The Journal of Biological Chemistry*, *254*(8), 2669–2676.

Reynolds, M. R., Lane, A. N., Robertson, B., Kemp, S., Liu, Y., Hill, B. G., Dean, D. C., & Clem, B. F. (2014). Control of glutamine metabolism by the tumor suppressor Rb. *Oncogene*, *33*(5), 556–566. https://doi.org/10.1038/onc.2012.635

Rizwan, A., Serganova, I., Khanin, R., Karabeber, H., Ni, X., Thakur, S., Zakian, K. L., Blasberg, R., & Koutcher, J. A. (2013). Relationships between LDH-A, Lactate and Metastases in 4T1 Breast Tumors. *Clinical Cancer Research : An Official Journal of the American Association for Cancer Research*, *19*(18). https://doi.org/10.1158/1078-0432.CCR-12-3300

Rodrigues, E., & Macauley, M. S. (2018). Hypersialylation in Cancer: Modulation of Inflammation and Therapeutic Opportunities. *Cancers*, *10*(6). https://doi.org/10.3390/cancers10060207

Romero-Garcia, S., Moreno-Altamirano, M. M. B., Prado-Garcia, H., & Sánchez-García, F. J. (2016). Lactate Contribution to the Tumor Microenvironment: Mechanisms, Effects on Immune Cells and Therapeutic Relevance. *Frontiers in Immunology*, *7*. https://doi.org/10.3389/fimmu.2016.00052

Saborano, R., Eraslan, Z., Roberts, J., Khanim, F. L., Lalor, P. F., Reed, M. A. C., & Günther, U. L. (2019). A framework for tracer-based metabolism in mammalian cells by NMR. *Scientific Reports*, *9*(1), 1–13. https://doi.org/10.1038/s41598-018-37525-3

Said, J. W. (2013). Aggressive B-cell lymphomas: How many categories do we need? *Modern Pathology : An Official Journal of the United States and Canadian Academy of Pathology, Inc*, *26*(0 1), S42–S56. https://doi.org/10.1038/modpathol.2012.178

Salesse, S., & Verfaillie, C. M. (2002). BCR/ABL: From molecular mechanisms of leukemia induction to treatment of chronic myelogenous leukemia. *Oncogene*, *21*(56), 8547–8559. https://doi.org/10.1038/sj.onc.1206082

Sánchez López de Nava, A., & Raja, A. (2020). Physiology, Metabolism. In *StatPearls*. StatPearls Publishing. http://www.ncbi.nlm.nih.gov/books/NBK546690/

San-Millán, I., & Brooks, G. A. (2017). Reexamining cancer metabolism: Lactate production for carcinogenesis could be the purpose and explanation of the Warburg Effect. *Carcinogenesis*, *38*(2), 119–133. https://doi.org/10.1093/carcin/bgw127

Savorani, F., Tomasi, G., & Engelsen, S. B. (2010). icoshift: A versatile tool for the rapid alignment of 1D NMR spectra. *Journal of Magnetic Resonance*, *202*(2), 190–202. https://doi.org/10.1016/j.jmr.2009.11.012

Saxton, R. A., & Sabatini, D. M. (2017). MTOR Signaling in Growth, Metabolism, and Disease. *Cell*, *168*(6), 960–976. https://doi.org/10.1016/j.cell.2017.02.004

Schafer, Z. T., Grassian, A. R., Song, L., Jiang, Z., Gerhart-Hines, Z., Irie, H. Y., Gao, S., Puigserver, P., & Brugge, J. S. (2009). Antioxidant and oncogene rescue of metabolic defects caused by loss of matrix attachment. *Nature*, *461*(7260), 109–113. https://doi.org/10.1038/nature08268

Scheller, H., Tobollik, S., Kutzera, A., Eder, M., Unterlehberg, J., Pfeil, I., & Jungnickel, B. (2010). C-Myc overexpression promotes a germinal center-like program in Burkitt's lymphoma. *Oncogene*, *29*(6), 888–897. https://doi.org/10.1038/onc.2009.377

Schmitz, R., Ceribelli, M., Pittaluga, S., Wright, G., & Staudt, L. M. (2014). Oncogenic Mechanisms in Burkitt Lymphoma. *Cold Spring Harbor Perspectives in Medicine*, *4*(2). https://doi.org/10.1101/cshperspect.a014282

Schwartzenberg-Bar-Yoseph, F., Armoni, M., & Karnieli, E. (2004). The Tumor Suppressor p53 Down-Regulates Glucose Transporters ***GLUT1*** and ***GLUT4*** Gene Expression. *Cancer Research*, *64*(7), 2627–2633. https://doi.org/10.1158/0008-5472.CAN-03-0846

Segawa, H., Fukasawa, Y., Miyamoto, K., Takeda, E., Endou, H., & Kanai, Y. (1999). Identification and functional characterization of a Na+-independent neutral amino acid transporter with broad substrate selectivity. *The Journal of Biological Chemistry*, *274*(28), 19745–19751. https://doi.org/10.1074/jbc.274.28.19745

Selwan, E. M., & Edinger, A. L. (2017). Branched chain amino acid metabolism and cancer: The importance of keeping things in context. *Translational Cancer Research*, *6*(Suppl 3), S578–S584. https://doi.org/10.21037/tcr.2017.05.05

Shanmugam, M., McBrayer, S. K., & Rosen, S. T. (2009). Targeting the Warburg Effect in Hematological Malignancies: From PET to Therapy. *Current Opinion in Oncology*, *21*(6), 531–536. https://doi.org/10.1097/CCO.0b013e32832f57ec

Shannon, P., Markiel, A., Ozier, O., Baliga, N. S., Wang, J. T., Ramage, D., Amin, N., Schwikowski, B., & Ideker, T. (2003). Cytoscape: A software environment for integrated models of biomolecular interaction networks. *Genome Research*, *13*(11), 2498–2504. https://doi.org/10.1101/gr.1239303

Shen, C., & Vakoc, C. R. (2015). Gain-of-function mutation of chromatin regulators as a tumorigenic mechanism and an opportunity for therapeutic intervention: *Current Opinion in Oncology*, *27*(1), 57–63. https://doi.org/10.1097/CCO.0000000000000151

Sherman, M. H., Yu, R. T., Tseng, T. W., Sousa, C. M., Liu, S., Truitt, M. L., He, N., Ding, N., Liddle, C., Atkins, A. R., Leblanc, M., Collisson, E. A., Asara, J. M., Kimmelman, A. C., Downes, M., & Evans, R. M. (2017). Stromal cues regulate the pancreatic cancer

epigenome and metabolome. *Proceedings of the National Academy of Sciences of the United States of America*, *114*(5), 1129–1134. https://doi.org/10.1073/pnas.1620164114

Shi, J., Fu, H., Jia, Z., He, K., Fu, L., & Wang, W. (2016). High Expression of CPT1A Predicts Adverse Outcomes: A Potential Therapeutic Target for Acute Myeloid Leukemia. *EBioMedicine*, *14*, 55–64. https://doi.org/10.1016/j.ebiom.2016.11.025

Shim, H., Dolde, C., Lewis, B. C., Wu, C.-S., Dang, G., Jungmann, R. A., Dalla-Favera, R., & Dang, C. V. (1997). c-Myc transactivation of LDH-A: Implications for tumor metabolism and growth. *Proceedings of the National Academy of Sciences*, *94*(13), 6658–6663. https://doi.org/10.1073/pnas.94.13.6658

Siddiqui, A., & Ceppi, P. (2020). A non-proliferative role of pyrimidine metabolism in cancer. *Molecular Metabolism*, *35*. https://doi.org/10.1016/j.molmet.2020.02.005

Sigoillot, F. D., Sigoillot, S. M., & Guy, H. I. (2004). Breakdown of the regulatory control of pyrimidine biosynthesis in human breast cancer cells. *International Journal of Cancer*, *109*(4), 491–498. https://doi.org/10.1002/ijc.11717

Simillion, C., Liechti, R., Lischer, H. E. L., Ioannidis, V., & Bruggmann, R. (2017). Avoiding the pitfalls of gene set enrichment analysis with SetRank. *BMC Bioinformatics*, *18*(1), 151. https://doi.org/10.1186/s12859-017-1571-6

Singh, N., & Ecker, G. F. (2018). Insights into the Structure, Function, and Ligand Discovery of the Large Neutral Amino Acid Transporter 1, LAT1. *International Journal of Molecular Sciences*, *19*(5). https://doi.org/10.3390/ijms19051278

Singleton, D. C., & Harris, A. L. (2012). Targeting the ATF4 pathway in cancer therapy. *Expert Opinion on Therapeutic Targets*, *16*(12), 1189–1202. https://doi.org/10.1517/14728222.2012.728207

Sinha, R., Nastoupil, L., & Flowers, C. R. (2012). Treatment Strategies for Patients with Diffuse Large B-Cell Lymphoma: Past, Present, and Future. *Blood and Lymphatic Cancer : Targets and Therapy*, *2012*(2), 87–98. https://doi.org/10.2147/BLCTT.S18701

Snowden, J. A., O'Connell, S., Hawkins, J., Dalley, C., Jack, A., Mannari, D., McNamara, C., Scott, M., Shenton, G., Soilleux, E., Macbeth, F., & Guideline Committee. (2017). Haematological cancers: Improving outcomes. A summary of updated NICE service guidance in relation to Specialist Integrated Haematological Malignancy Diagnostic Services (SIHMDS). *Journal of Clinical Pathology*, *70*(6), 461–468. https://doi.org/10.1136/jclinpath-2016-204029

Son, J., Lyssiotis, C. A., Ying, H., Wang, X., Hua, S., Ligorio, M., Perera, R. M., Ferrone, C. R., Mullarky, E., Shyh-Chang, N., Kang, Y., Fleming, J. B., Bardeesy, N., Asara, J. M., Haigis, M. C., DePinho, R. A., Cantley, L. C., & Kimmelman, A. C. (2013). Glutamine supports pancreatic cancer growth through a KRAS-regulated metabolic pathway. *Nature*, *496*(7443), 101–105. https://doi.org/10.1038/nature12040

Sontakke, P., Koczula, K. M., Jaques, J., Wierenga, A. T. J., Brouwers-Vos, A. Z., Pruis, M., Günther, U. L., Vellenga, E., & Schuringa, J. J. (2016). Hypoxia-Like Signatures Induced by BCR-ABL Potentially Alter the Glutamine Uptake for Maintaining Oxidative Phosphorylation. *PloS One*, *11*(4), e0153226. https://doi.org/10.1371/journal.pone.0153226

Stincone, A., Prigione, A., Cramer, T., Wamelink, M. M. C., Campbell, K., Cheung, E., Olin-Sandoval, V., Grüning, N.-M., Krüger, A., Alam, M. T., Keller, M. A., Breitenbach, M., Brindle, K. M., Rabinowitz, J. D., & Ralser, M. (2015). The return of metabolism: Biochemistry and physiology of the pentose phosphate pathway. *Biological Reviews of*

the Cambridge Philosophical Society, *90*(3), 927–963. https://doi.org/10.1111/brv.12140

Strickland, M., & Stoll, E. A. (2017). Metabolic Reprogramming in Glioma. *Frontiers in Cell and Developmental Biology*, *5*. https://doi.org/10.3389/fcell.2017.00043

Swerdlow, S. H., Campo, E., Pileri, S. A., Harris, N. L., Stein, H., Siebert, R., Advani, R., Ghielmini, M., Salles, G. A., Zelenetz, A. D., & Jaffe, E. S. (2016a). The 2016 revision of the World Health Organization classification of lymphoid neoplasms. *Blood*, *127*(20), 2375–2390. https://doi.org/10.1182/blood-2016-01-643569

Swerdlow, S. H., Campo, E., Pileri, S. A., Harris, N. L., Stein, H., Siebert, R., Advani, R., Ghielmini, M., Salles, G. A., Zelenetz, A. D., & Jaffe, E. S. (2016b). The 2016 revision of the World Health Organization classification of lymphoid neoplasms. *Blood*, *127*(20), 2375–2390. https://doi.org/10.1182/blood-2016-01-643569

Swinnen, J. V., Heemers, H., van de Sande, T., de Schrijver, E., Brusselmans, K., Heyns, W., & Verhoeven, G. (2004). Androgens, lipogenesis and prostate cancer. *The Journal of Steroid Biochemistry and Molecular Biology*, *92*(4), 273–279. https://doi.org/10.1016/j.jsbmb.2004.10.013

Szklarczyk, D., Gable, A. L., Lyon, D., Junge, A., Wyder, S., Huerta-Cepas, J., Simonovic, M., Doncheva, N. T., Morris, J. H., Bork, P., Jensen, L. J., & Mering, C. von. (2019). STRING v11: Protein-protein association networks with increased coverage, supporting functional discovery in genome-wide experimental datasets. *Nucleic Acids Research*, *47*(D1), D607–D613. https://doi.org/10.1093/nar/gky1131

Taegtmeyer, H., & Ingwall, J. S. (2013). Creatine – A Dispensable Metabolite? *Circulation Research*, *112*(6), 878–880. https://doi.org/10.1161/CIRCRESAHA.113.300974

Tan, W., Zhong, Z., Carney, R. P., Men, Y., Li, J., Pan, T., & Wang, Y. (2019). Deciphering the

metabolic role of AMPK in cancer multi-drug resistance. *Seminars in Cancer Biology*, *56*, 56–71. https://doi.org/10.1016/j.semcancer.2018.09.005

Taub, R., Kirsch, I., Morton, C., Lenoir, G., Swan, D., Tronick, S., Aaronson, S., & Leder, P. (1982). Translocation of the c-myc gene into the immunoglobulin heavy chain locus in human Burkitt lymphoma and murine plasmacytoma cells. *Proceedings of the National Academy of Sciences of the United States of America*, *79*(24), 7837–7841. https://doi.org/10.1073/pnas.79.24.7837

Teater, M., Dominguez, P. M., Redmond, D., Chen, Z., Ennishi, D., Scott, D. W., Cimmino, L., Ghione, P., Chaudhuri, J., Gascoyne, R. D., Aifantis, I., Inghirami, G., Elemento, O., Melnick, A., & Shaknovich, R. (2018). AICDA drives epigenetic heterogeneity and accelerates germinal center-derived lymphomagenesis. *Nature Communications*, *9*(1), 222. https://doi.org/10.1038/s41467-017-02595-w

Teoh, S. T., Ogrodzinski, M. P., Ross, C., Hunter, K. W., & Lunt, S. Y. (2018). Sialic Acid Metabolism: A Key Player in Breast Cancer Metastasis Revealed by Metabolomics. *Frontiers in Oncology*, *8*. https://doi.org/10.3389/fonc.2018.00174

Thomas, D. A., O'Brien, S., Faderl, S., Manning, J. T., Romaguera, J., Fayad, L., Hagemeister, F., Medeiros, J., Cortes, J., & Kantarjian, H. (2011). Burkitt Lymphoma and Atypical Burkitt or Burkitt-like Lymphoma: Should These be Treated as Different Diseases? *Current Hematologic Malignancy Reports*, *6*(1), 58–66. https://doi.org/10.1007/s11899-010-0076-4

Tiefenthaler, M., Amberger, A., Bacher, N., Hartmann, B. L., Margreiter, R., Kofler, R., & Konwalinka, G. (2001). Increased lactate production follows loss of mitochondrial membrane potential during apoptosis of human leukaemia cells. *British Journal of*

Haematology, *114*(3), 574–580. https://doi.org/10.1046/j.1365-2141.2001.02988.x

Todisco, S., Convertini, P., Iacobazzi, V., & Infantino, V. (2019). TCA Cycle Rewiring as Emerging Metabolic Signature of Hepatocellular Carcinoma. *Cancers*, *12*(1). https://doi.org/10.3390/cancers12010068

Tönjes, M., Barbus, S., Park, Y. J., Wang, W., Schlotter, M., Lindroth, A. M., Pleier, S. V., Bai, A. H. C., Karra, D., Piro, R. M., Felsberg, J., Addington, A., Lemke, D., Weibrecht, I., Hovestadt, V., Rolli, C. G., Campos, B., Turcan, S., Sturm, D., … Radlwimmer, B. (2013). BCAT1 promotes cell proliferation through amino acid catabolism in gliomas carrying wild-type IDH1. *Nature Medicine*, *19*(7), 901–908. https://doi.org/10.1038/nm.3217

Tortora, G. J., & Derrickson, B. H. (2018). *Principles of Anatomy and Physiology*. John Wiley & Sons.

Vardiman, J. W., Thiele, J., Arber, D. A., Brunning, R. D., Borowitz, M. J., Porwit, A., Harris, N. L., Le Beau, M. M., Hellström-Lindberg, E., Tefferi, A., & Bloomfield, C. D. (2009). The 2008 revision of the World Health Organization (WHO) classification of myeloid neoplasms and acute leukemia: Rationale and important changes. *Blood*, *114*(5), 937–951. https://doi.org/10.1182/blood-2009-03-209262

Vazquez, A., Liu, J., Zhou, Y., & Oltvai, Z. N. (2010). Catabolic efficiency of aerobic glycolysis: The Warburg effect revisited. *BMC Systems Biology*, *4*(1), 58. https://doi.org/10.1186/1752-0509-4-58

Villa, E., Ali, E. S., Sahu, U., & Ben-Sahra, I. (2019). Cancer Cells Tune the Signaling Pathways to Empower de Novo Synthesis of Nucleotides. *Cancers*, *11*(5). https://doi.org/10.3390/cancers11050688

Wang, Q., & Holst, J. (2015a). L-type amino acid transport and cancer: Targeting the mTORC1 pathway to inhibit neoplasia. *American Journal of Cancer Research*, *5*(4), 1281–1294.

Wang, Q., & Holst, J. (2015b). L-type amino acid transport and cancer: Targeting the mTORC1 pathway to inhibit neoplasia. *American Journal of Cancer Research*, *5*(4), 1281–1294.

Wang, X., Wang, J., & Zhang, L. (2019). Characterization of atypical acute promyelocytic leukaemia: Three cases report and literature review. *Medicine*, *98*(19), e15537. https://doi.org/10.1097/MD.0000000000015537

Wang, Y., Zhang, L., Chen, W.-L., Wang, J.-H., Li, N., Li, J.-M., Mi, J.-Q., Zhang, W.-N., Li, Y., Wu, S.-F., Jin, J., Wang, Y.-G., Huang, H., Chen, Z., Chen, S.-J., & Tang, H. (2013). Rapid diagnosis and prognosis of de novo acute myeloid leukemia by serum metabonomic analysis. *Journal of Proteome Research*, *12*(10), 4393–4401. https://doi.org/10.1021/pr400403p

Warburg, O., Wind, F., & Negelein, E. (1927). THE METABOLISM OF TUMORS IN THE BODY. *The Journal of General Physiology*, *8*(6), 519–530.

Ward, P. S., Patel, J., Wise, D. R., Abdel-Wahab, O., Bennett, B. D., Coller, H. A., Cross, J. R., Fantin, V. R., Hedvat, C. V., Perl, A. E., Rabinowitz, J. D., Carroll, M., Su, S. M., Sharp, K. A., Levine, R. L., & Thompson, C. B. (2010). The common feature of leukemia-associated IDH1 and IDH2 mutations is a neomorphic enzyme activity converting alpha-ketoglutarate to 2-hydroxyglutarate. *Cancer Cell*, *17*(3), 225–234. https://doi.org/10.1016/j.ccr.2010.01.020

Ward, P. S., & Thompson, C. B. (2012). Metabolic Reprogramming: A Cancer Hallmark Even Warburg Did Not Anticipate. *Cancer Cell*, *21*(3), 297–308. https://doi.org/10.1016/j.ccr.2012.02.014

Weaver, C. J., & Tariman, J. D. (2017). Multiple Myeloma Genomics: A Systematic Review. *Seminars in Oncology Nursing*, *33*(3), 237–253. https://doi.org/10.1016/j.soncn.2017.05.001

Weber, G. (2001). Ordered biochemical program of gene expression in cancer cells. *Biochemistry. Biokhimiia*, *66*(10), 1164–1173. https://doi.org/10.1023/a:1012493232344

Wise, D. R., DeBerardinis, R. J., Mancuso, A., Sayed, N., Zhang, X.-Y., Pfeiffer, H. K., Nissim, I., Daikhin, E., Yudkoff, M., McMahon, S. B., & Thompson, C. B. (2008). Myc regulates a transcriptional program that stimulates mitochondrial glutaminolysis and leads to glutamine addiction. *Proceedings of the National Academy of Sciences*, *105*(48), 18782–18787. https://doi.org/10.1073/pnas.0810199105

Wojtowicz, W., Chachaj, A., Olczak, A., Ząbek, A., Piątkowska, E., Rybka, J., Butrym, A., Biedroń, M., Mazur, G., Wróbel, T., Szuba, A., & Młynarz, P. (2018). Serum NMR metabolomics to differentiate haematologic malignancies. *Oncotarget*, *9*(36), 24414–24427. https://doi.org/10.18632/oncotarget.25311

Xiang, Y., Stine, Z. E., Xia, J., Lu, Y., O'Connor, R. S., Altman, B. J., Hsieh, A. L., Gouw, A. M., Thomas, A. G., Gao, P., Sun, L., Song, L., Yan, B., Slusher, B. S., Zhuo, J., Ooi, L. L., Lee, C. G. L., Mancuso, A., McCallion, A. S., … Dang, C. V. (2015). Targeted inhibition of tumor-specific glutaminase diminishes cell-autonomous tumorigenesis. *The Journal of Clinical Investigation*, *125*(6), 2293–2306. https://doi.org/10.1172/JCI75836

Xiao, D., Ren, P., Su, H., Yue, M., Xiu, R., Hu, Y., Liu, H., & Qing, G. (2015). Myc promotes glutaminolysis in human neuroblastoma through direct activation of glutaminase 2. *Oncotarget*, *6*(38). https://doi.org/10.18632/oncotarget.5821

Xiao, G., Chan, L. N., Klemm, L., Braas, D., Chen, Z., Geng, H., Zhang, Q. C., Aghajanirefah,

A., Cosgun, K. N., Sadras, T., Lee, J., Mirzapoiazova, T., Salgia, R., Ernst, T., Hochhaus, A., Jumaa, H., Jiang, X., Weinstock, D. M., Graeber, T. G., & Müschen, M. (2018). B-Cell-Specific Diversion of Glucose Carbon Utilization Reveals a Unique Vulnerability in B Cell Malignancies. *Cell*, *173*(2), 470-484.e18. https://doi.org/10.1016/j.cell.2018.02.048

Xiao, L., Hu, Z.-Y., Dong, X., Tan, Z., Li, W., Tang, M., Chen, L., Yang, L., Tao, Y., Jiang, Y., Li, J., Yi, B., Li, B., Fan, S., You, S., Deng, X., Hu, F., Feng, L., Bode, A. M., … Cao, Y. (2014). Targeting Epstein-Barr virus oncoprotein LMP1-mediated glycolysis sensitizes nasopharyngeal carcinoma to radiation therapy. *Oncogene*, *33*(37), 4568–4578. https://doi.org/10.1038/onc.2014.32

Yang, F., Du, J., Zhang, H., Ruan, G., Xiang, J., Wang, L., Sun, H., Guan, A., Shen, G., Liu, Y., Guo, X., Li, Q., & Tang, Y. (2017). Serum Metabolomics of Burkitt Lymphoma Mouse Models. *PLoS ONE*, *12*(1). https://doi.org/10.1371/journal.pone.0170896

Yang, L. V. (2017). Tumor Microenvironment and Metabolism. *International Journal of Molecular Sciences*, *18*(12). https://doi.org/10.3390/ijms18122729

Yang, L., Venneti, S., & Nagrath, D. (2017). Glutaminolysis: A Hallmark of Cancer Metabolism. *Annual Review of Biomedical Engineering*, *19*, 163–194. https://doi.org/10.1146/annurev-bioeng-071516-044546

Yang, T., Ren, C., Qiao, P., Han, X., Wang, L., Lv, S., Sun, Y., Liu, Z., Du, Y., & Yu, Z. (2018). PIM2-mediated phosphorylation of hexokinase 2 is critical for tumor growth and paclitaxel resistance in breast cancer. *Oncogene*, *37*(45), 5997–6009. https://doi.org/10.1038/s41388-018-0386-x

Yao, Y., Jones, E., & Inoki, K. (2017). Lysosomal Regulation of mTORC1 by Amino Acids in

Mammalian Cells. *Biomolecules*, *7*(3). https://doi.org/10.3390/biom7030051

Ye, B. H., Lista, F., Lo Coco, F., Knowles, D. M., Offit, K., Chaganti, R. S., & Dalla-Favera, R. (1993). Alterations of a zinc finger-encoding gene, BCL-6, in diffuse large-cell lymphoma. *Science (New York, N.Y.)*, *262*(5134), 747–750. https://doi.org/10.1126/science.8235596

Yin, J., Ren, W., Huang, X., Deng, J., Li, T., & Yin, Y. (2018). Potential Mechanisms Connecting Purine Metabolism and Cancer Therapy. *Frontiers in Immunology*, *9*. https://doi.org/10.3389/fimmu.2018.01697

Yu, L., Chen, X., Sun, X., Wang, L., & Chen, S. (2017). The Glycolytic Switch in Tumors: How Many Players Are Involved? *Journal of Cancer*, *8*(17), 3430–3440. https://doi.org/10.7150/jca.21125

Yu, X., & Li, S. (2017). Non-metabolic functions of glycolytic enzymes in tumorigenesis. *Oncogene*, *36*(19), 2629–2636. https://doi.org/10.1038/onc.2016.410

Zheng, Y.-H., Hu, W.-J., Chen, B.-C., Grahn, T.-H.-M., Zhao, Y.-R., Bao, H.-L., Zhu, Y.-F., & Zhang, Q.-Y. (2016). BCAT1, a key prognostic predictor of hepatocellular carcinoma, promotes cell proliferation and induces chemoresistance to cisplatin. *Liver International: Official Journal of the International Association for the Study of the Liver*, *36*(12), 1836–1847. https://doi.org/10.1111/liv.13178

Zhou, K., Xu, D., Cao, Y., Wang, J., Yang, Y., & Huang, M. (2014). C-MYC Aberrations as Prognostic Factors in Diffuse Large B-cell Lymphoma: A Meta-Analysis of Epidemiological Studies. *PLoS ONE*, *9*(4), e95020. https://doi.org/10.1371/journal.pone.0095020